

# Modulation of amyloid peptides aggregation by hydrophilic polymers

## Dissertation

zur Erlangung des Doktorgrades der Naturwissenschaften

(Dr. rer. nat.)

der

Naturwissenschaftlichen Fakultät II

Chemie, Physik und Mathematik

der Martin-Luther-Universität  
Halle-Wittenberg

vorgelegt von

Frau Zhanna Evgrafova

geb. am 29.09.1989 in Dimitrovgrad (Russland)

Gutachter

1. Prof. Dr. Wolfgang H. Binder
2. Prof. Dr. Felix Schacher

Verteidigung: 01.09.2020

## Acknowledgments

First of all, I would like to express my sincere gratitude and appreciation to my supervisor Prof. Dr. Wolfgang H. Binder for the opportunity to work in this fascinating field of science in his group. I am very thankful for his guidelines, advice, patience, and support he gave me within all these years. I would never be able to finish this scientific work without our discussions of my work, his professional revision of the publications, which became a part of the given thesis, and constant motivation.

I am also very thankful to Prof. Dr. Jochen Balbach for allowing me to conduct measurements on facilities of his group, which considerably reinforced my publications and supported my ideas. Furthermore, I would like to send my special thanks to Bruno Voigt who taught me a number of techniques, carried out all the TEM measurements, and contributed in 3 out of 4 publications included into this work.

I want to thank Prof. Dr. Dariush Hinderberger for allowing me to carry out experiments in his laboratory and for the effective collaboration in the framework of the SFB project. I also thank the members of his group, Dr. Andreas Kerth, for his help in explaining the turbidimetry technique as well as Andreas Roos for conducting the EPR experiments and a fruitful discussion of the results.

In addition, I thank Prof. Dr. Daniel Huster and Dr. Juliane Adler for their time and cooperation invested in the creation of the publication included within this cumulative dissertation. I also thank the Core Unit Peptid-Technologie in Leipzig and especially Dr. Sven Rothmund for the production of amyloid beta-polymer conjugates and a successful collaboration.

Moreover, I would like to thank the entire group of Prof. Dr. Wolfgang H. Binder for the pleasant working atmosphere and many good memories over these years. I thank Merve B. Canalp, Dr. Stefanie Deike, and Dr. Steve Neumann for the friendly support I have received from them. I am grateful to the latter two for their help and patience at the beginning of my learning process of the German language. Also, I thank Dr. Diana Döhler and Dr. Philipp Michael for their help at the beginning of work at AG Binder. Finally, I would like to thank Anke Hassi for her kind support in all the administrative issues as well as Susanne Tanner and Julia Großert for providing chemicals and conducting some of the measurements.

Last but not least, I am also very grateful to my husband Dr. Anton Mordvinkin for the understanding, love, and support he gave me during my PhD time. He supported me with deeds and words like no other. I also would like to thank him for the critical review of this thesis. Особенная благодарность также направляется моей семье в Россию. Без поддержки моей мамы, папы и бабушек этот тезис никогда не был бы написан. Вы всегда верили в меня, поддерживали и помогали мне во всех моих начинаниях. Без лишнего пафоса я просто скажу спасибо и то, что я вас очень-очень люблю!

## ABSTRACT

A spontaneous self-assembly process which a particular type of peptides and proteins are subject to, commonly termed as amyloids or amyloidogenic peptides/proteins, can lead to development of incurable neurodegenerative diseases known as Alzheimer's, Parkinson's, or Huntington's diseases. The presence of small molecules, peptides and proteins, nanoparticles, lipid membranes or synthetic polymers strongly affects fibrillation of amyloids *in vitro*. In contribution to this topic, fibrillogenesis of the irreversibly aggregating amyloid- $\beta$  1–40 peptide ( $A\beta_{1-40}$ ) here is investigated in a physical mixture or in covalent conjugation with hydrophilic thermoresponsive poly(oligo(ethylene glycol)<sub>m</sub> acrylates). Different molecular parameters of the polymers such as molecular weight, polydispersity index (PDI), cloud point temperature ( $T_{cp}$ ), and hydrophilicity are expected to affect on the fibrillation process. The designed polymers are synthesized via RAFT-polymerization technique allowing us to prepare a series of polymers with different molecular masses ( $M_n = 700$  to  $14\,600$  g/mol, PDI = 1.10 to 1.25) and adjustable  $T_{cp}$ . The polymer's hydrophilicity is altered by variation of the number of ethylene glycol-units in the side chain ( $m = 1-9$ ), nature of the end group (B = butoxy; C = carboxy; D = dodecyl; P = pyridyldisulfide) and the degree of polymerization ( $n$ ) of the polymers. The appropriate combination of hydrophobic end groups with hydrophilic side chains controls overall polymer's hydrophilicity and thus the polymer's  $T_{cp}$ , what in turn influences fibrillation pathways of the  $A\beta_{1-40}$  admixed with the polymers.

Polymer-peptide conjugates comprising the  $A\beta_{1-40}$  peptide and the poly(oligo(ethylene glycol)<sub>m</sub> acrylates) ( $m=2, 3$ ) ( $M_n$  up to  $6000$  g/mol) are successfully synthesized via two different coupling techniques. The obtained conjugates exhibit no detectable  $T_{cp}$  up to  $90$  °C. The aggregation behavior of the polymer- $A\beta_{1-40}$  conjugates is investigated via ThT detected fluorescence measurements. It is observed that the conjugates with the highest molecular weights aggregate faster than the analogues with the lower molecular weights or the  $A\beta_{1-40}$  alone. The final morphology of the obtained aggregates is significantly different from the conventional amyloid fibrils. Instead of long and straight fibrils, bundles of short aggregated are detected.

Furthermore, the chosen polymers are coupled with a reversibly aggregating peptide, namely with the parathyroid peptide hormone ( $PTH_{1-84}$ ). The transition of molecular conformations from the random coil to the collapsed state of these polymers above and below the  $T_{cp}$ , respectively, is monitored by means of NMR spectroscopy of  $^{15}N$  labeled parathyroid hormone ( $PTH_{1-84}$ ) for the first time. We observe stimulation of the  $PTH_{1-84}$  aggregation by the employed polymers, while keeping the morphology of the obtained fibrils unchanged.

## KURZFASSUNG

Die Fibrillierung bestimmter Peptide und Proteine kann zur Entwicklung unheilbarer neurodegenerativer Erkrankungen führen, die als Alzheimer-, Parkinson- oder Huntington-Krankheit bekannt sind. Die damit assoziierten Proteine bzw. Peptide werden als Amyloide bezeichnet. Das Vorhandensein kleiner Moleküle, Peptide und Proteine, Nanopartikel, Lipidmembranen oder synthetischer Polymere beeinflusst das Fibrillieren von Amyloiden *in vitro* stark. Als Beitrag zu diesem Thema wird die Fibrillogenese des irreversibel aggregierenden Amyloid- $\beta$  1–40-Peptids ( $A\beta_{1-40}$ ) sowie des reversibel aggregierenden Nebenschilddrüsenpeptidhormon (PTH<sub>1-84</sub>) in physikalischer Mischung oder in kovalenter Konjugation mit hydrophilen thermoresponsiven Poly(oligo(ethylene glycol)<sub>m</sub> acrylaten) untersucht.

Verschiedene molekulare Parameter der Polymere wie Molekulargewicht, Polydispersitätsindex (PDI), Trübungspunkttemperatur ( $T_{cp}$ ), Endgruppen und Hydrophilie werden in Hinblick auf den Fibrillationsprozess untersucht. Die Polymere werden mittels RAFT-Polymerisationstechnik synthetisiert, wodurch eine Serie von analog-strukturierten Polymeren mit unterschiedlichen Molekularmassen ( $M_n = 700$  bis  $14\,600$  g/mol, PDI = 1,10 bis 1,25) und einstellbarer  $T_{cp}$  herstellen werden konnten. Die Hydrophilie der Polymere wird durch Variation der Anzahl der Ethylenglykoleinheiten in der Seitenkette ( $m = 1-9$ ), der Art der Endgruppe (B = Butoxy; C = Carboxy; D = Dodecyl; P = Pyridyldisulfid) und des Polymerisationsgrades ( $n$ ) der Polymere verändert. Die geeignete Kombination von hydrophoben Endgruppen mit hydrophilen Seitenketten steuert die Hydrophilie des gesamten Polymers und dadurch die  $T_{cp}$  des Polymers, die wiederum die Fibrillationswege des mit den Polymeren vermischten  $A\beta_{1-40}$  beeinflussen. Es wird eine deutliche Abhängigkeit der Fibrillierung in Abhängigkeit von der Endgruppe, des Molekulargewichtes, wie auch der hydrophilen Seitenketten beobachtet, wobei mit steigender Trübungspunkttemperatur ( $T_{cp}$ ) eine Reduktion der Fibrillierung im Vergleich zu nativem  $A\beta_{1-40}$  detektiert wird.

Polymer-Peptid-Konjugate, die aus dem  $A\beta_{1-40}$ -Peptid und Poly(oligo(ethylene glycol)<sub>m</sub> acrylaten) ( $m = 2, 3$ ) ( $M_n$  bis zu  $6000$  g/mol) bestehen werden erfolgreich über zwei verschiedene Kupplungstechniken synthetisiert. Die erhaltenen Konjugate zeigen bis zu  $90$  °C keine nachweisbare  $T_{cp}$ . Das Aggregationsverhalten der Polymer- $A\beta_{1-40}$ -Konjugate wird über ThT-detektierte Fluoreszenzmessungen untersucht. Es wird beobachtet, dass die Konjugate mit den höchsten Molekulargewichten schneller aggregieren als die Analoga mit den niedrigeren Molekulargewichten oder nur mit  $A\beta_{1-40}$  alleine. Die endgültige Morphologie der erhaltenen Aggregate unterscheidet sich signifikant von den herkömmlichen Amyloidfibrillen. Anstelle von langen und geraden Fibrillen entstehen Bündel von kurzen aggregierten Fibrillen.

Darüber hinaus werden ausgewählte Polymere mit dem reversibel aggregierenden Peptid (PTH<sub>1-84</sub>) gekoppelt. Der Übergang molekularer Konformationen von einem "Random coil" zum kollabierten Zustand dieser Polymere oberhalb bzw. unterhalb der  $T_{cp}$  wird erstmals mittels NMR-Spektroskopie von <sup>15</sup>N-markiertem Nebenschilddrüsenhormon (PTH<sub>1-84</sub>) verfolgt. Wir beobachten eine Stimulation der PTH<sub>1-84</sub>-Aggregation durch die verwendeten Polymere, wohingegen die Morphologie der erhaltenen Fibrillen unverändert bleibt.

I.	INTRODUCTION .....	1
1.	Thermoresponsive polymers.....	1
1.1.	LCST behavior of polymers in aqueous medium.....	2
1.2.	Factors affecting the LCST of diverse polymers .....	4
1.2.1.	Influence of the polymer molecular weight .....	4
1.2.2.	Influence of the polymer end groups .....	4
1.2.3.	Influence of the polymer concentration .....	5
1.2.4.	Influence of added salts .....	5
2.	Amyloidogenic peptides and disease-causing proteins .....	6
2.1.	Methods to monitor aggregation pathway.....	11
2.2.	Factors affecting aggregation pathway of A $\beta$ <sub>1-40/42</sub> peptides .....	12
2.2.1.	Influence of small molecules on aggregation of A $\beta$ <sub>1-40/42</sub> peptides.....	13
2.2.2.	Influence of nanoparticles on aggregation of A $\beta$ <sub>1-40/42</sub> peptides .....	14
2.2.3.	Influence of proteins and peptides on aggregation of A $\beta$ <sub>1-40/42</sub> peptides.....	17
2.2.4.	Influence of lipids and lipid membranes on aggregation of A $\beta$ <sub>1-40/42</sub> peptides ...	20
2.2.5.	Influence of surfactants on aggregation of A $\beta$ <sub>1-40/42</sub> peptides .....	23
2.2.6.	Influence of synthetic polymers on aggregation of A $\beta$ <sub>1-40/42</sub> peptides .....	24
2.3.	The reversibly aggregating parathyroid peptide hormone .....	26
II.	SCOPE OF THE THESIS .....	28
1.	Objectives .....	28
2.	Concept.....	29
III.	RESULTS AND DISCUSSION .....	32
1.	Amyloid Beta Aggregation in the Presence of Temperature-Sensitive Polymers.....	33
2.	Modulation of amyloid $\beta$ peptide aggregation by hydrophilic polymers .....	49
3.	Synthesis and Aggregation of Polymer-Amyloid $\beta$ Conjugates.....	57
4.	Probing Polymer Chain Conformation and Fibril Formation of Peptide Conjugates ...	63
IV.	SUMMARY .....	68
V.	REFERENCES .....	71
VI.	Appendix .....	83

## I. INTRODUCTION

### 1. Thermoresponsive polymers

Various biomacromolecules undergo formation of well-defined supramolecular structures via development of non-covalent interactions in aqueous media.<sup>1</sup> Many of such molecules found in animals and plants experience conformational changes by responding external stimuli such as changes in salinity,<sup>2</sup> heavy metal concentration,<sup>3</sup> pH<sup>4</sup> or temperature<sup>5</sup>. The desire to imitate nature inspired preparation of wide range of macromolecules or polymers able to experience reversible phase transition upon minimal changes of environmental conditions. These macromolecules are known as stimuli-responsive, “smart” or “intelligent” materials.<sup>6</sup> Similar to nature-created biomacromolecules, the macroscopic changes of stimuli-responsive polymers most often take place under changes in pH, temperature or light. Polymers whose alteration of properties is temperature triggered can be described as thermoresponsive polymers. If a temperature increase leads to polymer precipitation from a solution, a polymer features a lower critical solution temperature (LCST). In contrast, if a polymer precipitates upon a temperature decrease, it features an upper critical solution temperature (UCST). The thermoresponsive behavior is mainly demonstrated by polymers displaying a miscibility gap in solution where two phases are coexisting in equilibrium with each other. In this case, one phase has a higher polymer concentration, while another one has a lower polymer concentration. The miscibility gap is confined within the region of the diagram restricted by the binodal curve. Between the binodal and spinodal curves, one can distinguish a metastable region. In turn, within the diagram’s region marked by the spinodal curve there is the instability region where even a slight fluctuation of density or composition leads to a phase separation (spinodal decomposition) (Figure 1).<sup>7</sup>

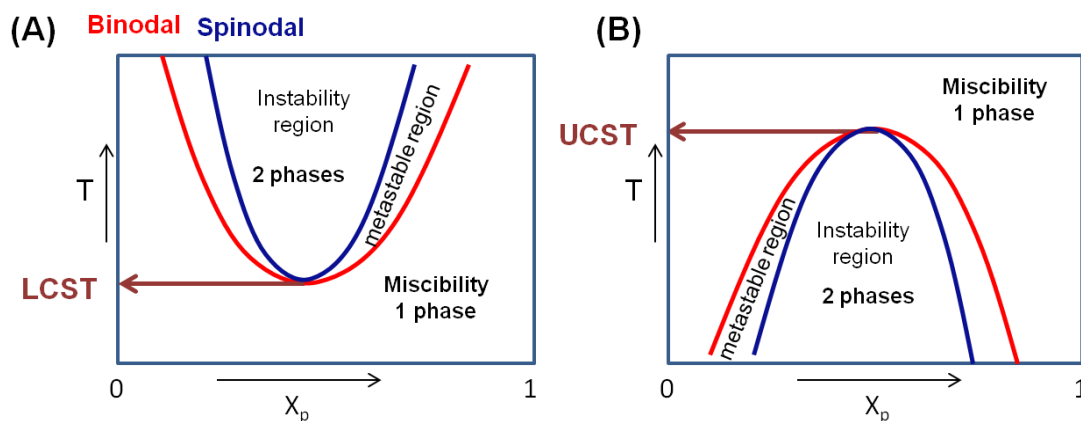


**Figure 1.** Phase diagram of polymer solutions featuring (A) a lower critical solution temperature and (B) an upper critical solution temperature.<sup>8</sup>

It is considered that the reversible phase transition occurs due to a complex interplay between hydrophobic and hydrophilic groups within a polymer chain upon heating, whereas reorganization of hydrogen bonds between the polymer and the solvent together with hydrophobic/hydrophilic interactions of a polymer chain significantly alters the phase transition temperature.<sup>9-10</sup> The phase transition temperature is practically determined by a cloud point temperature ( $T_{cp}$ ), the temperature at which a polymer experiences conformational transition from a fully hydrated and solubilized expanded coil state to a collapsed state, releasing most of the hydration molecules (Figure 2).<sup>11</sup> The “coil-to-globule transition” is considered to be a gradual process. Thus, some parts of the polymer chain may undergo a conformational transition earlier than the main collapse occurs, termed as “incipient

collapse".<sup>11-13</sup> Such a conformational transition in fact may occur for any polymer with a rational combination of hydrophobic-hydrophilic balance.

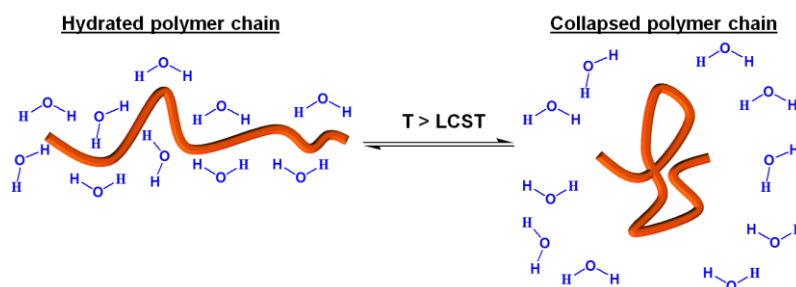


**Figure 2.** Reversible temperature-induced transition of a thermoresponsive polymer with LCST from a hydrated to a collapsed state.<sup>14</sup> Figure 2 was adapted from ref<sup>14</sup>.

The most common methods for determination of the phase transition temperature include dynamic light scattering (DLS),<sup>15-16</sup> differential scanning calorimetry (DSC),<sup>17-18</sup> proton nuclear magnetic resonance spectroscopy (<sup>1</sup>H NMR) in deuterated water,<sup>13-14</sup> infrared (IR) spectroscopy<sup>19-20</sup> and turbidimetry<sup>6, 21</sup>. The first mention of a particular smart polymer featuring a thermoresponsive behavior with a phase transition was made in 1968 by Heskins and Guillet.<sup>22</sup> Upon studies of solution properties of poly(*N*-isopropylacrylamide) (PNIPAM) in water an LCST of 32 °C was determined. Since then, many researches were published covering a large number of water-soluble polymers of different classes.

### 1.1. LCST behavior of polymers in aqueous medium

There is a large number of publications describing different classes of polymers featuring an LCST behavior.<sup>14, 23-26</sup> An overview of non-ionic thermoresponsive polymers featuring an LCST in aqueous solutions, including examples of poly(oxazoline)s, *N*-substituted poly(acrylamide)s and poly(methacrylamide)s, poly(*N*-vinyl amide)s, polymers containing PEG in the side chain, and protein-related polymers, is presented in Figure 3.<sup>1</sup>

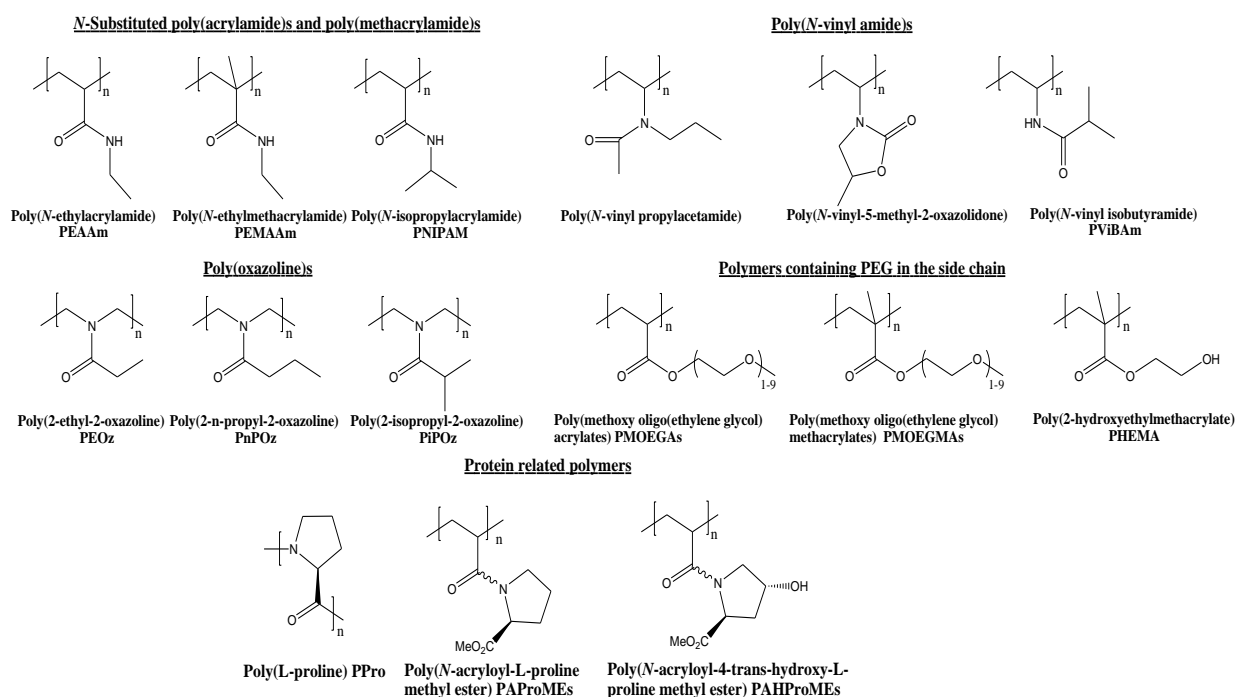


**Figure 3.** Representative examples of non-ionic thermoresponsive polymers featuring an LCST in aqueous media taken from ref<sup>1</sup>.

The phase separation and thus the “coil-to-globule transition” of thermoresponsive polymers with an LCST can be thermodynamically explained by Legendre transformation of the Gibbs equation:

$$\Delta G_{\text{mix}} = \Delta H_{\text{mix}} - T\Delta S_{\text{mix}}$$

where  $\Delta G_{\text{mix}}$  is the Gibbs free energy of mixing,  $\Delta S_{\text{mix}}$  and  $\Delta H_{\text{mix}}$  are the entropy and enthalpy of mixing at temperature  $T$ , respectively.

Below the LCST, the enthalpy of mixing is negative due to hydrogen bonding between polymer chains and solvent’s molecules ( $\Delta H_{\text{mix}} < 0$ ). The entropy of mixing in this case is also negative ( $\Delta S_{\text{mix}} < 0$ ) due to an increased ordering (Figure 4A).<sup>11</sup> Since a necessary thermodynamic condition for miscibility of a binary mixture requires  $\Delta G_{\text{mix}} < 0$ , one can assume that the enthalpy term is responsible for mixing at a given temperature.<sup>11, 27</sup> Further, approaching the LCST, the temperature increase causes disruption of hydrogen bonds, thus decreasing solubilization of polymer chains which leads to their ordering ( $\Delta S_{\text{mix}} < 0$ ). The breakage of hydrogen bonds leads to an increase of  $\Delta H_{\text{mix}}$ . At the same time,  $T\Delta S_{\text{mix}}$  further decreases. Finally, upon exceeding the LCST, the entropy term prevails over the enthalpy term and the free energy of mixing becomes positive, which leads to phase segregation (Figure 4B).<sup>11</sup>

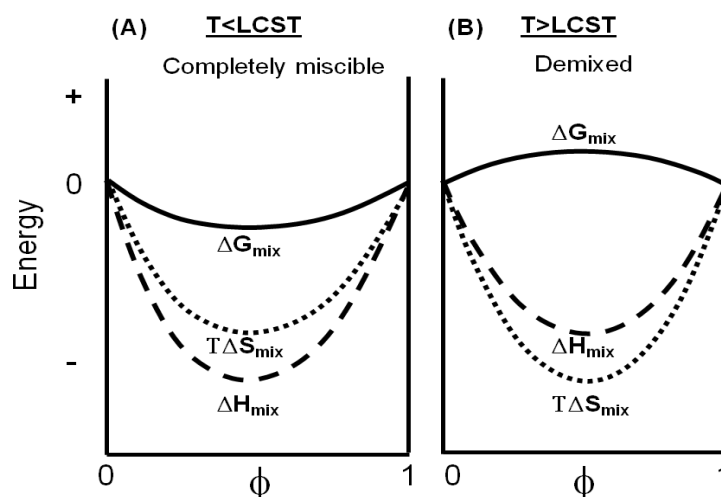


**Figure 4.** Change of thermodynamic properties for a binary polymer/solvent mixture below (A) and above (B) LCST of the polymer.<sup>11, 27</sup>

Thermoresponsive polymers featuring LCST behavior find application in different areas of bioscience such as drug delivery,<sup>28</sup> gene delivery,<sup>29</sup> regenerative medicine,<sup>30</sup> and tissue engineering.<sup>30</sup> Drug delivery process is often complicated due to inability to achieve the desired drug-release rate. Moreover, the concentration of the drug in the target area is often either too high or too low. Using smart polymers as drug carriers can solve many problems associated with the issue. Such carriers are able to release a desired concentration of the drug at the target area responding to small temperature changes which significantly increases the control over the process.<sup>24</sup>

Delivery of a therapeutic gene (DNA) into the cell, also known as transfection, can be enhanced using complexes consisting of thermoresponsive polymers and DNA. Since the DNA molecule is hydrophilic and the cell membrane is hydrophobic, thermoresponsive polymers can serve as an efficient gene-delivery vehicle due to its ability of rapid transition from a hydrophilic expanded coil state to a hydrophobic collapsed state.<sup>24</sup>

Smart thermoresponsive polymers can also be used for formation of a scaffold in tissue engineering. For this purpose, solutions comprising thermoresponsive polymer and cells are prepared below the polymer's LCST (below body temperature) and then injected to the body. The temperature increase up to the body temperature leads to conformational changes and formation of polymer gel with cells encapsulated inside. These 3D gels provide the cells with the necessary mechanical support, and also do not interfere with their nutrition.<sup>24</sup>

In addition to the representative examples described above, thermoresponsive polymers can also be used in smart clothing fabrication,<sup>31</sup> bioseparation,<sup>32</sup> smart surfaces,<sup>33</sup> catalysis,<sup>34</sup> green chemistry,<sup>35</sup> anticancer therapy,<sup>36</sup> cancer cell imaging,<sup>37</sup> protein adsorption, cell adhesion,<sup>38</sup> wound dressing,<sup>39</sup> and many others due to an opportunity to adjust polymers' conformation by simply increasing temperature of the system.

## 1.2. Factors affecting the LCST of diverse polymers

A number of factors can influence a phase transition of thermoresponsive polymers, which can be divided into several groups.

### 1.2.1. Influence of the polymer molecular weight

It is well-known that molecular weight of the polymer can significantly influence the LCST value. The reports dedicated to this issue are, however, controversial.<sup>40</sup> In some cases, they point to an inverse molecular-weight dependence<sup>41-44</sup> on the LCST value, whereas others report on a direct dependence or a lack of dependence. For instance, refs<sup>41-43</sup> suggest that the LCST decreases with increasing molecular weight in case of poly(*N,N*-diethylacrylamide), PNIPAM, and poly(*N*-ethylacrylamide), respectively. In turn, it was found in refs<sup>45-47</sup> that the LCST increases with increasing molecular weight of PNIPAM. Finally, no significant molecular weight effect on the LCST was observed in the case of PNIPAM and poly(*N*-isopropylmethacrylamide) in ref<sup>48</sup>. In view of the above, additional factors including polymers' end groups, concentration, and environment must be considered to explain the altering of the LCST value.

### 1.2.2. Influence of the polymer end groups

Hydrophilicity/hydrophobicity of the polymers' end groups is an important factor affecting the LCST.<sup>49-50</sup> In general, under the same experimental conditions polymers with hydrophobic end groups usually exhibit relatively low LCSTs, while polymers with hydrophilic end groups tend to elevate LCSTs. The cloud point temperature ( $T_{cp}$ ) of PNIPAM with more hydrophilic propionamide end group increases up to 45.3 °C compared to more hydrophobic ethoxypropionate and phenylpropionamide end groups, having  $T_{cp}$  of 40.6 and 37.4 °C, respectively.<sup>51</sup> The same trend was observed upon replacing a hydrophilic amino end group with a long hydrophobic 12-carbon end group.<sup>52</sup> Hydrophilic end groups are able to form hydrogen bonds with water molecules, thus improving solubility of the polymer in water, thus increasing its LCST. In turn, hydrophobic end groups have a tendency to form complex architectures in aqueous media such as polymeric micelles<sup>53</sup> polymer loops<sup>40</sup> and interchain associates<sup>54</sup>. An influence of the end group on an LCST is more pronounced in low molecular weight polymers solutions, since the end group concentration in this case is higher, than in high molecular weight systems.<sup>40</sup> Thus, it can be noted that polymers carrying hydrophilic end groups are characterized by higher cloud-point temperatures in comparison with similar polymers possessing hydrophobic end groups (Figure 5).

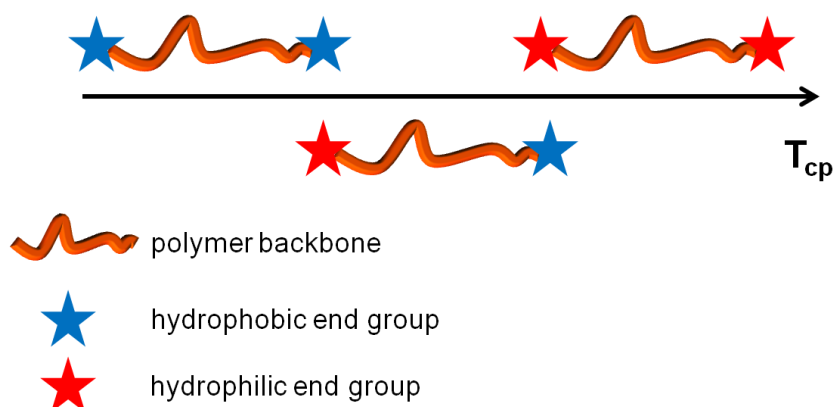


**Figure 5.** Influence of the polymers' end group on the  $T_{cp}$ . Higher levels of the overall polymers hydrophilicity leads to higher expected  $T_{cp}$  values.

### 1.2.3. Influence of the polymer concentration

According to the phase diagram, polymer concentration is one of the most important parameters affecting  $T_{cp}$ . For systems possessing an LCST, an inverse dependence of  $T_{cp}$  from the concentration of the polymer was observed within a certain concentration range.<sup>55-57</sup> As a representative example,  $T_{cp}$  of poly(2-hydroxypropyl acrylate) increases from 18.3 °C at 1.5 wt % to 33.3 °C at 0.25 wt %.<sup>58</sup> Moreover,  $T_{cp}$  increases with decreasing concentration of poly(2-isopropyl-2-oxazolines) of different molecular weights, namely,  $T_{cp}$  increases from 37.3 to 39.8 °C ( $M_n$  9700), from 38.7 to 42 °C ( $M_n$  7800) and from 43.7 to 50 °C ( $M_n$  4300) as the concentration decreases from 1.0 to 0.1 wt %.<sup>59</sup> Thus, one must always consider polymers' concentration for determination of  $T_{cp}$  values.

### 1.2.4. Influence of added salts

It is known that addition of different salts to a polymer solution can influence its LCST. Thus, salting-in and salting-out effects are applicable for solutions of thermoresponsive polymers. The salting-in effect is solubility enhancement caused by increase of ionic strength of a solution upon addition of salts, while salting-out, also known as salt-induced precipitation, refers to solubility decrease upon salts addition. Several experiments found that the effect of salt ions on the phase transition temperature follows the Hofmeister series (Figure 6).<sup>60-62</sup>



**kosmotropes**       $\text{N}(\text{CH}_3)_4^+$     $\text{NH}_4^+$     $\text{Cs}^+$     $\text{Rb}^+$     $\text{K}^+$     $\text{Na}^+$     $\text{Li}^+$     $\text{Mg}^{2+}$     $\text{Ca}^{2+}$       **chaotropes**

**Figure 6.** Hofmeister series for anions and cations.<sup>63</sup> Chloride and sodium are considered as reference ions.<sup>60-62</sup>

The anions and cations from the left side are strongly hydrated and known as kosmotropes, whereas anions and cations from the right side are weakly hydrated and known as chaotropes. An influence of sodium salts of  $\text{CO}_3^{2-}$ ,  $\text{SO}_4^{2-}$ ,  $\text{H}_2\text{PO}_4^-$ ,  $\text{F}^-$ ,  $\text{Cl}^-$ ,  $\text{Br}^-$ ,  $\text{NO}_3^-$ ,  $\text{I}^-$ ,  $\text{ClO}_4^-$  and  $\text{SCN}^-$  on the LCST of PNIPAM was studied, and three possible interaction effects within the system were proposed (Figure 7).<sup>61</sup> Firstly, it was found that chaotropic sodium salts lead to a decrease in LCST by increasing the surface tension between the hydrophobic parts of PNIPAM and the adjacent water (Figure 7A). Secondly, association of the chaotropic anions

(from  $\text{Cl}^-$  to  $\text{SCN}^-$ )  $\text{X}^-$  with the amide group of the polymer leads to a moderate salting-in effect (Figure 7B), whereas no salting-in effect was observed when using kosmotropic anions ( $\text{CO}_3^{2-}$ ,  $\text{SO}_4^{2-}$ ,  $\text{H}_2\text{PO}_4^-$ , and  $\text{F}^-$ ). Thirdly, destabilization of the hydrogen bonding between hydrophilic parts of the polymer and water induced by polarization of adjacent water molecules by anion  $\text{X}^-$  (Figure 7C) can happen.

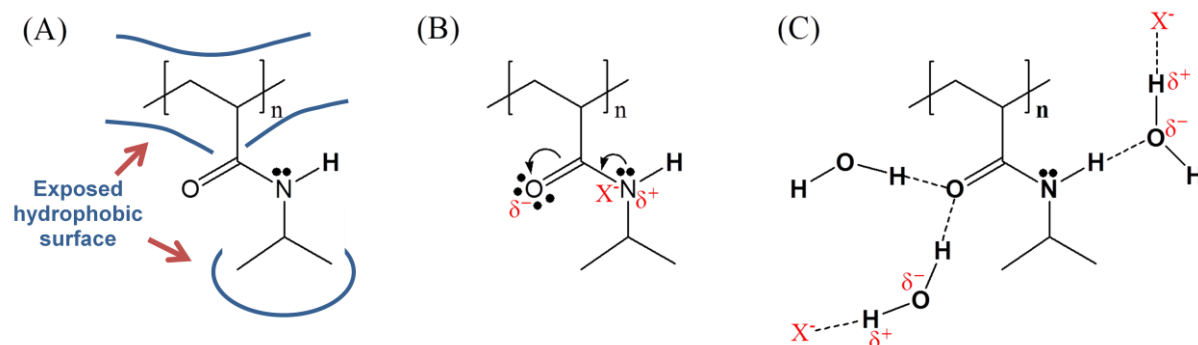


**Figure 7.** Possible mechanisms of interactions between PNIPAM, hydration water, and anions. Figure 7 is adapted from ref <sup>61</sup>.

Additionally, an increase of the salt concentration led to a decrease of the LCST of PNIPAM in the following sequence:



Moreover, a two-step phase transition was observed for PNIPAMs of different molecular weight ( $M_n$  of 360 000, 121 000, and 30 700 g/mol) in 0.3 M  $\text{Na}_2\text{SO}_4$  solutions. The dehydration of the amide group was ascribed to the first step, while liberation of the hydrophobically hydrating water molecules was taking place during the second step. Furthermore, the heating rate, presence and intensity of stirring, the method selected for the measurement and path length of the employed cuvette may influence the final values. Thus, the exact experimental conditions are crucial for evaluation of transition temperature and comparison of the obtained results. All the foregoing discussion brings us to understanding that “hydrophobic collapse” or “hydrophobic self association” play a very important role in the mechanism of thermotransition. Phase separation resulting from hydrophobic collapse is also often found in nature. For example in case of amyloids – the peptides or proteins tending to self-assembly in aqueous solutions, hydrophobic interactions play an equally significant role as in case of thermoresponsive polymers.

## 2. Amyloidogenic peptides and disease-causing proteins

A significant number of amyloidoses such as Alzheimer’s, Parkinson’s, or Prion diseases leads to malfunction and permanent damage of essential functions of human body. It is widely discussed that misfolding and aggregation of particular amyloidogenic peptides and proteins or simply “amyloids” leads to progression of dementia. Notably, more than 40 diverse native peptides and proteins with different amino acid sequences and thus a different structure undergo thermodynamically favorable conformational transition with formation of similar long, unbranched, water insoluble,  $\beta$ -sheet rich fibrils<sup>64-65</sup>. Contemporaneously, owing to their enhanced mechanical properties and compact package, amyloids often implement a storage function for peptides and proteins and known as “functional amyloids”.<sup>66</sup> They in turn do not cause and do not participate in any disease and are found in many organisms including mammalian skin<sup>67</sup>, *Escherichia coli*<sup>68</sup>, silkworms<sup>69</sup>, and fungi<sup>70</sup>. Examples of amyloidogenic peptides and proteins associated with human diseases along with the affected tissues are given

in Table 1. Thus, besides of A $\beta$  peptides, widely discussed in subsequent chapters of this dissertation, a broad number of other amyloids is given.

**Table 1.** Aggregating peptides and proteins leading to diverse amyloidoses and location of affected tissues.<sup>71-78</sup>

<b>Disease</b>	<b>Aggregating peptide/protein</b>	<b>Affected Tissues</b>
<b>Alzheimer's disease (AD)</b>	A $\beta$ peptides	Brain (hippocampus, cerebral cortex)
<b>Parkinson's disease (PD)</b>	$\alpha$ -Synuclein	Brain (substantia nigra, brain stem)
<b>Dementia with Lewy bodies</b>		Brain (frontal, temporal lobes)
<b>Prion disease</b>	Pr protein	Brain (gray matter), peripheral nervous system
<b>Huntington's disease (HD)</b>	Huntingtin	Brain (striatum)
<b>Spinocerebral ataxia</b>	Ataxin	Brain (cerebellum, spinocerebellar)
<b>Frontotemporal dementia</b>	Tau	Brain (frontal, temporal lobes)
<b>Corticobasal degeneration (CBD)</b>		Brain (cerebral cortex, basal ganglia)
<b>Multiple tauopathies</b>		Brain (cerebellum)
<b>Amyloid lateral sclerosis</b>	Superoxide dismutase 1	Brain (motor cortex, brain stem, spinal cord)
<b>Transmissible spongiform encephalopathy</b>	Pr protein	Brain, nervous system
<b>Spinal and bulbar muscular atrophy</b>	Androgen receptor with PolyQ expansion	Brain (brain stem, spinal cord)
<b>Familial British dementia</b>	ABri peptide	Brain
<b>Familial Danish dementia</b>	ADan peptide	Brain
<b>Dentatorubral-pallidoluysianatrophy</b>	Atrophin 1	Brain
<b>Finnish hereditary amyloidosis</b>	Fragments of gelsolin	Peripheral nervous system, cornea
<b>Familial amyloidotic polyneuropathy (FAP)</b>	Transthyretin (mutant forms)	Peripheral nervous system
<b>Spinocerebellar ataxia</b>	Ataxin with PolyQ expansion	Cerebellum

---

<b>Type II diabetes</b>	IAPP or “amylin”	Pancreas
<b>Cataract</b>	$\gamma$ -Crystallin	Eyes
<b>Amyotrophic lateral sclerosis</b>	TDP-43, SOD1, FUS	Motor neurons
<b>Multiple System Atrophy</b>	Tau, ubiquitin, crystallin	Multiple organs
<b>Light chain amyloidosis</b>	Immunoglobulin light chain (AL)	Multiple organs
<b>Transthyretin amyloidosis</b>		Peripheral nervous system, heart, kidney, eyes
<b>Cardiac transthyretin amyloidosis</b>	Transthyretin	Heart
<b>Senile systemic amyloidosis</b>		Heart, peripheral nervous system, eye, leptomen
<b>Apo AI amyloidosis</b>	N-terminal fragment of apolipoprotein	Heart, liver, kidney, PNS, testis, larynx (C-terminal variants), skin (C-terminal variants)
<b>Dialysis related amyloidosis</b>	$\beta_2$ -microglobulin	Autonomic nervous system and musculoskeletal system
<b>AA amyloidosis Familial Mediterranean fever</b>	Fragments of serum amyloid A protein	All organs except central nervous system
<b>Heavy chain amyloidosis</b>	Immunoglobulin heavy chain	All organs except central nervous system
<b>Medullary carcinoma of the thyroid</b>	Calcitonin	C-cell thyroid tumors
<b>Hypotrichosis simplex of the scalp</b>	Corneodesmin	Hair follicles, cornified epithelia
<b>Lysozyme amyloidosis</b>	Lysozyme	Kidney, liver, spleen
<b>Renal leukocyte chemotactic factor 2 amyloidosis</b>	Leukocyte chemotactic factor-2	Kidney
<b>Fibrinogen amyloidosis</b>	Fibrinogen $\alpha$ -chain	Kidney
<b>Localized cutaneous amyloidosis</b>	Galectin 7	Skin
<b>Cystatin amyloidosis</b>	Cystatin C	Skin, peripheral nervous system
<b>Pulmonary alveolar proteinosis</b>	Surfactin Protein C	Lung
<b>Pituitary prolactinoma</b>	Prolactin	Pituitary gland

---

<b>Injection-localized amyloidosis</b>	Insulin	Iatrogenic
<b>Senile seminal vesicle amyloid</b>	Semenogelin 1	Vesicula seminalis
<b>Corneal amyloidosis associated with trichiasis</b>	Lactoferrin	Cornea
<b>Lattice corneal dystrophies</b>	Transforming growth factor $\beta$ -induced protein	Cornea
<b>Aortic medial amyloidosis</b>	Medin	Senile aorta, media

Formation of fibrils can be described by a sigmoidal curve divided into three main phases, namely, the lag phase (I), the growth phases (II), and the saturation phase (III) (Figure 8).<sup>64, 79</sup> The lag phase (I) must not only be considered as a simple “waiting time” for fibril formation. In fact, millions of monomeric molecules associate forming primary nuclei within the lag phase.<sup>80</sup> The size and length of the associates may vary, but their concentration in most cases is too low to be detected. The subsequent thermodynamically favorable growth phase (II) characterized by the fastest conversion rate of monomers and oligomers into fibrils within the all three phases of the self-assembly process. The species formed at this phase have a rather short lifetime, which makes it difficult to isolate them for a subsequent analysis. The final saturation phase (III) is a steady state where the concentration of monomers is constantly low and the concentration of fibrils is constantly high. It is assumed that the main species throughout the lag phase (I) are monomers, throughout the saturation phase (III) are mature fibrils and throughout the growth phase (II) the concentration of the monomers and the mature fibrils is about the same. Thus, the monomers and fibrils are the most abundant species within the self-assembly process. The concentration of all other species such as oligomers, protofilaments or short fibrils remains low and challenging to determine.

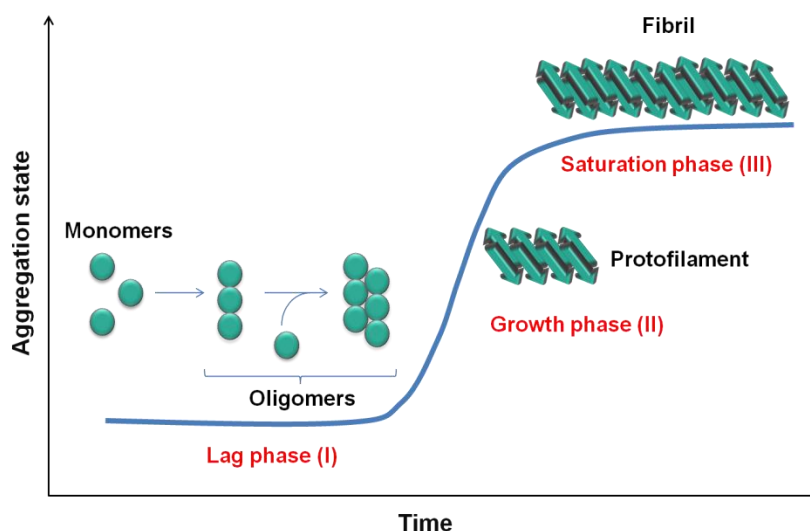


**Figure 8.** Simplified fibrillation pathway for amyloidogenic peptides and proteins.<sup>64, 79</sup>

There is a number of molecular events occurring within those three stages are commonly termed as primary nucleation (Figure 9A), characterized by association of native soluble peptide/protein with formation of nuclei, elongation (Figure 9B), described by attachment of monomers to ends of growing fibrils, monomer-dependent secondary nucleation (Figure 9C), where the body of the growing fibril serves as a catalytic surface for the fibril formation, and

finally fragmentation (Figure 9D) or simple breakage of fibrils with formation of new elongation sites.<sup>80</sup> Importantly, that all three molecular events can proceed within any phase of fibril formation, however, with different reaction rates and activities of the participating components (e.g. monomer, oligomers, fibrils of different sizes).

Primary nucleation is the only molecular event contributing to fibrillation at a very early stage of the fibrillation process when a pure monomer solution is examined and no intermediate species are present. The duration of the primary nucleation dominance is in fact very short and covers only  $10^{-7}$  % of the whole lag phase. After this time all other molecular events can proceed. As estimated by Arosio and coworkers<sup>80</sup> based on large data set from their previous works,<sup>81-82</sup> about 600 million primary nuclei are being generated until the completion of the lag phase.

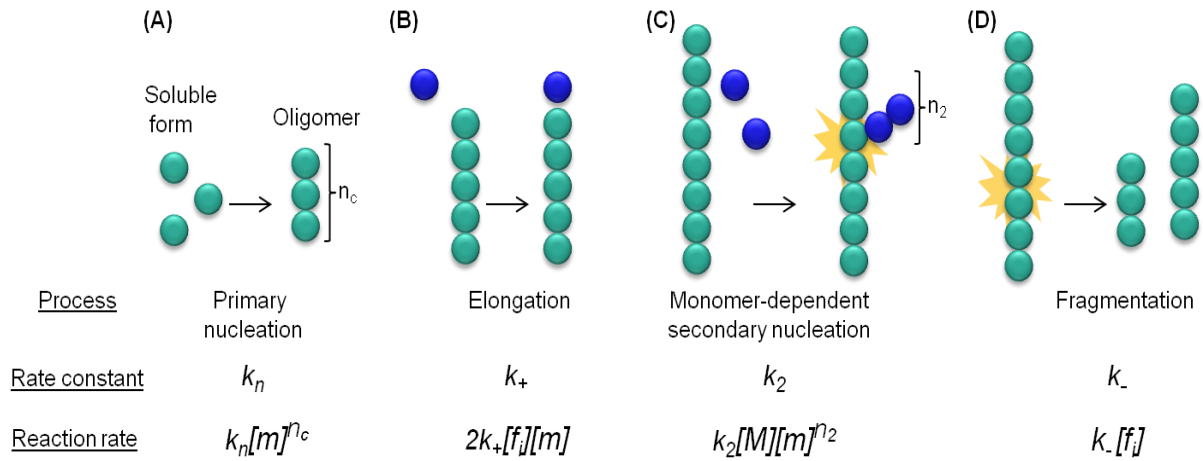


**Figure 9.** Molecular events occurring within the fibrillation process characterized by different reaction constants and reaction rates: (A) primary nucleation, (B) elongation, (C) monomer-dependent secondary nucleation and (D) fragmentation. Respective rate constants are given. The reaction rates are defined as expressions, where  $[m]$ ,  $[M]$  and  $[f_i]$  are the concentrations of the monomer, the total fibril mass and the fibril number, respectively. The primary and secondary nucleus sizes are given by  $n_c$  and  $n_2$ , respectively, and being  $n_c=n_2=2$ .<sup>80-81</sup> Figure 9 was reproduced from ref<sup>80</sup>.

Usually, the rate of elongation reaction is much higher than the rate of primary nucleation, which means that the primary nuclei very quickly turn into fibrils. Immediately afterwards, the secondary nucleation starts to contribute to the fibrillation process.

As determined previously<sup>81-82</sup> the rate constant of secondary nucleation exceeds the rate constant of primary nucleation ( $k_2 = 10^4 \text{ M}^{-2} \text{ s}^{-1}$  and  $k_n = 3 * 10^{-4} \text{ M}^{-1} \text{ s}^{-1}$ , respectively), thus after a particular threshold concentration  $[M^*]$  the number of nuclei formed by the secondary nucleation event will exceed the number of nuclei formed during the primary nucleation. The threshold concentration  $[M^*]$  can be estimated as proposed by Arosio<sup>80</sup>:

$$\text{Secondary nucleation} = \text{Primary nucleation}$$

$$k_2[M^*][m]^{n_2} = k_n[m]^{n_c}$$

$$[M^*] = \frac{k_n}{k_2} = \frac{3 * 10^{-4} \text{ M}^{-1} \text{ s}^{-1}}{10^4 \text{ M}^{-2} \text{ s}^{-1}} = 3 * 10^{-8} \text{ M}$$

Since the main species participating in secondary nucleation are monomers and fibrils (Figure 9C), the maximum rate of secondary nucleation is achieved during the growth phase when the concentration of these species is approximately the same. Thus, one must not associate the nucleation process solely with the lag phase, as a significant portion of the secondary nucleation also occurs within the growth phase. Thereby, the fibrillation process should not be considered as a simple simultaneous transformation of all monomers into fibrils of equal

length and size, but rather as a complex process in which various molecular events proceed in parallel at all conventional phases of fibrillation. Noteworthy to say, that the reaction constants of any molecular event described above, strictly depend on experimental conditions and should not be taken as universal units. It is known that primary nucleation and elongation occur faster with increasing temperature, while the rate of secondary nucleation is little higher at lower temperature.<sup>83-84</sup> The fibrillation rate also increases with increasing ionic strength of the solution due to reduced electrostatic repulsion between different reaction species.<sup>84-85</sup> The course of aggregation also depends on the environment and a presence of various molecules to the reaction volume. Various factors affecting aggregation pathway of amyloids will be discussed in detail in the chapters below.

## 2.1. Methods to monitor aggregation pathway

There are number of methods allowing to control fibril formation either directly during the aggregation process “*in situ*” or “*ex situ*” where a specific volume of peptide/protein solution is taken at regular intervals throughout the aggregation process.<sup>80</sup> Methods for monitoring aggregation “*in situ*” embrace various spectroscopic and light techniques including circular dichroism,<sup>86</sup> fluorescence,<sup>87</sup> NMR<sup>88</sup> and IR spectroscopy<sup>89</sup> as well as small angle X-ray<sup>90</sup> scattering or dynamic and static light scattering<sup>91-92</sup>. Specificity of “*ex situ*” analysis suggests that aliquots taken from the reaction are investigated separately from the reaction volume; accordingly, the methods used to study them, do not affect the development of fibrillation of the total amount of the studied amyloid. Thus, a wide range of methods can be used including different chromatographic and spectroscopic techniques, centrifugation, filtration or electrophoresis.<sup>80</sup> Table 2 summarizes the methods most widely used to study the process of amyloid aggregation.

**Table 2.** Methods allowing to monitor conversion of the monomeric amyloids and their key characteristics.<sup>80</sup>

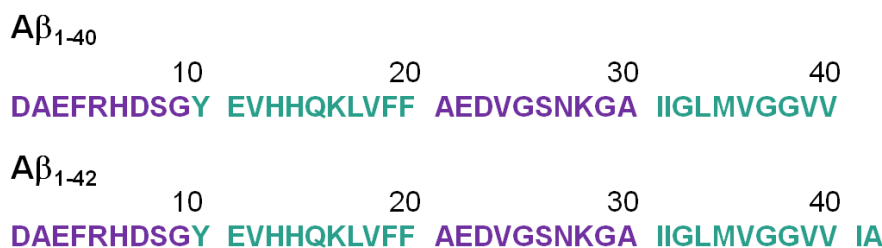
Method	Summary
Fluorescence spectroscopy	Method based on characteristic spectral changes during fibril formation. A fluorescent dye thioflavin T, widely used in the method, undergoes a sharp quantum yield increase by accession to the growing fibril. The mechanistic details of such an accession are still unclear, so the extraction of quantitative data is still complicated. In order to obtain a linear dependence of the obtained fluorescence signal from the aggregates concentration, the ThT to peptide/protein ratio must be optimized.
Circular dichroism spectroscopy (CD)	Determination of the peptide/protein conformation based on characteristic spectra. For instance, typical $\alpha$ -helical peptides/proteins possess two minima at 222 nm and 208 nm and a maximum at 193 nm. The $\beta$ -sheets-rich peptides/proteins possess a minimum at around 218 nm and a maximum at 195 nm, while intrinsically disordered samples have a minimum near 200 nm. <sup>93-94</sup> The conversion is evaluated by comparing the difference in the received signals starting from the unstructured monomer (or from any other initial conformation) to the $\beta$ -sheet-rich fibrils. Simultaneous quantification of monomer and fibril concentration is possible.
Fourier transform infrared (FTIR) spectroscopy	The conversion of peptide/protein can be estimated by the increase in intensity in the region characteristic for the $\beta$ -sheets-rich structure (1615–1643 $\text{cm}^{-1}$ ). A high peptide/protein

	concentration is needed.
NMR spectroscopy	The conversion can be estimated from the change in intensity of spectral signals, based on the fact that monomeric amyloids possess unique $^1\text{H}$ , $^{13}\text{C}$ or $^{15}\text{N}$ values. A relatively high peptide/protein concentration is needed.
Scattering methods	The usage of the small angle X-ray scattering or dynamic and static light scattering for the amyloid aggregation study is based on the fact that a particle size is largely responsible for the scattering intensity. Based on this, the scattering intensity of large aggregates exceeds the scattering intensity of small ones. Thus, the increase in scattering intensity gives information about fibril formation in real time. Information on the shape of the object can be obtained from the dependence of the scattering intensity on the scattering angle, however it still remains a challenging task for heterogeneous mixtures.
<i>Ex situ</i> methods	Aliquots taken from the reaction can be investigated separately from the reaction volume; accordingly, the methods used to study them do not affect the development of fibrillation of the total amount of amyloidogenic peptide/protein studied. Therefore, a broad range of methods can be used including various chromatographic and spectroscopic techniques, centrifugation, filtration, or electrophoresis.

## 2.2. Factors affecting aggregation pathway of $\text{A}\beta_{1-40/42}$ peptides

The  $\text{A}\beta_{1-40/42}$  peptides are not merely the main protein components of the senile plaques found in the brain of Alzheimer's patients, but also believed to cause the disease. Compared to the  $\text{A}\beta_{1-40}$  the  $\text{A}\beta_{1-42}$  has two additional amino acids in the C-terminus (Figure 10) and more prone to aggregation, which complicates its use in model systems. Thus, in this work, our interest was specifically attracted by amyloidogenic peptide  $\text{A}\beta_{1-40}$  due to its relative stability under physiological conditions. Nevertheless, both peptides will be discussed in subsequent chapters due to general similarity in their aggregation mechanisms.

In the last 30 years significant efforts have been made to study the influence of various factors on the course of their aggregation both *in vivo* and *in vitro*. Thus, one can easily find reports dedicated to an impact of small molecules,<sup>95-96</sup> nanoparticles,<sup>97-98</sup> membranes,<sup>99-100</sup> dendrimers,<sup>101-102</sup> polymers,<sup>103-104</sup> micelles,<sup>105-106</sup> molecular chaperon<sup>107-108</sup>, peptides and proteins<sup>109-110</sup> on the aggregation pathway and final morphology of the aggregates *in vitro*. Here, an influence of all above mentioned systems on the aggregation of the amyloidogenic peptide  $\text{A}\beta_{1-40/42}$  will be discussed in detail.

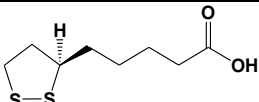
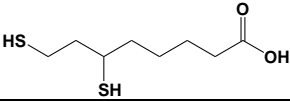
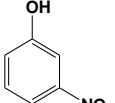
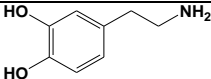


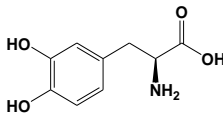
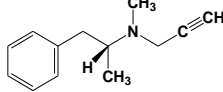
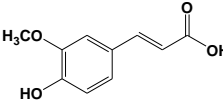
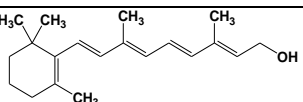
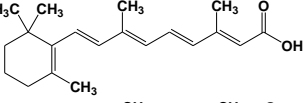
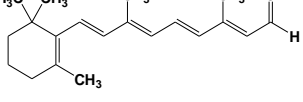
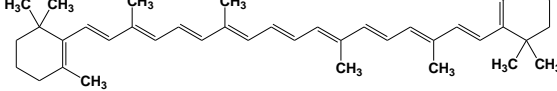
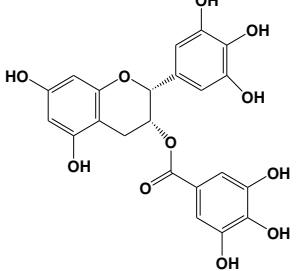
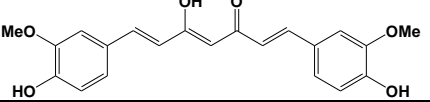
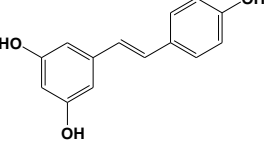
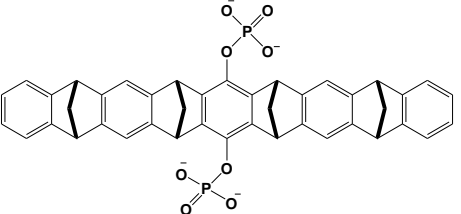
**Figure 10.** Amino acid sequence of amyloid  $\beta$  peptides  $\text{A}\beta_{1-40}$  and  $\text{A}\beta_{1-42}$ , where more hydrophilic regions are shown in violet and more hydrophobic regions in turquoise.<sup>111-112</sup>

### 2.2.1. Influence of small molecules on aggregation of A $\beta$ <sub>1-40/42</sub> peptides

Small molecules are considered to be promising modulators of the development of amyloid aggregation leading to neurodegenerative disease. Currently, a large number of small molecules are widely used as therapeutic drugs for treatment of mild to moderate cognitive symptoms of Alzheimer's disease.<sup>113</sup> Such molecules as donepezil (trade name Aricept<sup>®</sup>), rivastigmine (trade name Exelon<sup>®</sup>), galantamine (trade name Razadyne<sup>®</sup>, formerly Reminyl<sup>®</sup>) or tacrine (trade name Cognex<sup>®</sup>) positively contribute to the disease related cognitive deficiency *in vivo*.<sup>114</sup> The desire to achieve a persistent clinical effect in treatment of Alzheimer's disease prompted scientists to test various types of small molecules also as a modulator of A $\beta$ <sub>1-40/42</sub> aggregation *in vitro*. For instance, resveratrol (RES) and curcumin are able to bind to N-terminus (between amino acids R5-F20) of the A $\beta$ <sub>1-42</sub> thereby inhibiting formation of high molecular weight aggregates as determined by solution NMR spectroscopy and atomic force microscopy (AFM).<sup>115</sup> Moreover, RES can bind both to monomeric and fibril A $\beta$ <sub>1-40/42</sub>, however the binding response of RES to fibril A $\beta$ <sub>1-40</sub> was lower than to monomeric A $\beta$ <sub>1-40</sub>, whereas the binding response of RES to fibril A $\beta$ <sub>1-42</sub> was stronger than to monomeric A $\beta$ <sub>1-42</sub> as determined by NMR spectroscopy in solution.<sup>116</sup> RES is also able to remodel A $\beta$ <sub>1-42</sub> fibrils into unstructured aggregates as observed by AFM.<sup>96</sup> The flavanol epigallocatechin gallate (EGCG) is one of the components found in green tea, showing a promising inhibitory effect towards A $\beta$ <sub>1-40/42</sub> aggregation. The molecule can directly bind to both preformed oligomeric structures and mature fibrils through hydrophobic interactions and modify their morphology as discussed in a number of works.<sup>117-120</sup> Porat *et al.*<sup>121</sup> reviewed a wide number of polyphenols and noticed some similarities between the molecules able either to interfere an aggregation process or morphology of the aggregate. Thus, all these polyphenols have at "least two phenolic rings with two to six atom linkers, and a minimum number of three OH groups on the aromatic rings". Additional examples of small molecules capable of inhibiting an A $\beta$ <sub>1-40/42</sub> aggregation are shown in Table 3.

**Table 3.** Examples of small molecules able to inhibit fibrillation of A $\beta$ <sub>1-40/42</sub>.

Chemical compound	Structure	Key findings
Tramiprosate		Suppresses the A $\beta$ <sub>1-40/42</sub> self-assembly in a dose-dependent manner. <sup>122</sup> Strong interactions of sulfonic anion with K16 and K28 of the A $\beta$ <sub>1-42</sub> . <sup>123</sup>
$\alpha$ -Lipoic acid		Dose-dependent inhibition of the A $\beta$ <sub>1-40/42</sub> aggregation and destabilization of its fibrils. <sup>124</sup>
Dihydrolipoic acid		
3-Nitrophenol		Aggregation inhibition and fibril destabilization along with reduction of A $\beta$ <sub>1-42</sub> -induced cytotoxicity. <sup>125</sup>
Dopamine		Dose-dependent fibrillation inhibition and fibril

L-DOPA		destabilization of $A\beta_{1-40/42}$ . <sup>126</sup>
Selegiline		
Ferulic acid		Inhibition of $A\beta_{1-42}$ fibrillation and destabilization of the preformed fibrils. <sup>127</sup>
Retinol		
Retinoic acid		
Retinal		Dose-dependent aggregation inhibition and fibril destabilization of $A\beta_{1-40/42}$ . <sup>128</sup>
$\beta$ -Carotene		
Epigallocatechin gallate (EGCG)		Binds to both preformed oligomeric structures and mature $A\beta_{1-40/42}$ fibrils through hydrophobic interactions and modify their morphology. <sup>117-120</sup>
Curcumin		Binds to N-terminus (between amino acids R5-F20) of $A\beta_{1-42}$ . <sup>115</sup>
Resveratrol (RES)		Binds to N-terminus (between amino acids R5-F20) of the $A\beta_{1-42}$ . <sup>115</sup> Able to bind both to monomeric and fibril $A\beta_{1-40/42}$ . <sup>116</sup>
Molecular Tweezer CLR01		Binds to residues K16, K28, and R5 of monomeric $A\beta_{1-40}$ and efficiently inhibits its self-assembly. <sup>129</sup>

### 2.2.2. Influence of nanoparticles on aggregation of $A\beta_{1-40/42}$ peptides

A concern that certain types of nanoparticles (NPs) are capable of penetrating through the blood–brain barrier (BBB)<sup>130</sup> has led to a widespread research into the effect of NPs on the course of amyloid aggregation. In recent years, many articles have been published demonstrating the opposite effects ranging from overall fibrillation inhibition by means of

NPs, to acceleration of the process. The type of NPs and exact experimental conditions including concentration, pH, temperature, ionic strength, or shaking are important to consider for a detailed discussion of the altering mechanism. A strong violation of  $A\beta_{1-40/42}$  nucleation upon the presence of amino-modified polystyrene NPs was observed.<sup>131</sup> In particular, at low NPs concentration or surface area to peptide ratio, the NPs can serve as a catalytic surface for aggregation by increasing the local concentration of the peptide on their surface (Figure 11A). On the other hand, the opposite effect is observed upon increasing the concentration or surface area of the NPs over a certain value. Thus, the number of peptide molecules adsorbed by the surface of the NPs also grows decreasing the number of peptide molecules in solution able to nucleate, thereby inhibiting fibrillation rate (Figure 11B).

**(A) Low particle surface area**



**(B) High particle surface area**

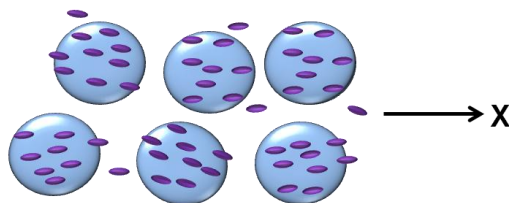


**Figure 11.** Peptide adsorption by NPs (A) at low particle surface area and (B) at high particle surface area with respect to peptide concentration.<sup>131</sup>

The mechanism of interaction of NPs with  $A\beta_{1-40/42}$  has diverse nature and includes various non-covalent interactions. For instance, an inhibition of  $A\beta_{1-40}$  fibrillation in the presence of (thioglycolic acid)-stabilized CdTe NPs was observed.<sup>132</sup> Based on scanning transmission electron microscopy (STEM), AFM and a series of 2D NMR experiments, a binding of the  $A\beta_{1-40}$  monomers and oligomers to the NPs through the van der Waals interactions related to “high electron density of atoms in the CdTe NPs” was found to take place. Moreover, oligomers showed a greater binding ability to the NPs than monomers.<sup>132</sup>

Hydrophobic interactions are also believed to be involved in the inhibitory mechanism of  $A\beta_{1-40}$  self-assembly rendered by poly(*N*-acryloyl-*L*-phenylalanyl-*L*-phenylalanine methyl ester) (polyA-FF-ME) NPs.<sup>133</sup> It is supposed that the alleged interactions occur between F19-F20 residues of  $A\beta_{1-40}$  and FF residues of the NPs. An influence of fluorinated and hydrogenated NPs on the course of  $A\beta_{1-40/42}$  fibrillation was discussed.<sup>134-135</sup> For example, complexes of polyampholyte and fluorinated dodecanoic acid (fluorinated NPs) promote formation of the  $\alpha$ -helical secondary structure of  $A\beta_{1-40}$  and prevent fibril development, while their hydrogenated counterparts (hydrogenated NPs) (Figure 12) induce formation of the  $\beta$ -sheet secondary structure and enhance fibrillation, as revealed by means of TEM, CD spectroscopy and dynamic light scattering (DLS).<sup>135</sup> It is supposed that a “highly negative zeta potential and hydrophobic fluorinated core” of the fluorinated NPs are responsible for the enhanced interactions with  $A\beta_{1-40}$  and observed inhibitory effect. Similar observations were later obtained for the  $A\beta_{1-42}$  case.<sup>134</sup> Moreover, the  $A\beta_{1-42}$ -induced cytotoxicity was reduced in the presence of fluorinated NPs and promoted in the presence of hydrogenated NPs.<sup>134</sup>

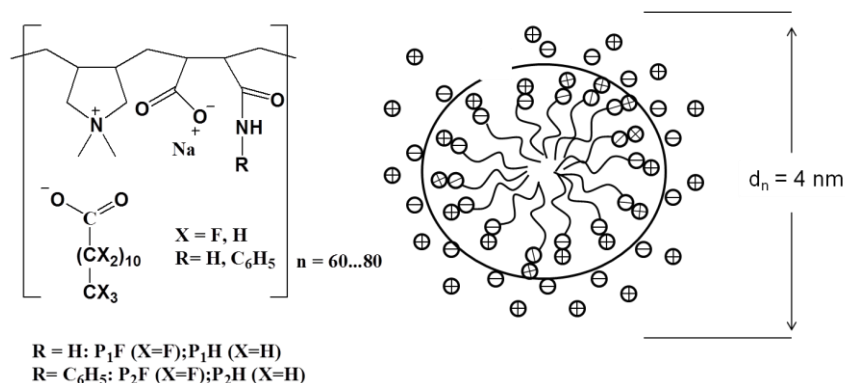


**Figure 12.** Complexation of polyampholyte and the sodium salt of perfluorododecanoic acid ( $X = F$ ) or sodium salt of the dodecanoic acid ( $X = H$ ). Figure 12 was reproduced from ref <sup>135</sup>.

Nowadays an influence of gold (Au) NPs on the fibrillation pathway is extensively investigated.<sup>136-139</sup> It was found that small L-glutathione-stabilized NPs AuNPs ( $6.0 \pm 2.0$  nm) inhibit  $A\beta_{1-40}$  fibrillation, whereas larger AuNPs ( $36.0 \pm 3.0$  nm and  $18.1 \pm 3.0$  nm) enhance formation of fibrils. At the same time, L-glutathione-stabilized nanoclusters (AuNCs) with a size of  $1.9 \pm 0.7$  nm proved to be more effective inhibitors towards  $A\beta_{1-40}$  fibrillogenesis completely suppressing fibrillation at a concentration of  $10 \mu\text{g}\cdot\text{mL}^{-1}$  and higher.<sup>139</sup> Further, gold NPs functionalized with four curcumin moieties (Au-curcumin) (Figure 13) inhibit  $A\beta_{1-40}$  self-assembly in a concentration-dependent manner and destabilize preformed fibrils.<sup>138</sup> The Au-curcumin NPs possess increased inhibitory performance towards  $A\beta_{1-40}$  fibrillation compared to a free curcumin supposedly due to its improved water solubility. It is presumed that the Au-curcumin NPs interact with  $A\beta_{1-40}$  through aromatic  $\pi$ -stacking and participate in multivalent interactions. A limiting factor in the use of the Au-curcumin NPs is their precipitation at neutral pH, so experiments should be carried out at acidic pH. Moreover, it is challenging to attach more than four curcumin moieties to the gold NPs without decreasing its aqueous solubility.

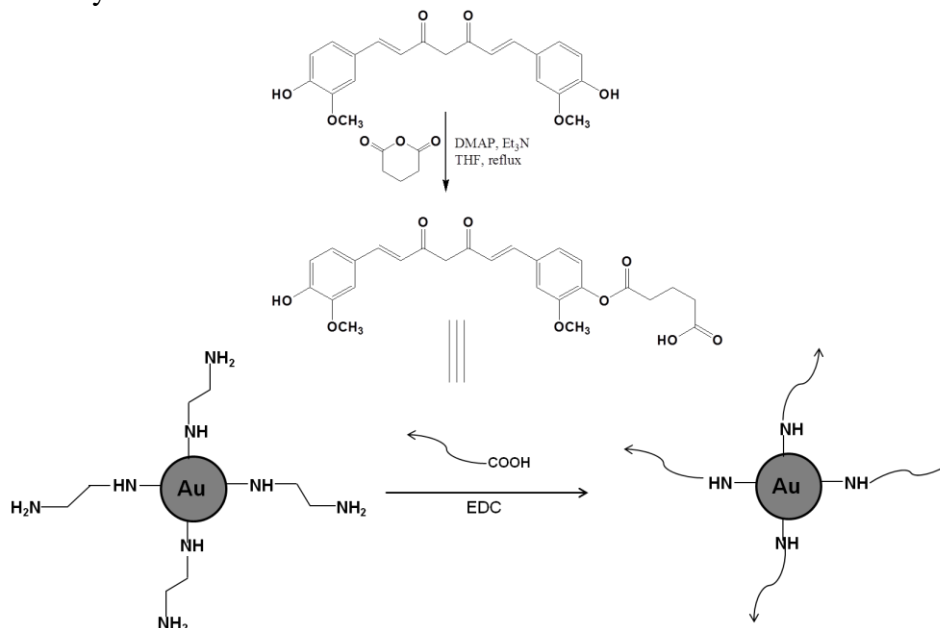


**Figure 13.** Preparation of curcumin-functionalized gold nanoparticles. DMAP is 4-dimethylaminopyridine, EDC is N<sup>7</sup>-(3-dimethylaminopropyl)-N-ethylcarbodiimide). Figure 13 was reproduced from ref <sup>138</sup>.

Gold NPs with anionic poly(acrylic acid) (PAA) or citrate surface chemistries appeared to be better inhibitors for A $\beta$ <sub>1-40</sub> fibrillation than the gold NPs with cationic surface chemistries, namely cetyltrimethylammonium bromide (CTAB) and polyelectrolytes poly(allylamine)hydrochloride (PAH).<sup>137</sup> Moreover, the PAA-coated NPs were more effective than the citrate-coated ones as observed ThT detected fluorescence measurements. The TEM data demonstrated that only the samples with cationic surface chemistries affect the morphology of the resulting aggregates. The presence of CTAB-coated NPs led to formation of short and thick aggregates, while PAH-coated NPs promoted development of thin and long fibrils. Furthermore, the PAA-coated NPs of the size 18 nm and 8 nm effectively suppress A $\beta$ <sub>1-40</sub> self-assembly at a substoichiometric ratio of 1:2,000,000, whereas their 40 nm analogues were not effective in A $\beta$ <sub>1-40</sub> inhibiting. Thus, the size, the surface chemistry, and the surface charging of NPs play an important role in the aggregation development and influence morphology of the obtained aggregates.<sup>137</sup> The NPs coated with histidine-based polymer (Figure 14) also possess inhibitory activity towards A $\beta$ <sub>1-40</sub> fibrillation, due to a proper combination of anionic and cationic surface charge in conjunction with weak hydrophobicity of methylene groups and imidazole ring was reported.<sup>140</sup> Taking into account the fact that the scope of nanomaterials is in a constant development, a library of potent inhibitors for amyloid aggregation will certainly be updated in the future.<sup>141</sup>

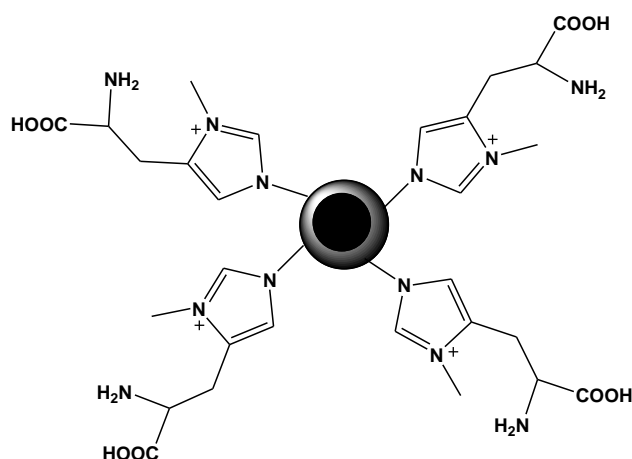


**Figure 14.** NP coated with a histidine-based polymer. Figure 14 was reproduced from ref <sup>140</sup>.

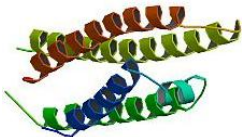
### 2.2.3. Influence of proteins and peptides on aggregation of A $\beta$ <sub>1-40/42</sub> peptides

Particular proteins also possess inhibitory properties towards A $\beta$ <sub>1-40/42</sub> self-assembly. Human serum albumin (HSA) is potentially effective moderator for A $\beta$ <sub>1-40/42</sub> fibrillation, however, the mechanism of inhibition is still widely debated. Some publications report a direct interaction of HSA with monomers, while others indicate an interplay with oligomers. A selective complexation of HSA with  $\beta$ -sheet-structured oligomers, rather than with monomers was reported in a number of researches.<sup>142-144</sup> At the same time, a fibrillation inhibition due to the interactions of HSA with monomers was found.<sup>145-146</sup> Results obtained by TEM indicated a possibility of formation of interactions of HSA with both monomeric and oligomeric A $\beta$ <sub>1-40/42</sub>, however, an oligomer should not consist of more than five monomers.<sup>109</sup> The most probable interactions involved in the inhibition process are hydrophobic interactions between respective exposed hydrophobic parts of HSA and A $\beta$ <sub>1-40/42</sub>.<sup>147</sup> Apolipoprotein E3 (apoE3) is another protein capable to suppress the amyloid aggregation through specific interaction with A $\beta$ <sub>1-40</sub> oligomers.<sup>148</sup> The nature of these interactions remains unclear. An ability to restrain fibrillation of A $\beta$ <sub>1-40</sub> is also inherent to cyclophilins.<sup>149</sup> As determined by NMR titration

experiments together with a SPOT peptide array approach,  $A\beta_{1-40}$  binds to a catalytic part of cyclophilin D through K16-E22 moieties. Blocking important sites involved in the fibrillation process leads to the preservation of the  $A\beta_{1-40}$  peptide in the monomeric form, which supposedly prevents its aggregation. The ability of small peptides to suppress fibrillogenesis was discussed in many publications in the last years.<sup>150-154</sup> A complete inhibition of  $A\beta_{1-40}$  fibril formation in the presence of the MAQTFWLSIQGKTLYWQIRIYAID (TJ10) peptide, as established by ThT assay followed by TEM was reported.<sup>150</sup> The presence of four aromatic amino acids (two W and two Y) together with the  $\beta$ -sheet conformation of TJ10 was assumed to be an important factor involved in the inhibition mechanism. The authors speculated that TJ10 hinders the oligomers and the protofilaments from further growth, thus preventing the formation of mature fibrils.

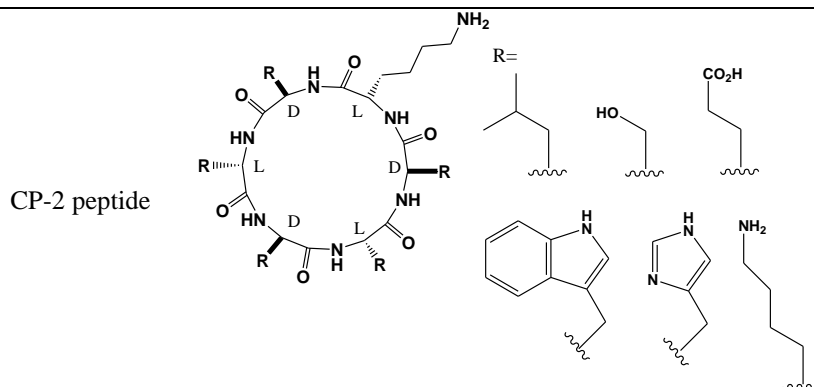
The desire to find a molecule or a class of molecules targeting specifically the amyloidogenic peptides/proteins, but having a simpler structure than antibodies, encouraged to study short peptides whose sequence would include a part of the peptide/protein molecule.<sup>150</sup> For example, an inhibition of  $A\beta_{1-40/42}$  aggregation in the presence of the short peptides RGKLVFFGR (OR1) and RGKLVFFGR-NH<sub>2</sub> (OR2) was reported.<sup>154</sup> The amino acids sequence KLVFF included in OR1 and OR2 is a part of the hydrophobic region of  $A\beta_{1-40/42}$  itself. Despite the fact that both OR1 and OR2 are able to prevent the fibril formation, only OR2 could also prevent the oligomer formation, as determined by enzyme-linked immunosorbent assay (ELISA). The toxicity of  $A\beta_{1-40/42}$  in the presence of OR2 toward human neuroblastoma cells (SH-SY5Y) has also decreased. The OR2 peptide differs from OR1 by the presence of an amide group at the C-terminus. The authors assumed that the presence of the amide group increases OR2 recognition by  $A\beta_{1-40/42}$  as a part of its molecule, thereby increasing the possibility of interactions between the peptides. A series of 20 short peptides consisting of different D-amino acid sequences corresponding to the amino acid sequences located at N-terminus of the  $A\beta_{1-40/42}$  was studied.<sup>151</sup> It was found that only D-peptides including KLVFF moiety ( $A\beta_{15-20}$  and  $A\beta_{16-22}$ ) can restrain the fibrillation process. A direct binding of these peptides to respective moiety of the  $A\beta_{1-40/42}$  peptide, as was previously established in the case of short L-peptides incorporating KLVFF segment, was suggested.<sup>155-156</sup> Thus, drugs displaying structural elements of the above mentioned peptides and proteins may serve as negative regulators of the fibril formation. Additional examples of peptides and proteins capable of inhibiting  $A\beta_{1-40/42}$  aggregation are shown in Table 4. The key findings are mentioned accordingly.

**Table 4.** Examples of peptides and proteins able to inhibit fibrillation of  $A\beta_{1-40/42}$ .<sup>157</sup>

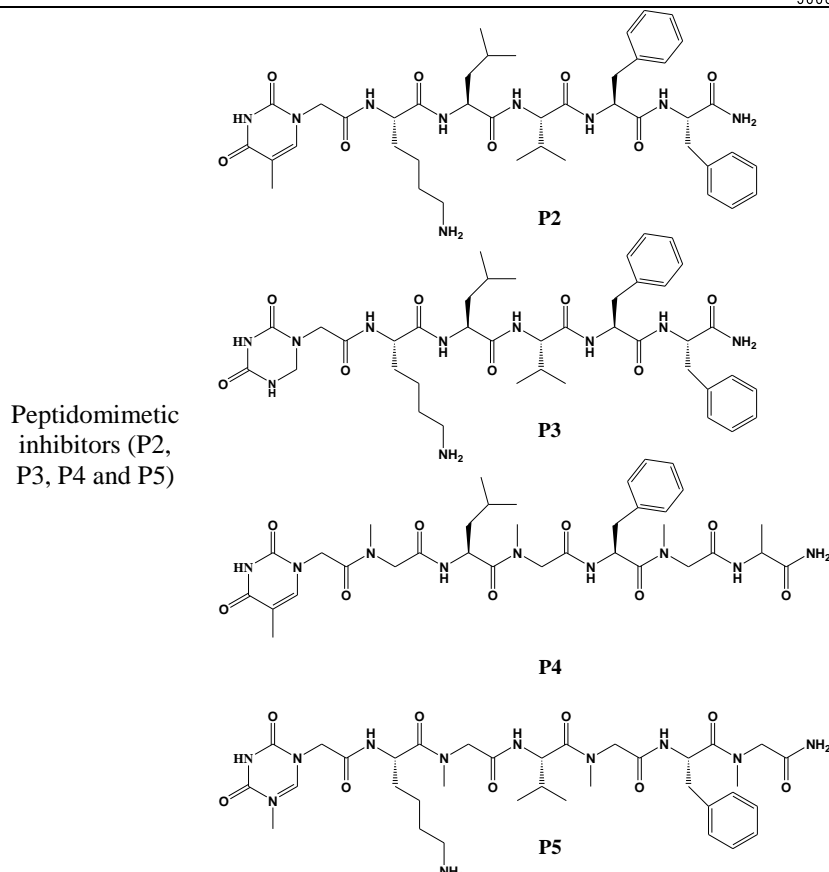
Chemical compound	Structure	Key findings
Human serum albumin*		Possibility of formation of interactions with both monomeric and oligomeric $A\beta_{1-40/42}$ . <sup>109</sup>
Apolipoprotein E3**		Inhibits the $A\beta_{1-40}$ aggregation through interaction with oligomers. <sup>148</sup>

(ribbon model of amino acids 1-191)

PP-Leu		<p>Strong inhibition of oligomerization and fibrillation through sequestration of <math>A\beta_{1-40}</math>.<sup>158</sup></p>
TJ10	MAQTFWLSIQGKTLYWQIRIY AID	<p>The presence of aromatic amino acids (two W and two Y) together with the <math>\beta</math>-sheet conformation of TJ10 was assumed to be an important factor involved in the <math>A\beta_{1-40}</math> inhibition mechanism.<sup>150</sup></p>
OR1 and OR2	RGKLVFFGR and RGKLVFFGR-NH <sub>2</sub>	<p>OR1 and OR2 prevent the fibril formation, while OR2 also prevents oligomerization. The presence of the amide group supposedly increases OR2 recognition by <math>A\beta_{1-40/42}</math> as a part of its molecule.<sup>154</sup></p>
$A\beta_{31-42}$ and $A\beta_{39-42}$	IIGLMVGGVVIA and VVIA	<p>Reduction of <math>A\beta_{1-42}</math>-induced cytotoxicity due to the formation of non-toxic hydrophobic heterooligomers.<sup>159</sup></p>
Pentapeptide amides	GVVIA-NH <sub>2</sub> and RVVIA-NH <sub>2</sub>	<p>Aggregation inhibition due to the affinity of the peptides to hydrophobic areas (FFA and VVI) of the <math>A\beta_{1-42}</math>.<sup>160</sup></p>
Decoy peptides	IAAGITGGGCOOH, TVIGTIGGGCONH <sub>2</sub> , TGIASGGGCOOH, TIVSTGGGCOOH, AGVISIGGGCOOH, TVIR <sup>+</sup> TIAAACOOH	<p>Aggregation inhibition supposedly due to their ability to complex with the <math>A\beta_{1-42}</math>.<sup>161</sup></p>
O-acyl isopeptide and [ <i>N</i> -Me- $\beta$ -Ala26] of $A\beta_{42}$		<p>Fibrillation inhibition compared to the wild type <math>A\beta_{1-42}</math> in both cases along with improved chemical stability in the [<i>N</i>-Me-<math>\beta</math>-Ala26] case.<sup>162</sup></p>
$A\beta_{25-35}$	GSNKGAIIGLM	<p>Aggregation inhibition along with reduction of <math>A\beta_{1-40}</math>-induced cytotoxicity was observed. The inhibition mechanism includes hydrophobic contacts and <math>\pi</math>-<math>\pi</math> interactions between the peptides and the <math>A\beta_{1-40}</math>.<sup>163</sup></p>
Neurokinin B	DMHDFVGLM	
Neurokinin A	HKTDSFVGLM	
Substance P	RPKPQFFGLM	
Physalaemin	pEADPNKFYGLM	
	pE – pyroglutamic acid	
Carnosine		<p>Inhibition of the <math>A\beta_{1-42}</math> aggregation due to the interactions between the <math>\beta</math>-alanine end and the imidazole ring of the carnosine with the <math>A\beta_{1-42}</math> residues K28 and D23, respectively.<sup>164</sup></p>



Significant inhibition of  $A\beta_{1-40/42}$  aggregation and disassembling of the performed aggregated structures. Reduction of the  $A\beta_{1-40/42}$ -induced cytotoxicity. Interactions of CP-2 with  $A\beta_{1-40/42}$  induces a “weak secondary structure in  $A\beta$ ”. Stabilization of the small oligomers (1-3 mers) in the presence of CP-2.<sup>165</sup>



Inhibition of the  $A\beta_{1-42}$  self-assembly process through hydrogen bonding and other non-covalent interactions with the peptidomimetics. Dissolution of the  $A\beta_{1-42}$  aggregates in the presence of the peptidomimetics was observed.<sup>166</sup>

\*Structure is taken from the public domain. \*\*Structure is taken from the RCSB Protein Data Bank.

#### 2.2.4. Influence of lipids and lipid membranes on aggregation of $A\beta_{1-40/42}$ peptides

A large number of researches have been devoted to the study of interaction mechanism between  $A\beta_{1-40/42}$  and lipid membranes. Despite the small contradictions obtained in different works, a strong interplay between  $A\beta_{1-40/42}$  and lipid membranes was established. Moreover, the latter can be permeable by  $A\beta_{1-40/42}$  during the fibrillation progression.<sup>99</sup> It is well known that the components of lipid rafts such as sphingomyelin,<sup>167</sup> gangliosides,<sup>168</sup> or cholesterol<sup>169</sup> participate in peptide-lipid interactions and were found in tissues obtained from Alzheimer's patients.<sup>170</sup> Lipid membranes can both inhibit and enhance self-assembly process, therefore, the experimental conditions are an important factor determining the process flow.<sup>99, 171-172</sup> An influence of phospholipid membranes on aggregation of  $A\beta_{1-40/42}$  under conditions close to physiological in a sense of low amyloid concentration and a low peptide to membrane surface area ratio was studied.<sup>99</sup> Small and large unilamellar vesicles composed of dioleoyl-phosphatidylcholine (DOPC) building a liquid disordered lamellar phase at physiological

conditions, dipalmitoyl-phosphatidylcholine (DPPC) forming a solid lamellar gel phase, or DPPC with cholesterol introduction making up a liquid ordered bilayer phase were designed (Figure 15). A prominent inhibition of  $A\beta_{1-40}$  fibrillation was observed in the presence of vesicles in the solid state (DPPC), whereas the vesicles in the liquid ordered or liquid disorder state (DPPC with cholesterol incorporation or DOPC) showed decreased inhibitory properties. Thus, the state of the lipid phase can be associated with the course of aggregation of the peptide. Two possible situations are proposed: (i) a part of the peptide may penetrate through the membrane, reducing the concentration of the available peptide in solution, which in turn reduces the rate of aggregation; (ii) a peptide demonstrates the largest binding to the gel phase. The observations obtained in this study indicated that membrane composition is an important factor affecting the self-assembly process.

Fibrillogenesis of N-terminally octanoyl or palmitoyl modified  $A\beta_{1-40}$  was investigated by means of fluorescence spectroscopy, TEM, X-ray diffraction, and solid-state NMR spectroscopy.<sup>173</sup> It was observed that such modification enhances formation of rigid heterogeneous  $\beta$ -sheet-rich fibrils. <sup>13</sup>C NMR of the labeled conjugates revealed that along with the amino acids commonly accepted as a part of the  $\beta$ -sheet conformation (F19 and V39), A2, F4, and V12 moieties located at the N-terminus of  $A\beta_{1-40}$  were also found within the  $\beta$ -sheet structure. Thus, conjugation of  $A\beta_{1-40}$  to lipids contributes to an increase of local hydrophobicity, which leads to incorporation of the N-terminus into the  $\beta$ -sheet conformation and enhanced fibrillation kinetics.

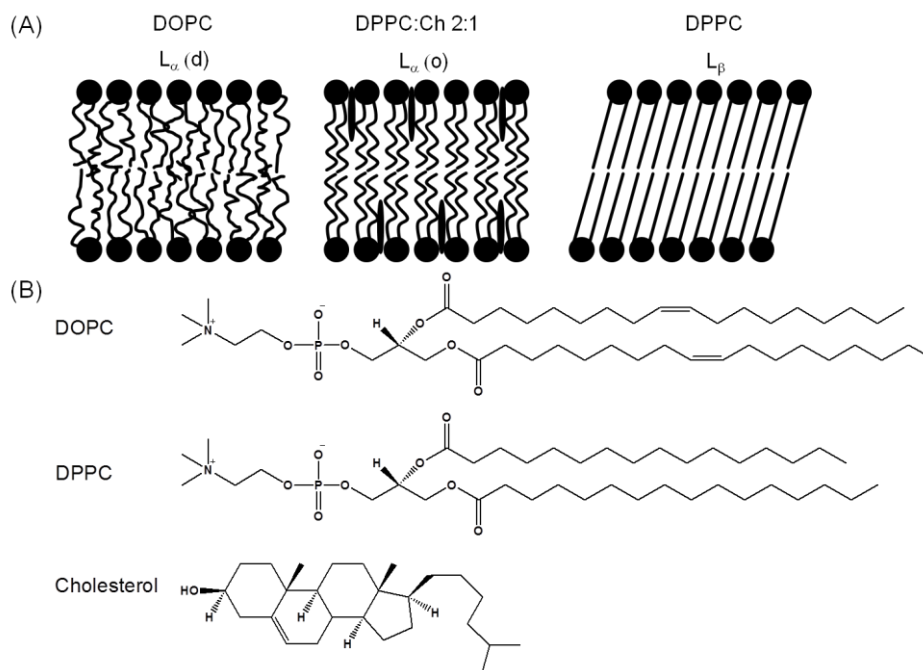


**Figure 15.** (A) Schematic representation of bilayer phospholipid membranes. (B) Structures of the employed lipids. Figure 15 was reproduced from ref<sup>99</sup>.

A lipid concentration may also have a strong effect on the course of the  $A\beta_{1-40}$  aggregation, as investigated on the example of 1,2-dihexanoyl-*sn*-glycero-3-phosphocholine (DHPC) (Figure 16).<sup>174</sup> Significant changes in aggregation kinetics of  $A\beta_{1-40}$  were observed in the presence of DHPC in a concentration dependent manner, as monitored by fluorescence spectroscopy. Thus, compared to a lipid-free  $A\beta_{1-40}$  sample, the duration of the lag phase was considerably decreased in the presence of 2 mM DHPC, but notably elongated in the presence of 4 mM DHPC. A specific interaction between  $A\beta_{1-40}$  and DHPC were determined by means of surface tension measurements, thus the CMC of DHPC was increased from  $13.1 \pm 0.3$  to

15.1±0.3 mM in the presence of 50μM Aβ<sub>1-40</sub>. An increase in the CMC value by approximately 2 mM implies that every Aβ<sub>1-40</sub> molecule captures about 40 DHPC molecules.

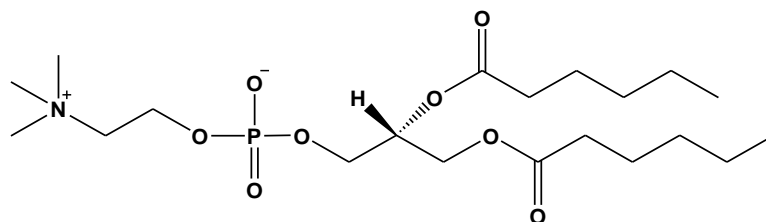


**Figure 16.** Chemical structure of DHPC.<sup>174</sup>

Interactions of Aβ<sub>1-40</sub> and Aβ<sub>1-42</sub> peptides with small unilamellar vesicles composed of palmitoyl-2-oleoyl-sn-glycero-3-phosphocholine (POPC) and 1-palmi-toyl-2-oleoyl-sn-glycero-3-[phospho-rac-(1-glycerol)] (POPG) were investigated via single-molecule imaging and tracking.<sup>175</sup> Relying on obtained data, a model describing interactions between the membrane and different species formed within the self-assembly process was proposed (Figure 17).

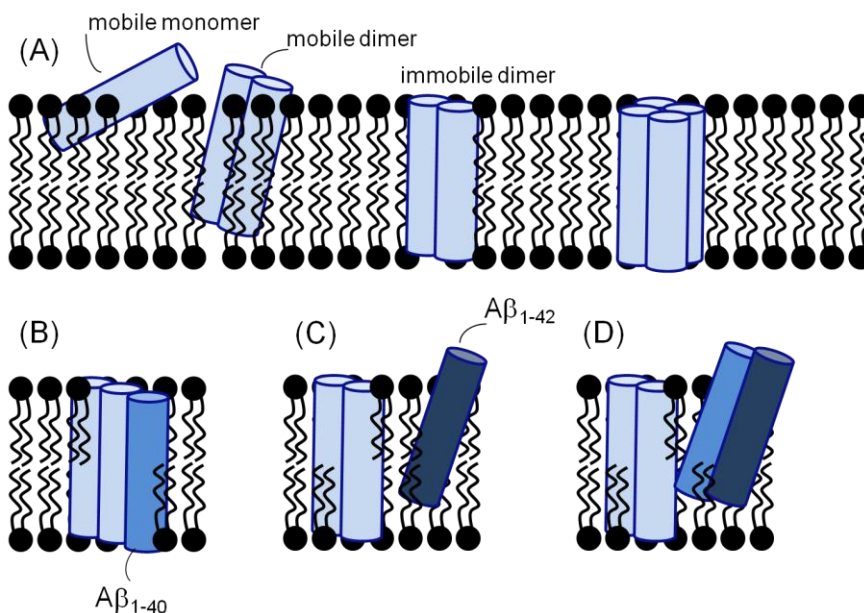


**Figure 17.** (A-D) Proposed models of interaction of different species involved in the aggregation process with the membrane. Figure 17 was reproduced from ref<sup>175</sup>.

Thus, different peptide species such as initially mobile monomers, mobile or immobile dimers or larger oligomers are able to bind to a phospholipid membrane (Figure 17A), although, at low saturation level. Additionally, different penetration of Aβ<sub>1-40</sub> and Aβ<sub>1-42</sub> species into the membrane was observed (Figure 17 B,C). Monte Carlo simulation data advise that two additional hydrophobic residues on the C-terminus of Aβ<sub>1-42</sub> lead to stabilization of Aβ<sub>1-42</sub> in the lipid tail groups (Figure 17C), whereas more polar C-terminus of Aβ<sub>1-40</sub> lead to its full incorporation (Figure 17B) into the membrane. It is interesting that by mixing of Aβ<sub>1-40</sub> and Aβ<sub>1-42</sub> a reduced number of oligomers and slower aggregation rate were observed. The authors suggested that specific interactions between two peptides lead to formation of a structure inhibiting development of the transmembrane conformation (Figure 17D).

Observation made on  $A\beta_{1-40/42}$  fibrillogenesis mixed or conjugated with lipids as well as at the model membranes *in vitro* may clarify the mechanism of the pathology *in vivo* and to move forward on the way to defeating Alzheimer's disease.

### 2.2.5. Influence of surfactants on aggregation of $A\beta_{1-40/42}$ peptides

Studying the interaction between amphiphilic amyloidogenic peptides and amphiphilic surfactants is an important step towards understanding of the interactions between the amyloids and other amphiphilic biological formations like membranes. Selected works dedicated to this topic will be discussed below.

An aggregation of the  $A\beta_{1-40}$  peptide in the presence of sodium dodecyl sulfate (SDS) was investigated by small-angle X-ray scattering (SAXS) and small-angle neutron scattering (SANS) techniques.<sup>105</sup> By addition of 115  $\mu\text{M}$   $A\beta_{1-40}$  solution to a solution containing 6 mM SDS (monomers) formation of “globular core-shell SDS- $A\beta_{1-40}$  complexes” was observed. The complexation occurs, however, slower than the transition of the  $A\beta_{1-40}$  structure from a random coil conformation to an  $\alpha$ -helical conformation.  $A\beta_{1-40}$  aggregates are coexisting with the SDS- $A\beta_{1-40}$  complexes forming mass-fractal-like clusters. It was also found that for each peptide molecule, the globular complex contains about 30 SDS molecules. Further, by addition of a 115  $\mu\text{M}$   $A\beta_{1-40}$  solution to a solution containing 20 mM SDS (micelles) extended core-shell SDS- $A\beta_{1-40}$  complexes can be formed. Such complexation in turn efficiently inhibits formation of amyloid aggregates due to association of hydrophilic and hydrophobic parts of the  $A\beta_{1-40}$  peptide with the respective parts of the preformed micelles (Figure 18).

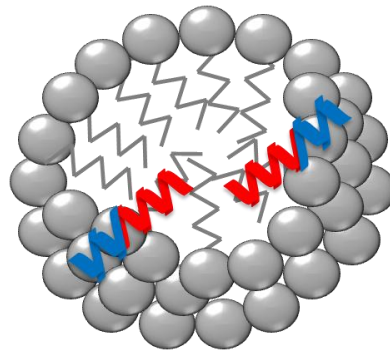


**Figure 18.** Schematic illustration of complexation of the  $A\beta_{1-40}$  monomers with SDS micelles (shown in gray). Hydrophilic residues of the  $A\beta_{1-40}$  are shown in blue, while hydrophobic in red. Figure 18 was reproduced from ref <sup>105</sup>.

Similarly,  $A\beta_{1-40/42}$  aggregation inhibition has been achieved in the presence of SDS micelles,<sup>176</sup> whereas changes of a secondary structure from a random coil state to a fully  $\alpha$ -helical conformation of the  $A\beta_{1-40}$  peptide could be induced by SDS and lithium dodecyl sulfate (LiDS) in a concentration-dependent way.<sup>106</sup> An influence of surfactants with different net charges, namely, anionic SDS, zwitterionic myristyl sulfobetaine, neutral dodecyl  $\beta$ -D-maltoside (DDM), and cationic cetyltrimethylammonium bromide (CTAB), on the course of the  $A\beta_{1-40}$  fibrillation was investigated.<sup>177</sup> By employment of cationic surfactant, formation of electrostatically linked amorphous peptide-surfactant coclusters was observed. In this state,  $A\beta_{1-40}$  adopts an  $\alpha$ -helical conformation which is compared to a  $\beta$ -sheet conformation not prone to self-assembly. Interactions between the anionic surfactant and negatively charged  $A\beta_{1-40}$  were in turn energetically unfavorable, leading to destabilization of monomers and

enhancement of their aggregation. Energetically unfavorable electrostatic interactions were less pronounced in case of the zwitterionic surfactant and were competitive with the hydrophobic interactions between the respective parts of the peptide and the surfactant. In case of the neutral surfactant electrostatic effect fully disappeared and hydrophobic interactions were dominant instead. Authors speculated that these interactions stabilize a monomer and either inhibit or completely suppress the self-assembly process. The knowledge obtained using different model systems, including surfactants of various nature, can be applied in the modeling of anti-amyloid inhibitors and other therapeutic strategies.

### 2.2.6. Influence of synthetic polymers on aggregation of $A\beta_{1-40/42}$ peptides

Usage of synthetic polymers as an additive to the systems containing aggregating peptides/proteins allows increasing the number of promising model systems for understanding the self-assembly process. Due to their good solubility, biocompatibility, diversity of chemical and morphological structures, an ability to control molecular weight and polydispersity while maintaining a given molecular structure, as well as a variety of synthesis methods, polymers are considered to be as effective modulators towards fibrillogenesis.

Despite the fact that a large number of researches are devoted to the study of amyloid aggregation in the presence of polymers, most of them described either an aggregation of short fragments of the  $A\beta_{1-40/42}$  molecules,<sup>103-104, 178</sup> or only targeted the  $A\beta_{1-42}$  variant<sup>179-181</sup>. Thus, at the moment, the aggregation behavior of the  $A\beta_{1-40}$  molecule in the presence of polymers is still poorly studied and requires additional knowledge. Nevertheless, several publications devoted specifically to the  $A\beta_{1-40}$  variant are present.

According to the data obtained through far-UV circular dichroism (CD) and ThT fluorescence aggregation assays, cationic polymethacrylate quaternary ammonium copolymer (PMAQA) (Figure 19) can induce formation of  $\beta$ -sheet rich fibrils of  $A\beta_{1-40}$  and thus promote its self-assembly process.<sup>182</sup> NMR spectroscopy analysis accompanied by microsecond scale atomistic molecular dynamics simulations indicate that interactions of PMAQA with central (K16-V24) and C-terminus (A30-V40) regions of  $A\beta_{1-40}$  lead to the above mentioned fibrillation enhancement.

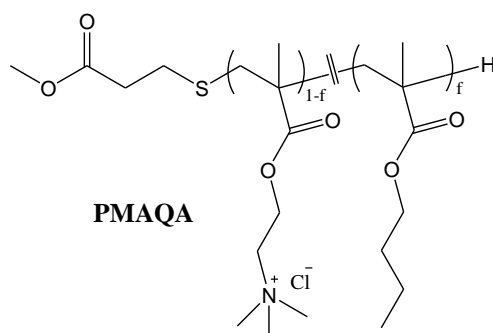


**Figure 19.** Polymethacrylate quaternary ammonium copolymer (PMAQA).<sup>182</sup>

A novel hydroxyquinoline appended polyfluorene (PF-HQ) (Figure 20) is also able to influence fibrillogenesis of the  $A\beta_{1-40}$  peptide.<sup>183</sup> Based on results obtained via AFM, ThT fluorescence, CD, and Fourier transform infrared (FTIR) spectroscopy, the PF-HQ possesses an “amyloid-like” surface structure and forms coaggregates with different intermediate species within the  $A\beta_{1-40}$  fibrillation. Capturing the prefibrillar intermediates within the coaggregates efficiently inhibits fibril formation and reduces peptide cytotoxicity.

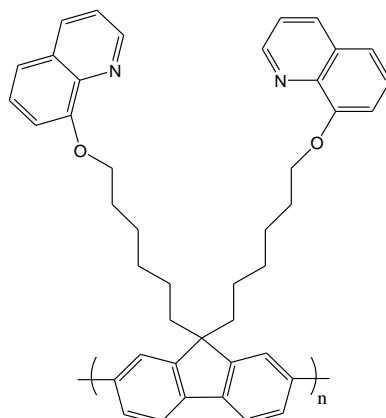


**Figure 20.** Hydroxyquinoline appended polyfluorene (PFHQ).<sup>183</sup>

Multivalent polymer-LPFFD conjugates (mP-LPFFD) (Figure 21) containing an LPFFD peptide fragment known for its ability to interact with the central hydrophobic sequence, namely L17–A21, of  $A\beta_{1-40}$  were designed.<sup>184</sup> Retaining the polymer backbone, but changing the content of the peptide fragment from 3 to 12 mol % per chain, a different inhibitory ability was observed. Thus, according to the ThT fluorescence studies, the conjugate with 7% LPFFD loading has the best inhibitory ability out of three variants. The authors suggested that the self-assembly process of conjugates with 12% LPFFD loading, competes with the LPFFD- $A\beta_{1-40}$  interactions, making the conjugates with the higher peptide load less effective. AFM and TEM experiments revealed formation of the zero-dimensional nanostructures with an approximate size of 5–35 nm in case of mP-LPFFD/ $A\beta_{1-40}$  systems, whereas conventional  $A\beta_{1-40}$  fibrils were detected in a micrometer size. It was further found that the polymer-LPFFD conjugates with a 7% peptide load can disassemble the structure of mature  $A\beta_{1-40}$  fibrils depending on the molecular weight of the conjugate. AFM and DLS results demonstrated that by increasing the molecular weight of the conjugate, the disassembling effect is also enhanced.

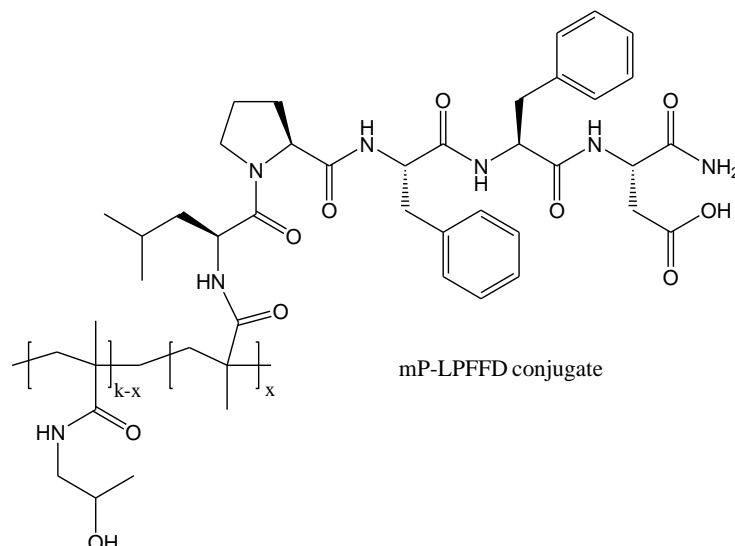


**Figure 21.** Structure of the multivalent polymer conjugate mP-LPFFD consisting of poly(hydroxypropyl methacrylamide) backbone and LPFFD peptide ligand.<sup>184</sup>

A modest number of articles devoted to the influence of various classes of polymers on the aggregation of particularly the  $A\beta_{1-40}$  peptide variant prompts us to conduct an additional research in this area, thus, opening the bridgehead for new discoveries.

### 2.3. The reversibly aggregating parathyroid peptide hormone

The parathyroid peptide hormone (PTH) is an important participant in human vital functions. PTH is produced by parathyroid glands in case of an increase in the concentration of phosphates or a decrease in the concentration of  $\text{Ca}^{2+}$  in the blood, thereby affecting bone metabolism.<sup>66, 185</sup> The structure of physiologically occurring PTH includes 84 amino acids (Figure 22), where I5-N10 and S17-F34 regions are predisposed to establish an  $\alpha$ -helix structure, H14-S17 region is stabilized by hydrophobic interactions, while V35-Q84 region is disordered.<sup>66, 185</sup>

#### PTH<sub>1-84</sub>

```

          10          20          30          40          50          60
SVSEIQLMHN LGKHLNSMER VEWLRKKLQD VHNFVALGAP LAPRDAGSQR PRKKEDNVLV

          70          80
ESHEKSLGEA DKADVNVLTAKSQ

```

**Figure 22.** Amino acid sequence of PTH<sub>1-84</sub>.

Nonetheless, only a PTH fragment including the 34 N-terminal amino acids S1-F34 is essential for its bioactivity. Currently, short and long forms of the peptide hormone are used in the treatment of osteoporosis as efficient agents promoting bone growth under the trade names Forteo<sup>®</sup> and Natpara<sup>®</sup>, respectively.

Similar to amyloid  $\beta$  peptides, the PTH hormone also aggregates forming fibrils with cross- $\beta$  structure both *in vivo* and *in vitro*. *In vitro* mature fibrils can be rapidly generated by heating up the system, containing the PTH<sub>1-84</sub> variant, up to 65 °C within minutes.<sup>66</sup> Solid-state NMR data indicate that the fibril cross- $\beta$  core structure is mostly formed by residues R25–P40, which is approximately 20% of the total peptide hormone length.<sup>66</sup> The N- and C-terminus regions are in turn very flexible and intrinsically disordered. The obtained fibrils, moreover, demonstrate low thermodynamic stability, since  $10.1 \pm 2.5\%$  of the monomer can be liberated again within 24 h, thus, the aggregation of PTH<sub>1-84</sub> in contrast to  $\text{A}\beta_{1-40/1-42}$  is reversible. It is suggested that such a fibrillation has a non-pathological, but storage function, and PTH<sub>1-84</sub> is a “functional amyloid in secretory granules”.<sup>66</sup> The factors affecting an aggregation pathway of the PTH hormone are poorly studied and thus of great interest. The only investigation currently devoted to this issue describes an influence of EGCG on the course of the PTH<sub>1-84</sub> fibrillation.<sup>66</sup> As a part of the research, the PTH<sub>1-84</sub> and EGCG were co-incubated for 48 h at 65 °C at a molar ratio of 1:2.4 or 1:10. Aliquots of these mixtures taken at different time intervals were subsequently investigated by TEM. Formation of amorphous aggregates noticeably different from the PTH<sub>1-84</sub> fibrils obtained in the absence of the EGCG was observed at both 1:2.4 and 1:10 molar ratio at any analyzed time. Formation of spherical particles with a diameter of up to 30 nm was detected in the case of the 1:10 mixture after an hour of incubation. Presence of tryptophan (W23) within the PTH<sub>1-84</sub> sequence, used as an internal fluorescent probe, allowed using fluorescence spectroscopy as a further investigation step. Fluorescence intensity of PTH<sub>1-84</sub> decreased upon titration as EGCG was added, indicating possible interactions between the PTH<sub>1-84</sub> and EGCG.<sup>66</sup> Similar observations were later obtained by means of NMR spectroscopy. The obtained 2D <sup>1</sup>H-<sup>15</sup>N HSQC spectra indicated a change in chemical shifts and intensity of the particular moieties of <sup>15</sup>N-PTH<sub>1-84</sub> upon titration with EGCG. Noteworthy changes of the chemical shift were obtained by increasing the PTH<sub>1-84</sub> : EGCG ratio from 1:1 to 1:3. As discussed in the previous chapters, EGCG is also able to inhibit the  $\text{A}\beta_{1-40/1-42}$  fibrillation<sup>117-120</sup> and suppress the  $\alpha$ -synuclein self-assembly.<sup>186</sup>

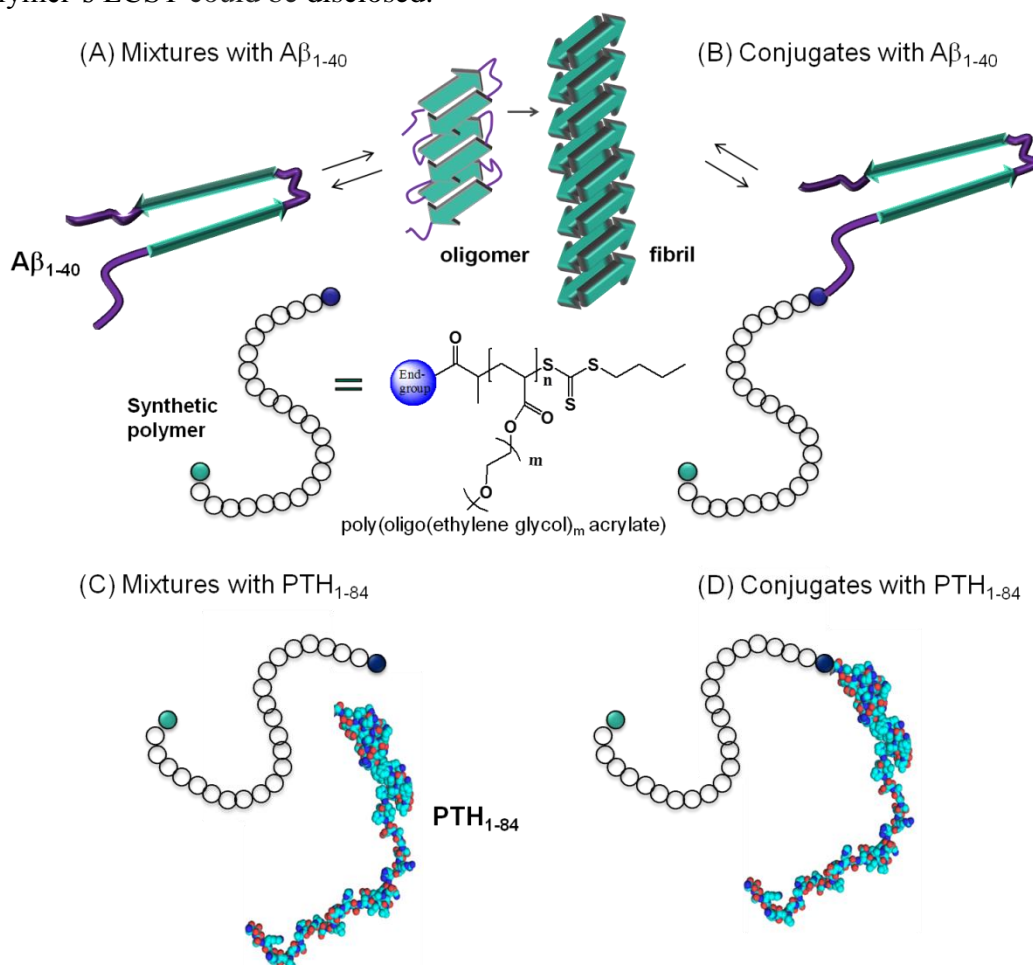
Recently, it has been found that pegylation of PTH<sub>1-34</sub> can prolong pharmacokinetic and pharmacodynamic actions of the peptide hormone *in vivo*,<sup>187</sup> thus indicating the need for further study of the effect of polymers on the biological activity of both peptide variants.

## II. SCOPE OF THE THESIS

### 1. Objectives

The main aim of this scientific work is to study the aggregation of amyloidogenic peptides in the presence of hydrophilic polymers whose conformation is controlled by small temperature changes via their LCST. Therefore, poly(oligo(ethylene glycol)<sub>m</sub> acrylates), in which the polymer's hydrophilicity, and hence the LCST, is adjusted by variation of the number of ethylene glycol-units in the side chain ( $m = 1-9$ ), the nature of end groups (B = butoxy; C = carboxy; D = dodecyl; P = pyridyldisulfide), and the degree of polymerization ( $n$ ) were synthesized (Scheme 1).

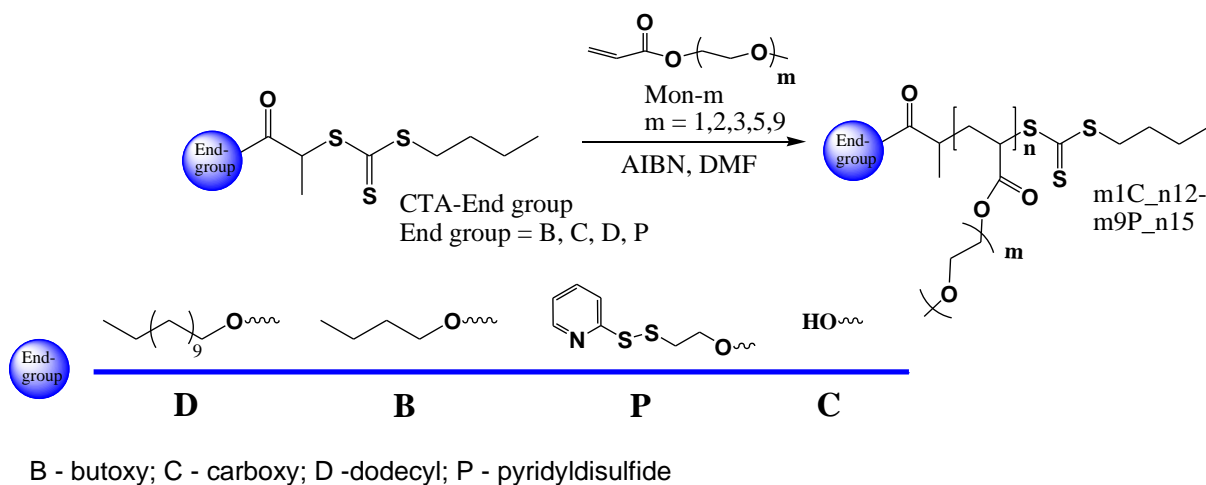
Subsequently, self-assembly of the irreversibly aggregating A $\beta$ <sub>1-40</sub> peptide or reversibly aggregating PTH<sub>1-84</sub> peptide hormone was investigated either upon mixing with the prepared hydrophilic polymers (Scheme 1A, 1C) or by covalent conjugation of the peptides with the polymers by means of resin-based synthesis or solution-based coupling chemistries (Scheme 1B, 1D). Furthermore, employing <sup>15</sup>N-NMR spectroscopy for the conjugated PTH<sub>1-84</sub> part, a chain conformation of poly(methoxy di(ethylene glycol)acrylates) ( $m=2$ ) above and below the polymer's LCST could be disclosed.



**Scheme 1.** Schematic illustration of (A and C) mixtures of the thermoresponsive polymers with A $\beta$ <sub>1-40</sub> and PTH<sub>1-84</sub>, respectively, (B and D) conjugates of the thermoresponsive polymers with the A $\beta$ <sub>1-40</sub> and PTH<sub>1-84</sub> peptides, respectively, and their subsequent self-assembly. The  $\alpha$  end group of the polymer (e.g. carboxy-) is shown as a blue circle, while the  $\omega$  end group is shown as a turquoise circle.

## 2. Concept

Reversible addition-fragmentation chain transfer (RAFT) polymerization of oligo(ethylene glycol)<sub>m</sub> acrylates using four different chain transfer agents (CTAs) and the azobisisobutyronitrile (AIBN) initiator was utilized to synthesize well-defined thermoresponsive poly(oligo(ethylene glycol)<sub>m</sub> acrylates), as shown in Scheme 2. The optimal combination of hydrophobicity of the end groups with hydrophilicity of the polymers' repeating unit allowed adjusting the LCST in the desired range. The given work aimed to investigate the influence of the synthesized polymers on the aggregation pathway of the irreversibly aggregating A $\beta$ <sub>1-40</sub> and reversibly aggregating PTH<sub>1-84</sub>.



**Scheme 2.** Synthetic pathway for preparation of various hydrophilic thermoresponsive polymers via RAFT polymerization using oligo(ethylene glycol)<sub>m</sub> acrylate monomers (Mon-m) functionalized with CTAs and AIBN as an initiator.

In order to follow all the possible conformational transitions within the studied system, different analytical methods were employed. The temperature induced transition of the polymers from an expanded coil to a collapsed globule was followed by turbidimetry measurements, while ThT detected fluorescence measurements were used to follow fibrillation kinetics of the peptides.

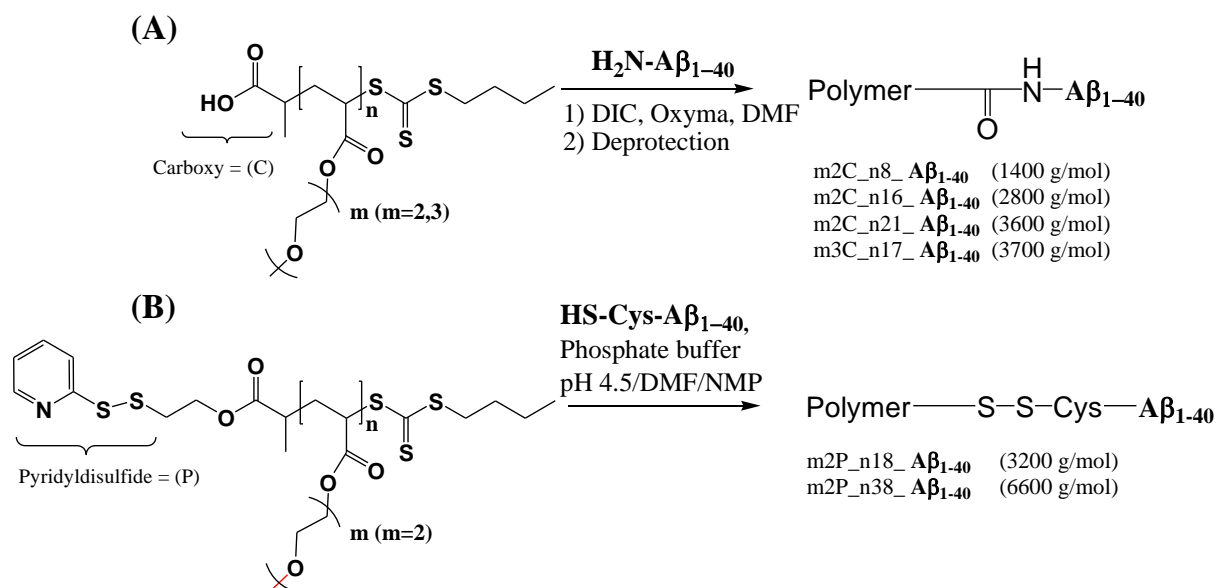
Firstly, only three poly(methoxy di(ethylene glycol)acrylates) (m=2) with diverse molecular weights (3600, 8500 and 14600 g/mol) carrying a carboxy end group were mixed with the A $\beta$ <sub>1-40</sub> peptide. The studied A $\beta$ <sub>1-40</sub>/polymer mixtures demonstrated accelerated aggregation kinetics compared to the A $\beta$ <sub>1-40</sub> alone, while all three polymeric samples were below their LCST temperature under conditions of ThT fluorescence assay.

These results are summarized in the first publication (*“Amyloid Beta Aggregation in the Presence of Temperature-Sensitive Polymers”* – *Polymers* **2016**, 8(5), 178; **1st chapter** of *Results and Discussion*) incorporated in this cumulative doctoral thesis comprising in total four chapters of Results and Discussion based on four publications. This publication also encompasses complementary data of Sebastian Funtan (synthesis and characterization of poly(oxazolines)) that were needed to support the observed trends, but are of no further relevance for my project. Note, the samples designated as 3a, 3b, and 3c in the article are assigned in the general nomenclature proposed in Scheme 2 as m2C\_n21, m2C\_n49, and m2C\_n84, respectively, to better distinguish samples in the overall set of samples.

In the continuation of the study, the second publication (*“Modulation of amyloid  $\beta$  peptide aggregation by hydrophilic polymers”* – *Physical Chemistry Chemical Physics* **2019**, 21,

20999; **2nd chapter** of *Results and Discussion*) described the modulation of the  $A\beta_{1-40}$  self-assembly process in the presence of additional thermoresponsive poly(oligo(ethylene glycol)<sub>m</sub> acrylates). There, polymer's hydrophilicity was adjusted by variation of the number of ethylene glycol-units in the side chain ( $m = 1-9$ ), the nature of end groups ( $B =$  butoxy;  $C =$  carboxy;  $D =$  dodecyl;  $P =$  pyridyldisulfide), and the degree of polymerization ( $n$ ) of the polymers. It was found that by a proper combination of hydrophilic side chains with hydrophobic end groups of the polymer one can efficiently tune its LCST and, as a result, notably influence on the  $A\beta_{1-40}$ 's aggregation pathway. In addition to ThT detected fluorescence measurements, TEM imaging allowed us to visualize and to evaluate morphology of the obtained aggregates. The secondary structure of the chosen polymer-peptide mixtures were, moreover, examined by means of circular dichroism (CD) spectroscopy. According to the data obtained by the above mentioned methods, the presence of the employed polymers did not seem to significantly influence on the morphology of the final fibrils compared to  $A\beta_{1-40}$  alone.

In the third publication ("*Synthesis and Aggregation of Polymer-Amyloid  $\beta$  Conjugates*" – *Macromolecular Rapid Communications* **2019**, *0*, 1900378; **3rd chapter** of *Results and Discussion*), selected poly(oligo(ethylene glycol)<sub>m</sub> acrylates) ( $m=2,3$ ) were covalently conjugated with the  $A\beta_{1-40}$  peptide *in situ* either by SPS/DIC-coupling (Scheme 3A) or by in-solution pyridyldisulfide coupling (Scheme 3B). Compared to the wild type  $A\beta_{1-40}$  peptide, the conjugates demonstrated enhanced fibrillation accompanied with changes in fibrils morphology. Thus, instead of long fibrils attributed to classical amyloid fibrils, bundles of short aggregates were detected.

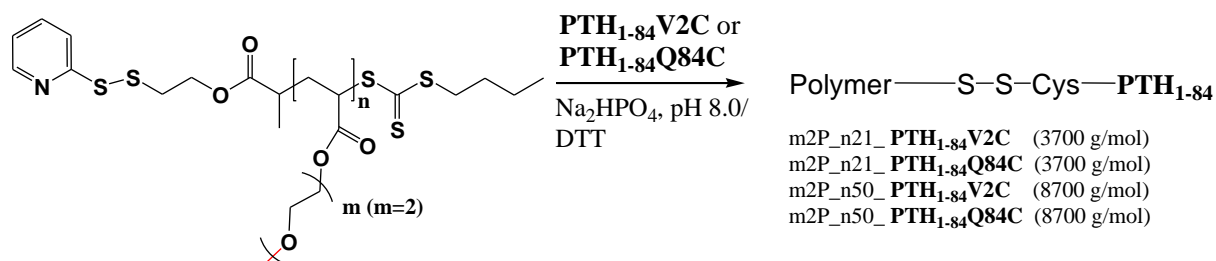


**Scheme 3.** Synthetic pathway for preparation of polymer- $A\beta_{1-40}$  conjugates. (A) Carboxy-functionalized polymers were amino-terminally coupled with the  $H_2N-A\beta_{1-40}$  peptide (1) on the preloaded resin followed by (2) deprotection in TFA, TIPS,  $H_2O$ , and phenol. (B) Polymer conjugation through thiol-disulfide exchange to the  $A\beta_{1-40}$  peptide with an additional cysteine at the amino-terminus  $HS-Cys-A\beta_{1-40}$ . Molecular weights of the employed polymers are shown in brackets.

Finally, the fourth publication ("*Probing Polymer Chain Conformation and Fibril Formation of Peptide Conjugates*" – *ChemPhysChem* **2019**, *20*, 236; **4th chapter** of *Results and Discussion*) described self-assembly of the reversibly aggregating peptide hormone  $PTH_{1-84}$  physically mixed or covalently conjugated with the poly(methoxy di(ethylene glycol)acrylates) ( $m=2$ ) through thiol-disulfide exchange (Scheme 4). Relying on the data obtained from ThT detected measurements and TEM,  $PTH_{1-84}$  aggregation was found to be

.....

enhanced by employed polymers, while the morphology of the final fibrils stayed unchanged. Employing  $^{15}\text{N}$ -NMR-spectroscopy for the conjugated peptide part, one could additionally follow the conformational transition of the polymer from the random coil to the collapsed state. Note, the samples designated as RP-22 and RP-23 in the article are assigned in the general nomenclature proposed in Scheme 2 as m2P\_n50, m2P\_n21, respectively, to better distinguish samples in the overall set of samples.



**Scheme 4.** Polymer conjugation through thiol-disulfide exchange to the  $\text{PTH}_{1-84}$  peptide with a cysteine introduced to the peptide either at the amino-terminus (V2C variant) or the carboxy-terminus (Q84C variant). Molecular weights of the employed polymers are shown in brackets.

---

### III. RESULTS AND DISCUSSION

The *Results and Discussion* part consists of four chapters based on the respective publications mentioned below. In the first three chapters influence of the hydrophilic thermoresponsive poly(oligo(ethylene glycol)<sub>m</sub> acrylates) mixed or conjugated with the irreversibly aggregating A $\beta$ <sub>1-40</sub> peptide is investigated. The fourth chapter discusses interactions of the employed polymers with the reversibly aggregating peptide, namely the PTH<sub>1-84</sub>. The fibrillogenesis of the peptides was investigated via ThT detected fluorescence measurements, CD spectroscopy and TEM. The aggregation behavior of the thermoresponsive polymers in the chapters 1-3 was monitored via turbidimetry, while additional <sup>15</sup>N-NMR-spectroscopy investigations were employed in the chapter 4.

- 1) Funtan, S.; Evgrafova, Z.; Adler, J.; Huster, D.; Binder, H. W., Amyloid Beta Aggregation in the Presence of Temperature-Sensitive Polymers. *Polymers* **2016**, *8* (5).
- 2) Evgrafova, Z.; Voigt, B.; Roos, A. H.; Hause, G.; Hinderberger, D.; Balbach, J.; Binder, W. H., Modulation of amyloid  $\beta$  peptide aggregation by hydrophilic polymers. *Physical Chemistry Chemical Physics* **2019**, *21* (37), 20999-21006.
- 3) Evgrafova, Z.; Rothmund, S.; Voigt, B.; Hause, G.; Balbach, J.; Binder, W. H., Synthesis and Aggregation of Polymer-Amyloid  $\beta$  Conjugates. *Macromolecular Rapid Communications* **2019**, *0* (0), 1900378.
- 4) Evgrafova, Z.; Voigt, B.; Baumann, M.; Stephani, M.; Binder, W. H.; Balbach, J., Probing Polymer Chain Conformation and Fibril Formation of Peptide Conjugates. *ChemPhysChem* **2019**, *20* (2), 236-240.

## 1. Amyloid Beta Aggregation in the Presence of Temperature-Sensitive Polymers



Article

# Amyloid Beta Aggregation in the Presence of Temperature-Sensitive Polymers

Sebastian Funtan <sup>1</sup>, Zhanna Evgrafova <sup>1</sup>, Juliane Adler <sup>2</sup>, Daniel Huster <sup>2</sup> and Wolfgang H. Binder <sup>1,\*</sup>

<sup>1</sup> Faculty of Natural Science II, Martin-Luther University Halle-Wittenberg, Von-Danckelmann-Platz 4, D-06120 Halle (Saale), Germany; sebastian.funtan@chemie.uni-halle.de (S.F.); zhanna.evgrafova@chemie.uni-halle.de (Z.E.)

<sup>2</sup> Institute for Medical Physics and Biophysics, Leipzig University, Härtelstraße 16-18, D-04107 Leipzig, Germany; juliane.adler@medizin.uni-leipzig.de (J.A.); daniel.huster@medizin.uni-leipzig.de (D.H.)

\* Correspondence: wolfgang.binder@chemie.uni-halle.de; Tel.: +49-345-55-25930

Academic Editor: André Laschewsky

Received: 31 March 2016; Accepted: 26 April 2016; Published: 2 May 2016

**Abstract:** The formation of amyloid fibrils is considered to be one of the main causes for many neurodegenerative diseases, such as Alzheimer's, Parkinson's or Huntington's disease. Current knowledge suggests that amyloid-aggregation represents a nucleation-dependent aggregation process *in vitro*, where a sigmoidal growth phase follows an induction period. Here, we studied the fibrillation of amyloid  $\beta$  1-40 ( $A\beta_{40}$ ) in the presence of thermoresponsive polymers, expected to alter the  $A\beta_{40}$  fibrillation kinetics due to their lower critical solution behavior. To probe the influence of molecular weight and the end groups of the polymer on its lower critical solution temperature (LCST), also considering its concentration dependence in the presence of buffer-salts needed for the aggregation studies of the amyloids, poly(oxazolines) (POx) with LCSTs ranging from 14.2–49.8 °C and poly(methoxy di(ethylene glycol)acrylates) with LCSTs ranging from 34.4–52.7 °C were synthesized. The two different polymers allowed the comparison of the influence of different molecular structures onto the fibrillation process. Mixtures of  $A\beta_{40}$  with these polymers in varying concentrations were studied via time-dependent measurements of the thioflavin T (ThT) fluorescence. The studies revealed that amyloid fibrillation was accelerated in, accompanied by an extension of the lag phase of  $A\beta_{40}$  fibrillation from 18.3 h in the absence to 19.3 h in the presence of the poly(methoxy di(ethylene glycol)acrylate) (3600 g/mol).

**Keywords:** amyloid  $\beta$ ; fibrillation; lower critical solution temperature; thermoresponsive polymer

### 1. Introduction

A wide range of neurodegenerative diseases, such as Alzheimer's, Parkinson's or Huntington's disease, is related to misfolding and aggregation of particular amyloid proteins, leading to the formation of insoluble fibrils [1]. Despite the fact that native soluble proteins associated with these illnesses have very different amino acid sequences and, therefore, different structures, the resulting insoluble aggregates are mainly straight, unbranched and share a common  $\beta$ -sheet secondary structure [2–7]. The fibrillation kinetics of the amyloid protein has been broadly studied and can be described by a sigmoidal curve featuring three characteristic regions known as the lag phase, the growth phase and the saturation phase or “plateau region” [3,4,8].

At the very early stage of the lag phase, when no (larger, detectable) aggregates are present, native soluble proteins combine to form primary nuclei, which are referred to as oligomeric species and protofibrils characterized by a significant  $\beta$ -sheet conformation (Figure 1a) [9,10]. These primary nuclei then elongate (Figure 1b), and a secondary nucleation catalyzed by the surface of a growing

filament takes place (Figure 1c). Fragmentation (Figure 1d) as a consequence of external forces (e.g., mixing or shaking), which will generate new active chain ends, is also possible and will accelerate fibril growth [11]. Although the fraction of the aggregated fibrils during the lag phase is relatively low and difficult to characterize, experimental proof confirms that the mature fibrils are already present in the system [3,12–15]. The second phase of the amyloid protein fibrillation is characterized via a growth phase, which is the thermodynamically-favorable addition of monomers to the growing prefibrillar structures, [3,8,14,15], followed by the last step, the saturation phase, where the concentration of the mature fibril is very high and the concentration of the monomeric species has achieved a constant value [3,8,14,15].

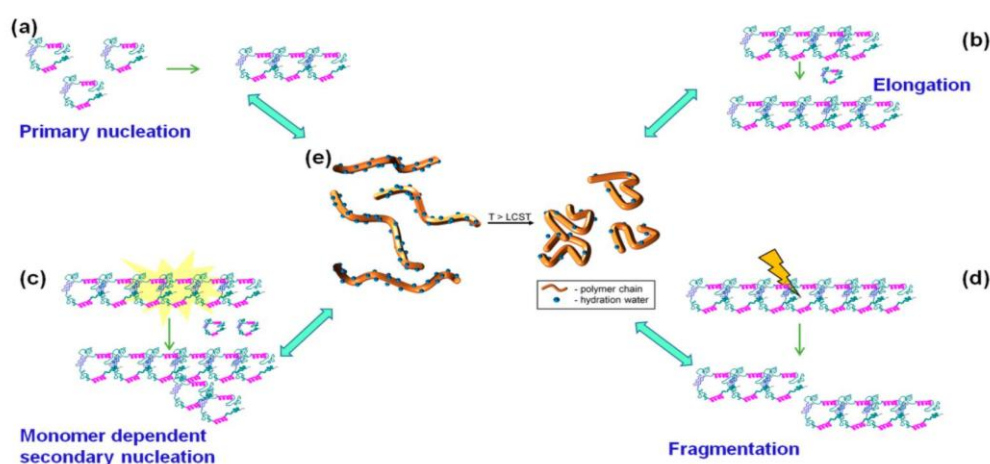


**Figure 1.** Molecular events during the lag time (a–d): (a) primary nucleation; (b) elongation; (c) monomer-dependent secondary nucleation; (d) fragmentation creates new elongation sites in the system; and (e) transition of a thermoresponsive polymer from the hydrated coil to the collapsed state. Prior to heating, the polymer chain (brown) is more hydrated. When the cloud point temperature ( $T_{CP}$ ) has been reached, the chain collapses to a compact globule by releasing most of the hydration water (blue), and further aggregation of the collapsed chains is possible [3,12–16]. LCST: lower critical solution temperature.

Beside small molecules [17,18] and proteins [19–22], especially polymers are promising candidates for the inhibition of the fibrillation as has been shown for the poly-(L)-lysine (PLL) [23], dendrimers [11,24,25] and polymeric nanoparticles [26–28]. Thus, the presence of bilayer membranes [3,29], micellar aggregates [3,30–33] and nanoparticles [27,34,35] has shown to significantly alter the aggregation process, where especially the interplay between  $A\beta$  with artificial membranes is often seen as an important factor of the  $A\beta$  fibrillation *in vivo* [3]. *In vitro* aggregation of the amyloid protein can be delayed by means of interaction with, e.g., phospholipid membranes, leading to a reduction of the amyloid-formation from initially 2–9 h in the presence of liposomes made from dioleoyl-phosphatidylcholine (DOPC) in the gel phase [29]. Furthermore, surfactant micelles interfere with the formation of the  $A\beta$  fibrils in a concentration-dependent manner [3,30–33], as in the presence of sodium dodecyl sulfate (SDS) the lag time for a solution containing 150  $\mu$ M  $A\beta_{40}$  is decreasing from  $7.5 \pm 2.0$ – $1.9 \pm 0.2$  h at 0.9 mM SDS and  $1.2 \pm 0.2$  h at 2.75 mM SDS (below its critical micelle concentration (cmc)), whereas a higher concentration of SDS (12.5 mM, above the cmc) suppressed fibrillation [33]. The same effect was observed for  $A\beta$ -nanoparticle systems [27,34,35], where the presence of 0.05 or 1.1 mg/mL of amine-modified polystyrene nanoparticles in a 16  $\mu$ M  $A\beta$  system changed the lag time from  $138 \pm 20$  min to around 50 and 500 min, respectively, also reporting the formation of stickier and shorter fibrils [27]. However, contradictory results have been achieved with regard to the interference of polymers and polyelectrolytes with  $A\beta$  fibrillation kinetics [36].

To the best of our knowledge, the influence of thermoresponsive polymers on the fibrillation pathways of amyloids has not yet been investigated. The current study provides a first report on the influence thermoresponsive polymers exert on the fibrillation of an amyloid protein, mixed noncovalently into a fibrillating amyloid system. An important requirement for such an experiment is the correct choice of the lower critical solution temperature (LCST) behavior of the polymer, which should be chosen close to the temperature, where amyloid aggregation is observed (experimentally *in vitro*). As the LCST is also referred to as the cloud point temperature ( $T_{CP}$ ), where the conformation changes from a hydrated coil to a collapsed globule by the release of most of the hydration water (coil-globule transition; see Figure 1e) [16], it is tempting to speculate about the effects of such a transition on the amyloid aggregation, most of all with respect to the macroscopic kinetic aggregation behavior.

Besides the well-known poly(*N*-isopropylacrylamide) (PNIPAM) [37–39], especially poly(oxazolines) (POx) [40–43] and polyacrylates containing a PEG part in the repeating unit [44,45] are widely-used thermoresponsive polymers, allowing one to tune the LCST behavior by variation of the nature and amount of the used (co)-monomers: hydrophilic monomers in the chain shift the LCST to higher values, whereas the incorporation of hydrophobic monomers will decrease the LCST [42,45]. Thus, hydrophilic PEtOx displays an LCST of  $T_{CP} = 60\text{--}68\text{ }^{\circ}\text{C}$  [40], whereas poly(2-isopropyl-2-oxazoline) (PiPrOx) shows an LCST around body temperature of  $T_{CP} = 36\text{--}39\text{ }^{\circ}\text{C}$  [41]. Nearly any value for the LCST can be adjusted, e.g., by copolymerization (P(*n*PrOx-EtOx) [42,46], P(*n*PrOx-*i*PrOx) [42], P(*i*PrOx-*n*BuOx) [47], P(*i*PrOx-NonOx) [47], P(*c*-PropOx-EtOx) [48]) or by adjusting the polymer concentration [40], the molecular weight [40,46] or the end groups [49,50]. Similarly, thermoresponsive polyacrylates, containing a PEG part in the repeating unit [44,45], display an LCST behavior [45,51]. It was found that the cloud point can be adjusted steplessly between 9 and 90  $^{\circ}\text{C}$ .

Here, we describe the design and syntheses of two different types of polymers (poly(oxazolines) and poly(methoxy di(ethylene glycol)acrylates)), both showing an LCST at temperatures close to the *in vitro*-aggregation temperature of amyloids. Subsequently, we study their effect on amyloid aggregation probed by conventional aggregation assays. A special focus was placed on the comparison of the two different hydrophilic polymers.

## 2. Materials and Methods

### 2.1. Materials

The following chemicals were purchased from Sigma Aldrich (Taufkirchen, Germany): 2,2'-azobis(2-methylpropionitrile) (AIBN), ethanolamine, deuterated chloroform, isobutyronitrile, methyl trifluoromethanesulfonate, *N*-methylpropargylamine, THF (HPLC grade), valeronitrile and zinc acetate dihydrate. *N,N*-diethylamine and propargyl tosylate were purchased from Fluka (Taufkirchen, Germany). Calcium hydride was bought from Alfa Aesar (Karlsruhe, Germany). Sodium chloride and sodium sulfate were bought from Roth (Karlsruhe, Germany).  $\text{Ce}(\text{SO}_4)\cdot 4\text{H}_2\text{O}$  and  $(\text{NH}_4)_6\text{Mo}_7\text{O}_{24}\cdot 4\text{H}_2\text{O}$  were obtained from VEB (Eschborn, Germany). Concentrated sulfuric acid was purchased from Th. Geyer (Renningen, Germany). Deuterated chloroform was obtained from Chemotrade (Düsseldorf, Germany), and DMF (HPLC grade) was purchased from VWR-Prolabo (Darmstadt, Germany).

A $\beta_{40}$  peptide was synthesized using the standard F-moc solid phase synthesis strategy at the core unit "Peptid-Technologien" of the Medical Faculty of the University of Leipzig [52].

The oxazoline monomers were stored over calcium hydride and were freshly distilled before usage. All solvents were freshly distilled and degassed by bubbling with nitrogen for at least 20 min prior to usage. Acetonitrile (ACN) was dried with calcium hydride by boiling for several hours followed by distillation. AIBN was recrystallized from ethanol twice before usage.

## 2.2. Methods

$^1\text{H}$ -NMR spectra were recorded on a Varian Gemini 2000 (400 MHz) (Agilent, Waldbronn, Germany) or on a Varian Unity Inova 500 (500 MHz) (Agilent, Waldbronn, Germany) using MestReNova software (Version 6.0.2-5475) (Mestrelab Research, Santiago de Compostela, Spain) for the evaluation of the results. NMR spectra were measured at 27 °C using deuterated chloroform ( $\text{CDCl}_3$ ). All chemical shifts ( $\delta$ ) were given in parts per million (ppm) relative to trimethylsilane (TMS) and referred to the solvent signal ( $\text{CDCl}_3$ : 7.26 ppm ( $^1\text{H}$ ), 77.0 ppm ( $^{13}\text{C}$ )).

MALDI-TOF-MS analysis was carried out using a Autoflex III Smartbeam (Bruker Daltonics, Bremen, Germany) equipped with a nitrogen laser (337 nm) working in linear and reflection modes. The obtained data were evaluated using flexAnalysis software (Version 3.0) (Bruker Daltonics, Bremen, Germany). The matrix solution was prepared by dissolving 1,8,9-anthracenetriol (dithranol) in THF at a concentration of 20 mg/mL. The polymer was dissolved in THF (10 mg/mL) and mixed with sodium trifluoroacetate (10 mg/mL in THF). The ratio between the matrix, the analyte and the salt was 100:10:1.

Gel permeation chromatography (GPC) for the poly(methoxy di(ethylene glycol)acrylates) was performed on a Viscotek GPCmax VE 2002 (Malvern, Crowthorne, UK) using a  $\text{H}_{\text{HR}}\text{-H}$  Guard-17360 precolumn and a  $\text{GMH}_{\text{HR}}\text{-N-18055}$  column with THF as the solvent and a VE 3580 IR detector for refractive index determination. A polystyrene standard ( $M_{\text{P}} = 1000\text{--}115,000$  g/mol) was used for external calibration. Column and detector temperatures were held at 22 and 35 °C, respectively, and the flow rate was set to 1 mL/min. The concentration of all samples was 3 mg/mL.

GPC measurements of the POx were performed on a Viscotek GPCmax VE 2001 (Malvern, Crowthorne, UK) using a  $\text{H}_{\text{HR}}\text{-H}$  Guard-17369 and a  $\text{GMH}_{\text{HR}}\text{-N-18055}$  column with DMF as the eluent at 60 °C and via detection of the refractive index with a VE 3580 RI detector from Viscotek at 35 °C. The external calibration was done using a polystyrene standard ( $M_{\text{P}} = 1000\text{--}115,000$  g/mol). The concentration of all samples was 5 mg/mL, and the flow rate was 1 mL/min.

Turbidimetry measurements were done using the UV-Vis spectrometer HP 8543 (Hewlett-Packard, Waldbronn, Germany). By coupling with a Peltier element HP 89090A (Hewlett-Packard, Waldbronn, Germany), controlled heating with a heating rate of 0.5 °C/min was possible. The observed wavelength was  $\lambda = 500$  nm. For all measurements in water, a 1 wt % solution of the polymer was used. Measurements in buffers were done as follows: for the poly(methoxy di(ethylene glycol)acrylates), sodium phosphate buffer (25 mmol/L), containing sodium chloride (150 mmol/L) at pH = 9.2, was used.  $T_{\text{CP}}$  was detected at 50% of transmission. The POx were measured in sodium borate buffer (50 mmol/L, pH = 9.0) as 1 wt % solutions. Only the P(*i*PrOx-*n*BuOx) copolymers were measured as 0.25 wt % solutions due to their poor solubility.  $T_{\text{CP}}$  was chosen as the onset temperature, when the first drop of the transmission was observed.

Fluorescence measurements for the fibrillation kinetics of the  $\text{A}\beta_{40}$  peptide in the absence and in the presence of the polymers were measured on a Tecan infinite M200 microplate reader (Tecan Group AG, Männedorf, Switzerland). Data were analyzed using standard protocols from the literature [53]. Thioflavin T (ThT) was used as a fibril indicator, because it shows increasing fluorescence intensity at  $\lambda = 482$  nm by binding to  $\beta$ -sheet-rich structures, such as the formed  $\text{A}\beta_{40}$  fibrils [54]. Measurements were performed in a 96-well plate. Mixtures of  $\text{A}\beta_{40}$  and the polymers were dissolved in sodium phosphate buffer (25 mmol/L) at pH 9.2, containing sodium chloride (150 mmol/L), ThT (20  $\mu\text{mol/L}$ ) and 0.01%  $\text{NaN}_3$  to prevent bacterial growth. The used concentrations were:  $\text{A}\beta_{40}$ : 230  $\mu\text{M}$ ; polymer **3a**: 196  $\mu\text{M}$ ; polymer **3b**: 113  $\mu\text{M}$ ; polymer **3c**: 260  $\mu\text{M}$ ; and polymer **6c**: 230  $\mu\text{M}$ . One hundred fifty microliters of each solution were pipetted into the wells. The temperature was 37 °C; the excitation wavelength was set to 450 nm; and the emission was measured at 485 nm every 30 min for at least three days. Two different shaking protocols were used: 30 min cycles of 5 min shaking (at a 1-mm shaking amplitude), 5 min waiting, 5 min shaking followed by the measurement (Protocol I) and 25 min and

subsequent 10 s shaking followed by the measurement (Protocol II). The fluorescence intensity was fitted using the following equation [53]:

$$I = F_1 + m_1 t + \frac{F_2 + m_2 t}{1 + e^{-[(t-t_{\text{char}})/\tau]}} \quad (1)$$

where  $t_{\text{char}}$  is the characteristic time, where the fluorescence intensity reaches half its maximum and the lag time is given by  $t_{\text{char}} - 2\tau$  with  $\tau$  as the inverse of the rate constant [53].

Thin-layer chromatography (TLC) was performed using “Merck silica gel 60” plates (Merck, Darmstadt, Germany). Spots on the TLC plate were visualized using oxidizing agent “blue” stain or UV light (254 or 366 nm). “Blue” stain was prepared as follows:  $(\text{NH}_4)_6\text{Mo}_7\text{O}_{24} \cdot 4\text{H}_2\text{O}$  (1 g) and  $\text{Ce}(\text{SO}_4)_2 \cdot 4\text{H}_2\text{O}$  (1 g) were dissolved in a mixture of distilled water (90 mL) and concentrated sulfuric acid (6 mL). Subsequent column chromatography was carried out using high purity-grade Merck 60 (230–400 mesh particle size) silica gel (Darmstadt, Germany).

### 2.3. General Procedure for the Syntheses of the Poly(methoxy di(ethylene glycol)acrylates) 3

As an example, the synthesis for a projected molecular weight of  $M_n = 3800$  g/mol is described. The reaction was carried out using a round-bottomed flask equipped with a magnetic stirrer, a rubber septum and a balloon filled with argon. Prior to the reaction, a mixture of monomer **1** (242.60 mg, 234.80  $\mu\text{L}$ , 1.39 mmol), chain transfer agent (CTA) **2** (15.10 mg, 0.063 mmol), AIBN (1.04 mg, 0.0063 mmol) and DMF (0.34 mL) was bubbled with argon for 25 min and subsequently placed into a preheated oil bath at 70 °C. The reaction was stirred for six hours before it was opened to air and cooled by means of an ice bath. The resulting bright yellow polymer was precipitated into *n*-hexane (3  $\times$  70 mL) and dried in a high vacuum within two days. The polymeric product **3** was characterized via size exclusion chromatography (SEC), matrix-assisted laser desorption/ionization mass spectrometry (MALDI-TOF MS) (for isotopic pattern simulation see Supplementary Materials, Figure S1),  $^1\text{H-NMR}$  (see Supplementary Materials, Figure S2) and turbidimetry (Table 1). Thus, the expected final polymer was obtained as truly proven via these experimental methods.

$^1\text{H-NMR}$  (400 MHz,  $\text{CDCl}_3$ ):  $\delta =$  ppm 4.83 (m, 1H<sub>a</sub>, -CH), 4.19 (s, 42H<sub>e</sub>, -CH<sub>2</sub>), 3.62 (m, 84H<sub>f,g</sub>, -CH<sub>2</sub>), 3.53 (m, 42H<sub>h</sub>, -CH<sub>2</sub>), 3.36 (m, 63H<sub>i</sub>, -CH<sub>3</sub>), 2.34 (s, 21H<sub>d</sub>, -CH), 1.92–1.41 (m, 46H<sub>c,k,l</sub>, -CH<sub>2</sub>), 1.15 (m, 3H<sub>b</sub>, -CH<sub>3</sub>), 0.93 (t, 3H<sub>m</sub>, -CH<sub>3</sub>).

### 2.4. Syntheses of the Poly(oxazolines) 6–9

Similar to known procedures [47,55], 2-isopropyl-2-oxazoline **4** (iPrOx) and 2-*n*-butyl-2-oxazoline **5** (nBuOx), served as the monomers [56] for the cationic ring-opening polymerization for the POx. Polymers **6**, **7** and **9** were all initiated with propargyl tosylate, but polymers **6** and **9** were quenched with water, whereas polymer **7** was quenched with *N,N*-diethylamine. The synthesis of polymer **8** was initiated with methyl trifluoromethanesulfonate and quenched with *N*-methylpropargylamine. Results for the characterization and the measured LCSTs for all polymers are given in Table 1 (turbidimetry, molecular weights and polydispersities). Detailed procedures for all reactions and the corresponding characterizations are given in the Supplementary Materials.

### 2.5. General Procedure for the Syntheses of the Poly(oxazolines) 6–8

2-Isopropyl-2-oxazoline (2.00 g, 2.10 mL, 17.63 mmol), dry ACN (8.81 mL) and the appropriate amount of initiator (propargyl tosylate for polymers **6** and **7**, methyl trifluoromethanesulfonate for polymer **8**) were added to a Schlenk tube, which was subsequently sealed with a rubber septum. The mixture was stirred at room temperature for one hour and consecutively for 48 h at 80 °C. Living chain ends were quenched by the addition of the respective quencher (**6**: water; **7**: *N,N*-diethylamine; **8**: *N*-methylpropargylamine) and further stirring for 24 h at 60 °C. After evaporation of the solvent, the residue was dissolved in dichloromethane DCM (5.0 mL) and was extracted with water (5  $\times$  30.0 mL). The combined aqueous phases were back extracted using DCM (10  $\times$  30.0 mL). Subsequently, the

organic phases were combined and dried over sodium sulfate. After filtration, most of the solvent was removed, and the remaining viscous solution was precipitated three times in a cold mixture of diethyl ether/*n*-hexane (1:1) to obtain the pure polymer. A representative <sup>1</sup>H-NMR spectrum is given in the Supplementary Materials for polymers **6**, **7** and **8** (Figures S3–S5).

<sup>1</sup>H-NMR (400 MHz, CDCl<sub>3</sub>, 27 °C): δ (ppm) = 4.09 (s, 2H, H<sub>4</sub>), 3.76–3.26 (m, CH<sub>2</sub> of the repetitive unit), 3.01–2.55 (m, CH of the repetitive unit), 1.09 (s, CH<sub>3</sub> of the repetitive unit).

### 2.6. General Procedure for the Syntheses of Poly(2-isopropyl-2-oxazoline-*grad*-2-*n*-butyl-2-oxazoline) **9**

The procedure was done as described for the homopolymerization of 2-isopropyl-oxazoline. A mixture of 2-isopropyl-2-oxazoline (0.54 mL, 0.51 g, 4.50 mmol), 2-*n*-butyl-oxazoline (63.60 mg, 0.50 mmol), propargyl tosylate (50.86 μL, 61.80 mg, 0.29 mmol) and ACN (2.50 mL) was stirred for one hour at room temperature in a Schlenk tube. After stirring for 48 h at 80 °C, the reaction was quenched by the addition of water (20.90 μL, 20.90 mg, 1.16 mmol). The reaction was stirred for a further 24 h at 60 °C, and the work-up was done as described for the poly(2-isopropyl-2-oxazoline). A representative <sup>1</sup>H-NMR spectrum is given in the Supplementary Materials (Figure S6), as well as a table with full characterization of the synthesized copolymers (initial monomer ratio, molecular weight as determined from <sup>1</sup>H-NMR and GPC, polydispersity index (PDI) and copolymer composition as determined from <sup>1</sup>H-NMR) (Table S1).

<sup>1</sup>H-NMR (400 MHz, CDCl<sub>3</sub>, 27 °C): δ (ppm) = 4.03 (s, 2H, H<sub>9</sub>), 3.50–3.25 (m, CH<sub>2</sub> of the repetitive unit, H<sub>1</sub> + H<sub>4</sub>), 2.90–2.50 (m, CH of the repetitive unit), 2.32–2.15 (m, CH<sub>2</sub> of the repetitive unit, H<sub>5</sub>), 1.50 (s, CH<sub>2</sub> of the repetitive unit, H<sub>6</sub>), 1.25 (s, CH<sub>2</sub> of the repetitive unit, H<sub>7</sub>), 1.02 (s, CH<sub>3</sub> of the repetitive unit, H<sub>3</sub>), 0.82 (s, CH<sub>3</sub> of the repetitive unit, H<sub>8</sub>).

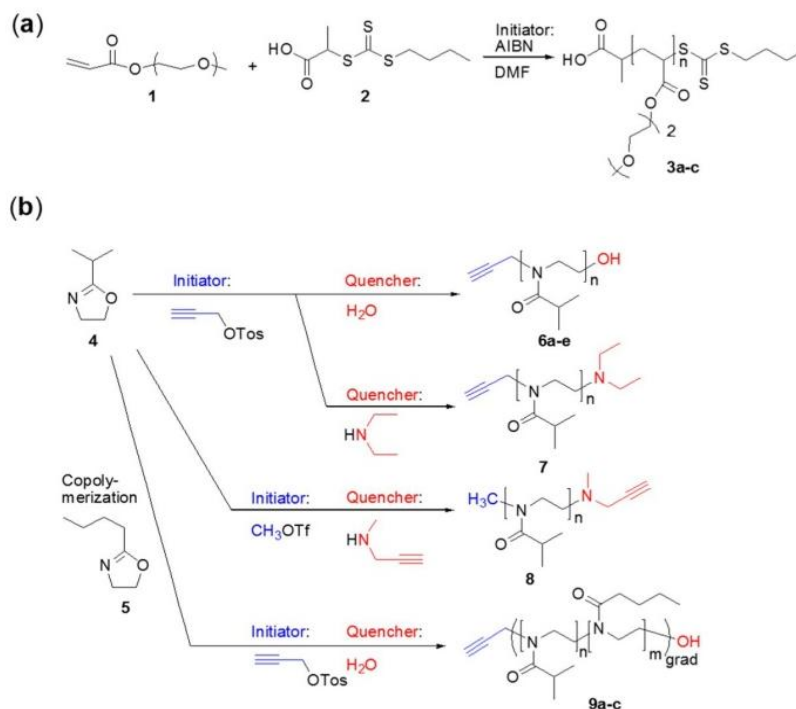
## 3. Results and Discussion

### 3.1. Syntheses of the Polymers

We synthesized two different polymers, both displaying an LCST (see Scheme 1a,b): on the one hand, poly(methoxy di(ethylene glycol)acrylates) **3a–c** were prepared by reversible addition-fragmentation chain-transfer polymerization (RAFT) [57,58] starting from methoxy di(ethylene glycol)acrylate **1** [59] and a chain transfer agent (CTA) (2-(*n*-butyltrithiocarbonylthio) propionic acid **2** [60]) with AIBN as the initiator. The molar ratio between monomer:CTA:AIBN (**3a**: 22:1:0.1; **3b**: 50:1:0.1; **3c**: 90:1:0.1) was used to adjust the intended molecular weight, generating polymers with an LCST varying from ~34–45 °C, whereas the poly(oxazolines) **6–9** were designed as homo- and co-polymers, thus addressing a wide range of different LCSTs and molecular weights via living cationic ring-opening polymerization.

As a representative example, the MALDI-TOF of polymer **3a** is shown in Figure 2, displaying three different series (Series S1–S3), corresponding to the repeating unit (difference ~174 Da) and different types of attached ions. The first series at 3047.179 Da can be assigned to poly(methoxy di(ethylene glycol)acrylate) with a formula of [HOCC<sub>2</sub>H<sub>4</sub>(C<sub>8</sub>H<sub>14</sub>O<sub>4</sub>)<sub>16</sub>S<sub>3</sub>C<sub>5</sub>H<sub>9</sub>]<sup>Na</sup><sup>+</sup>. The main signal of the multiplet chosen for Series S2, which appears at 3069.360 Da, can be assigned to [NaOCC<sub>2</sub>H<sub>4</sub>(C<sub>8</sub>H<sub>14</sub>O<sub>4</sub>)<sub>16</sub>S<sub>3</sub>C<sub>5</sub>H<sub>9</sub>]<sup>Na</sup><sup>+</sup>, whereas the minor Series S3 appears at 3084.645 Da and is assigned to the polymer with the formula of [NaOCC<sub>2</sub>H<sub>4</sub>(C<sub>8</sub>H<sub>14</sub>O<sub>4</sub>)<sub>16</sub>S<sub>3</sub>C<sub>5</sub>H<sub>9</sub>]<sup>K</sup><sup>+</sup>. For simulation of the isotopic pattern, check the Supplementary Materials (Figure S1).

Further characterization via NMR spectroscopy is shown in the Supplementary Materials (Figure S2), finally proving both the end groups and the true structure of polymer **3**. Similarly, the poly(oxazolines) **6–9** were characterized via NMR spectroscopy and GPC (see Supplementary Materials Figures S3–S6).



**Scheme 1.** Synthetic pathway for the thermoresponsive polymers that were used for the LCST and fibrillation measurements: (a) preparation of poly(methoxy di(ethylene glycol)acrylates) **3**; (b) preparation of the poly(2-isopropyl-2-oxazoline) homopolymers **6–8** (using different initiation and quenching methods) and the poly(2-isopropyl-2-oxazoline-*grad*-2-*n*-butyl-2-oxazoline) copolymers **9** ( $n = 9–11$ ;  $m = 3–6$ ).

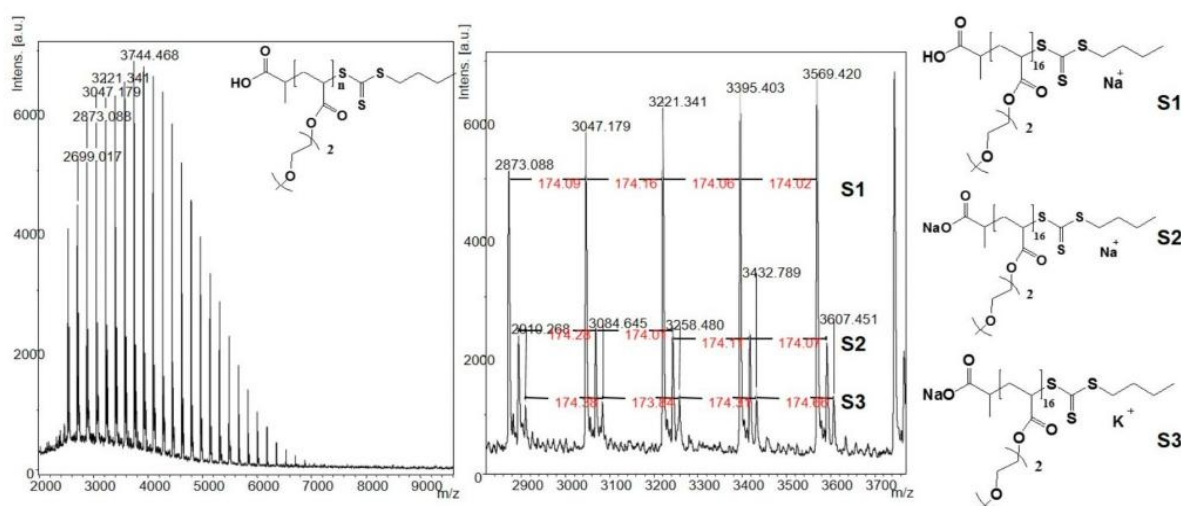


**Figure 2.** MALDI-TOF spectrum of poly(methoxy di(ethylene glycol)acrylate) (**3a**). S1, Series 1.

### 3.2. Turbidimetry of the Polymers **3**, **6–9**

In preparation of the subsequent fibrillation experiments (amyloid aggregation in the presence of polymers), first-hand experimental information on the LCST influence of the molecular weight and the addition of salts (buffer solutions are required for respective fibrillation conditions), the concentration of the polymer via appropriate extensive turbidimetric measurements was accomplished.

literature [41,42,47,50], followed by poly(methoxy diethylene glycol)acrylate, which is less intensely studied in the literature [45,61,62]. The results of the turbidimetric measurements are given in Table 1.

**Table 1.** Measured  $T_{CP}$  for the synthesized poly(methoxy diethylene glycol)acrylates (3), poly(2-isopropyl-2-oxazoline) (PiPrOx) (6–8) and P(iPrOx-*n*BuOx) (9) in sodium borate buffer and in water. For the homopolymers, 1 wt % solutions were used, whereas for the copolymers, 0.25 wt % solutions were used due to poor solubility in water. The samples were heated at a rate of 0.5 K/min. PDI = Polydispersity Index

Polymer	$n_{NMR}^1$ (4)	$n_{NMR}^1$ (5)	$M_{NMR}$ (g/mol)	$M_{GPC}$ (g/mol)	PDI	$T_{CP}$ (°C) (Sodium borate buffer)	$T_{CP}$ (°C) (H <sub>2</sub> O)
3a	–	–	3,600	2,700	1.1	– <sup>4,5</sup>	34.4
3b	–	–	8,500	6,600	1.2	52.7 <sup>4</sup>	40.4
3c	–	–	14,600	13,700	1.2	49.5 <sup>4</sup>	45.1
6a	1	–	1,600 <sup>2</sup>	2,600 <sup>3</sup>	1.2	43.6	47.5
7	1	–	2,000 <sup>2</sup>	3,100 <sup>3</sup>	1.1	42.6	43.4
6b	1	–	4,300 <sup>2</sup>	4,200 <sup>3</sup>	1.3	40.1	42.3
6c	1	–	5,600 <sup>2</sup>	11,000 <sup>3</sup>	2.0	32.2 <sup>6</sup> (36.2) <sup>4</sup>	36.4 <sup>6</sup>
6d	1	–	2,800 <sup>2</sup>	7,400 <sup>3</sup>	1.9	31.1/36.5 <sup>6</sup>	37.8 <sup>6</sup>
6e	1	–	2,300 <sup>2</sup>	6,200 <sup>3</sup>	2.0	37.6 <sup>6</sup>	38.1 <sup>6</sup>
8	1	–	5,200 <sup>2</sup>	3,000 <sup>3</sup>	1.3 <sup>7</sup>	49.8	46.5
9a	0.79	0.21	1,700 <sup>2</sup>	3,600 <sup>3</sup>	1.3	24.9	27.2
9b	0.80	0.20	1,600 <sup>2</sup>	3,600 <sup>3</sup>	1.3	24.7	25.7
9c	0.61	0.39	1,700 <sup>2</sup>	4,200 <sup>3</sup>	1.4	14.2	15.3

<sup>1</sup> Ratios of the monomers (4 and 5) within the copolymers as calculated from <sup>1</sup>H-NMR; <sup>2</sup> the <sup>1</sup>H-NMR signal from the methylene group next to the alkyne group at  $\delta = 4.05$  ppm was used as a reference for polymers 6, 7 and 9, whereas for polymer 8, the signal from the methyl-initiator group at  $\delta = 3.05$  ppm was used; <sup>3</sup> measured in DMF with polystyrene ( $M_p = 1000$ – $115,000$  g/mol) as the standard; <sup>4</sup> sodium phosphate buffer (pH = 9.2, 150 mmol NaCl) was used instead with a polymer concentration of 230  $\mu$ mol/L; <sup>5</sup> no LCST detectable under the used conditions; <sup>6</sup> due to the higher PDI, the drop in transmission is much less pronounced in comparison to the other samples; polymer 6d exhibits two LCSTs when measured in buffer solution; this might be due to its relatively high polydispersity; <sup>7</sup> bimodal distribution according to GPC.

For the PiPrOx polymers (6, 7 and 8), the same influence of the molecular weight on the LCST was found as described in the literature [46,55,63]. Thus, an increase in the molecular weight led to a decrease of the LCST. By varying the molecular weight, it was possible to tune the LCST in a range of  $\pm 5$  K. PiPrOx 6a with a molecular weight of 2600 g/mol (GPC) exhibits an LCST of 47.5 °C (in H<sub>2</sub>O), whereas PiPrOx 6c with a molecular weight of 11,000 g/mol (GPC) displays an LCST of 36.4 °C (in H<sub>2</sub>O). The measured curves of some of the PiPrOx are shown in Figure 3a and illustrate the influence of the molecular weight on the LCST.

A significant influence of the used buffer on the LCST was observed when changing to sodium borate buffer as the solvent (required for the amyloid fibrillation assays; 50 mmol/L, pH = 9.0), as the presence of the sodium borate provoked a decrease of the LCST in the range of 1–4 °C, except for polymer 8. As the ions in the buffer are able to weaken the hydrogen bonds between the polymer chains and water molecules, the release of water is facilitated, consequently shifting the LCST to lower temperatures (salting out effect). Figure 3b exemplary shows the measured curves for the polymer 6a in pure water and in sodium borate buffer as a comparison.

Furthermore, the concentration dependency of the LCST was measured for polymer 7 in the range from 0.25–1.5 wt % in water. The results are presented in the Supplementary Materials (Table S2), and the measured curves are shown in Figure 3c. For the lowest concentration (0.25 wt %), an LCST of 48.2 °C and for the highest concentration (1.5 wt %) an LCST of 41.3 °C were measured. Apparently, a change of the concentration by 0.25 wt % has a significant effect on the LCST, especially at lower concentrations.

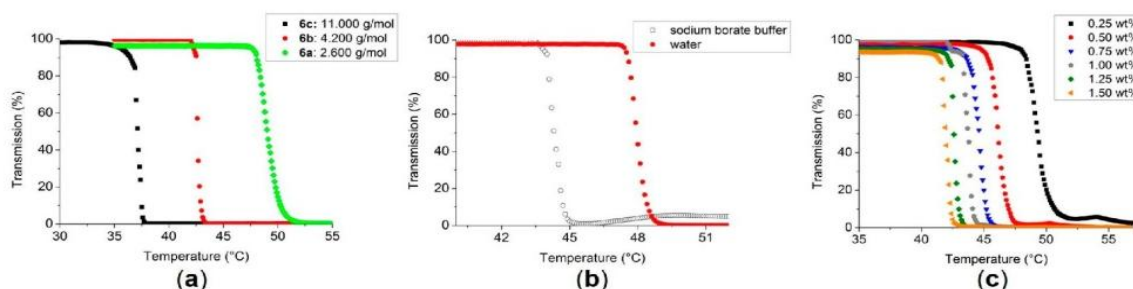


**Figure 3.** LCST measurements for the POx as 1 wt % solutions: (a) influence of the molecular weight for the polymers **6a**, **6b** and **6c**; with an increasing molecular weight, the LCST is decreasing; (b) sodium borate (50 mmol/L, pH = 9.0) decreases the LCST of PiPrOx **6a** (2600 g/mol) by nearly 4 K from 47.5 down to 43.6 °C; the curve with the filled symbols (red) refers to a measurement in water, whereas the curve with the open symbols (black) refers to a measurement in buffer; (c) with an increasing concentration, the LCST for polymer **7** (3100 g/mol) is shifted to lower values and can be tuned between 48.2 °C (0.25 wt %) and 41.3 °C (1.50 wt %) within the tested concentration range.

As expected, the copolymerization with the more hydrophobic *n*BuOx resulted in a decrease of the LCST as described in the literature [47]. Because of the high amount of *n*BuOx from 21%–35%, the LCST was reduced to 27.2 and 15.3 °C respectively, illustrating the strong influence of the hydrophilic/hydrophobic ratio of a polymer on its LCST. By measuring the samples in sodium borate buffer, the LCST could be further decreased to 14.2 °C (see Supplementary Materials, Figure S7).

In a similar manner, LCST data were obtained via turbidimetric measurements for the polyacrylates **3** as explained in the experimental part, showing the same unexpected influence of the molecular weight on the LCST as described in the literature [59,61,62] (see Table 1). Thus, LCSTs ranging from 34.4 °C (polymer **3a**) to 45.1 °C (polymer **3c**) could be determined, demonstrating a strong increase of the  $T_{CP}$  with increasing molecular weight [62].

Upon determining the LCST in sodium phosphate buffer at pH = 9.2, keeping the polymer concentration at 230  $\mu$ M, polymer **3a** does not display an LCST under the applied conditions (measurement range = 25–70 °C). Cloud point temperatures of samples **3b** and **3c** were detected at 52.7 °C (40.4 °C in water) and 49.5 °C (45.1 °C in water), indicating that the addition of ions stabilize the macromolecules in solution, however with a less pronounced effect for higher molecular weights (**3b**:  $\Delta T_{CP}$  = 12.3 °C; **3c**:  $\Delta T_{CP}$  = 4.4 °C) (see Supplementary Materials for details on the measured curves, Figures S8 and S9).

### 3.3. Fibrillation of A $\beta$ <sub>40</sub> in the Presence of Polymers **6** and **3**

The choice of the polymers for the amyloid fibrillation measurements was based on the reverse thermoresponsive behavior of the POx and polyacrylates. These polymers are water and buffer soluble, and the  $T_{CP}$  could be adjusted over a wide range of temperatures. Polyacrylates **3a**, **3b** and **3c** (displaying molecular weights below and above the molecular weight of A $\beta$ <sub>40</sub>) serve as a good selection for the A $\beta$  aggregation studies due to the different LCSTs. PiPrOx **6c** was chosen due to the molecular weight of the polymers **3c** and **6c** being close to each other (14,600 g/mol and 11,000 g/mol, respectively), thus probing whether there is an influence on the fibrillation of the A $\beta$ <sub>40</sub> due to the structural differences of the polymers.

Upon addition of an LCST-type polymer to an aggregating amyloid, a number of possible scenarios can be considered. Thus, by mixing of the polymer with the A $\beta$  protein, the polymer can either inhibit or enhance fibrillation, as observed before [36]. At  $T < T_{LCST}$  and a concentration  $C_{amyloid} < C_{polymer}$ , the amyloid could evenly distribute within the polymer phase, in turn preventing the amyloid/amyloid contact formation and, thus, reducing or even eliminating fibrillation. At a concentration  $C_{amyloid} < C_{polymer}$ , the polymer could also form a protective layer around the native

proteins, and at  $C_{\text{amyloid}} > C_{\text{polymer}}$ , the polymer might boost the fibrillation by acting as a catalytic surface. If present above its LCST, several scenarios are possible, e.g., that the polymer can hinder the fibrillation of the amyloid by evenly binding the native proteins to its surface and therefore preventing the formation of bigger oligomers or alternatively accelerating the fibrillation by acting as a seed.

### 3.3.1. Effect of Poly(oxazolines) on $A\beta_{40}$ Aggregation

For the first fibrillation measurements, equimolar amounts of  $A\beta_{40}$  (wild-type, WT) and the corresponding polymer were dissolved in sodium phosphate buffer (25 mM, pH = 9.2, containing 150 mM NaCl) at a concentration of 230  $\mu\text{mol/L}$  for both  $A\beta_{40}$  and the polymer. Tracking of the fibril growth was done by using the fluorescence dye thioflavin T (ThT) (20  $\mu\text{mol/L}$ ), as ThT binds to  $\beta$ -sheet-rich structures showing an increasing fluorescence at  $\lambda = 482$  nm, which in turn allows the measurement of the kinetics of the fibril growth [54]. Measurements were done at 37  $^{\circ}\text{C}$  using a well plate, which allowed the triple measurement of each sample simultaneously (Protocol I, see Methods). The time-dependent development of the ThT at  $\lambda = 482$  nm is shown in Figure 4. Upon the addition of PiPrOx 6c,  $A\beta_{40}$  shows a significantly increased fluorescence (Trace b), indicative of fibril formation with a characteristic time  $t_{\text{char}} = 4.5$  h in the presence of polymer 6c. To exclude interactions between the polymer and ThT, the fluorescence of the pure PiPrOx in buffer solution in the absence of  $A\beta_{40}$  was measured as a control experiment (Trace c), in turn excluding nonspecific ThT/PiPrOx (6c) interactions. For a comparison, the time-dependent development for the ThT fluorescence at  $\lambda = 482$  nm for WT  $A\beta_{40}$  is given in the figure (Trace a), indicating a characteristic time for fibrillation of  $A\beta_{40}$  of  $t_{\text{char}} = 6.4$  h.

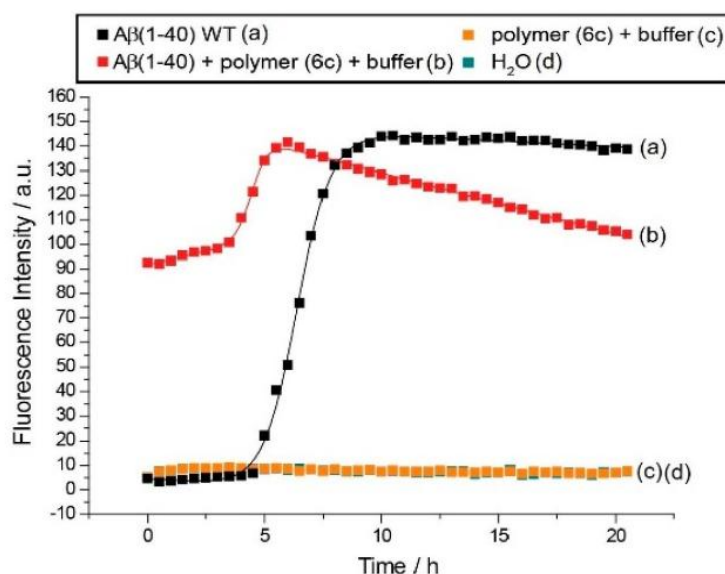


**Figure 4.** Thioflavin T fluorescence intensity of the  $A\beta_{40}$ /polymer (6c) mixture (b) compared to WT  $A\beta_{40}$  (a) and the pure polymer (6c) (c) in buffer solution, as well as pure water (d). Both the characteristic and lag time are shortened for the peptide/polymer mixture compared to WT  $A\beta_{40}$  fibrillation kinetics. The characteristic time, which reports the time at which half the fluorescence maximum is reached, decreases from 6.4 down to 4.5 h, and the lag time is reduced from 4.9 down to 3.7 h. The higher initial thioflavin T (ThT) fluorescence of  $A\beta_{40}$  in the presence of 6c (b) could be related to an initial nucleation that was too fast to be recorded in our experimental setup. The observed decrease of the fluorescence after  $t = 5$  h (b) often is the result of the precipitation of the sample.

Thus, the faster fibril growth upon the addition of polymer 6c can be attributed to a shortening of the lag phase of fibrillation. As under the used conditions the LCST of 6c was 36.2  $^{\circ}\text{C}$ , the polymer

was above its LCST and consequently precipitated during the measurement, in turn acting as a seed for the A $\beta$ <sub>40</sub> monomers and favoring oligomerization.

### 3.3.2. Effect of Poly(methoxy di(ethylene glycol)acrylates) on A $\beta$ <sub>40</sub> Fibrillation

Measuring amyloid aggregation via the ThT fluorescence assay (Protocol II, see Methods) in the presence of the acrylates **3a**, **3b** and **3c** was accomplished in 230  $\mu$ M A $\beta$ <sub>40</sub> buffered solutions, mixing with buffered solutions of the polymers with different chain lengths and concentrations (Figure 5). In all cases, the lag time was reduced, and the saturation phase of fibrillation was achieved more quickly. Furthermore, the slope of all three aggregation curves became steeper, in comparison to WT A $\beta$ <sub>40</sub>, implying that the presence of the polymer is boosting the protein fibrillation and enhancing secondary nucleation and the elongation rates.

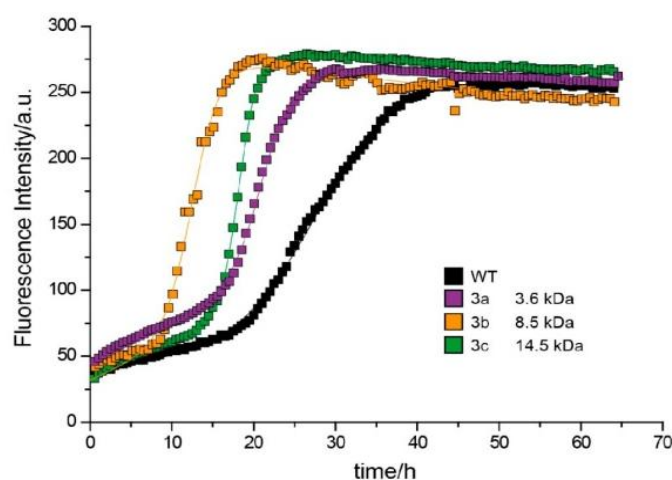


**Figure 5.** Time-dependent evolution of the ThT fluorescence intensity at  $\lambda = 482$  nm of the polymer/A $\beta$ <sub>40</sub> mixtures. For polymers **3b** and **3c**, the lag phase is shortened, while for polymer **3a**, the lag phase is increased by one hour from  $t = 18.3$  h (for pure A $\beta$ <sub>40</sub>) to  $t = 19.3$  h.

Remarkably, the duration of the lag phase seems to be decreased in the case of the polymers **3b** and **3c**, but slightly increased from  $t = 18.3$  h to  $t = 19.3$  h in the case of the polymer **3a**, indicating that polymer **3a**, having the closest molecular weight compared to the A $\beta$ <sub>40</sub> ( $\sim 4300$  g/mol), is able to interact with the native protein interfering with the primary nucleation process. This phenomenon is extremely interesting due to the prospective control over the A $\beta$ <sub>40</sub> fibrillation upon the change of the molecular weight or the concentration of the polymer and will be studied in detail in the upcoming publications. Nevertheless, the WT A $\beta$ <sub>40</sub> peptide shows the longest characteristic times compared to the peptide/polymer mixtures.

The summarized values for the *PiPrOx*, as well as for the poly(methoxy di(ethylene glycol)acrylates) are given in Table 2, as well as the cloud points for those polymers under the conditions that were used for the fibrillation experiments.

### 3.3.3. Discussion of A $\beta$ <sub>40</sub> Aggregation Experiments

The influence of polymers, such as neutral polymers [36], polyelectrolytes [36], dendrimers [11,24,25] or polymeric nanoparticles [26–28], on amyloid aggregation has been studied. Often, retarding effects on the fibrillation of A $\beta$  have been observed. Amyloid formation has been found to be promoted by glycosaminoglycans [64] and positively-charged polymers, such as poly(diallyldimethylammonium chloride) (PDDA), poly(ethylenimine) (PEI) and poly(lysine) hydrobromide [36]. Most relevant to our situation is the study by Assarsson *et al.*, in which the effect of charged polymers and polyamino acids on the A $\beta$  fibril formation was studied [36]. While an accelerating effect of all positively-charged

polyelectrolytes on A $\beta$  fibril formation was found, neutral (poly(threonine)) and negatively-charged polymers poly(acrylic acid sodium salt) (PAA) and poly-glutamic acid sodium salt did not interfere with the kinetics of A $\beta$  fibrillation. In contrast, all neutral polymers investigated in our study also accelerated the fibrillation kinetics of A $\beta_{40}$ . In agreement with the aforementioned results, the lag time of A $\beta$  fibril formation decreased, and the growth phase showed a steeper slope. This is akin to the situation where the A $\beta$  concentration is systematically increased [65].

**Table 2.** Measured data for the fibrillation kinetics of the A $\beta_{40}$  fibrillation in the presence of the polymers **3a**, **3b**, **3c** (Fluorescence Protocol II) and **6c** (Fluorescence Protocol I, see Methods) at 37 °C. The characteristic time and lag time vary between the different protocols, as shaking times varied between the two protocols. Shaking increases the probability of molecular contacts, thus enhancing aggregation.

Name	$T_{CP}$ (°C)	WT concentration <sup>1</sup>	Mn (kDa)	Polymer concentration <sup>1</sup>	$t_{char}$ (h)	$t_{lag}$ (h)	Kinetic protocol
A $\beta_{40}$ WT	–	230 $\mu$ M	4.3	0	27.9 h	18.3 h	II
<b>3c</b>	49.5 <sup>1</sup>	230 $\mu$ M	14.6	260 $\mu$ M	18.3 h	15.9 h	II
<b>3b</b>	52.7 <sup>1</sup>	230 $\mu$ M	8.5	113 $\mu$ M	12.5 h	9.1 h	II
<b>3a</b>	– <sup>1,2</sup>	230 $\mu$ M	3.6	196 $\mu$ M	21.1 h	19.3 h	II
A $\beta_{40}$ WT	–	230 $\mu$ M	4.3	0	6.4 h	4.9 h	I
<b>6c</b>	36.2	230 $\mu$ M	11.0	230 $\mu$ M	4.5 h	3.7 h	I

<sup>1</sup> Cloud points were determined in sodium phosphate buffer (pH = 9.2, 150 mmol NaCl) with a polymer concentration of 230  $\mu$ mol/L; <sup>2</sup> no LCST detectable under the used conditions.

It should finally be mentioned that the concentration of the polymers added to the A $\beta$  preparations is too low to influence the A $\beta$  fibrillation by crowding through excluded volume effects. However, somehow, it is likely that the presence of the polymer leads to an increase in the local A $\beta$  concentration, which favors nucleation of the peptide and leads to the observed increased fibrillation kinetics.

#### 4. Conclusions

Amyloid aggregation was studied in the presence of hydrophilic polymers, able to display an LCST in the range between 35 and 45 °C. For this effect, we have synthetically prepared a large number of hydrophilic polymers, adjusting the LCST to 35–45 °C by either homo- or co-polymerization. Poly(oxazolines) **6–9**, prepared via cationic ring opening polymerization, served as one class of hydrophilic polymer, whereas poly(methoxy di(ethylene glycol)acrylates) **3a–3c** prepared via RAFT polymerization were the second class of polymers. For all polymers, a significant influence of the end groups, as well as the molecular weight on the final LCSTs was observed, restricting the investigations to a total of four polymers (the acrylates **3a**, **3b** and **3c**, as well as the poly(oxazoline) **6c**) for the amyloid-fibrillation experiments. Furthermore, the used buffers did show a significant influence on the LCSTs of the polymer in solution, with a significant increase in the case of the poly(acrylates) **3b** and **3c** and a decrease in the case of the poly(oxazoline) **6c**. The polymers (**6c**, **3b**, **3c**) do show a reduction of the lag time of amyloid-aggregation, indicative of an enhanced fibrillation. Although one polymer **3a** did not show an LCST in the used buffer solution, an increase of the lag time of the fibril formation from 18.34–19.33 h was observed.

In summary, several factors can be considered as being influential for the polymer/amyloid aggregation in the current system: (1) enhanced nucleation due to A $\beta$ -cluster formation at the polymer chains at temperatures below the LCST [36,66]; (2) steric shielding of the amyloids as a consequence of polymer adsorption (polymers **3a**, **3b** and **3c**) [15,30–32]; (3) enhanced nucleation of amyloid aggregation via the formed polymer particles at temperatures above the LCST (polymer **6c**) [3,27]. Among the discussed possibilities, the enhanced nucleation by all of the used polymers seems the most probable scenario, as in all cases, fibrillation of the amyloids is enhanced, irrespective of their chemical or physical nature. Research is proceeding in this direction, as currently, other mechanisms cannot be ruled out.

**Supplementary Materials:** The following are available online at [www.mdpi.com/2073-4360/8/5/178/s1](http://www.mdpi.com/2073-4360/8/5/178/s1). Figure S1: MALDI of **3a**, Figure S2:  $^1\text{H-NMR}$  spectrum of **3a**, Figure S3:  $^1\text{H-NMR}$  spectrum of propargyl-initiated PiPrOx **6a**, Figure S4:  $^1\text{H-NMR}$  spectrum of propargyl-initiated PiPrOx **7**, Figure S5:  $^1\text{H-NMR}$  spectrum of methyl-initiated PiPrOx **8**, Figure S6:  $^1\text{H-NMR}$  spectrum of P(*n*BuOx-*grad*-iPrOx) **9**, Table S1: Characterization of P(*n*BuOx-*grad*-iPrOx) copolymers **9**, Table S2: Concentration dependency of the LCST for PiPrOx **7**, Figure S7: LCST curves for the P(*n*BuOx-*grad*-iPrOx) copolymers **9** (in buffer), Figure S8: Molecular weight dependency of the LCST for poly(methoxy di(ethylene glycol)acrylates) **3** (in water), Figure S9: Molecular weight dependency of the LCST for poly(methoxy di(ethylene glycol)acrylates) **3** (in buffer).

**Acknowledgments:** We acknowledge funding from the SFB Transregio 102 “Polymers under multiple constraints”, Projects A03 and A06.

**Author Contributions:** Zhanna Evgrafova and Sebastian Funtan have prepared all of the polymers, performed all LCST experiments and did the polymer characterization. Juliane Adler did the amyloid-aggregation assays. Wolfgang H. Binder and Daniel Huster designed the research, analyzed the data and wrote the paper.

**Conflicts of Interest:** The authors declare no conflict of interest.

## References

1. Chiti, F.; Dobson, C.M. Protein misfolding, functional amyloid, and human disease. *Annu. Rev. Biochem.* **2006**, *75*, 333–366. [[CrossRef](#)] [[PubMed](#)]
2. Hamley, I.W. Peptide fibrillization. *Angew. Chem. Int. Ed.* **2007**, *46*, 8128–8147. [[CrossRef](#)] [[PubMed](#)]
3. Hamley, I.W. The amyloid beta peptide: A chemist’s perspective. Role in alzheimer’s and fibrillization. *Chem. Rev.* **2012**, *112*, 5147–5192. [[CrossRef](#)] [[PubMed](#)]
4. Sgarbossa, A. Natural biomolecules and protein aggregation: Emerging strategies against amyloidogenesis. *Int. J. Mol. Sci.* **2012**. [[CrossRef](#)] [[PubMed](#)]
5. Arosio, P.; Cukalevski, R.; Frohm, B.; Knowles, T.P.J.; Linse, S. Quantification of the concentration of a $\beta$ 42 propagons during the lag phase by an amyloid chain reaction assay. *J. Am. Chem. Soc.* **2014**, *136*, 219–225. [[CrossRef](#)] [[PubMed](#)]
6. Meisl, G.; Yang, X.; Hellstrand, E.; Frohm, B.; Kirkegaard, J.B.; Cohen, S.I.A.; Dobson, C.M.; Linse, S.; Knowles, T.P.J. Differences in nucleation behavior underlie the contrasting aggregation kinetics of the A $\beta$ 40 and A $\beta$ 42 peptides. *Proc. Natl. Acad. Sci. USA* **2014**, *111*, 9384–9389. [[CrossRef](#)] [[PubMed](#)]
7. Sackler, A.M. *Self-Perpetuating Structural States in Biology, Disease, and Genetics*; National Academy of Sciences: Washington, DC, USA, 2002.
8. Adamcik, J.; Mezzenga, R. Proteins fibrils from a polymer physics perspective. *Macromolecules* **2012**, *45*, 1137–1150. [[CrossRef](#)]
9. Scheidt, H.A.; Morgado, I.; Rothmund, S.; Huster, D.; Fändrich, M. Solid-state NMR spectroscopic investigation of A $\beta$  protofibrils: Implication of a  $\beta$ -sheet remodeling upon maturation into terminal amyloid fibrils. *Angew. Chem. Int. Ed.* **2011**, *50*, 2837–2840. [[CrossRef](#)] [[PubMed](#)]
10. Chimon, S.; Shaibat, M.A.; Jones, C.R.; Calero, D.C.; Aizezi, B.; Ishii, Y. Evidence of fibril-like  $\beta$ -sheet structures in a neurotoxic amyloid intermediate of Alzheimer’s  $\beta$ -amyloid. *Nat. Struct. Mol. Biol.* **2007**, *14*, 1157–1164. [[CrossRef](#)] [[PubMed](#)]
11. Klajnert, B.; Cortijo-Arellano, M.; Cladera, J.; Bryszewska, M. Influence of dendrimer’s structure on its activity against amyloid fibril formation. *Biochem. Biophys. Res. Commun.* **2006**, *345*, 21–28. [[CrossRef](#)] [[PubMed](#)]
12. Ferrone, F.A.; Hofrichter, J.; Eaton, W.A. Kinetics of sickle hemoglobin polymerization: I. Studies using temperature-jump and laser photolysis techniques. *J. Mol. Biol.* **1985**, *183*, 591–610. [[CrossRef](#)]
13. Ferrone, F.A.; Hofrichter, J.; Eaton, W.A. Kinetics of sickle hemoglobin polymerization: II. A double nucleation mechanism. *J. Mol. Biol.* **1985**, *183*, 611–631. [[CrossRef](#)]
14. Cohen, S.I.A.; Vendruscolo, M.; Dobson, C.M.; Knowles, T.P.J. From macroscopic measurements to microscopic mechanisms of protein aggregation. *J. Mol. Biol.* **2012**, *421*, 160–171. [[CrossRef](#)] [[PubMed](#)]
15. Cohen, S.I.A.; Arosio, P.; Presto, J.; Kurudenkandy, F.R.; Biverstål, H.; Dolfe, L.; Dunning, C.; Yang, X.; Frohm, B.; Vendruscolo, M.; *et al.* A molecular chaperone breaks the catalytic cycle that generates toxic A $\beta$  oligomers. *Nat. Struct. Mol. Biol.* **2015**, *22*, 207–213. [[CrossRef](#)] [[PubMed](#)]

16. Necula, M.; Kaye, R.; Milton, S.; Glabe, C.G. Small molecule inhibitors of aggregation indicate that amyloid  $\beta$  oligomerization and fibrillization pathways are independent and distinct. *J. Biol. Chem.* **2007**, *282*, 10311–10324. [[CrossRef](#)] [[PubMed](#)]
17. Hård, T.; Lendel, C. Inhibition of amyloid formation. *J. Mol. Biol.* **2012**, *421*, 441–465. [[CrossRef](#)] [[PubMed](#)]
18. Hoyer, W.; Grönwall, C.; Jonsson, A.; Ståhl, S.; Hård, T. Stabilization of a  $\beta$ -hairpin in monomeric alzheimer's amyloid- $\beta$  peptide inhibits amyloid formation. *Proc. Natl. Acad. Sci. USA* **2008**, *105*, 5099–5104. [[CrossRef](#)] [[PubMed](#)]
19. Madine, J.; Doig, A.J.; Middleton, D.A. Design of an n-methylated peptide inhibitor of  $\alpha$ -synuclein aggregation guided by solid-state NMR. *J. Am. Chem. Soc.* **2008**, *130*, 7873–7881. [[CrossRef](#)] [[PubMed](#)]
20. Stanyon, H.F.; Viles, J.H. Human serum albumin can regulate amyloid- $\beta$  peptide fiber growth in the brain interstitium: Implications for Alzheimer disease. *J. Biol. Chem.* **2012**, *287*, 28163–28168. [[CrossRef](#)] [[PubMed](#)]
21. Assarsson, A.; Hellstrand, E.; Cabaleiro-Lago, C.; Linse, S. Charge dependent retardation of amyloid  $\beta$  aggregation by hydrophilic proteins. *ACS Chem. Neurosci.* **2014**, *5*, 266–274. [[CrossRef](#)] [[PubMed](#)]
22. Nguyen, K.V.; Gendrault, J.-L.; Wolff, C.-M. Poly-L-lysine dissolves fibrillar aggregation of the alzheimer  $\beta$ -amyloid peptide *in vitro*. *Biochem. Biophys. Res. Commun.* **2002**, *291*, 764–768. [[CrossRef](#)] [[PubMed](#)]
23. Klajnert, B.; Cladera, J.; Bryszewska, M. Molecular interactions of dendrimers with amyloid peptides: pH dependence. *Biomacromolecules* **2006**, *7*, 2186–2191. [[CrossRef](#)] [[PubMed](#)]
24. Heegaard, P.M.H.; Boas, U.; Otzen, D.E. Dendrimer effects on peptide and protein fibrillation. *Macromol. Biosci.* **2007**, *7*, 1047–1059. [[CrossRef](#)] [[PubMed](#)]
25. Cabaleiro-Lago, C.; Quinlan-Pluck, F.; Lynch, I.; Lindman, S.; Minogue, A.M.; Thulin, E.; Walsh, D.M.; Dawson, K.A.; Linse, S. Inhibition of amyloid  $\beta$  protein fibrillation by polymeric nanoparticles. *J. Am. Chem. Soc.* **2008**, *130*, 15437–15443. [[CrossRef](#)] [[PubMed](#)]
26. Cabaleiro-Lago, C.; Quinlan-Pluck, F.; Lynch, I.; Dawson, K.A.; Linse, S. Dual effect of amino modified polystyrene nanoparticles on amyloid  $\beta$  protein fibrillation. *ACS Chem. Neurosci.* **2010**, *1*, 279–287. [[CrossRef](#)] [[PubMed](#)]
27. Skaat, H.; Chen, R.; Grinberg, I.; Margel, S. Engineered polymer nanoparticles containing hydrophobic dipeptide for inhibition of amyloid- $\beta$  fibrillation. *Biomacromolecules* **2012**, *13*, 2662–2670. [[CrossRef](#)] [[PubMed](#)]
28. Hellstrand, E.; Sparr, E.; Linse, S. Retardation of A $\beta$  fibril formation by phospholipid vesicles depends on membrane phase behavior. *Biophys. J.* **2010**, *98*, 2206–2214. [[CrossRef](#)] [[PubMed](#)]
29. Shao, H.; Jao, S.-C.; Ma, K.; Zagorski, M.G. Solution structures of micelle-bound amyloid  $\beta$ -(1-40) and  $\beta$ -(1-42) peptides of Alzheimer's disease. *J. Mol. Biol.* **1999**, *285*, 755–773. [[CrossRef](#)] [[PubMed](#)]
30. Rangachari, V.; Moore, B.D.; Reed, D.K.; Sonoda, L.K.; Bridges, A.W.; Conboy, E.; Hartigan, D.; Rosenberry, T.L. Amyloid- $\beta$ (1-42) rapidly forms protofibrils and oligomers by distinct pathways in low concentrations of sodium dodecylsulfate. *Biochemistry* **2007**, *46*, 12451–12462. [[CrossRef](#)] [[PubMed](#)]
31. Lin, J.-M.; Lin, T.-L.; Jeng, U.S.; Huang, Z.-H.; Huang, Y.-S. Aggregation structure of alzheimer amyloid- $\beta$ (1-40) peptide with sodium dodecyl sulfate as revealed by small-angle X-ray and neutron scattering. *Soft Matter* **2009**, *5*, 3913–3919. [[CrossRef](#)]
32. Abelein, A.; Kaspersen, J.D.; Nielsen, S.B.; Jensen, G.V.; Christiansen, G.; Pedersen, J.S.; Danielsson, J.; Otzen, D.E.; Gräslund, A. Formation of dynamic soluble surfactant-induced amyloid  $\beta$  peptide aggregation intermediates. *J. Biol. Chem.* **2013**, *288*, 23518–23528. [[CrossRef](#)] [[PubMed](#)]
33. Cabaleiro-Lago, C.; Szczepankiewicz, O.; Linse, S. The effect of nanoparticles on amyloid aggregation depends on the protein stability and intrinsic aggregation rate. *Langmuir* **2012**, *28*, 1852–1857. [[CrossRef](#)] [[PubMed](#)]
34. Palmal, S.; Jana, N.R.; Jana, N.R. Inhibition of amyloid fibril growth by nanoparticle coated with histidine-based polymer. *J. Phys. Chem. C* **2014**, *118*, 21630–21638.
35. Assarsson, A.; Linse, S.; Cabaleiro-Lago, C. Effects of polyamino acids and polyelectrolytes on amyloid  $\beta$  fibril formation. *Langmuir* **2014**, *30*, 8812–8818. [[CrossRef](#)] [[PubMed](#)]
36. Hocine, S.; Li, M.-H. Thermoresponsive self-assembled polymer colloids in water. *Soft Matter* **2013**, *9*, 5839–5861. [[CrossRef](#)]
37. Heskins, M.; Guillet, J.E. Solution properties of poly(*N*-isopropylacrylamide). *J. Macromol. Sci. A* **1968**, *2*, 1441–1455. [[CrossRef](#)]
38. Fujishige, S.; Kubota, K.; Ando, I. Phase transition of aqueous solutions of poly(*N*-isopropylacrylamide) and poly(*N*-isopropylmethacrylamide). *J. Phys. Chem.* **1989**, *93*, 3311–3313. [[CrossRef](#)]

39. Graziano, G. On the temperature-induced coil to globule transition of poly-*N*-isopropylacrylamide in dilute aqueous solutions. *Int. J. Biol. Macromol.* **2000**, *27*, 89–97. [CrossRef]
40. Lin, P.; Clash, C.; Pearce, E.M.; Kwei, T.K.; Aponte, M.A. Solubility and miscibility of poly(ethyl oxazoline). *J. Polym. Sci. B Polym. Phys.* **1988**, *26*, 603–619. [CrossRef]
41. Uyama, H.; Kobayashi, S. A novel thermo-sensitive polymer. Poly(2-iso-propyl-2-oxazoline). *Chem. Lett.* **1992**, *21*, 1643–1646. [CrossRef]
42. Park, J.-S.; Kataoka, K. Comprehensive and accurate control of thermosensitivity of poly(2-alkyl-2-oxazoline)s via well-defined gradient or random copolymerization. *Macromolecules* **2007**, *40*, 3599–3609. [CrossRef]
43. Hoogenboom, R. Poly(2-oxazoline)s: A polymer class with numerous potential applications. *Angew. Chem. Int. Ed.* **2009**, *48*, 7978–7994. [CrossRef] [PubMed]
44. Gil, E.S.; Hudson, S.M. Stimuli-responsive polymers and their bioconjugates. *Prog. Polym. Sci.* **2004**, *29*, 1173–1222. [CrossRef]
45. Aseyev, V.; Tenhu, H.; Winnik, F.M. Non-ionic thermoresponsive polymers in water. *Adv. Polym. Sci.* **2011**, *242*, 29–89.
46. Hoogenboom, R.; Thijs, H.M.L.; Jochems, M.J.H.C.; van Lankvelt, B.M.; Fijten, M.W.M.; Schubert, U.S. Tuning the lcst of poly(2-oxazoline)s by varying composition and molecular weight: Alternatives to poly(*N*-isopropylacrylamide)? *Chem. Commun.* **2008**, 5758–5760. [CrossRef] [PubMed]
47. Huber, S.; Jordan, R. Modulation of the lower critical solution temperature of 2-alkyl-2-oxazoline copolymers. *Colloid Polym. Sci.* **2008**, *286*, 395–402. [CrossRef]
48. Glassner, M.; Lava, K.; de la Rosa, V.R.; Hoogenboom, R. Tuning the lcst of poly(2-cyclopropyl-2-oxazoline) via gradient copolymerization with 2-ethyl-2-oxazoline. *J. Polym. Sci. A Polym. Chem.* **2014**, *52*, 3118–3122. [CrossRef]
49. Xia, Y.; Burke, N.A.D.; Stöver, H.D.H. End group effect on the thermal response of narrow-disperse poly(*N*-isopropylacrylamide) prepared by atom transfer radical polymerization. *Macromolecules* **2006**, *39*, 2275–2283. [CrossRef]
50. Huber, S.; Hutter, N.; Jordan, R. Effect of end group polarity upon the lower critical solution temperature of poly(2-isopropyl-2-oxazoline). *Colloid Polym. Sci.* **2008**, *286*, 1653–1661. [CrossRef]
51. Ishizone, T.; Han, S.; Okuyama, S.; Nakahama, S. Synthesis of water-soluble polymethacrylates by living anionic polymerization of trialkylsilyl-protected oligo(ethylene glycol) methacrylates. *Macromolecules* **2003**, *36*, 42–49. [CrossRef]
52. Adler, J.; Scheidt, H.A.; Kruger, M.; Thomas, L.; Huster, D. Local interactions influence the fibrillation kinetics, structure and dynamics of A $\beta$ (1–40) but leave the general fibril structure unchanged. *Phys. Chem. Chem. Phys.* **2014**, *16*, 7461–7471. [CrossRef] [PubMed]
53. Nielsen, L.; Khurana, R.; Coats, A.; Frokjaer, S.; Brange, J.; Vyas, S.; Uversky, V.N.; Fink, A.L. Effect of environmental factors on the kinetics of insulin fibril formation: Elucidation of the molecular mechanism. *Biochemistry* **2001**, *40*, 6036–6046. [CrossRef] [PubMed]
54. Bolder, S.G.; Sagis, L.M.C.; Venema, P.; van der Linden, E. Thioflavin t and birefringence assays to determine the conversion of proteins into fibrils. *Langmuir* **2007**, *23*, 4144–4147. [CrossRef] [PubMed]
55. Park, J.-S.; Akiyama, Y.; Winnik, F.M.; Kataoka, K. Versatile synthesis of end-functionalized thermosensitive poly(2-isopropyl-2-oxazolines). *Macromolecules* **2004**, *37*, 6786–6792. [CrossRef]
56. Witte, H.; Seeliger, W. Cyclische imidsäureester aus nitrilen und aminoalkoholen. *Justus Liebigs Ann. Chem.* **1974**, *1974*, 996–1009. [CrossRef]
57. Zhong, Q.; Wang, W.; Adelsberger, J.; Golosova, A.; Bivigou Koumba, A.M.; Laschewsky, A.; Funari, S.S.; Perlich, J.; Roth, S.V.; Papadakis, C.M.; *et al.* Collapse transition in thin films of poly(methoxydiethylenglycol acrylate). *Colloid Polym. Sci.* **2011**, *289*, 569–581. [CrossRef]
58. Vanparijs, N.; Maji, S.; Louage, B.; Voorhaar, L.; Laplace, D.; Zhang, Q.; Shi, Y.; Hennink, W.E.; Hoogenboom, R.; de Geest, B.G. Polymer-protein conjugation via a ‘grafting to’ approach—A comparative study of the performance of protein-reactive raft chain transfer agents. *Polym. Chem.* **2015**, *6*, 5602–5614. [CrossRef]
59. Hua, F.; Jiang, X.; Li, D.; Zhao, B. Well-defined thermosensitive, water-soluble polyacrylates and polystyrenics with short pendant oligo(ethylene glycol) groups synthesized by nitroxide-mediated radical polymerization. *J. Polym. Sci. A Polym. Chem.* **2006**, *44*, 2454–2467. [CrossRef]

60. Ferguson, C.J.; Hughes, R.J.; Nguyen, D.; Pham, B.T.T.; Gilbert, R.G.; Serelis, A.K.; Such, C.H.; Hawket, B.S. Ab initio emulsion polymerization by raft-controlled self-assembly. *Macromolecules* **2005**, *38*, 2191–2204. [[CrossRef](#)]
61. Zhong, Q.; Metwalli, E.; Rawolle, M.; Kaune, G.; Bivigou-Koumba, A.M.; Laschewsky, A.; Papadakis, C.M.; Cubitt, R.; Wang, J.; Müller-Buschbaum, P. Influence of hydrophobic polystyrene blocks on the rehydration of polystyrene-*block*-poly(methoxy diethylene glycol acrylate)-*block*-polystyrene films investigated by *in situ* neutron reflectivity. *Macromolecules* **2016**, *49*, 317–326. [[CrossRef](#)]
62. Miasnikova, A.; Laschewsky, A. Influencing the phase transition temperature of poly(methoxy diethylene glycol acrylate) by molar mass, end groups, and polymer architecture. *J. Polym. Sci. Part A* **2012**, *50*, 3313–3323. [[CrossRef](#)]
63. Christova, D.; Velichkova, R.; Loos, W.; Goethals, E.J.; Prez, F.D. New thermo-responsive polymer materials based on poly(2-ethyl-2-oxazoline) segments. *Polymer* **2003**, *44*, 2255–2261. [[CrossRef](#)]
64. Calamai, M.; Kumita, J.R.; Mifsud, J.; Parrini, C.; Ramazzotti, M.; Ramponi, G.; Taddei, N.; Chiti, F.; Dobson, C.M. Nature and significance of the interactions between amyloid fibrils and biological polyelectrolytes. *Biochemistry* **2006**, *45*, 12806–12815. [[CrossRef](#)] [[PubMed](#)]
65. Hellstrand, E.; Boland, B.; Walsh, D.M.; Linse, S. Amyloid  $\beta$ -protein aggregation produces highly reproducible kinetic data and occurs by a two-phase process. *ACS Chem. Neurosci.* **2010**, *1*, 13–18. [[CrossRef](#)] [[PubMed](#)]
66. Ghosh, D.; Dutta, P.; Chakraborty, C.; Singh, P.K.; Anoop, A.; Jha, N.N.; Jacob, R.S.; Mondal, M.; Mankar, S.; Das, S.; *et al.* Complexation of amyloid fibrils with charged conjugated polymers. *Langmuir* **2014**, *30*, 3775–3786. [[CrossRef](#)] [[PubMed](#)]



© 2016 by the authors; licensee MDPI, Basel, Switzerland. This article is an open access article distributed under the terms and conditions of the Creative Commons Attribution (CC-BY) license (<http://creativecommons.org/licenses/by/4.0/>).

2. Modulation of amyloid  $\beta$  peptide aggregation by hydrophilic polymers

PCCP

PAPER

View Article Online  
View Journal | View IssueCite this: *Phys. Chem. Chem. Phys.*,  
2019, 21, 20999Modulation of amyloid  $\beta$  peptide aggregation  
by hydrophilic polymers†Zhanna Evgrafova,<sup>a</sup> Bruno Voigt,<sup>b</sup> Andreas H. Roos,<sup>a</sup> Gerd Hause,<sup>c</sup>  
Dariush Hinderberger,<sup>a</sup> Jochen Balbach<sup>b</sup> and Wolfgang H. Binder<sup>a\*</sup>

A substantial number of diseases leading to loss of neurologic functions such as Morbus Alzheimer, Morbus Parkinson, or Chorea Huntington are related to the fibrillation of particular amyloidogenic peptides. *In vitro* amyloid fibrillation strongly depends on admixture with other proteins and peptides, lipids, nanoparticles, surfactants and polymers. We investigated amyloid-beta 1–40 peptide ( $A\beta_{1-40}$ ) fibrillation in mixture with thermoresponsive poly(oligo(ethylene glycol)<sub>m</sub>acrylates), in which the polymer's hydrophobicity is tuned by variation of the number of ethylene glycol-units in the side chain ( $m = 1-9$ ), the end groups (**B** = butoxy; **C** = carboxy; **D** = dodecyl; **P** = pyridyldisulfide) and the degree of polymerization ( $n$ ) of the polymers. The polymers were prepared *via* RAFT-polymerization, obtaining a broad range of molecular masses ( $M_n = 700$  to  $14\,600$  g mol<sup>-1</sup> kDa<sup>-1</sup>, polydispersity indices PDI = 1.10 to 1.25) and tunable cloud point temperatures ( $T_{cp}$ ), ranging from 42.4 °C to 80 °C, respectively. Proper combination of hydrophobic end groups with hydrophilic side chains of the polymer allowed to alter the hydrophilicity/hydrophobicity of these polymers, which is shown to enhance  $A\beta_{1-40}$  aggregation significantly in case of the endgroup D (with  $n = 16, 23, 56$ ). We observed that the less hydrophilic polymers ( $m = 1-2$ ) were able to both decrease and elongate the lag (t<sub>lag</sub>) and characteristic times (t<sub>char</sub>) of  $A\beta_{1-40}$  fibril formation in dependence of their end groups, molecular mass and hydrophilicity. On the other hand, highly hydrophilic polymers ( $m = 3, 5, 9$ ) either decreased, or only marginally influenced the lag and characteristic times of  $A\beta_{1-40}$  fibrillation, in all cases forming  $\beta$ -sheet rich fibrils as observed by TEM and CD-spectroscopy. Our results support that balanced hydrophobic and hydrophilic interactions of a polymer with  $A\beta_{1-40}$  is important for inhibiting amyloid-formation pathways.

Received 12th May 2019,  
Accepted 5th September 2019

DOI: 10.1039/c9cp02683e

rsc.li/pccp

## 1 Introduction

Fibrillar aggregation of peptides and proteins has received increasing attention due to the involvement of these molecules in a variety of neurodegenerative diseases, such as Alzheimer's,<sup>1</sup> Parkinson's and prion diseases.<sup>2</sup> The molecular basis of protein fibrillation can be described as a stepwise association of polypeptide chains such as the amyloid  $\beta$  peptides  $A\beta_{1-40}$  and  $A\beta_{1-42}$  into fibrillar aggregates with a cross- $\beta$  structure, subsequently forming macroscopic protein-plaques.<sup>3</sup> During aggregation, soluble monomeric proteins or peptides are converted into oligomers and finally into the amyloid fibrils<sup>4</sup> similar to the *in vitro*

formation of protein-fibrils.<sup>5</sup> There is a strong interest to inhibit fibril-formation and growth by interfering with the primordial stages of fibrillation by small or larger molecules, capable of interacting with the  $A\beta$  monomers/oligomers to prohibit further aggregation. To this end, a plethora of different small molecules,<sup>6-11</sup> peptides<sup>12,13</sup> and proteins,<sup>14,15</sup> nanoparticles and nanomaterials<sup>16</sup> has been shown to influence the aggregation process and therefore the kinetic behaviour of  $A\beta_{1-40}/A\beta_{1-42}$  fibril formation *in vitro*.<sup>17</sup> Besides electrostatics<sup>18</sup> and crowding,<sup>19</sup> surface induced seeding effects<sup>20</sup> can be responsible for these often counterbalancing effects of nanomaterials on amyloid-aggregation.<sup>16</sup>

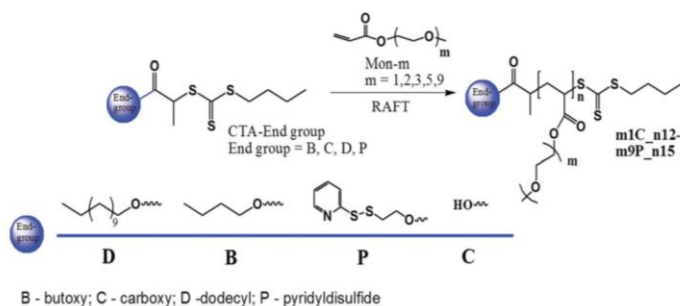
In contrast to previous works on model PEG peptide assemblies,<sup>21-24</sup> where the investigated peptides are remote from actual biology and often induce gelation of the peptide-amphiphiles,<sup>21</sup> we here intended to study the biologically relevant  $A\beta_{1-40}$  peptide instead of its small peptide analogs. We report on modulating  $A\beta_{1-40}$  fibrillation *via* hydrophilic polymers as additives in solution, where the polymers (see Scheme 1) are based on hydrophilic oligo-ethylene-acrylates, known to display a lower critical solution temperature in dependence on their side chain length and end group.<sup>25,26</sup> Variation of the oligo-ethylene side

<sup>a</sup> Martin-Luther University Halle-Wittenberg, Faculty of Natural Science II, Institute of Chemistry, Von-Danckelmann-Platz 4, D-06120 Halle (Saale), Germany. E-mail: wolfgang.binder@chemie.uni-halle.de; Tel: +49 345 55 25930

<sup>b</sup> Martin-Luther University Halle-Wittenberg, Faculty of Natural Science II, Institute of Physics, Betty-Heimann-Str., 7, D-06120 Halle (Saale), Germany

<sup>c</sup> Martin-Luther University Halle-Wittenberg, Biocenter, Weinbergweg 22, D-06120 Halle (Saale), Germany

† Electronic supplementary information (ESI) available. See DOI: 10.1039/c9cp02683e



**Scheme 1** Synthetic pathway for preparation of poly(oligo(ethylene glycol)<sub>m</sub>acrylates) **m1C<sub>n</sub>12–m9P<sub>n</sub>15** using the respective chain transfer agents. (for details on chemical structure, end groups, and molecular weights see Table S1 in the ESI†). The name of every sample comprises: *m*(1–9) – the number of ethylene glycol units in the side chain of the polymer; (C), (D), (B), (P) – the end group of the polymer; (*n*) followed by a number – the degree of polymerization.

chains enables to tune the hydrophobicity of the polymer, still maintaining water solubility.<sup>27–29</sup> The choice of a suitable end group, chosen according to solubility parameters,<sup>30</sup> additionally contributes to the overall hydrophobicity/hydrophilicity-profiles. As the fibrillation of Aβ<sub>1–40</sub> is a nucleation dependent process, it is assumed that the addition of polymers with adjustable hydrophilicity/hydrophobicity could lead to changes in the primordial stages of fibrillation, either by modifying nuclei properties or by direct interaction with monomeric Aβ<sub>1–40</sub>.

## 2 Materials and methods

### 2.1 Materials

Deuterated chloroform was purchased from Chemotrade, DMF (HPLC grade) and THF (HPLC grade) was purchased from Grüssing and VWR – ProLabo, respectively. Hexane was bought from Overlack. Aβ<sub>1–40</sub> peptide (DAEFRHDSGY EVHHQKLVFF AEDVGSNKGAIIGLMVGGVV) was synthesized using standard Fmoc solid phase synthesis (Peptide Core Unit, Leipzig University, Germany). All other chemicals were purchased from Sigma Aldrich and used without further purification unless otherwise stated.

### 2.2 Methods

**2.2.1 <sup>1</sup>H NMR, MALDI TOF MS, gel permeation chromatography, turbidimetry, CW EPR spectroscopy.** <sup>1</sup>H NMR spectra were recorded on a Varian Gemini 2000 (400 MHz) or a Varian Unity Inova 500 (500 MHz) using MestReNova software (version 6.0.2-5475) for the evaluation of the spectra. NMR spectra of polymers in deuterated chloroform were measured at 27 °C. All chemical shifts are reported relative to trimethylsilane (TMS) and referred to the solvent signal (CDCl<sub>3</sub>: 7.26 ppm (<sup>1</sup>H), 77.0 ppm (<sup>13</sup>C)).

MALDI TOF MS analysis was carried out using a Bruker Autoflex III Smartbeam equipped with a nitrogen laser (337 nm) operating in linear and reflection modes. Data were evaluated using flexAnalysis software (version 3.0). The matrix solution was prepared by dissolving trans-2-[3-(4-*tert*-butylphenyl)-2-methyl-2-propenylidene]malononitrile (DCTB) in THF at a

concentration of 20 mg mL<sup>-1</sup>. The polymer was dissolved in THF (20 mg mL<sup>-1</sup>) and mixed with sodium trifluoroacetate (20 mg mL<sup>-1</sup> in THF). The ratio between the matrix, the analyte and the salt was 100 : 10 : 1.

Gel permeation chromatography (GPC) measurements were performed on a Viscotek GPCmax VE 2002 using a H<sub>HR</sub>-H Guard-17360 precolumn and a GMH<sub>HR</sub>-N-18055 column with THF as solvent and VE 3580 IR detector for refractive index determination. Polystyrene standards (*M*<sub>p</sub> = 1000–115 000 g mol<sup>-1</sup>) were used for external calibration. Column and detector temperatures were held at 22 °C and 35 °C, respectively, and the flow rate was set to 1 mL min<sup>-1</sup>. The concentration of all samples was 3 mg mL<sup>-1</sup>.

Turbidimetry measurements were carried out using an UV-VIS spectrometer JASCO Corp., J-815 using a 0.1 cm diameter quartz cuvette. By coupling with a Peltier element PTC-423L from Jasco a controlled heating rate of 1 K min<sup>-1</sup> could be utilized. The observed wavelength was λ = 500 nm. For all measurements in water, a 10 μM solution of the polymer was used. For measurements in buffer 10 μM solutions of poly(oligo(ethylene glycol)<sub>m</sub>acrylates) in 50 mM Na<sub>2</sub>HPO<sub>4</sub> buffer (pH 7.4), supplemented with 150 mM NaCl were used. Cloud point temperatures (*T*<sub>cp</sub>) were detected at 50% of maximum absorbance. Due to the low signal to noise ratio, the sample **m1C<sub>n</sub>32** was measured using a cell with a larger optical path (1 cm). Note that the results obtained using cells with different optical paths agreed within 2–3 °C, as was tested on selected samples.

The temperature series of CW EPR spectra were measured in 2 K steps with the Miniscope MS 5000 and the MS 5000 temperature controller (magnettech GmbH, Berlin, Germany). By using the Freiberg Instruments software the spectra are measured with a sweep width of 10 mT, a modulation amplitude of 0.02 mT, a digital RC filter with a time constant of 0.2 s and a microwave attenuation of 20 dB. Each spectra represents an accumulation of 3 scans. For preparing the samples TEMPO, polymer and Aβ were dissolved in 50 mM Na<sub>2</sub>HPO<sub>4</sub> buffer (pH 7.4). These stock solutions were mixed together in Rotilabo<sup>®</sup> sample vials and convicted for measuring in Blaubrand<sup>®</sup> Micropipettes. The resulting concentration for the physical mixture of polymer and Aβ are 10 μM with a TEMPO concentration of 34.5 μM.

**2.2.2 Fibrillation kinetics, CD spectroscopy and general morphology.** ThT dependent kinetics of A $\beta_{1-40}$  fibrillation as a wild type (WT), in the absence and in mixtures with poly-(oligo(ethylene glycol) $_m$ acrylates) were recorded on a BMG Labtech FLUOStar Omega platereader using a 96-well plate (150  $\mu$ L each).<sup>31,32</sup> The polymers and A $\beta_{1-40}$  were individually dissolved in 50 mM Na<sub>2</sub>HPO<sub>4</sub> buffer (pH 7.4), supplemented with 150 mM NaCl and 10  $\mu$ M ThT. Solutions of the polymers were filtered through 17 mm PTFE syringe filters with a pore size 0.2  $\mu$ m. In order to completely dissolve A $\beta_{1-40}$ , an ultrasound treatment for 2 min was applied.<sup>33</sup> To start from the monomeric state of the peptide, a consequent centrifugation at 4 °C and 10 000 rpm for 2 hours prior to every measurement was carried out, according to previously reported protocols.<sup>33-35</sup> Subsequently, the concentration of the samples was determined using a Jasco J-650 UV-VIS spectrometer and set to 10  $\mu$ M. The shaking protocol comprised of 300 s long cycles including 240 s double-orbital shaking at 300 rpm before the measurement, using an excitation wavelength of 450 nm and an emission wavelength of 480 nm. All experiments were performed independently three times at 37 °C. Fluorescence intensities were normalized to the range from 0 to 1. The lag times ( $t_{lag}$ ) were determined as intercepts of piecewise linear fits performed from the zero-intensity up to the inflexion points of the ThT fluorescence intensity curves

$$\begin{cases} at, & t < t_{lag} \\ at_{lag} + b(t - t_{lag}), & t \geq t_{lag} \end{cases},$$

where  $a$ ,  $b$  are the slopes of the linear fits before and after the lag time  $t_{lag}$ , respectively, and  $t$  is the experimental time. The characteristic times ( $t_{char}$ ) were determined as times at which the fluorescence intensity reaches a half of its maximum.

Circular Dichroism Spectroscopy (CD) spectra were obtained on a JASCO Corp., J-815 at a temperature of 20 °C using a 0.1 cm diameter quartz cuvette. The samples for the measurements were taken just before or just after the fibrillation behaviour was studied by ThT dependent kinetics of A $\beta_{1-40}$  (see detailed sample preparation above). In every case a peptide-to-polymer ratio of 1 : 1 (10  $\mu$ M : 10  $\mu$ M) was used. The molar ellipticity [ $\theta$ ] [deg cm<sup>2</sup> dmol<sup>-1</sup>] was determined using the equation<sup>36</sup>

$$[\theta] = \frac{\theta \times (MW_{protein}/40)}{10 \times c \times l}$$

where,  $\theta$  is the ellipticity,  $c$  is the concentration of the sample (g L<sup>-1</sup>),  $l$  is the UV-cuvette cell diameter (0.1 cm),  $MW_{protein}$  is the molecular mass of the A $\beta_{1-40}$  (g mol<sup>-1</sup>), and 40 is the number of amino acids in A $\beta_{1-40}$  peptide.

Transmission Electron Microscopy (TEM) was employed to elucidate the morphology of selected aggregated samples. 5  $\mu$ L samples, taken from the well plates after ThT dependent kinetic measurements, were applied on carbon film coated copper grids and incubated for three minutes. The grids were further washed three times (20 seconds each time) in double distilled water and incubated for 60 seconds in 1% (w/v) uranyl acetate solution. The grids were dried for 24 h on filter paper.

TEM analysis was done with a Zeiss EM 900 transmission electron microscope (acceleration voltage 80 kV). Images were taken by a Variospeed SSCCD camera (SM-1k-120, TRS, Moorenweis) operating with ImageSP Viewer software.

## 3 Results and discussion

### 3.1 Polymer synthesis and characterization

The synthesis of the poly(oligo(ethylene glycol) $_m$ acrylates) was accomplished by RAFT-polymerization, allowing to introduce defined endgroups (B = butoxy; C = carboxy; D = dodecyl; P = pyridyldisulfide, see Scheme 1 and Table S1 in the ESI<sup>†</sup>).<sup>32,37</sup> The polymeric products were characterized *via* <sup>1</sup>H NMR spectroscopy (Fig. S2–S11, ESI<sup>†</sup>), matrix-assisted laser desorption/ionization mass spectrometry (MALDI-TOF MS) (Fig. S12–S15, ESI<sup>†</sup>), size exclusion chromatography (SEC), and turbidimetry (Fig. 1 and Fig. S16, ESI<sup>†</sup>), proving their chemical structure including the presence of the respective end groups (B, C, D, P). The synthesized polymers possess low polydispersities, ranging from 1.11 to 1.25, and molecular masses from 700 g mol<sup>-1</sup> to 14 600 g mol<sup>-1</sup>, obtained in a controlled way. Further details on the synthetic and experimental methods can be found in the ESI<sup>†</sup> (Fig. S1–S16).

### 3.2 LCST measurements of polymers

The effect of hydrophilicity, molecular mass, end groups, and addition of salts on the lower critical solution temperature (LCST) of the synthesized poly(oligo(ethylene glycol) $_m$ acrylates) was investigated.<sup>38-40</sup> The LCST is experimentally determined by the cloud point temperature, where polymers undergo a conformational transition from a fully hydrated expanded coil to a collapsed globule, liberating most of the hydration molecules.<sup>38</sup>

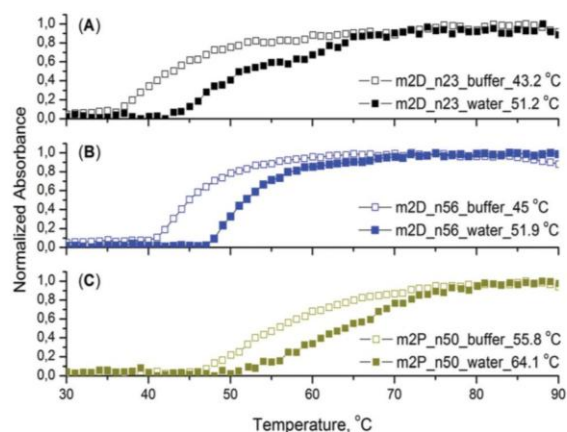


Fig. 1 LCST measurements for the poly(methoxy di(ethylene glycol) $_m$ -acrylates) either as 10  $\mu$ M solution in 50 mM Na<sub>2</sub>HPO<sub>4</sub> buffer (pH 7.4), supplemented with 150 mM NaCl, or as 10  $\mu$ M solution in deionized water. (A–C) Demonstration of  $T_{cp}$  elevation in water as compared to the buffer for polymers with end groups of different polarity as indicated. Comparison of data in (A) and (B) demonstrates the effect of the molecular weight on  $T_{cp}$ , comparison of data in (B) and (C) shows, additionally, the effect of end group polarity on  $T_{cp}$ .

Since subsequent fibrillation experiments of  $A\beta_{1-40}$  were conducted in a 50 mM  $Na_2HPO_4$  buffer (pH 7.4) supplemented with 150 mM NaCl, LCST measurements were also performed under these conditions. Additional LCST investigations, carried out in water, were performed to demonstrate the influence of the environment, namely salts and pH, on the  $T_{cp}$ . Table S1 in the ESI<sup>†</sup> documents that more hydrophilic poly(oligo(ethylene glycol)<sub>m</sub>acrylates), carrying three to nine ethylene glycol units ( $m = 3-9$ ) in the backbone, irrespective of their end group (**B**, **C**, **P**), do not collapse under the measuring conditions up to 90 °C. In contrast, less hydrophilic polymers with  $m = 1, 2$  demonstrate a growing tendency to collapse with increasing molecular mass, in line with previously published data.<sup>29</sup> Another important aspect is the influence of the polymers' end group on its LCST under the same experimental conditions. We found that more hydrophobic end groups (e.g. **B** and **D**), in contrast to their more hydrophilic counterparts (e.g. **C**), can severely decrease  $T_{cp}$ . Therefore, it was possible to tune  $T_{cp}$  of similar poly(methoxy di(ethylene glycol)acrylates) to be 78 °C for the polymer **m2C\_n49** 8500 g mol<sup>-1</sup> with a carboxy-end group, to  $T_{cp} = 55.8$  °C for the polymer **m2P\_n50** 8700 g mol<sup>-1</sup> with a pyridyldisulfide - end group, and to  $T_{cp} = 45$  °C for the polymer **m2D\_n56** 9800 g mol<sup>-1</sup> with a dodecyl- end group. A noteworthy effect of the used buffer on  $T_{cp}$  correlated with the choice of the end group: the most hydrophilic carboxy- end group led to elevated  $T_{cp}$  in the buffer compared to water due to specific non-covalent interactions of the end group with the components of the buffer. **B**, **D** and **P** end groups show an opposite effect: these polymers revealed slightly higher  $T_{cp}$  values in water compared to those in buffer. The LCST results of three representative polymers **m2D\_n23**, **m2D\_n56**, **m2P\_n50** are shown in Fig. 1 and demonstrate the influence of molecular mass (Fig. 1A and B), end groups (Fig. 1B and C) and the medium (pH and salts addition) on the

LCST. Additional figures for various other polymers of this study can be found in the ESI<sup>†</sup> (Fig. S16).

### 3.3 $A\beta_{1-40}$ fibril formation in physical mixtures with polymers

Next, fibril formation of  $A\beta_{1-40}$  in the presence of thermo-responsive poly(oligo(ethylene glycol)<sub>m</sub>acrylates) ( $m = 1-9$ ) carrying **B** = butoxy, **C** = carboxy, **D** = dodecyl and **P** = pyridyldisulfide end groups was investigated, and the following issues were raised: (i) does the number of ethylene glycol units (**m**) within the polymer backbone affect the  $A\beta_{1-40}$  aggregation? (ii) Does the degree of polymerization (**n**) alter the  $A\beta_{1-40}$  fibrillation process? (iii) Is there an end group influence on the  $A\beta_{1-40}$  aggregation rate? (iv) If yes, what explanation can be provided? (v) Does addition of these polymers influence the morphology of the obtained fibrils?

All presented fibrillation kinetics were followed by a change in the ThT fluorescence at a fixed polymer/ $A\beta_{1-40}$  ratio of 10  $\mu$ M/10  $\mu$ M. Under the here used conditions,  $A\beta_{1-40}$  fibrillation occurs at a lag time of  $t_{lag} = 3.25 \pm 0.12$  h and a characteristic time  $t_{char} = 3.83 \pm 0.1$  h in the absence of polymers and all influences of the physically mixed polymers are discussed in correspondence to this reference values. In order to ensure that the pure polymer itself does not exert a modification of the ThT assay, it was conducted in the presence of polymers **m1C\_n32**, **m2C\_n49**, **m2B\_n36**, and **m2D\_n56**, but devoid of  $A\beta_{1-40}$ . We found no contribution to the ThT fluorescence from the polymers (see ESI<sup>†</sup> Fig. S23).

First, the influence of the number of ethylene glycol units (**m**) within the polymer backbone of poly(oligo(ethylene glycol)<sub>m</sub>acrylates) ( $m = 1-9$ ) on the fibrillation kinetic was investigated (Fig. 2). For clarity only samples with comparable degrees of polymerization and a carboxy end group are depicted. All further curves can be found in the ESI<sup>†</sup> (Fig. S17). From Fig. 2 and Table S1 (ESI<sup>†</sup>) it is

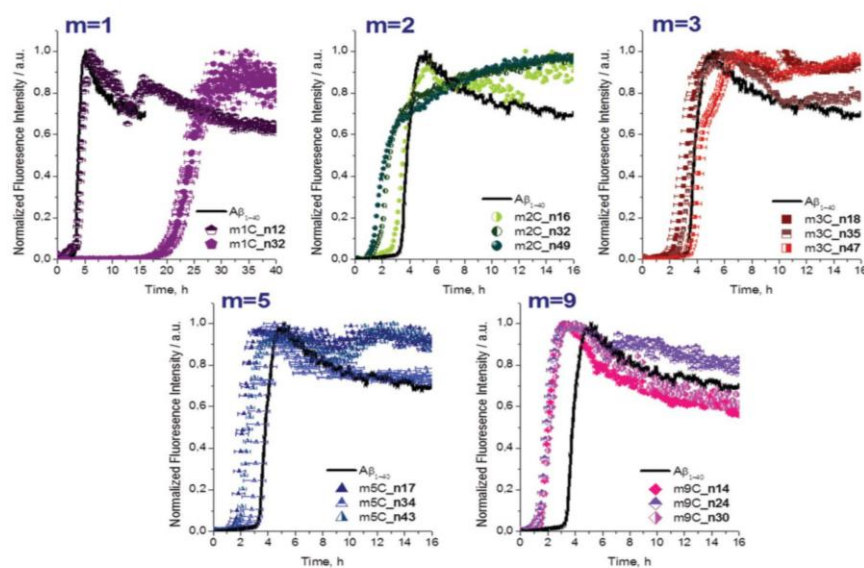


Fig. 2 Time evolution of the ThT fluorescence intensity of the poly(oligo(ethylene glycol)<sub>m</sub> acrylates)/ $A\beta_{1-40}$  mixtures at  $\lambda = 480$  nm. Black solid line corresponds to  $A\beta_{1-40}$  wild type. The hydrophilicity is varied by the number of ethylene glycol units (**m**). Degree of polymerization (**n**) is indicated for every sample and highlighted in bold. Error bars based on three independent measurements are shown.

notable that almost all polymers with  $m = 2-9$  (featuring high  $T_{cp}$  values above 78 °C) either do not influence or, as observed in most cases, accelerate formation of  $A\beta_{1-40}$  fibrils. All corresponding  $t_{lag}$  and  $t_{char}$  values from a quantitative analysis are listed in Table S1 and a graphical representation is given in Fig. 4B.

In contrast, one polymer with  $m = 1$  disclosed a high potency to retard aggregation of  $A\beta_{1-40}$ . Since only two  $m = 1$  samples within the prepared  $M_n$  range are soluble in the employed buffer, ThT fibrillation kinetics were only measured for **m1C\_n12** 1600 g mol<sup>-1</sup> and **m1C\_n32** 4200 g mol<sup>-1</sup>. Polymer **m1C\_n12** ( $T_{cp}$  n/a) only slightly influence  $t_{lag}$  and  $t_{char}$  of  $A\beta_{1-40}$  fibrillation (from  $3.25 \pm 0.12$  h to  $3.88 \pm 0.75$  h and from  $3.83 \pm 0.1$  h to  $4.3 \pm 0.75$  h, respectively), whereas the polymer **m1C\_n32** with a low cloud temperature of  $T_{cp} = 42.4$  °C substantially delayed fibrillation (see Fig. 2).

Within the same set of polymers with a carboxy- end group, the influence of the degree of polymerization  $n$  on  $A\beta_{1-40}$  fibrillation could be followed. In case of  $m = 2$ , lower molecular mass samples only marginally influence  $A\beta_{1-40}$  fibrillation (Table S1 (ESI<sup>†</sup>) no. 5-7). In contrast, their higher molecular mass counterparts (Table S1 (ESI<sup>†</sup>) no. 8-10) accelerate the fibril formation by shortening  $t_{lag}$  and  $t_{char}$ . This effect of the molecular mass is not pronounced for the mixtures of  $A\beta_{1-40}$  with more hydrophilic polymers  $m = 3-9$  but a general trend of slight acceleration of  $A\beta_{1-40}$  fibrillation for these polymers is obvious from Fig. 2.

With the next set of polymers, we tested end group effects on  $t_{lag}$  and  $t_{char}$  of  $A\beta_{1-40}$  fibrillation. As demonstrated in Fig. 3, the poly(methoxy di(ethylene glycol)acrylates) with the same side chains ( $m = 2$ ) and similar molecular masses between 4000 g mol<sup>-1</sup> and 9800 g mol<sup>-1</sup>, but different hydrophobic end groups (**B**, **D**, **P**) notably increased  $t_{lag}$  and  $t_{char}$  concomitantly with a decreasing slope during the growth phase. This contrasts the previously finding for the hydrophilic carboxy (**C**) end group, which accelerated aggregation (Fig. 2,  $m = 2$ ). This strong retardation by polymers with end groups **B**, **C**, **P** was not present for lower molecular masses (700-3600 g mol<sup>-1</sup>), which do not display thermo-responsive behaviour. With increase of molecular masses, the cloud point temperature of the samples decreases, yet to a

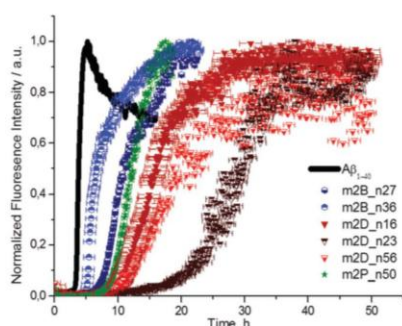


Fig. 3 Effect of the polymer's end group on  $t_{lag}$  and  $t_{char}$  of  $A\beta_{1-40}$  fibrillation demonstrated as a time evolution of the ThT fluorescence intensity at  $\lambda = 480$  nm. Error bars based on three independent measurements are shown.

different extent due to the different hydrophilicity of their end groups. Furthermore, for the samples with comparable molecular masses, but different end groups (**B**, **P**, **C**) **m2B\_n36** 6300 g mol<sup>-1</sup> ( $T_{cp}$  54.1 °C) (Table S1 no. 13, ESI<sup>†</sup>), **m2P\_n38** 6600 g mol<sup>-1</sup> ( $T_{cp}$  65.2 °C) (Table S1 no. 18, ESI<sup>†</sup>), and **m2C\_n32** 5600 g mol<sup>-1</sup> ( $T_{cp}$  80.4 °C) (Table S1 no. 9, ESI<sup>†</sup>), only the most hydrophobic sample with the lowest cloud temperature, **m2B\_n36**, can retard  $A\beta_{1-40}$  aggregation extending both the  $t_{lag}$  and the  $t_{char}$  (see Fig. 3).

The end group (**D**) harbours the 12-carbon long dodecyl- end group with pronounced hydrophobic character compared to the hydrophilic polymers' repeating unit. End group (**D**) retarded most the  $A\beta_{1-40}$  aggregation kinetics of all studied end groups with maximal factor of 6.4 for  $t_{lag}$  and 7.7 for  $t_{char}$  revealed by **m2D\_n23** (Fig. 3 and 4A). This strong end group effect even overwrites the cloud point dependence found for the other 3 end groups (**m2D\_n16** in Fig. 4A and C). All trends corresponding to the end groups, cloud point temperatures, and molecular masses are summarized in Fig. 4.

### 3.4 CD spectroscopy and TEM measurements of amyloid $A\beta_{1-40}$ /polymer mixtures

To identify possible conformational changes of  $A\beta_{1-40}$  due to interactions with the here studied polymers (Table S1, ESI<sup>†</sup>), UV circular dichroism spectroscopy<sup>36,41</sup> was employed in the absence of polymer and in the presence of four selected samples **m2C\_n16** 2800 g mol<sup>-1</sup> (NMR), **m3C\_n18** 3900 g mol<sup>-1</sup>, **m5C\_n17** 5200 g mol<sup>-1</sup>, **m9C\_n14** 6700 g mol<sup>-1</sup>. All non-aggregated monomeric samples taken before the ThT dependent kinetic measurements demonstrate prominent negative ellipticities at around 200 nm, exhibiting a random coil conformation of  $A\beta_{1-40}$  both alone and in mixtures with the polymers (Fig. 5). In contrast, all samples taken after the ThT dependent kinetic measurements showed changes in the spectra, confirming the transition to cross- $\beta$  structures due to the characteristic negative ellipticities in the range between 215 and 218 nm. Additional spectra can be found in the ESI<sup>†</sup> (Fig. S21). Also, transmission electron microscopy (TEM) was employed to elucidate the morphological appearance of  $A\beta_{1-40}$  fibrils in the presence of the poly(methoxy di(ethylene glycol)acrylates). We found in all preparations in the absence and presence of polymers fibrillar aggregates sharing some common features, namely, they are long, straight, entangled, and unbranched irrespective of the used polymer. There are some non-systematic variations in the length of the fibrils. Dark spots on the images can be explained by clustering of uranyl acetate during drying on the surface of the TEM grid. Selected micrographs are shown in Fig. 6. Additional images can be found in the ESI<sup>†</sup> (Fig. S22).

### 3.5 Discussion

Systems involving synthetic polymers and natural proteins gained a lot of attention in the last decades due to their tremendous properties they can offer.<sup>42,43</sup> Misfolding and aggregation of proteins can lead to the formation of cytotoxic oligomers and accumulation of extended fibrils in different body tissues causing a wide range of amyloidoses.<sup>4,17</sup> The origin of this phenomenon is still largely

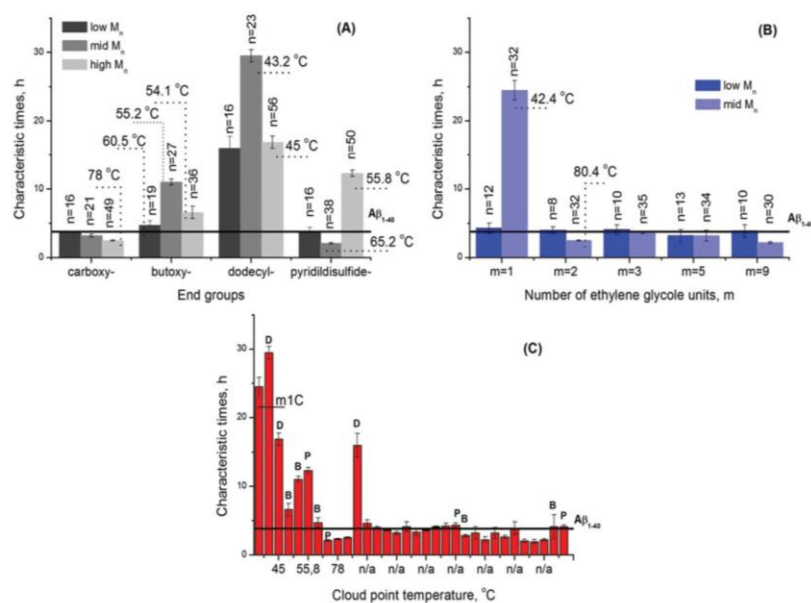


**Fig. 4** Summary of various factors affecting  $A\beta_{1-40}$  characterization time. The data are obtained from the ThT detected fibrillation kinetics of  $A\beta_{1-40}$  in the absence (showed as a bold line) or in the presence of thermoresponsive polymers. The dotted lines indicate  $T_{cp}$  values of the corresponding samples. In case  $T_{cp}$  is not specified, it means that  $T_{cp}$  is above 90 °C. (A) Influence of the poly(methoxy di(ethylene glycol)acrylates ( $m = 2$ ) with different end groups, but comparable degree of polymerization ( $n$ ). (B) Influence of the number of ethylene glycol units ( $m$ ) in the side chain of polymers with comparable  $n$  and carboxy- end groups. (C) Influence of  $T_{cp}$  in a series of studied polymers ( $m = 1-9$ ). N/a:  $T_{cp}$  above 90 °C. The end group of the polymer is indicated as a letter (**B** = butoxy; **D** = dodecyl; **P** = pyridyldisulfide) above the respective bar. In case the end group is not specified, it means that it is **C** = carboxy. The sample **m1C\_n32** is additionally marked as **m1C**. Error bars based on three independent measurements are also shown.

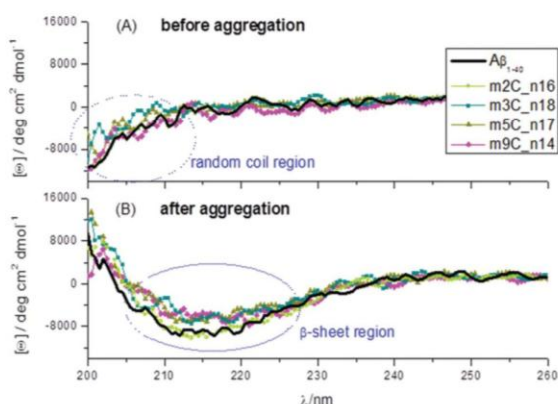


**Fig. 5** Far-UV CD spectra of the  $A\beta_{1-40}$ /poly(oligo(ethylene glycol) $_m$ acrylates) **m2C\_n16**, **m3C\_n18**, **m5C\_n17**, **m9C\_n14** 10  $\mu M$ /10  $\mu M$  mixtures as solution in a 50 mM  $Na_2HPO_4$  buffer (pH 7.4) supplemented with 150 mM NaCl, measured (A) just before and (B) just after ThT dependent kinetic measurements. The resulting CD spectra display a transition from the non-aggregated freshly prepared native peptides (A) to the  $\beta$ -sheet rich fibrils (B).

unclear, but it was established that the *in vitro* formation of fibrils takes place through the following phases, namely, the lag phase, the growth phase, and the saturation phase.<sup>44</sup> In the here presented study, the influence of thermoresponsive poly(oligo(ethylene glycol) $_m$ acrylates) ( $m = 1-9$ ) carrying **B** = butoxy, **C** = carboxy, **D** = dodecyl and **P** = pyridyldisulfide end groups on the progression of  $A\beta_{1-40}$  aggregation was investigated. We followed the fibrillation kinetics of the  $A\beta_{1-40}$  peptide by ThT

fluorescence at a 10  $\mu M$ /10  $\mu M$  peptide/polymer ratio, monitored the transition of the  $A\beta_{1-40}$  native peptide from the random coil conformation to the  $\beta$ -sheet rich fibrils by CD spectroscopy, and analyzed the morphology of the obtained fibrils by transmission electron microscopy (TEM). The obtained data indicate that the thermoresponsive poly(oligo(ethylene glycol) $_m$ acrylates) ( $m = 1-9$ ) can effectively alter the fibrillation kinetics of the  $A\beta_{1-40}$  peptide, at the same time keeping the morphology of the final fibrils almost unaffected as proven by CD and TEM. Both the lag phase and the slope during the growth phase get altered in the presence of these polymers indicating that early nucleation and fibril elongation are affected. Despite the fact that  $t_{lag}$  and  $t_{char}$  of the studied samples are close, the shapes and slopes of the curves are dissimilar, which can indicate differences in the aggregation mechanism upon the presence of polymers. This observation will be considered for future investigations.

We propose that the overall hydrophobicity of the polymer, regulated by the variation of ethylene glycol units ( $m$ ) in the side chain of the polymer backbone and by defined end groups (**B**, **C**, **D**, **P**), leading to a decreased cloud point temperature, plays the major role in the observed changes. This implies that the formation of  $A\beta_{1-40}$  fibrils can be retarded by lowering  $T_{cp}$  of the poly(oligo(ethylene glycol) $_m$ acrylates) (Fig. 4). Since the fibrillation kinetic measurements were conducted at 37 °C, and the polymer's transition from an expanded coil conformation below  $T_{cp}$  to a globular chain conformation above  $T_{cp}$  is a gradual process, some chains can collapse even before the main transition can be detected, known as "incipient collapse".<sup>38,45-48</sup> The latter

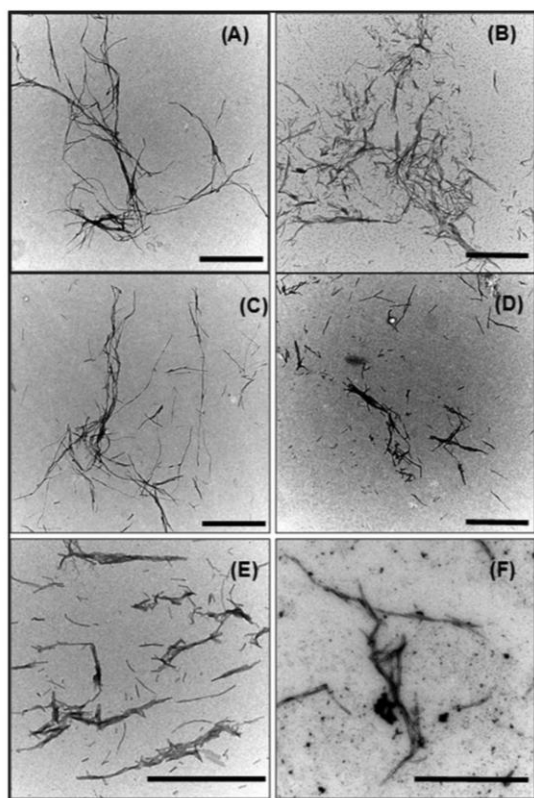


Fig. 6 TEM images of the fibrils obtained after ThT kinetic measurements (A)  $A\beta_{1-40}$  in the absence of polymers; (B)  $A\beta_{1-40}/m2P_n50$ ; (C)  $A\beta_{1-40}/m2C_n4$ ; (D)  $A\beta_{1-40}/m2D_n16$ ; (E)  $A\beta_{1-40}/m2P_n18$ ; (F)  $A\beta_{1-40}/m2C_n8$ . The scale bar corresponds to 1000 nm.

increases the amount of hydrophobic domains in the mixture. Such a “pre-transition” or early onset of a broad collapse has on several occasions been observed in thermoresponsive polymer systems using electron paramagnetic resonance (EPR) on amphiphilic spin probes like TEMPO.<sup>49</sup> Often, these early collapse processes only lead to very small volume fractions of slightly polymer-enriched, water-depleted regions that are very difficult to detect or quantify with typically used light scattering methods. The favorable partition coefficient towards hydrophobic environments of TEMPO together with the specificity of EPR spectroscopy allows a characterization of these pre-collapsed regions. For the samples of polymer **m2D\_n23**, we have indeed detected the onset of nanoscopic phase segregation at 34 °C, which is 9–10 °C below the macroscopic cloud point (see Table S1 and Fig. S26 in the ESI†). Owing to the fact that the  $A\beta_{1-40}$  peptide has two distinct hydrophobic regions, localized between amino acids Y10–F20 and A30–V40,<sup>50,51</sup> the aforementioned hydrophobic domains, formed by collapsed or partially collapsed macromolecules, can bind to the peptide through hydrophobic interactions.<sup>52–54</sup> We also observed that in the case of the poly(methoxy di(ethylene glycol)-acrylates, with a dodecyl- end group, the LCST influence was, though, important, but not decisive, since all the samples carrying this end group could retard aggregation of the  $A\beta_{1-40}$  regardless of  $T_{cp}$ . We hypothesize that the long hydrophobic 12-carbon end

group interacts with hydrophobic regions of  $A\beta_{1-40}$ , blocking important interaction sites and thus productively postpone the fibrillation process both above and near the LCST. This hypothesis will be investigated in structural terms in the near future *e.g.* by NMR- or EPR-spectroscopy.<sup>48</sup>

In all cases, where the addition of polymers accelerated or insignificantly changed the fibrillation rate,  $T_{cp}$  was at least higher than 60 °C. We presume that hydration-effects can play an important role when it comes to possible polymer–protein interactions. Regardless of the differences in fibrillation, all the samples chosen for morphological analyses displayed common secondary  $\beta$ -sheet structure, determined by characteristic negative ellipticities in the range between 215 and 218 nm. Transmission electron microscopy imaging confirmed formation of straight, long, unbranched fibrils.

Summarizing the obtained result, we can conclude that a rational combination of hydrophobicity of the end groups with hydrophilicity of the repeating units of thermoresponsive poly(oligo(ethylene glycol)<sub>m</sub>acrylates) can predictably alter the fibrillation kinetics of the  $A\beta_{1-40}$  peptide, at the same time keeping the common morphology of the final fibrils.

## Author contributions

Zhanna Evgrafova has prepared all the polymers, performed all CD and LCST-experiments, did the polymer characterization, and the amyloid-aggregation assays; B. Voigt and G. Hause did TEM assays, Andreas H. Roos and Dariush Hinderberger performed EPR spectroscopic measurements and analysis. Wolfgang H. Binder and Jochen Balbach designed research and analyzed data. The paper was written by Zhanna Evgrafova, Jochen Balbach, and Wolfgang H. Binder.

## Conflicts of interest

There are no conflicts to declare.

## Acknowledgements

We thank the DFG – Deutsche Forschungsgemeinschaft, DFG, ProjektNr 189853844, TRR-SFB 102, A03 and A12, as well as the Leistungszentrum Chemie/Systembiologie, UNI-CBS, Project “Biologisch Abbaubare Partikel über Encapsulierungsmethoden, Emulsions-/Evaporationsverfahren und 3D Printing” for financial support. We would like to acknowledge Dr Juliane Adler for valuable discussions regarding the project and Dr Sven Rothmund for synthesis of the native  $A\beta_{1-40}$  peptide.

## References

- 1 A. Alzheimer, *Z. Gesamte Neurol. Psychiatr.*, 1911, **4**, 356.
- 2 T. P. J. Knowles, M. Vendruscolo and C. M. Dobson, *Nat. Rev. Mol. Cell Biol.*, 2014, **15**, 384.
- 3 I. W. Hamley, *Angew. Chem., Int. Ed.*, 2007, **46**, 8128–8147.

- 4 P. Arosio, T. P. J. Knowles and S. Linse, *Phys. Chem. Chem. Phys.*, 2015, **17**, 7606–7618.
- 5 J. Adamcik and R. Mezzenga, *Macromolecules*, 2012, **45**, 1137–1150.
- 6 J. Bieschke, M. Herbst, T. Wiglenda, R. P. Friedrich, A. Boeddrich, F. Schiele, D. Kleckers, J. M. Lopez del Amo, B. A. Grüning, Q. Wang, M. R. Schmidt, R. Lurz, R. Anwyl, S. Schnoegl, M. Fändrich, R. F. Frank, B. Reif, S. Günther, D. M. Walsh and E. E. Wanker, *Nat. Chem. Biol.*, 2011, **8**, 93.
- 7 K. Debnath, S. Shekhar, V. Kumar and N. R. Jana, *ACS Appl. Mater. Interfaces*, 2016, **8**, 20309–20318.
- 8 J. McLaurin, R. Golomb, A. Jurewicz, J. P. Antel and P. E. Fraser, *J. Biol. Chem.*, 2000, **275**, 18495–18502.
- 9 F. L. Palhano, J. Lee, N. P. Grimster and J. W. Kelly, *J. Am. Chem. Soc.*, 2013, **135**, 7503–7510.
- 10 J. Habchi, P. Arosio, M. Perni, A. R. Costa, M. Yagi-Utsumi, P. Joshi, S. Chia, S. I. A. Cohen, M. B. D. Müller, S. Linse, E. A. Nollen, C. M. Dobson, T. P. J. Knowles and M. Vendruscolo, *Sci. Adv.*, 2016, **2**, e1501244.
- 11 K. Dahse, M. Garvey, M. Kovermann, A. Vogel, J. Balbach, M. Fändrich and A. Fahr, *J. Mol. Biol.*, 2010, **403**, 643–659.
- 12 S. Rocha, I. Cardoso, H. Börner, M. C. Pereira, M. J. Saraiva and M. Coelho, *Biochem. Biophys. Res. Commun.*, 2009, **380**, 397–401.
- 13 T. Takahashi and H. Mihara, *Acc. Chem. Res.*, 2008, **41**, 1309–1318.
- 14 A. Assarsson, E. Hellstrand, C. Cabaleiro-Lago and S. Linse, *ACS Chem. Neurosci.*, 2014, **5**, 266–274.
- 15 M. Villmow, M. Baumann, M. Malesevic, R. Sachs, G. Hause, M. Fändrich, J. Balbach and C. Schiene-Fischer, *Biochem. J.*, 2016, **473**, 1355–1368.
- 16 B. Wang, E. H. Pilkington, Y. Sun, T. P. Davis, P. C. Ke and F. Ding, *Environ. Sci.: Nano*, 2017, **4**, 1772–1783.
- 17 I. W. Hamley, *Chem. Rev.*, 2012, **112**, 5147–5192.
- 18 S. Palmal, N. R. Jana and N. R. Jana, *J. Phys. Chem. C*, 2014, **118**, 21630–21638.
- 19 C. Cabaleiro-Lago, F. Quinlan-Pluck, I. Lynch, K. A. Dawson and S. Linse, *ACS Chem. Neurosci.*, 2010, **1**, 279–287.
- 20 A. Gladysz, B. Abel and H. J. Risselada, *Angew. Chem., Int. Ed.*, 2016, **55**, 11242–11246.
- 21 A. R. Hirst, I. A. Coates, T. R. Boucheteau, J. F. Miravet, B. Escuder, V. Castelletto, I. W. Hamley and D. K. Smith, *J. Am. Chem. Soc.*, 2008, **130**, 9113–9121.
- 22 V. Castelletto and I. W. Hamley, *Biophys. Chem.*, 2009, **141**, 169–174.
- 23 I. W. Hamley, *Biomacromolecules*, 2014, **15**, 1543–1559.
- 24 I. W. Hamley and V. Castelletto, *Bioconjugate Chem.*, 2017, **28**, 731–739.
- 25 J.-F. Lutz, *J. Polym. Sci., Part A: Polym. Chem.*, 2008, **46**, 3459–3470.
- 26 G. Vancoillie, D. Frank and R. Hoogenboom, *Prog. Polym. Sci.*, 2014, **39**, 1074–1095.
- 27 V. Aseyev, H. Tenhu and F. Winnik, *Non-Ionic Thermoresponsive Polymers in Water*, 2010.
- 28 F. Hua, X. Jiang, D. Li and B. Zhao, *J. Polym. Sci., Part A: Polym. Chem.*, 2006, **44**, 2454–2467.
- 29 J.-F. Lutz, *J. Polym. Sci., Part A: Polym. Chem.*, 2008, **46**, 3459–3470.
- 30 A. F. M. Barton, *Handbook of Polymer-Liquid Interaction Parameters and Solubility Parameters*, CRC Press, 1990.
- 31 J. Wägele, S. De Sio, B. Voigt, J. Balbach and M. Ott, *Biophys. J.*, 2019, **116**, 227–238.
- 32 Z. Evgrafova, B. Voigt, M. Baumann, M. Stephani, W. H. Binder and J. Balbach, *ChemPhysChem*, 2019, **20**, 236–240.
- 33 D. Jiang, I. Rauda, S. Han, S. Chen and F. Zhou, *Langmuir*, 2012, **28**, 12711–12721.
- 34 T. J. Esparza, N. C. Wildburger, H. Jiang, M. Gangolli, N. J. Cairns, R. J. Bateman and D. L. Brody, *Sci. Rep.*, 2016, **6**, 38187.
- 35 P. Arosio, T. Cedervall, T. P. J. Knowles and S. Linse, *Anal. Biochem.*, 2016, **504**, 7–13.
- 36 D. Huesmann, A. Birke, K. Klinker, S. Türk, H. J. Räder and M. Barz, *Macromolecules*, 2014, **47**, 928–936.
- 37 S. Funtan, Z. Evgrafova, J. Adler, D. Huster and W. Binder, *Polymers*, 2016, **8**, 178.
- 38 Q. Zhang, C. Weber, U. S. Schubert and R. Hoogenboom, *Mater. Horiz.*, 2017, **4**, 109–116.
- 39 K. Skrabania, J. Kristen, A. Laschewsky, Ö. Akdemir, A. Hoth and J.-F. Lutz, *Langmuir*, 2007, **23**, 84–93.
- 40 J. Liao, S. Liu, Y. Yuan and H. Zhang, *New J. Chem.*, 2018, **42**, 5698–5708.
- 41 N. J. Greenfield, *Nat. Protoc.*, 2006, **1**, 2876–2890.
- 42 K. L. Heredia and H. D. Maynard, *Org. Biomol. Chem.*, 2007, **5**, 45–53.
- 43 B. Trzebicka, R. Szweda, D. Kosowski, D. Szweda, Ł. Otulakowski, E. Haladjova and A. Dworak, *Prog. Polym. Sci.*, 2017, **68**, 35–76.
- 44 F. Chiti and C. M. Dobson, *Annu. Rev. Biochem.*, 2017, **86**, 27–68.
- 45 Y. Liu, Y. Dai and X. Xu, *J. Phys. Chem. B*, 2017, **121**, 9469–9475.
- 46 X. Zheng, M. A. Anisimov, J. V. Sengers and M. He, *Phys. Rev. Lett.*, 2018, **121**, 207802.
- 47 G. Luna-Bárceñas, D. G. Gromov, J. C. Meredith, I. C. Sanchez, J. J. de Pablo and K. P. Johnston, *Chem. Phys. Lett.*, 1997, **278**, 302–306.
- 48 D. Kurzbach, M. J. N. Junk and D. Hinderberger, *Macromol. Rapid Commun.*, 2013, **34**, 119–134.
- 49 J. Hunold, T. Wolf, F. R. Wurm and D. Hinderberger, *Chem. Commun.*, 2019, **55**, 3414–3417.
- 50 A. T. Petkova, W.-M. Yau and R. Tycko, *Biochemistry*, 2006, **45**, 498–512.
- 51 L. C. Serpell, *Biochim. Biophys. Acta, Mol. Basis Dis.*, 2000, **1502**, 16–30.
- 52 H. Liu, B. Xie, X. Dong, L. Zhang, Y. Wang, F. Liu and Y. Sun, *React. Funct. Polym.*, 2016, **103**, 108–116.
- 53 T. Ziehm, A. K. Buell and D. Willbold, *ACS Chem. Neurosci.*, 2018, **9**, 2679–2688.
- 54 H. Skaat, R. Chen, I. Grinberg and S. Margel, *Biomacromolecules*, 2012, **13**, 2662–2670.

### 3. Synthesis and Aggregation of Polymer-Amyloid $\beta$ Conjugates

#### COMMUNICATION



Macromolecular  
Rapid Communications  
www.mrc-journal.de

## Synthesis and Aggregation of Polymer-Amyloid $\beta$ Conjugates

Zhanna Evgrafova, Sven Rothemund, Bruno Voigt, Gerd Hause, Jochen Balbach, and Wolfgang H. Binder\*

Modulating the assembly of medically relevant peptides and proteins via macromolecular engineering is an important step in modifying their overall pathological effects. The synthesis of polymer-peptide conjugates composed of the amyloidogenic Alzheimer peptide,  $A\beta_{1-40}$ , and poly(oligo(ethylene glycol)<sub>m</sub> acrylates) ( $m = 2,3$ ) with different molecular weights ( $M_n = 1400\text{--}6600\text{ g mol}^{-1}$ ) is presented here. The challenging conjugation of a synthetic polymer to an in situ aggregating protein is established via two different coupling strategies, only successful for polymers with molecular weights not exceeding  $6600\text{ g mol}^{-1}$ , relying on resin-based synthesis or solution-based coupling chemistries. The conjugates are characterized by high-performance liquid chromatography and matrix-assisted laser desorption ionization time-of-flight mass spectrometry. The aggregation of these polymer- $A\beta_{1-40}$  conjugates, as monitored via thioflavine-T (ThT)-fluorescence spectroscopy, is accelerated mainly upon attaching the polymers. However, the appearance of the observed fibrils is different from those composed of native  $A\beta_{1-40}$ , specifically with respect to length and morphology of the obtained aggregates. Instead of long, unbranched fibrils characteristic for  $A\beta_{1-40}$ , bundles of short aggregates are observed for the conjugates. Finally, the ThT kinetics and morphologies of  $A\beta_{1-40}$  fibrils formed in the presence of the conjugates give some mechanistic insights.

Polymer-protein conjugates belong to a very important class of hybrid molecules, displaying both, the biological properties of the protein moieties and the function of the attached synthetic polymer chain.<sup>[1]</sup> On the one hand, synthetic polymers can endow a protein with advanced properties, such as an improved stability,<sup>[2]</sup> modulated bioavailability,<sup>[3]</sup> enhanced biocompatibility,<sup>[1]</sup> and improved pharmacokinetics.<sup>[4]</sup> On the other hand, proteins exhibit a unique architectural complexity, including defined secondary and tertiary structures and often quaternary assembly profiles.<sup>[5,6]</sup> Synthetic polymers can also form well-organized complex architectures, yet with a different degree of three dimensional (3D)-arrangement. This complexity extends for the increasing class of well-recognized intrinsically disordered proteins since the induction of structural motifs is only observed during binding events or aggregation.<sup>[7]</sup> Aggregation of a large variety of peptides and proteins into amyloid fibrils leads to a plethora of neurodegenerative disorders,<sup>[8-10]</sup> so-called amyloidoses. A significant number of attempts

have been made to find a system capable of either redirecting the aggregation process or disassembling well-organized secondary structures of fibrils.<sup>[11-20]</sup> These include admixture of small organic molecules,<sup>[21]</sup> proteins mimics,<sup>[22]</sup> or nanoparticles,<sup>[23]</sup> or a coupling of amyloidogenic short peptides to synthetic polymers to feature inhibition and even disassembly of already aggregated fibrils.<sup>[24,25]</sup> Song and coworkers have demonstrated that multivalent peptide-polymer conjugates are able to efficiently disrupt preformed  $A\beta_{1-40}$  fibrils.<sup>[24]</sup> Castelletto et al. stated significant changes of fibril packing pattern along with a prominent difference of “self-assembled nanostructures,” detected by conjugation of a model amyloid peptide  $A\beta_{16-20}$ (KLVFF) with poly(ethylene glycol) (PEG) of different chain lengths.<sup>[26]</sup> Previously, Castelletto et al. also reported on a change of persistence length of YYKLVFF-PEG conjugate's fibrils, depending on the molecular weights of PEG.<sup>[27]</sup> The self-assembly properties of the model amyloid peptide  $A\beta_{16-20}$ (KLVFF) were notably interfered by conjugation of the peptide with poly(*N*-isopropylacrylamide) and poly(hydroxyethylacrylate) of low molecular weights.<sup>[28]</sup>

We here investigate how the conjugation of poly(oligo(ethylene glycol)<sub>m</sub> acrylates), whose hydrophilicity is varied by changing the number of ethylene glycol units in the

Z. Evgrafova, Prof. W. H. Binder  
Faculty of Natural Science II, Institute of Chemistry  
Martin-Luther University Halle-Wittenberg  
Von-Danckelmann-Platz 4, D-06120 Halle (Saale), Germany  
E-mail: wolfgang.binder@chemie.uni-halle.de

Dr. S. Rothemund  
Core Unit Peptide Technologies  
Liebigstraße 21, D-04103 Leipzig, Germany

B. Voigt, Prof. J. Balbach  
Faculty of Natural Science II  
Institute of Physics  
Martin-Luther University Halle-Wittenberg  
Betty-Heimann-Str. 7, D-06120 Halle (Saale), Germany

Dr. Gerd Hause  
Martin-Luther University Halle-Wittenberg  
Biocenter, Weinbergweg 22, D-06120 Halle (Saale), Germany

The ORCID identification number(s) for the author(s) of this article can be found under <https://doi.org/10.1002/marc.201900378>.

© 2019 The Authors. Published by WILEY-VCH Verlag GmbH & Co. KGaA, Weinheim. This is an open access article under the terms of the Creative Commons Attribution-NonCommercial-NoDerivs License, which permits use and distribution in any medium, provided the original work is properly cited, the use is non-commercial and no modifications or adaptations are made.

DOI: 10.1002/marc.201900378

side chain ( $m = 2,3$ ), to  $A\beta_{1-40}$  can influence its aggregation. In the presented study, we have primarily focused on the biologically significant amyloidogenic peptide  $A\beta_{1-40}$  instead of its short fragments, thus facing the synthetic challenge to link the synthetic polymers to an in situ assembling protein. To this end, we have synthesized and characterized a series of covalently

bonded polymer-peptide conjugates based on hydrophilic poly(oligo(ethylene glycol) $_m$  acrylates) ( $m = 2,3$ ) (for general procedure, see Tables S1 and S2 and Figures S9–S18, Supporting Information) to the N-terminus of the  $A\beta_{1-40}$  peptide (Figure 1 and Figure S1, Supporting Information). We aimed to follow the aggregation kinetics of the conjugates and subsequently

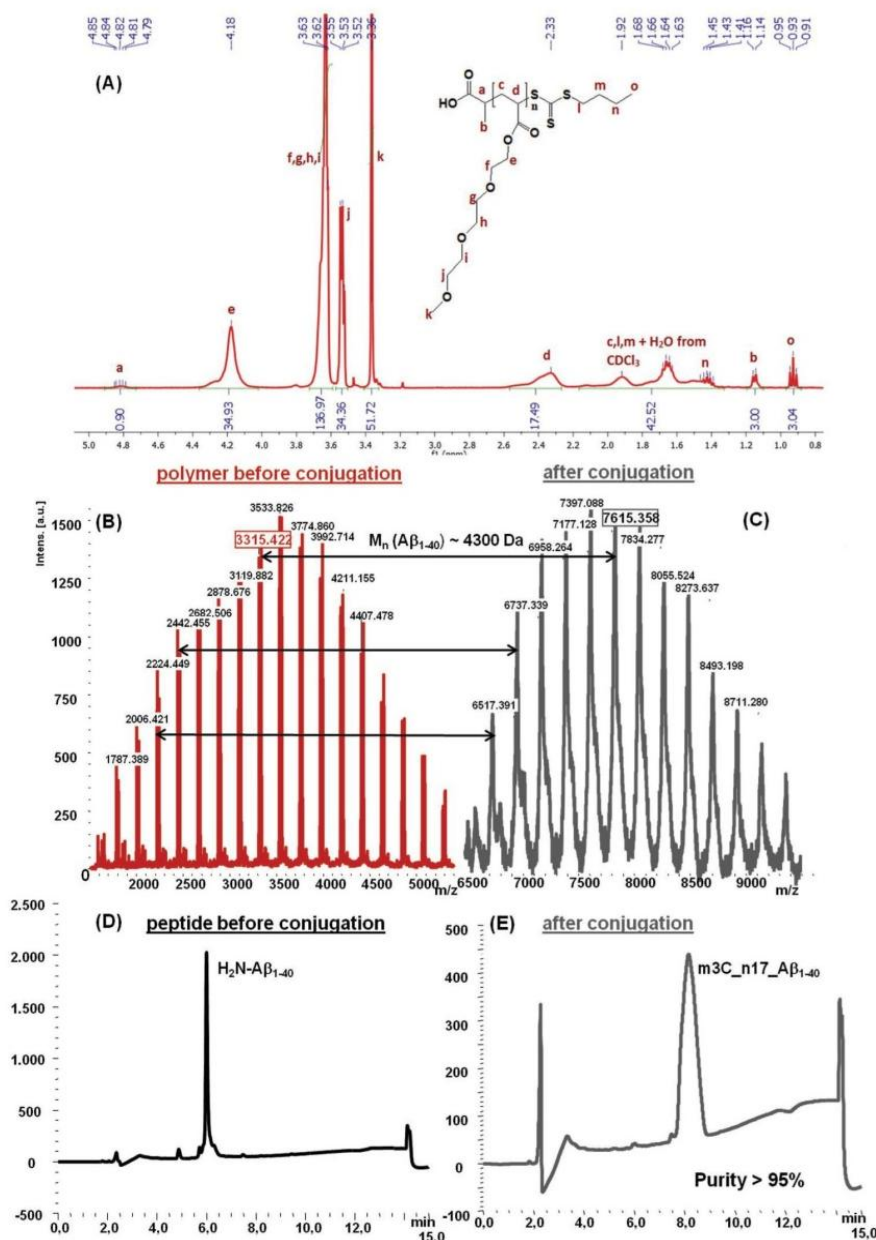


**Figure 1.** A)  $^1\text{H}$  NMR spectrum of the polymer  $m3C_{n17}$ , B) MALDI-TOF MS spectrum of the polymer  $m3C_{n17}$  obtained before conjugation (dark red). Simulated isotopic patterns of the chosen series are shown in Figure S18, Supporting Information. C) MALDI-TOF MS spectrum of the conjugate  $m3C_{n17}\text{-}A\beta_{1-40}$  obtained after conjugation (gray). Arrows represent the molecular mass difference corresponding to the  $A\beta_{1-40}$  peptide conjugated to the polymer. D) HPLC chromatogram of the  $\text{H}_2\text{N-}A\beta_{1-40}$  before conjugation. E) HPLC chromatogram of the  $m3C_{n17}\text{-}A\beta_{1-40}$  conjugate. The peak at 8.2 min represents the purified product.

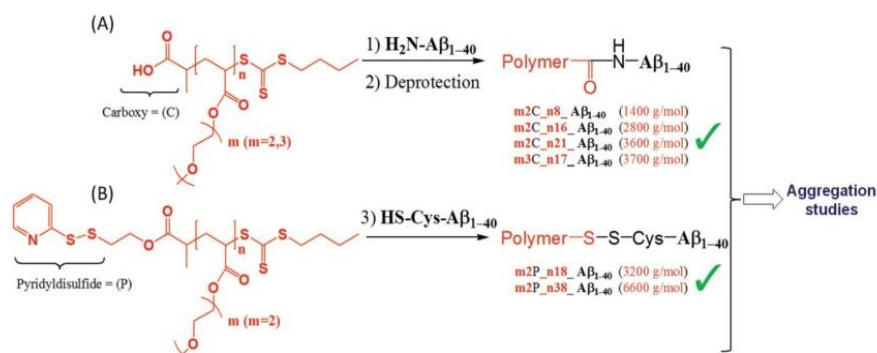
analyze the morphology and structure of the obtained aggregates by transmission electron microscopy (TEM) (Scheme 1 and Scheme S1, Supporting Information).

The successful attachment of synthetic polymers onto assembling proteins such as  $A\beta_{1-40}$  presents a significant challenge, as—during solution linkage—the protein can already start fibrillation, thus blocking possible conjugation sites for the chemical linkage process. A plethora of different linking methods has been already probed, covering Staudinger ligation,<sup>[29]</sup> Michael's addition,<sup>[30]</sup> thio-bromo “click” reaction,<sup>[31]</sup> oxime/hydrazone chemistry,<sup>[32]</sup> Diels–Alder cycloaddition,<sup>[33]</sup> and Suzuki coupling;<sup>[34]</sup> however, none of them on truly in situ assembling peptides or proteins. Our chosen approach used two different strategies as shown in Scheme 1, namely either an on-resin solid phase synthesis (SPS, pathway A) based on carbodiimide (DIC-) coupling or a solution-based coupling via thiol-exchange chemistry (via pyridyldisulfides) (pathway B). The synthetic polymers, poly(oligo(ethylene glycol)<sub>m</sub> acrylates), were synthesized by RAFT-polymerization, enabling the introduction of protein-reactive end groups, namely P = pyridyldisulfide and C = carboxy group for the subsequent attachments to  $A\beta_{1-40}$  (Scheme 1 and Scheme S1, Supporting Information). All polymers were obtained in yields up to 95%, and fully characterized by NMR spectroscopy (Figure 1A and Supporting Information), MALDI-TOF MS (Figure 1B and Supporting Information) and GPC, with low polydispersity indices (PDIs) and defined molecular weights ( $M_n$ ), ranging from 1.1 to 1.2 and 1400 to 11 700 g mol<sup>-1</sup>, respectively, (see Table S2, Supporting Information, for details).

We first probed the in situ linkage on the preloaded resin, where  $H_2N-A\beta_{1-40}$  was amino terminally coupled to the carboxy-functionalized polymers with molecular weights of 1400–11 700 g mol<sup>-1</sup> (Scheme 1A and Tables S2 and S3, Supporting Information) using conventional DIC coupling. When probing different molecular weights of the polymers, a successful conjugation took place only in the case of polymers whose molecular mass did not exceed 3700 g mol<sup>-1</sup> (NMR).<sup>[35–37]</sup> In the case of polymers with a higher molecular

mass (6700–11 700 g mol<sup>-1</sup>, Table S2, Supporting Information), coupling was not efficient leading to a low yield of the conjugated product (<1%). The so obtained crude conjugates were purified to >95% purity using preparative RP-HPLC, furnishing the final, purified conjugates in final yields of 8.1–26.5% (Table S3, Supporting Information). In order to improve the coupling yields, we also probed another strategy, namely, the solution-coupling of the pyridyldisulfide-functionalized polymers with molecular weights of 3200–7700 g mol<sup>-1</sup> (Table S2, Supporting Information) with an additional cysteine at the amino terminus of HS-Cys- $A\beta_{1-40}$  for 2 h at room temperature (Scheme 1B). In this case, two polymers with molecular weights of 3200 and 6600 g mol<sup>-1</sup> (Table S2, Supporting Information) were successfully conjugated to  $A\beta_{1-40}$ , yielding the purified conjugates (purity >95% via RP-HPLC) in yields of 21.7% and 33.6% (Table S3, Supporting Information), respectively.<sup>[35–37]</sup> The higher-molecular mass of the pyridyldisulfide-functionalized polymers (7200–7700 g mol<sup>-1</sup>) (Table S2, Supporting Information) in turn enhanced the oligomerization of the  $A\beta_{1-40}$  peptide, which resulted in a low yield of the conjugated product (<1%). In all cases, the successful coupling could be proven using analytical HPLC and matrix-assisted laser desorption/ionization time-of-flight mass spectrometry (MALDI-TOF MS), which revealed the mass peaks in the expected range (see Figure 1 and Figures S1–S8, Supporting Information).

MALDI-TOF MS analysis of the product prepared via coupling of the carboxy-functionalized polymer m3C\_n17 to the amino terminus of  $A\beta_{1-40}$  is depicted in Figure 1C compared to the starting polymer m3C\_n17 (Figure 1B). In Figure 1B,C, a significant shift of the mass signals of the conjugate relative to the uncoupled polymer can be seen; for example, the mass signal is shifted from 2224 Da (Figure 1B) to 6517 Da (Figure 1B), corresponding to the mass difference of  $A\beta_{1-40}$ . HPLC results also prove the formation of the respective conjugates, demonstrating a disappearance of the signal at 6 min retention time, assigned to  $A\beta_{1-40}$  (Figure 1D) and emergence of the broad signal at 8.2 min of the conjugate.



**Scheme 1.** Experimental concept of the synthesis and aggregation of poly(oligo(ethylene glycol)<sub>m</sub> acrylate)- $A\beta_{1-40}$  conjugates. The polymers are shown in red and  $A\beta_{1-40}$  in bold black. Successful conjugation attempts are indicated with a check mark (green). Molecular weights of the employed polymers are shown in brackets. A) Synthetic pathway for the preparation of the conjugates between poly(oligo(ethylene glycol)<sub>m</sub> acrylates) ( $m = 2,3$ ) displaying a reactive carboxy-end group, and  $A\beta_{1-40}$  utilizing DIC, Oxyma coupling chemistry. B) Synthesis of conjugates between poly(oligo(ethylene glycol)<sub>m</sub> acrylates) ( $m = 2$ ) carrying a pyridyldisulfide-reactive end group. The name of every sample comprises:  $m(2,3)$ , the number of ethylene glycol units in the side chain of the polymer; (C), (P), the end-group of the polymer; (n) followed by a number, the degree of polymerization.

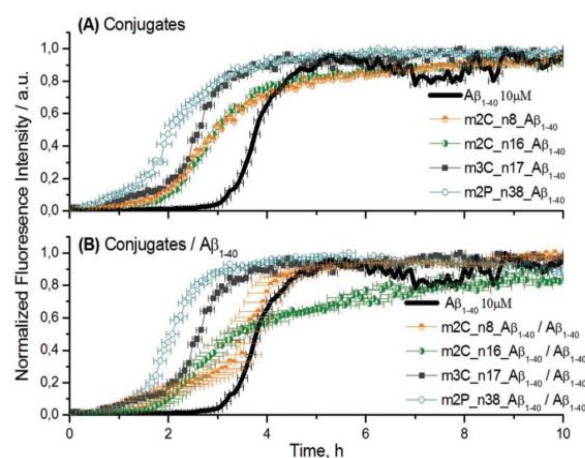


**Figure 2.** Time evolution of the ThT fluorescence intensity at  $\lambda_{\text{em}} = 480$  nm of the A)  $10 \mu\text{M}$  solutions of poly(oligo(ethylene glycol)<sub>m</sub> acrylates)- $A\beta_{1-40}$  conjugates and B)  $10 \mu\text{M}/10 \mu\text{M}$  solutions of poly(oligo(ethylene glycol)<sub>m</sub> acrylates)- $A\beta_{1-40}$  conjugates/ $A\beta_{1-40}$ . For all the measurements  $50 \text{ mM}$   $\text{Na}_2\text{HPO}_4$ ,  $150 \text{ mM}$   $\text{NaCl}$  buffer (pH 7.4), supplemented with  $10 \mu\text{M}$  ThT were used. The black solid line corresponds to sole  $A\beta_{1-40}$ . A representative example along with error bars based on three independent measurements at  $37^\circ\text{C}$  is shown. For raw data see Figure S19, Supporting Information.

All further investigations were conducted with the polymer- $A\beta_{1-40}$  conjugates with  $M_n(\text{polymer}) < 6600 \text{ g mol}^{-1}$ , prepared by either the thiol-based or the amino-based linkages.

ThT-dependent fibrillation kinetics of the conjugates were followed by fluorescence spectroscopy at  $37^\circ\text{C}$ . Four conjugates with different molecular weights ( $5200\text{--}9100 \text{ g mol}^{-1}$  as estimated by MALDI-TOF MS), synthesized by both coupling methods and displaying two to three ethylene glycol units ( $m = 2, 3$ ) in the side chain were chosen. As in previous studies, all experiments were recorded under physiological pH = 7.4.<sup>[38]</sup> (For further details of sample preparations see Supporting Information).

Conjugation of the poly(oligo(ethylene glycol)<sub>m</sub> acrylates) to  $A\beta_{1-40}$  enhances its aggregation in comparison to the uncoupled  $A\beta_{1-40}$  (Figure 2A and Table 1), thereby decreasing the lag ( $t_{\text{lag}}$ )

and characteristic ( $t_{\text{char}}$ ) times of fibril formation to  $1.54 \pm 0.13$  and  $2.04 \pm 0.15$  h, compared to  $3.25 \pm 0.12$  and  $3.83 \pm 0.1$  h for native  $A\beta_{1-40}$ . Additionally, the rate of aggregation was correlated mainly to the molecular mass of the conjugated polymer: For example, the fastest aggregation was observed in case of the conjugate with the highest molecular weight (Table 1 and Scheme S2, Supporting Information). The fibrillation of the native amyloid  $A\beta_{1-40}$  peptide is complex and—especially in its first steps—only poorly understood, primarily guided by a kinetically controlled, nucleation-based assembly process. We assume that conjugation of  $A\beta_{1-40}$  to the chosen polymers reduces their overall mobility, as often observed for protein/polymer conjugates. However, we propose a significant increase of local hydrophobicity of the  $A\beta_{1-40}$  due to the contribution of the hydrophobic backbone<sup>[39]</sup> of the conjugated polymer. We imagine that this alteration of the hydrophobicity leads to the enhanced assembly process, similar to those observed in lipid- $A\beta_{1-40}$  conjugates.<sup>[13]</sup>

Important in such aggregation processes is the final morphology of the obtained aggregates, most of all in comparison to the non-conjugated  $A\beta_{1-40}$  fibrils. Thus, the morphologies of the acquired aggregates were analyzed by TEM, indicating that the here studied polymer-peptide conjugates build bundles of short aggregates (Figure 3D–F) as compared to long and straight fibrils characteristic for uncoupled  $A\beta_{1-40}$  (Figure 3A).

Since polymer-peptide conjugates in some cases are able to modulate a fibrillation pathway of the  $A\beta_{1-40}$  as well as the morphology of the obtained fibrils,<sup>[24]</sup> the aggregation of the  $A\beta_{1-40}$  physically mixed with the here prepared conjugates was additionally investigated. The obtained data (Figure 2B and Table 1) indicate the preservation of the trend, namely enhancement of the ThT-detected kinetics, as revealed for the conjugates alone (Scheme S2, Supporting Information). At the same time, the prepared conjugates do not protect the mixed  $A\beta_{1-40}$  from the formation of long fibrils (Figure 3B,C) as sometimes observed by others.<sup>[24,25]</sup> The presented data indicate that by conjugation of  $A\beta_{1-40}$  to the poly(oligo(ethylene glycol)<sub>m</sub> acrylates) one can effectively prevent formation of the long, straight fibrils, but these conjugates do not disrupt the morphology of the fibrils obtained from the non-conjugated  $A\beta_{1-40}$ .

**Table 1.** Summary of the investigated polymer- $A\beta_{1-40}$  conjugates and polymer- $A\beta_{1-40}/A\beta_{1-40}$  mixtures.

Name	m	$M_n^{\text{MALDI}}$ [ $\text{g mol}^{-1}$ ]	Appearance of aggregates	$t_{\text{lag}}$ [h]	$t_{\text{char}}$ [h]
m2C_n8_ $A\beta_{1-40}$	2	5274.2	Bundles	$1.75 \pm 0.06$	$2.96 \pm 0.02$
m2C_n16_ $A\beta_{1-40}$	2	6132.7	Bundles	$1.93 \pm 0.3$	$2.96 \pm 0.1$
m2P_n38_ $A\beta_{1-40}$	2	9091.5	Bundles	$1.54 \pm 0.13$	$2.04 \pm 0.15$
m3C_n17_ $A\beta_{1-40}$	3	7397.1	Bundles	$1.84 \pm 0.14$	$2.63 \pm 0.1$
m2C_n8_ $A\beta_{1-40}/A\beta_{1-40}$	2	5274.2/4328	Fibrils	$1.55 \pm 0.5$	$3.56 \pm 0.39$
m2C_n16_ $A\beta_{1-40}/A\beta_{1-40}$	2	6132.7/4328	Fibrils	$1.66 \pm 0.06$	$2.79 \pm 0.28$
m2P_n38_ $A\beta_{1-40}/A\beta_{1-40}$	2	9091.5/4328	Fibrils	$1.27 \pm 0.12$	$1.83 \pm 0.1$
m3C_n17_ $A\beta_{1-40}/A\beta_{1-40}$	3	7397.1/4328	Fibrils	$2.03 \pm 0.19$	$2.55 \pm 0.13$
$A\beta_{1-40}$	—	4328	Fibrils	$3.25 \pm 0.12$	$3.83 \pm 0.1$

Molecular mass  $M_n$  of  $A\beta_{1-40}$  and the conjugates obtained via MALDI-TOF MS. The standard deviation ( $\pm$ ) for  $t_{\text{lag}}$  and  $t_{\text{char}}$  obtained from three independent measurements is given. The examples of piecewise linear fits are shown in Figure S20, Supporting Information.

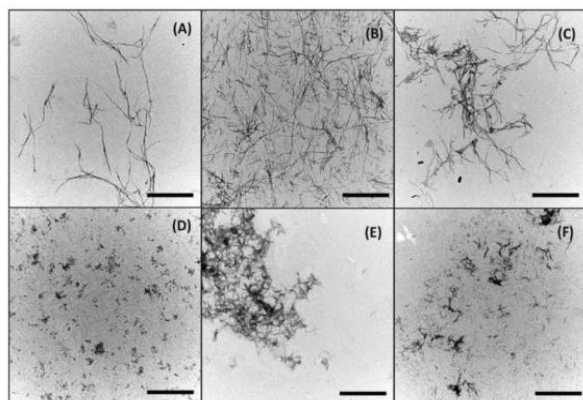


**Figure 3.** TEM images of the fibrils obtained after ThT kinetic measurements A)  $A\beta_{1-40}$ , B)  $m2C\_n8\_A\beta_{1-40}/A\beta_{1-40}$  (mixture of conjugate/ $A\beta_{1-40}$ ), C)  $m3C\_n17\_A\beta_{1-40}/A\beta_{1-40}$ , D)  $m2P\_n38\_A\beta_{1-40}$  (only conjugate), E)  $m2C\_n8\_A\beta_{1-40}$ , and F)  $m3C\_n17\_A\beta_{1-40}$ . The scale bar corresponds to 1000 nm.

The acceleration of  $A\beta_{1-40}$  fibril formation in the presence of the conjugates (Figure 2B) can clearly be addressed to the polymer moiety because about the same acceleration had been observed for the conjugates alone (Figure 2A). This crossover between  $A\beta_{1-40}$  and conjugate fibrillation is manifested in the ThT fibrillation kinetics, which is not simply a superposition of the ThT kinetics of  $A\beta_{1-40}$  and the kinetics of the conjugate in physical mixture of both molecules, but a cooperative single transition step (see, e.g., the dark gray kinetics in Figure 2B). This intertwined mechanism is supported by the TEM images. A qualitative inspection shows no superposition of long fibrils and short fibril bundles in the mixtures of  $A\beta_{1-40}$  and the conjugates but mostly long, straight fibrils (comparison, e.g., of Figure 3B,E).

Acceleration of fibril formation can be potentially a prospective strategy for reduction of the  $A\beta_{1-40}$  oligomers lifespan,<sup>[40]</sup> which are supposed to be the toxic species for neurons. The observation that poly(oligo(ethylene glycol)<sub>m</sub> acrylates) accelerate amyloid fibril formation seems to be a generic property, because we reported recently the same phenomenon for the parathyroid hormone.<sup>[38]</sup> This peptide is completely unrelated in length and primary sequence to  $A\beta_{1-40}$  but both ThT kinetics of physical mixture and of conjugates with the here studied polyacrylates were accelerated.

Finally, we have investigated LCST behavior of all the employed polymers and the conjugates under fibrillation experiment conditions. First, we checked the native polymers, namely  $m2C\_n8$ ,  $m2C\_n16$ ,  $m3C\_n18$ , and  $m2P\_n38$ , which after conjugation were used for the fibrillation experiment. Only polymer  $m2P\_n38$  possesses an LCST under the applied conditions (65.2 °C), with all other polymers devoid of a transition up to 90 °C. Second, we examined the four  $A\beta_{1-40}$  conjugates in view of their potential transition temperatures: none of the conjugates displayed LCST behavior at temperatures up to 90 °C, in line with observations on similar poly(di(ethylene glycol) acrylates), considering the low concentration of our samples (10  $\mu$ M), the use of the phosphate buffer required for the ThT assay, the end groups, and the molecular weight of our

current samples.<sup>[11,41–43]</sup> A further increase of  $T_{cp}$  in the case of  $m2P\_n38\_A\beta_{1-40}$  conjugate compared to the non-conjugated polymer could arise from the steric hindrance<sup>[44]</sup> associated with the attachment of the peptide.

In summary, effective strategies for preparation and purification of conjugates between the amyloidogenic peptide  $A\beta_{1-40}$  and poly(oligo(ethylene glycol)<sub>m</sub> acrylates) were developed, placing both, in situ SPS/DIC-coupling and in-solution pyridyldisulfide coupling in the synthetic focus. In both approaches, we found that the initial molecular mass of the polymer plays an important role in the aggregation behavior of the conjugates, since all the attempts to prepare a conjugate with polymers whose molecular mass surpassing 6600 g mol<sup>-1</sup> failed. This trend was also observed during the aggregation experiment of the prepared conjugates via ThT-dependent kinetic measurements: The conjugate with the highest molecular mass aggregate faster than the counterparts with lower molecular weights or native  $A\beta_{1-40}$  itself. Notably, the length and morphology of the obtained aggregates from the conjugates turned out to be considerably different to  $A\beta_{1-40}$  fibrils. In lieu of straight, long, unbranched fibrils, we observed bundles of short aggregates, still capable to bind ThT. Additionally, the conjugates do not significantly alter the morphology of  $A\beta_{1-40}$  fibrils when added in physical mixtures during fibril formation. Thereby, the conjugation of polymers to amyloidogenic peptides or proteins can modulate their aggregation pathway and open a foothold for many future potential strategies for hybrid-systems, composed of aggregating proteins and synthetic polymers.

### Supporting Information

Supporting Information is available from the Wiley Online Library or from the author.

### Acknowledgements

The study was supported by the Deutsche Forschungsgemeinschaft (DFG, ProjektNr 189853844, TRR-SFB 102, A03, and A12). The authors further acknowledge a grant from the "Leistungszentrum Chemie und Systembiologie," Biologisch abbaubare Partikel über Enkapsulierungsmethoden: Emulsions-/Evaporationsverfahren und 3D-Printing (Uni-CBS1) from the Land-Sachsen-Anhalt. The authors would like to acknowledge Dr. Juliane Adler for enlightening discussions regarding the project.

### Conflict of Interest

The authors declare no conflict of interest.

### Keywords

aggregation, amyloid  $\beta$ , coupling, fibrils, polymer–peptide conjugates

Received: July 29, 2019

Revised: September 20, 2019

Published online: October 21, 2019



- [1] K. L. Heredia, H. D. Maynard, *Org. Biomol. Chem.* **2007**, *5*, 45.
- [2] V. Thilakarathne, V. A. Briand, Y. Zhou, R. M. Kasi, C. V. Kumar, *Langmuir* **2011**, *27*, 7663.
- [3] N. V. Katre, *Adv. Drug Delivery Rev.* **1993**, *10*, 91.
- [4] W. Gao, W. Liu, T. Christensen, M. R. Zalutsky, A. Chilkoti, *Proc. Natl. Acad. Sci. USA* **2010**, *107*, 16432.
- [5] S. W. Englander, L. Mayne, *Proc. Natl. Acad. Sci. USA* **2014**, *111*, 15873.
- [6] N. H. Andersen, *J. Am. Chem. Soc.* **2001**, *123*, 12933.
- [7] P. Dogra, M. Bhattacharya, S. Mukhopadhyay, *J. Phys. Chem. B* **2017**, *121*, 412.
- [8] A. Alzheimer, *Z. Gesamte Neurol. Psychiatr.* **1911**, *4*, 356.
- [9] T. P. J. Knowles, M. Vendruscolo, C. M. Dobson, *Nat. Rev. Mol. Cell Biol.* **2014**, *15*, 384.
- [10] I. W. Hamley, *Angew. Chem., Int. Ed.* **2007**, *46*, 8128.
- [11] S. Funtan, Z. Evgrafova, J. Adler, D. Huster, H. W. Binder, *Polymers* **2016**, *8*, 178.
- [12] P. M. H. Heegaard, U. Boas, D. E. Otzen, *Macromol. Biosci.* **2007**, *7*, 1047.
- [13] J. Adler, H. A. Scheidt, K. Lemmnitzer, M. Krueger, D. Huster, *Phys. Chem. Chem. Phys.* **2017**, *19*, 1839.
- [14] E. Hellstrand, E. Sparr, S. Linse, *Biophys. J.* **2010**, *98*, 2206.
- [15] J.-M. Lin, T.-L. Lin, U. S. Jeng, Z.-H. Huang, Y.-S. Huang, *Soft Matter* **2009**, *5*, 3913.
- [16] A. Assarsson, E. Hellstrand, C. Cabaleiro-Lago, S. Linse, *ACS Chem. Neurosci.* **2014**, *5*, 266.
- [17] M. Villmow, M. Baumann, M. Malesevic, R. Sachs, G. Hause, M. Fändrich, J. Balbach, C. Schiene-Fischer, *Biochem. J.* **2016**, *473*, 1355.
- [18] S. Kumar, A. D. Hamilton, *J. Am. Chem. Soc.* **2017**, *139*, 5744.
- [19] K. Dahse, M. Garvey, M. Kovermann, A. Vogel, J. Balbach, M. Fändrich, A. Fahr, *J. Mol. Biol.* **2010**, *403*, 643.
- [20] H. Sun, J. Liu, S. Li, L. Zhou, J. Wang, L. Liu, F. Lv, Q. Gu, B. Hu, Y. Ma, S. Wang, *Angew. Chem., Int. Ed.* **2019**, *58*, 5988.
- [21] D. E. Ehrnhoefer, J. Bieschke, A. Boeddrich, M. Herbst, L. Masino, R. Lurz, S. Engemann, A. Pastore, E. E. Wanker, *Nat. Struct. Mol. Biol.* **2008**, *15*, 558.
- [22] T. Takahashi, H. Mihara, *Acc. Chem. Res.* **2008**, *41*, 1309.
- [23] C. Cabaleiro-Lago, F. Quinlan-Pluck, I. Lynch, S. Lindman, A. M. Minogue, E. Thulin, D. M. Walsh, K. A. Dawson, S. Linse, *J. Am. Chem. Soc.* **2008**, *130*, 15437.
- [24] Y. Song, E. G. Moore, Y. Guo, J. S. Moore, *J. Am. Chem. Soc.* **2017**, *139*, 4298.
- [25] H. Kakwere, R. J. Payne, K. A. Jolliffe, S. Perrier, *Soft Matter* **2011**, *7*, 3754.
- [26] V. Castelletto, G. Cheng, S. Fuzeland, D. Atkins, I. W. Hamley, *Soft Matter* **2012**, *8*, 5434.
- [27] V. Castelletto, G. E. Newby, D. Hermida Merino, I. W. Hamley, D. Liu, L. Noirez, *Polym. Chem.* **2010**, *1*, 453.
- [28] S. Dehn, V. Castelletto, I. W. Hamley, S. Perrier, *Biomacromolecules* **2012**, *13*, 2739.
- [29] B. L. Nilsson, L. L. Kiessling, R. T. Raines, *Org. Lett.* **2000**, *2*, 1939.
- [30] M. P. Lutolf, N. Tirelli, S. Cerritelli, L. Cavalli, J. A. Hubbell, *Bioconjugate Chem.* **2001**, *12*, 1051.
- [31] S. Kumar, S. Deike, W. H. Binder, *Macromol. Rapid Commun.* **2018**, *39*, 1700507.
- [32] D. K. Kölmel, E. T. Kool, *Chem. Rev.* **2017**, *117*, 10358.
- [33] A. Sanyal, *Macromol. Chem. Phys.* **2010**, *211*, 1417.
- [34] M. A. Gauthier, H.-A. Klok, *ChemComm* **2008**, 2591.
- [35] Y.-A. Lu, A. M. Felix, *React. Polym.* **1994**, *22*, 221.
- [36] L. A. Canalle, D. W. P. M. Löwik, J. C. M. van Hest, *Chem. Soc. Rev.* **2010**, *39*, 329.
- [37] I. W. Hamley, *Biomacromolecules* **2014**, *15*, 1543.
- [38] Z. Evgrafova, B. Voigt, M. Baumann, M. Stephani, W. H. Binder, J. Balbach, *ChemPhysChem* **2019**, *20*, 236.
- [39] J.-F. Lutz, *J. Polym. Sci., Part A: Polym. Chem.* **2008**, *46*, 3459.
- [40] E. H. Pilkington, M. Lai, X. Ge, W. J. Stanley, B. Wang, M. Wang, A. Kaminen, M.-A. Sani, M. R. Whittaker, E. N. Gurzov, F. Ding, J. F. Quinn, T. P. Davis, P. C. Ke, *Biomacromolecules* **2017**, *18*, 4249.
- [41] X. Qiu, T. Koga, F. Tanaka, F. M. Winnik, *Sci. China: Chem.* **2013**, *56*, 56.
- [42] G. Vancoillie, D. Frank, R. Hoogenboom, *Prog. Polym. Sci.* **2014**, *39*, 1074.
- [43] V. Aseyev, H. Tenhu, F. M. Winnik, in *Self Organized Nanostructures of Amphiphilic Block Copolymers II* (Eds: A. H. E. Müller, O. Borisov), Springer, Berlin **2011**, p. 29.
- [44] J. Liao, S. Liu, Y. Yuan, H. Zhang, *New J. Chem.* **2018**, *42*, 5698.

## 4. Probing Polymer Chain Conformation and Fibril Formation of Peptide Conjugates



DOI: 10.1002/cphc.201800867

CHEMPHYSICHEM  
Communications

### Probing Polymer Chain Conformation and Fibril Formation of Peptide Conjugates

Zhanna Evgrafova<sup>+, [a]</sup>, Bruno Voigt<sup>+, [b]</sup>, Monika Baumann,<sup>[b]</sup> Madlen Stephani,<sup>[b]</sup> Wolfgang H. Binder,<sup>\*, [a]</sup> and Jochen Balbach<sup>\*, [b]</sup>

Covalent conjugates between a synthetic polymer and a peptide hormone were used to probe the molecular extension of these macromolecules and how the polymer modifies the fibril formation of the hormone. NMR spectroscopy of <sup>15</sup>N labeled parathyroid hormone (PTH) was employed to visualize the conformation of the conjugated synthetic polymer, triggered by small temperature changes via its lower critical solution temperature. A shroud-like polymer conformation dominated the molecular architecture of the conjugated chimeras. PTH readily forms amyloid fibrils, which is probably the physiological storage form of the hormone. The polyacrylate based polymers stimulated the nucleation processes of the peptide.

Chimeras between a synthetic polymer and a biological peptide or protein moiety are valuable molecules because they combine the different functional properties of both entities often generating added values.<sup>[1]</sup> In case of the here studied thermo-responsive polymers, the conjugated peptide can modify the phase transition temperature, which is of high importance in many material science applications. On the other hand, the responsive polymer entity changes the solubility and activity of the biological entity utilized in various biomedical applications including prolonged pharmacokinetics.<sup>[2]</sup> These large variety of properties is based upon the molecular architecture of both conjugated entities.

In contrast to the well studied structural biology of peptides and proteins adopting mainly  $\alpha$ -helical and  $\beta$ -sheet structures,<sup>[3]</sup> synthetic polymer chains are usually unfolded, unless specific structure forming elements have been introduced.<sup>[4]</sup> Thus typically the shape of most polymers is regarded as a random coil, described by collective models to predict chain extension and conformation.<sup>[5]</sup> A large variety of experimental and theoretical methods has been used in the past to investigate the shape and form of unfolded macromolecules, such as static-

and dynamic light scattering<sup>[6]</sup> or viscosimetry, dating back to the fundamental investigations of Staudinger.<sup>[7]</sup> Modern methods to probe e.g. distance-relations between the ends of macromolecules including methods such as fluorescence resonance energy transfer (FRET),<sup>[8]</sup> triplet/triplet-energy transfer (TTET),<sup>[9]</sup> or ESR-spectroscopy<sup>[10]</sup> provide an average picture of chain extension. Especially the largely growing field of single-chain folded macromolecules,<sup>[5,11]</sup> where an individual chain of a synthetic macromolecule is folding into a singular nanoparticle,<sup>[12]</sup> is still elusively explored, because of a lack of specific methods to probe the folding of individual polymer based nanoparticles.

In the here presented study, we characterized chimeras of the parathyroid hormone with a thermo-responsive polymer. Structural biology tools applied to the peptide entity allowed us to characterize the molecular conformation of the synthetic polymer moiety. *Vice versa* the latter moiety modified a biological property of the hormone, which is the formation of functional amyloids.

The parathyroid peptide hormone (PTH) controls the Ca<sup>2+</sup> and phosphate homeostasis in blood and thus the bone and kidney metabolism.<sup>[13]</sup> It comprises 84 amino acid residues of which I5-N10 and S17-F34 show a high  $\alpha$ -helix propensity<sup>[14]</sup> required to bind to its cognate G protein coupled receptor.<sup>[15]</sup> Residues V35-Q84 are intrinsically disordered.<sup>[16]</sup> Both, PTH(1-34) and the here studied PTH(1-84) are approved drugs against osteoporosis (Forteo<sup>®</sup> and Natpara<sup>®</sup>, respectively). Chimeras of PTH(1-34) and polyethylene glycol displayed prolonged pharmacokinetic/pharmacodynamic properties *in vivo*.<sup>[17]</sup> Before PTH gets released to the blood it is stored in secretory granules,<sup>[18]</sup> where it forms functional amyloid fibrils.<sup>[16]</sup> This biological property of PTH has been employed to follow the influence of the synthetic polymer entity in the here studied chimeras (see below).

<sup>15</sup>N-NMR-spectroscopy of the peptide entity of the PTH chimeras was applied to judge the spatial extension and thus the conformation of the conjugated synthetic macromolecule (Figure 1). This molecular probe monitors contacts between the polymer and the individual amino acid residues of PTH. Towards this end we covalently conjugated the thermo-responsive pyridyl-disulfide-polyacrylate based polymer entity to <sup>15</sup>N labeled PTH (blue spheres in Scheme 1).

Two different synthetic polymers RP-22 and RP-23 (Scheme 1) were employed, both displaying a thermal transition, above which a conformational collapse is known to take place, characterized by a lower critical solution temperature: above this temperature, the polymers undergo a transition

[a] Z. Evgrafova,<sup>\*</sup> Prof. Dr. W. H. Binder  
Institute of Chemistry, Martin Luther University Halle-Wittenberg, Von-Danckelmann-Platz 4, 06120 Halle (Saale), Germany  
E-mail: wolfgang.binder@chemie.uni-halle.de

[b] B. Voigt,<sup>\*</sup> Dr. M. Baumann, M. Stephani, Prof. Dr. J. Balbach  
Institute of Physics, Martin Luther University Halle-Wittenberg, Betty-Heimann-Str. 7, 06120 Halle (Saale), Germany  
E-mail: jochen.balbach@physik.uni-halle.de

[†] These authors contributed equally to this work.

Supporting information for this article is available on the WWW under <https://doi.org/10.1002/cphc.201800867>

An invited contribution to a Special Issue on BioNMR Spectroscopy

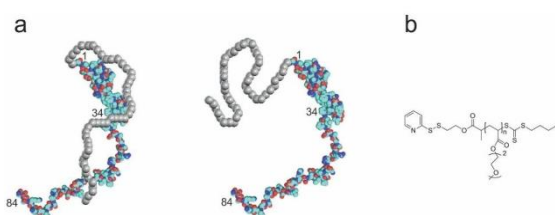


**Figure 1.** Experimental concept to study the conformation of the synthetic polymer (grey). Amino acids of the attached protein probe interactions with the polymer by NMR chemical shift changes in order to differentiate between a shroud-like structure with the polymer wrapping around the protein (left) and a dumbbell structure with a coil extending away from the protein (right). (B) Employed thermo-responsive polymer to switch between conformations by a temperature change.

from an expanded state (at  $T < T_{LCST}$ ) to a coiled state (at  $T > T_{LCST}$ ). Polymers were prepared by living polymerization methods (RAFT),<sup>[19]</sup> introducing the required linkage to PTH via the pyridyl-disulfide functionalized chain transfer agent. As shown in Scheme 1, RAFT-polymerization did enable to introduce the pyridyl-linkage quantitatively at one end of the polymer-chain, allowing concomitant chain-length control of the polymer (see Table 1; all experimental details including MALDI-MS and NMR-

**Table 1.** Synthetic polymers and polymer-conjugates, molecular masses, polydispersities and apparent hydrodynamic radii ( $r_{H,app}$ ) at 15 °C.

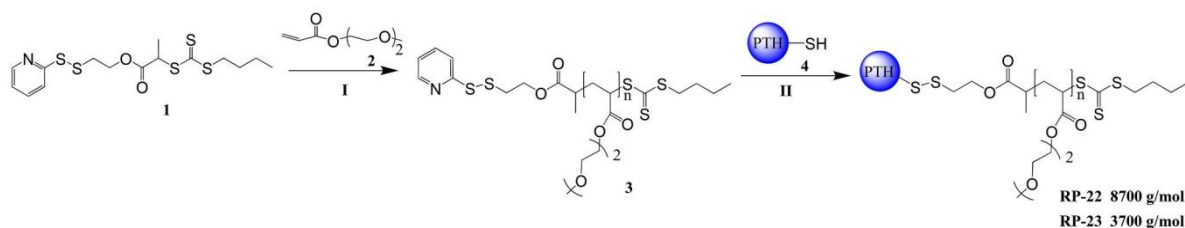
Molecule	Molecular mass [g mol <sup>-1</sup> ]	Polydispersity	$r_{H,app}$ [nm]
RP-22	8700	1.15	1.97 ± 0.01
RP-23	3700	1.11	1.34 ± 0.01
<sup>15</sup> N PTH	9550	–	2.48 ± 0.06
<sup>15</sup> N PTH V2 C-RP-22	ca. 18000	1.15	2.40 ± 0.04
<sup>15</sup> N PTH V2 C-RP-23	ca. 13200	1.11	2.61 ± 0.06
<sup>15</sup> N PTH Q84 C-RP-22	ca. 18000	1.15	2.58 ± 0.03
<sup>15</sup> N PTH Q84 C-RP-23	ca. 13200	1.11	2.62 ± 0.07

spectra are given in the Supporting Information). Adjustment of the  $T_{LCST}$  to physiological temperatures was accomplished by carefully adjusting the chain length to  $n=21$  (RP-23) and  $n=50$  (RP-22). The lower critical solution temperatures of the pure polymers RP-22 and RP-23 were determined by means of turbidimetry and found to be 38.6 °C and 24.7 °C (SI, Figure S1), respectively. Subsequent conjugation to the PTH peptide was achieved by a thiol disulfide exchange reaction with terminal

cysteine side chains introduced to the peptide either at the N-terminus (V2 C variant) or the C-terminus (Q84 C variant). Both cysteine variants <sup>15</sup>N PTH V2 C and <sup>15</sup>N PTH Q84 C were recombinantly expressed in *E. coli* according to published protocols<sup>[16]</sup> enabling the conjugation of the two thermo-responsive polymers RP-22 and RP-23 to these PTH variants by disulfide-exchange (Scheme 1) in yields of about 30%. Excessive polymer was removed by centrifugation above the  $T_{LCST}$  and the conjugate was purified (Figure 2) by ion exchange chromatography to remove PTH dimers and by size exclusion chromatography (SEC). MALDI-TOF mass spectrometry (e.g. for <sup>15</sup>N PTH Q84 C-RP-23 at 14.5 ml elution volume in Figure 2 and SI, Figure S2 and S3) confirmed the successful purification of the conjugates.

As the protein backbone chemical shifts and line widths are sensitive to changes in the local environment (within a few Å) of each amino acid residue of PTH, they can be employed to probe the conformation of the attached synthetic polymer. Comparison of the 2D <sup>15</sup>N HSQC spectra of <sup>15</sup>N PTH(1-84) (red in Figure 3 and with residue assignments in SI, Figure S4) and <sup>15</sup>N PTH Q84 C-RP-23 (black in Figure 3) revealed residues in close proximity to the C-terminally conjugated polymer chain by differences in the chemical shifts. E.g. the cross peak of Ser83 at 8.26 ppm (<sup>1</sup>H) and 117.8 ppm (<sup>15</sup>N) shifted to a new position in the RP-23 conjugate, whereas Glu61 at 8.41 ppm (<sup>1</sup>H) and 125.2 ppm (<sup>15</sup>N) did not. For other residues, NMR intensities significantly dropped (e.g. Gly12 and Gly38 at 25 °C in Figure 3). Plotting these changes along the peptide sequence showed that the RP-23 polymer conjugated at the C-terminus of PTH caused at 15 °C, a temperature below the  $T_{LCST}$  of RP-23, major changes only at the last 6 residues at the C-terminus. This indicates that RP-23 has an extended dumbbell conformation. At 25 °C RP-23 formed a much more compact shroud-like conformation in the PTH conjugates because residues all the way to the N-terminus are strongly affected when reaching the  $T_{LCST}$ . Note that the presence of non-conjugated RP-23 in the <sup>15</sup>N PTH samples had no effect on the NMR resonances of the peptide at both temperatures (SI, Figure S5).

Conjugated RP-23 at the N-terminus of PTH significantly affected the NMR resonances up to alanine 39 (SI, Figure S6) with a less pronounced difference between 15 °C and 25 °C. Note that the N-terminus has a high  $\alpha$ -helical propensity up to Phe34, whereas the C-terminal residues are intrinsically disordered. This difference in secondary structure of PTH might



**Scheme 1.** Synthetic pathway for the protein/thermo-responsive polymer conjugates: I – RAFT polymerization; II – polymer-protein conjugation through thiol-disulfide exchange.

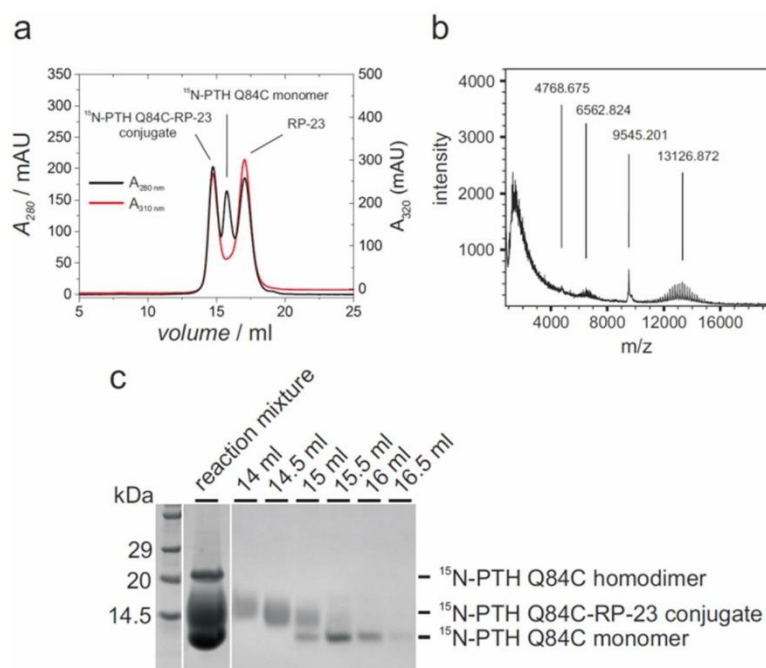


**Figure 2.** The purification of the  $^{15}\text{N}$  PTH Q84 C + RP-23 reaction mixture leads to the isolated conjugated product. Size exclusion chromatography (a) is shown as the last step of the purification protocol. The absorbance at 310 nm, which only detects the trithiocarbonyl group of the polymer, shows two peaks corresponding to the free polymer and to the conjugate. Mass spectrometric (MALDI-TOF) (b) and SDS-PAGE (c) analysis confirm the successful linkage of the polymer RP-23 to  $^{15}\text{N}$  PTH Q84 C (expected masses:  $M(^{15}\text{N}$  PTH Q84 C) =  $9524.74 \text{ g mol}^{-1}$ ,  $M(\text{RP-23}) = \text{ca. } 3700 \text{ g mol}^{-1}$ ,  $M(^{15}\text{N}$  PTH Q84 C-RP-23) =  $\text{ca. } 13200 \text{ g mol}^{-1}$ ).

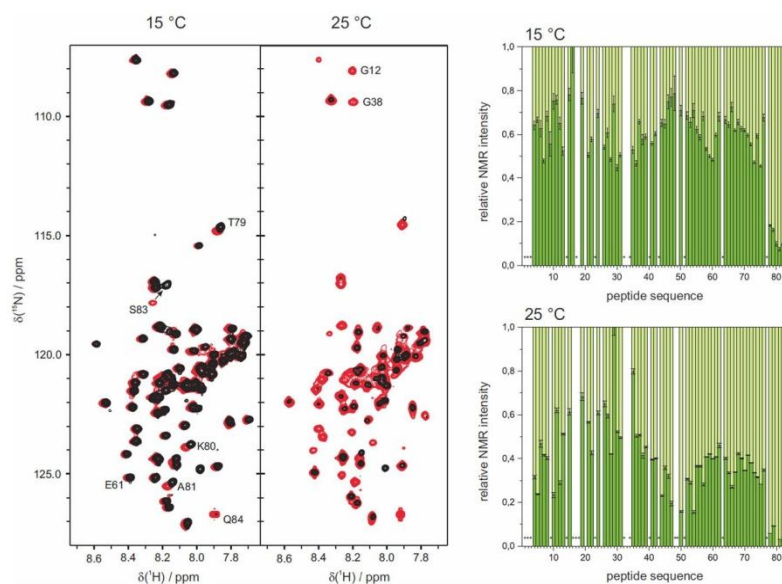


**Figure 3.** 2D  $^1\text{H}$ - $^{15}\text{N}$  HSQC NMR spectra of  $^{15}\text{N}$  PTH Q84 C-RP23 (black) at  $15^\circ\text{C}$  and  $25^\circ\text{C}$  compared to the spectra of the non-conjugated  $^{15}\text{N}$  PTH variants (red). The diagrams illustrate the relative NMR intensity changes at the respective cross peak positions in the  $^{15}\text{N}$  PTH spectrum along the peptide sequence. Prolines and residues with non-detectable cross peaks are indicated by an asterisk.

cause the different NMR signature for RP-23 when attached to the N- or the C-terminus of PTH.

Conjugated RP-22 with a more than 2-fold higher molecular mass showed about the same NMR signature as RP-23 when

conjugated to the C-terminus of PTH (SI, Figure S7). In contrast, basically all PTH residues sensed RP-22 when N-terminally attached indicating a shroud-like conformation. Hydrodynamic radii derived from NMR diffusion experiments pointed into the same direction (Table 1). Conjugation of RP-23 to the N- or C-terminus of PTH and of RP-22 to the C-terminus increased the apparent radius, whereas N-terminal attachment of RP-22 did not. These results document that standard protein NMR spectroscopy can be employed to monitor the conformation of polymers in chimeric conjugates.

Next, we asked the question whether the here studied polymers affect the biological function of the peptide. For this purpose we focused on the ability of PTH to form amyloid fibrils as reported earlier.<sup>[16]</sup> This process can be followed by thioflavin T (ThT) dependent fluorescence assays. Although the <sup>15</sup>N HSQC spectrum of the peptide did not indicate noteworthy interactions with RP-22 and RP-23 in physical mixtures (SI, Figure S5), we observed an acceleration of PTH fibrillation, which we could not screen under high salt concentrations (Figure 4). This indicates that the polymer stimulated downstream nucleation processes of the peptide without detectable interactions with the monomers. The same ThT assay was performed for the conjugates. Surprisingly, only PTH V2 C-RP-23

showed some increase in ThT fluorescence (blue in Figure 5a). Compared to the non-modified peptide, this increase occurred much earlier. Even more surprising was the inspection of the samples after the ThT assays by electron microscopy. PTH(1-84) and all four conjugates formed fibrils even though with different morphologies. We speculate that the strongly reduced or fully missing ThT fluorescence of the conjugate fibrils results

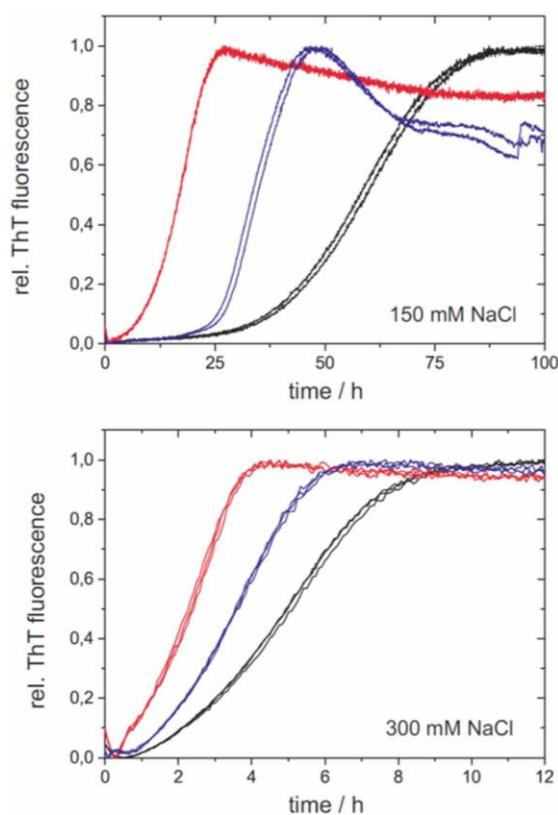


**Figure 4.** Thioflavin T detected fibrillation kinetics of PTH at 37 °C and pH 7.4 in the absence (black) and presence of RP-23 (blue) and RP-22 (red) at different salt concentrations. Equimolar concentrations (600  $\mu$ M) of peptide and polymer have been used.

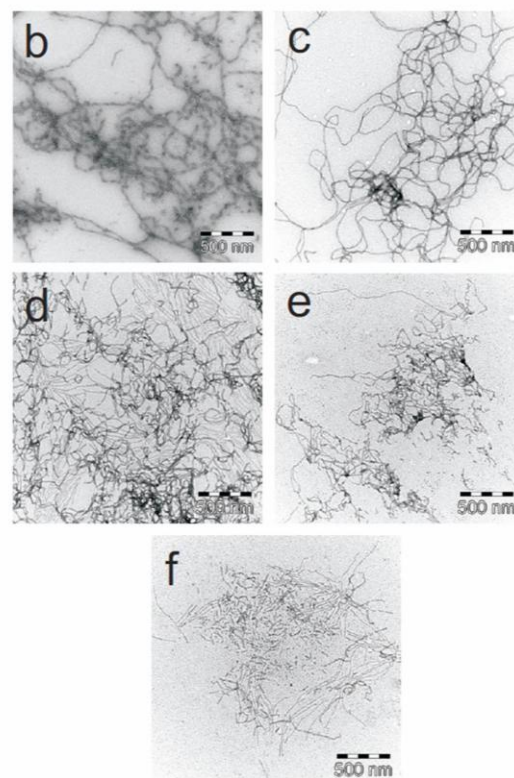
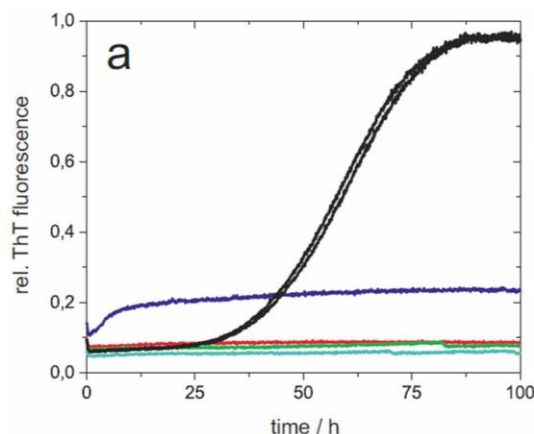


**Figure 5.** Fibril formation of PTH conjugates: a) thioflavin T detected fibrillation kinetics of PTH (black), PTH V2 C-RP-23 (blue), PTH Q84 C-RP-23 (cyan), PTH V2 C-RP-22 (red), and PTH Q84 C-RP-22 (green) at 37 °C, pH 7.4, and 150 mM NaCl. Electron micrographs are given in the same order: b) PTH, c) PTH V2 C-RP-23, d) PTH Q84 C-RP-23, e) PTH V2 C-RP-22, and f) PTH Q84 C-RP-22.

from RP-22 and RP-23, which might cover the fibril surface and thus occupy the binding sites for the fluorescence dye.

Polyethylene glycol (PEG) conjugation with peptides and proteins is a very common protein modification for various reasons, including pharmacological advances. A comparison of pegylated  $^{15}\text{N}$  protein therapeutics (Neulasta<sup>®</sup>, Pegasys<sup>®</sup>, PEG-Intron<sup>®</sup>) with unmodified samples by 2D  $^1\text{H}$ - $^{15}\text{N}$  NMR spectroscopy showed for example that the higher order secondary and tertiary structure of the proteins was not affected because only minor chemical shift changes were observed.<sup>[28]</sup> We came to the same conclusion for the here presented conjugated PTH, which shows an  $\alpha$ -helical propensity for residues 5–10 and 17–34<sup>[15]</sup> and no major changes of the backbone chemical shifts and thus of the peptide conformation. NMR mapping of the PTH conjugates and their hydrodynamic radii indicated that RP-23 close to the  $T_{\text{LCSP}}$  C-terminally attached RP-22, and probably their fibrils share a more shroud-like polymer conformation. Corresponding results have been reported for  $r_{\text{H}}$  of pegylated  $\alpha$ -lactalbumin,  $\beta$ -lactoglobulin<sup>[29]</sup> and helix bundle proteins.<sup>[20]</sup> In contrast, pegylation of lysozyme and an underlying dumbbell model more than doubled  $r_{\text{H}}$ .<sup>[21]</sup> A confirmation of the suggested shroud-like structure for the RP-22 and RP-23 conjugates of PTH requires DLS and SANS data,<sup>[22]</sup> which is future work.

In summary, the presented chimeric conjugates of PTH allowed for the first time to monitor the actual conformation and molecular extension of the synthetic macromolecule entity. The  $^{15}\text{N}$ -labelled PTH as a probe in the 2D  $^{15}\text{N}$  HSQC measurements revealed that a shroud-like polymer conformation dominated in these chimeras. In biological terms, the secondary structure of the PTH entity was not affected by conjugation of the thermo-responsive polymers but fibrillation was accelerated. The here presented analysis method can be generally applied and is not restricted to the here studied synthetic polymer.

## Experimental Section

Experimental details to the synthesis and characterization of RP-22 and RP-23 and the PTH conjugates are given in the Supporting Information.

## Acknowledgements

This work has been supported by grants from the Deutsche Forschungsgemeinschaft (TP A03 and A06 within the collaborative research project SFB TRR102) and ERDF by the EU.

## Conflict of Interest

The authors declare no conflict of interest.

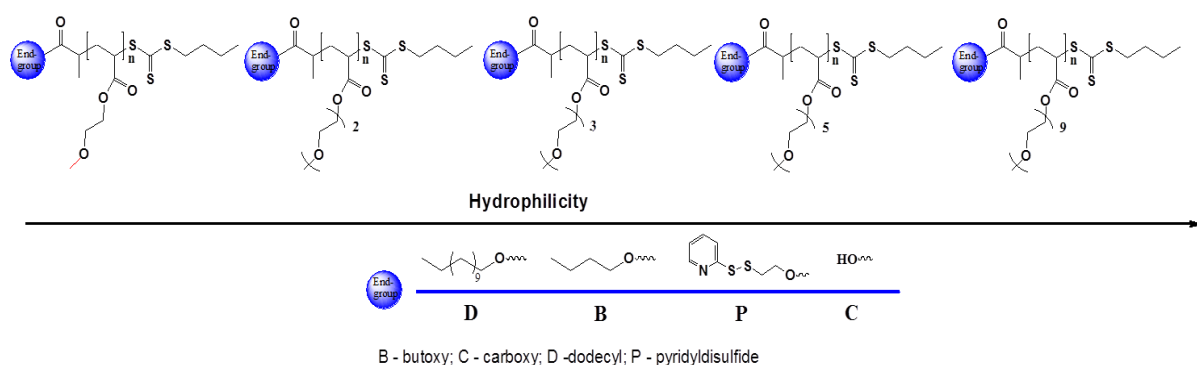
**Keywords:** macromolecular conformation · NMR spectroscopy · thermo-responsive polymer · parathyroid hormone · protein fibrils

- [1] B. Trzebicka, R. Szweda, D. Kosowski, D. Szweda, L. Otulakowski, E. Haladjova, A. Dworak, *Prog. Polym. Sci.* **2017**, *68*, 35.
- [2] R. Haag, F. Kratz, *Angew. Chem. Int. Ed.* **2006**, *45*, 1198.
- [3] a) C. M. Dobson, A. Sali, M. Karplus, *Angew. Chem. Int. Ed.* **1998**, *37*, 868; b) D. J. Hill, M. J. Mio, R. B. Prince, T. S. Hughes, J. S. Moore, *Chem. Rev.* **2001**, *101*, 3893.
- [4] a) Z.-T. Li, J.-L. Hou, C. Li, *Acc. Chem. Res.* **2008**, *41*, 1343; b) W. S. Horne, S. H. Gellman, *Acc. Chem. Res.* **2008**, *41*, 1399; c) M. B. J. Otten, G. A. Metselaar, J. J. L. M. Cornelissen, A. E. Rowan, R. J. M. Nolte, Wiley-VCH Verlag GmbH & Co. KGaA, **2007**, pp. 367.
- [5] A. Sanchez-Sanchez, S. Akbari, A. J. Moreno, F. L. Verso, A. Arbe, J. Colmenero, J. A. Pomposo, *Macromol. Rapid Commun.* **2013**, *34*, 1681.
- [6] J. Stetefeld, S. A. McKenna, T. R. Patel, *Biophys. Rev.* **2016**, *8*, 409.
- [7] a) H. Staudinger, *Berichte der deutschen chemischen Gesellschaft (A and B Series)* **1920**, *53*, 1073; b) H. Staudinger, *Trans. Faraday Soc.* **1933**, *29*, 18.
- [8] M. H. Jacob, R. N. Dsouza, I. Ghosh, A. Norouzy, T. Schwarzlose, W. M. Nau, *J. Phys. Chem. B* **2013**, *117*, 185.
- [9] B. Fierz, T. Kieffhaber, *J. Am. Chem. Soc.* **2007**, *129*, 672.
- [10] D. Kurzbach, M. J. N. Junk, D. Hinderberger, *Macromol. Rapid Commun.* **2013**, *34*, 119.
- [11] a) S. Basasoro, M. Gonzalez-Burgos, A. J. Moreno, F. L. Verso, A. Arbe, J. Colmenero, J. A. Pomposo, *Macromol. Rapid Commun.* **2016**, *37*, 1060; b) A. J. Moreno, F. Lo Verso, A. Arbe, J. A. Pomposo, J. Colmenero, *J. Phys. Chem. Lett.* **2016**, *7*, 838.
- [12] S. Mavila, O. Eivgi, I. Berkovich, N. G. Lemcoff, *Chem. Rev.* **2016**, *116*, 878.
- [13] Z. Agus, L. Gardner, L. Beck, M. Goldberg, *Am. J. Physiol.* **1973**, *224*, 1143.
- [14] U. C. Marx, K. Adermann, P. Bayer, W.-G. Forstmann, P. Rösch, *Biochem. Biophys. Res. Commun.* **2000**, *267*, 213.
- [15] a) R. C. Gensure, T. J. Gardella, H. Juppner, *Biochem. Biophys. Res. Commun.* **2005**, *328*, 666; b) R. W. Cheloha, S. H. Gellman, J. P. Vilardaga, T. J. Gardella, *Nat. Rev. Endocrinol.* **2012**, *8*, 712.
- [16] M. Gopalswamy, A. Kumar, J. Adler, M. Baumann, M. Henze, S. T. Kumar, M. Fändrich, H. A. Scheidt, D. Huster, J. Balbach, *Biochim. Biophys. Acta* **2015**, *1854*, 249.
- [17] J. Guo, A. Khatri, A. Maeda, J. T. Potts, H. Juppner, T. J. Gardella, *J. Bone Miner. Res.* **2017**, *32*, 86.
- [18] P. Westermark, *Amyloid* **1994**, *1*, 47.
- [19] A. B. Lowe, C. L. McCormick, *Prog. Polym. Sci.* **2007**, *32*, 283.
- [20] J. Y. Shu, R. Lund, T. Xu, *Biomacromolecules* **2012**, *13*, 1945.
- [21] S. S. Pai, B. Hammouda, K. Hong, D. C. Pozzo, T. M. Przybycien, R. D. Tilton, *Bioconjugate Chem.* **2011**, *22*, 2317.
- [22] C. N. Lam, D. Chang, M. Wang, W.-R. Chen, B. D. Olsen, *J. Polymer Sci. Part A: Polymer Chem.* **2016**, *54*, 292.
- [23] K. L. Heredia, T. H. Nguyen, C.-W. Chang, V. Bulmus, T. P. Davis, H. D. Maynard, *Chem. Commun.* **2008**, 3245.
- [24] F. Hua, X. Jiang, D. Li, B. Zhao, *J. Polymer Sci. Part A: Polymer Chem.* **2006**, *44*, 2454.
- [25] E. Bosse-Doenecke, U. Weiningner, M. Gopalswamy, J. Balbach, S. M. Knudsen, R. Rudolph, *Protein Expression Purif.* **2008**, *58*, 114.
- [26] D. K. Wilkins, S. B. Grimshaw, V. Receveur, C. M. Dobson, J. A. Jones, L. J. Smith, *Biochemistry* **1999**, *38*, 16424.
- [27] A. Kumar, M. Gopalswamy, C. Wishart, M. Henze, L. Eschen-Lippold, D. Donnelly, J. Balbach, *ACS Chem. Biol.* **2014**, *9*, 2465.
- [28] D. J. Hodgson, Y. Aubin, *J. Pharm. Biomed. Anal.* **2017**, *138*, 351.
- [29] C. J. Fee, J. M. Van Alstine, *Bioconjugate Chem.* **2004**, *15*, 1304.

Manuscript received: September 13, 2018  
Accepted manuscript online: September 17, 2018  
Version of record online: November 13, 2018

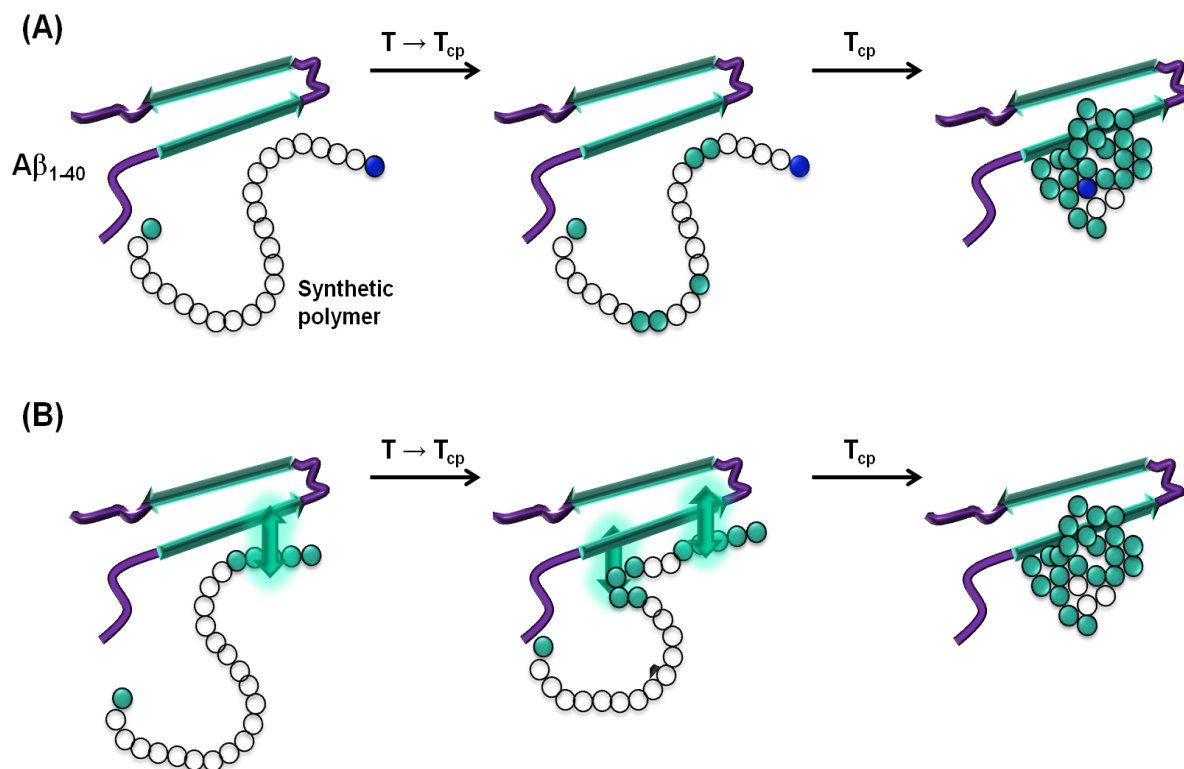
## IV. SUMMARY

Summarizing, this scientific work was devoted to the study of fibrillogenesis of amyloids, namely, irreversibly aggregating  $A\beta_{1-40}$  or reversibly aggregating  $PTH_{1-84}$ , either in a physical mixture or in a covalent conjugation with hydrophilic thermoresponsive poly(oligo(ethylene glycol) $_m$  acrylate)s. Reversible addition-fragmentation chain transfer (RAFT) polymerization of oligo(ethylene glycol) $_m$  acrylates using azobisisobutyronitrile (AIBN) initiator and four functional chain transfer agents (CTAs) allowed a successful preparation of the polymers with desired properties (Scheme 5).



**Scheme 5.** Overview of the thermoresponsive polymers used in this study with five different side chain lengths  $m$  and four different end groups (**D** = dodecyl; **B** = butoxy; **P** = pyridyldisulfide; **C** = carboxy), ordered according to their rising hydrophilicity.

Firstly, the thermoresponsive polymers were used as an admixture to the  $A\beta_{1-40}$ -containing systems. The increase of total hydrophobicity of the polymer controlled by adjustment of its molecular weight ( $M_n = 700$  to  $14\,600$  g/mol), side-chain length ( $m$ ) and end groups (**B**, **C**, **D**, **P**) led to reduction of  $T_{cp}$  from  $80$  to  $42.4$  °C, as was determined by turbidimetry measurements. Results obtained by ThT-detected fluorescence measurements conducted at  $37$  °C, a temperature close to physiological conditions, demonstrated that polymers with low  $T_{cp}$  values possess an inhibitory ability against amyloid aggregation. The transition of a polymer from a fully hydrated expanded coil state below  $T_{cp}$  to a collapsed state above  $T_{cp}$  was found to be a gradual process. Therefore, the nanoscopic phase segregation was often detected before the main macroscopic transition occurred, which is known as “incipient collapse”.<sup>11-13</sup> Such segregation increased an amount of hydrophobic domains in the system. Thus, it was hypothesized that the hydrophobic domains of the polymer are able to interact with the hydrophobic regions of the  $A\beta_{1-40}$  peptide, thereby slowing down the aggregation process (Scheme 6A). Moreover, all the samples carrying a dodecyl-end group could also suppress an aggregation rate regardless of  $T_{cp}$ . It was assumed that hydrophobic regions of the  $A\beta_{1-40}$  peptide and a long hydrophobic dodecyl-chain interact with each other, thereby delaying an aggregation process blocking the regions involved in the fibril development (Scheme 6B). On the other hand, well hydrated hydrophilic polymers carrying a carboxy-end group and having from two to nine ethylene glycol units in the side chain did not have a significant impact on the course of aggregation, or slightly accelerated it. Regardless of whether the aggregation process has been slowed down or accelerated by the presence of the polymers, formation of long  $\beta$ -sheet rich fibrils was detected for all the aggregated samples selected for CD and TEM analysis.



**Scheme 6.** Schematic mechanism of interactions between monomeric  $A\beta_{1-40}$ , represented here as a “ $\beta$ -hair pin”, and studied thermoresponsive polymers. For simplicity, water molecules are not shown, and the hydrated repeating units of the polymer chain are designated as empty circles. Hydrophobic regions of the  $A\beta_{1-40}$  and the hydrophobic end groups of the polymer are represented in turquoise, while hydrophilic regions of the  $A\beta_{1-40}$  are shown in violet. (A) Above  $T_{cp}$ , polymers carrying a hydrophilic  $\alpha$  end group (e.g. carboxy-, shown as a blue circle) are fully hydrated. Approaching  $T_{cp}$ , the polymer undergoes a so-called “incipient collapse”, upon which the dehydrated parts of the macromolecule bind to the hydrophobic parts of monomeric  $A\beta_{1-40}$ . (B) Polymers carrying hydrophobic (e.g. dodecyl-) end groups are hypothesized to directly bind to the hydrophobic regions of monomeric  $A\beta_{1-40}$  even below  $T_{cp}$ . With an increasing temperature towards  $T_{cp}$ , the number of hydrophobic domains in the polymer chain increases, which in turn elevates the affinity of the polymer to the hydrophobic parts of monomeric  $A\beta_{1-40}$ . Potential hydrophobic interactions are indicated with arrows.

Secondly, covalent conjugation of the selected polymeric samples with the irreversibly aggregating  $A\beta_{1-40}$  peptide was accomplished by means of the resin-based synthesis or solution-based coupling chemistries. A successful synthesis of the conjugates was accomplished for polymers whose molecular weight did not exceed 6600 g/mol. Fibrillogenesis of the chosen conjugates was monitored by means of ThT-detected fluorescence measurements. Thus, all the studied conjugates demonstrated accelerated fibrillation kinetics as compared to the unconjugated  $A\beta_{1-40}$  peptide. Additionally, the conjugate with the highest molecular weight aggregated faster than its lower molecular weight analogues. Notably, instead of conventional long and straight fibrils characteristic for  $A\beta_{1-40}$  self-assembly, bundles of short aggregates were observed by TEM for all studied conjugates (Figure 23). Hence, the rate of  $A\beta_{1-40}$  self-assembly and appearance of the preformed aggregates can be modulated by conjugation with hydrophilic polymers.

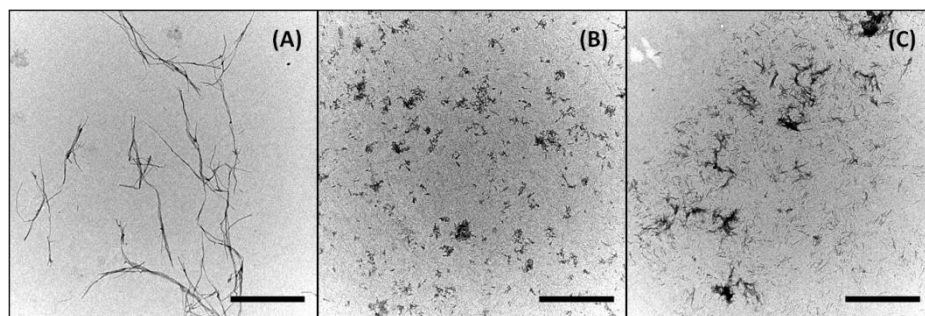
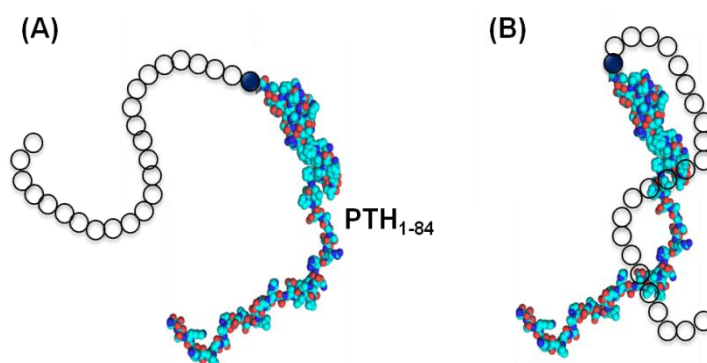


**Figure 23.** TEM images of the fibrils obtained after ThT kinetic measurements of the (A)  $A\beta_{1-40}$ , and the conjugates (B) m2P\_n38\_ $A\beta_{1-40}$ , (B) m3C\_n17\_ $A\beta_{1-40}$ . The scale bar corresponds to 1000 nm. Figure 23 is adapted from ref<sup>188</sup>.

Finally, the chosen poly(methoxy di(ethylene glycol)acrylate)s ( $m=2$ ) were coupled with reversibly aggregating  $PTH_{1-84}$  via solution-based coupling chemistry. The conformational transition of the polymer from the random coil to a collapsed state was confirmed by means of NMR spectroscopy of  $^{15}N$  labeled  $PTH_{1-84}$  for the first time. Thus, relying on changes of chemical shifts, an extended dumbbell conformation in which a polymer chain located away from the peptide body was observed below  $T_{cp}$  (Scheme 7A), whereas a compact shroud-like conformation in which the polymer chain is wrapped around the peptide was observed above  $T_{cp}$  (Scheme 7B). Additionally, the employed polymers enhanced the  $PTH_{1-84}$  self-assembly, at the same time leaving the morphology of the resulting fibrils unchanged compared to wild type  $PTH_{1-84}$  fibrils.

Thus, despite the divergence of chemical structure and properties of the  $A\beta_{1-40}$  and the  $PTH_{1-84}$  peptides, the pathway of their aggregation can be noticeably modulated by hydrophilic thermoresponsive poly(oligo(ethylene glycol) $m$  acrylate)s.



**Scheme 7.** Transition of a thermoresponsive polymer conformational state from the (A) extended dumbbell conformation below its  $T_{cp}$  to the (B) compact shroud-like conformation above its  $T_{cp}$ , confirmed by means of  $^{15}N$ - NMR spectroscopy.

The results of this work provide a solid basis for further research in the field of amyloid aggregation and contributes to understanding of the factors affecting the self-assembly process of peptides and proteins.

---

**V. REFERENCES**

1. Aseyev, V.; Tenhu, H.; Winnik, F. M., Non-ionic Thermoresponsive Polymers in Water. In *Self Organized Nanostructures of Amphiphilic Block Copolymers II*, Müller, A. H. E.; Borisov, O., Eds. Springer Berlin Heidelberg: Berlin, Heidelberg, 2011; pp 29-89.
2. Tan, Z.-J.; Chen, S.-J., Salt Contribution to RNA Tertiary Structure Folding Stability. *Biophysical Journal* **2011**, *101* (1), 176-187.
3. Yang, X.; Yang, M.; Deng, H.; Ding, Y., New Era of Studying RNA Secondary Structure and Its Influence on Gene Regulation in Plants. *Frontiers in Plant Science* **2018**, *9* (671).
4. Carius, A. B.; Rogne, P.; Duchoslav, M.; Wolf-Watz, M.; Samuelsson, G.; Shutova, T., Dynamic pH-induced conformational changes of the PsbO protein in the fluctuating acidity of the thylakoid lumen. *Physiologia Plantarum* **2019**, *166* (1), 288-299.
5. Su, Z.; Tang, Y.; Ritchey, L. E.; Tack, D. C.; Zhu, M.; Bevilacqua, P. C.; Assmann, S. M., Genome-wide RNA structurome reprogramming by acute heat shock globally regulates mRNA abundance. *Proceedings of the National Academy of Sciences* **2018**, *115* (48), 12170-12175.
6. Papadakis, C. M.; Müller-Buschbaum, P.; Laschewsky, A., Switch It Inside-Out: “Schizophrenic” Behavior of All Thermoresponsive UCST–LCST Diblock Copolymers. *Langmuir* **2019**, *35* (30), 9660-9676.
7. Rubinstein, M.; Colby, R. H., *Polymer Physics*. Oxford University Press: New York, 2003.
8. Weber, C.; Hoogenboom, R.; Schubert, U. S., Temperature responsive bio-compatible polymers based on poly(ethylene oxide) and poly(2-oxazoline)s. *Progress in Polymer Science* **2012**, *37* (5), 686-714.
9. Lanzalaco, S.; Armelin, E., Poly(N-isopropylacrylamide) and Copolymers: A Review on Recent Progresses in Biomedical Applications. *Gels* **2017**, *3* (4), 36.
10. Djokpé, E.; Vogt, W., N-Isopropylacrylamide and N-Isopropylmethacrylamide: Cloud Points of Mixtures and Copolymers. *Macromolecular Chemistry and Physics* **2001**, *202* (5), 750-757.
11. Zhang, Q.; Weber, C.; Schubert, U. S.; Hoogenboom, R., Thermoresponsive polymers with lower critical solution temperature: from fundamental aspects and measuring techniques to recommended turbidimetry conditions. *Mater. Horizons* **2017**, *4* (2), 109-116.
12. Zheng, X.; Anisimov, M. A.; Sengers, J. V.; He, M., Unusual Transformation of Polymer Coils in a Mixed Solvent Close to the Critical Point. *Phys. Rev. Lett.* **2018**, *121* (20), 207802.
13. Liu, Y.; Dai, Y.; Xu, X., Dynamic Feature of Incipient Polymer Collapse below the Theta Point. *J. Phys. Chem. B* **2017**, *121* (40), 9469-9475.
14. Vancoillie, G.; Frank, D.; Hoogenboom, R., Thermoresponsive poly(oligo ethylene glycol acrylates). *Progress in Polymer Science* **2014**, *39* (6), 1074-1095.
15. Lutz, J.-F.; Weichenhan, K.; Akdemir, Ö.; Hoth, A., About the Phase Transitions in Aqueous Solutions of Thermoresponsive Copolymers and Hydrogels Based on 2-(2-methoxyethoxy)ethyl Methacrylate and Oligo(ethylene glycol) Methacrylate. *Macromolecules* **2007**, *40* (7), 2503-2508.
16. Monge, S.; Antoniacomi, S.; Lapinte, V.; Darcos, V.; Robin, J.-J., Poly(tris(hydroxymethyl)acrylamidomethane)-based copolymers: a new class of acid-labile thermosensitive polymers. *Polymer Chemistry* **2012**, *3* (9), 2502-2507.
17. Niskanen, J.; Karesoja, M.; Rossi, T.; Tenhu, H., Temperature and pH responsive hybrid nanoclay grafted with PDMAEMA. *Polymer Chemistry* **2011**, *2* (9), 2027-2036.

- .....
18. Laukkanen, A.; Valtola, L.; Winnik, F. M.; Tenhu, H., Thermosensitive graft copolymers of an amphiphilic macromonomer and N-vinylcaprolactam: synthesis and solution properties in dilute aqueous solutions below and above the LCST. *Polymer* **2005**, *46* (18), 7055-7065.
  19. Hidaka, T.; Sugihara, S.; Maeda, Y., Infrared spectroscopic study on LCST behavior of poly(N,N-bis(2-methoxyethyl)acrylamide). *European Polymer Journal* **2013**, *49* (3), 675-681.
  20. Yamauchi, H.; Maeda, Y., LCST and UCST Behavior of Poly(N-isopropylacrylamide) in DMSO/Water Mixed Solvents Studied by IR and Micro-Raman Spectroscopy. *The Journal of Physical Chemistry B* **2007**, *111* (45), 12964-12968.
  21. Miasnikova, A.; Laschewsky, A., Influencing the phase transition temperature of poly(methoxy diethylene glycol acrylate) by molar mass, end groups, and polymer architecture. *J. Polym. Sci. A* **2012**, *50* (16), 3313-3323.
  22. Heskins, M.; Guillet, J. E., Solution Properties of Poly(N-isopropylacrylamide). *Journal of Macromolecular Science: Part A - Chemistry* **1968**, *2* (8), 1441-1455.
  23. Aseyev, V.; Tenhu, H.; Winnik, F., *Non-Ionic Thermoresponsive Polymers in Water*. 2010; Vol. 242, p 29-89.
  24. Ward, M. A.; Georgiou, T. K., Thermoresponsive Polymers for Biomedical Applications. *Polymers* **2011**, *3* (3), 1215-1242.
  25. Skrabania, K.; Kristen, J.; Laschewsky, A.; Akdemir, Ö.; Hoth, A.; Lutz, J.-F., Design, Synthesis, and Aqueous Aggregation Behavior of Nonionic Single and Multiple Thermoresponsive Polymers. *Langmuir* **2007**, *23* (1), 84-93.
  26. Lutz, J.-F., Polymerization of oligo(ethylene glycol) (meth)acrylates: Toward new generations of smart biocompatible materials. *Journal of Polymer Science Part A: Polymer Chemistry* **2008**, *46* (11), 3459-3470.
  27. Ruzette, A.-V. G.; Mayes, A. M., A Simple Free Energy Model for Weakly Interacting Polymer Blends. *Macromolecules* **2001**, *34* (6), 1894-1907.
  28. Vihola, H.; Laukkanen, A.; Tenhu, H.; Hirvonen, J., Drug release characteristics of physically cross-linked thermosensitive poly(N-vinylcaprolactam) hydrogel particles. *Journal of Pharmaceutical Sciences* **2008**, *97* (11), 4783-4793.
  29. Twaites, B. R.; de las Heras Alarcón, C.; Lavigne, M.; Saulnier, A.; Pennadam, S. S.; Cunliffe, D.; Górecki, D. C.; Alexander, C., Thermoresponsive polymers as gene delivery vectors: Cell viability, DNA transport and transfection studies. *Journal of Controlled Release* **2005**, *108* (2), 472-483.
  30. Shimizu, K.; Fujita, H.; Nagamori, E., Oxygen plasma-treated thermoresponsive polymer surfaces for cell sheet engineering. *Biotechnology and Bioengineering* **2010**, *106* (2), 303-310.
  31. Crespy, D.; Rossi, R. M., Temperature-responsive polymers with LCST in the physiological range and their applications in textiles. *Polymer International* **2007**, *56* (12), 1461-1468.
  32. Ohnishi, N.; Furukawa, H.; Hideyuki, H.; Wang, J.-M.; An, C.-I.; Fukusaki, E.; Kataoka, K.; Ueno, K.; Kondo, A., High-efficiency bioaffinity separation of cells and proteins using novel thermoresponsive biotinylated magnetic nanoparticles. *NanoBiotechnology* **2006**, *2* (1), 43-49.
  33. Pasparakis, G.; Vamvakaki, M., Multiresponsive polymers: nano-sized assemblies, stimuli-sensitive gels and smart surfaces. *Polymer Chemistry* **2011**, *2* (6), 1234-1248.
  34. Bergbreiter, D. E.; Mariagnanam, V. M.; Zhang, L., Polymer ligands that can regulate reaction temperature in "smart" catalysts. *Advanced Materials* **1995**, *7* (1), 69-71.

- .....
35. Huang, X.; Witte, Krista L.; Bergbreiter, David E.; Wong, C.-H., Homogenous Enzymatic Synthesis Using a Thermo-Responsive Water-Soluble Polymer Support. *Advanced Synthesis & Catalysis* **2001**, *343* (6-7), 675-681.
  36. Purushotham, S.; Chang, P. E. J.; Rumpel, H.; Kee, I. H. C.; Ng, R. T. H.; Chow, P. K. H.; Tan, C. K.; Ramanujan, R. V., Thermoresponsive core-shell magnetic nanoparticles for combined modalities of cancer therapy. *Nanotechnology* **2009**, *20* (30), 305101.
  37. Wu, W.; Zhou, T.; Berliner, A.; Banerjee, P.; Zhou, S., Smart Core-Shell Hybrid Nanogels with Ag Nanoparticle Core for Cancer Cell Imaging and Gel Shell for pH-Regulated Drug Delivery. *Chemistry of Materials* **2010**, *22* (6), 1966-1976.
  38. Psarra, E.; König, U.; Ueda, Y.; Bellmann, C.; Janke, A.; Bittrich, E.; Eichhorn, K.-J.; Uhlmann, P., Nanostructured Biointerfaces: Nanoarchitectonics of Thermoresponsive Polymer Brushes Impact Protein Adsorption and Cell Adhesion. *ACS Applied Materials & Interfaces* **2015**, *7* (23), 12516-12529.
  39. Zubik, K.; Singhsa, P.; Wang, Y.; Manuspiya, H.; Narain, R., Thermo-Responsive Poly(N-Isopropylacrylamide)-Cellulose Nanocrystals Hybrid Hydrogels for Wound Dressing. *Polymers* **2017**, *9* (4), 119.
  40. Qiu, X.; Koga, T.; Tanaka, F.; Winnik, F. M., New insights into the effects of molecular weight and end group on the temperature-induced phase transition of poly(N-isopropylacrylamide) in water. *Science China Chemistry* **2013**, *56* (1), 56-64.
  41. Lessard, D. G.; Ousalem, M.; Zhu, X. X., Effect of the molecular weight on the lower critical solution temperature of poly(N,N-diethylacrylamide) in aqueous solutions. *Canadian Journal of Chemistry* **2001**, *79* (12), 1870-1874.
  42. Schild, H. G.; Tirrell, D. A., Microcalorimetric detection of lower critical solution temperatures in aqueous polymer solutions. *The Journal of Physical Chemistry* **1990**, *94* (10), 4352-4356.
  43. Xue, W.; Huglin, M. B.; Jones, T. G. J., Parameters Affecting the Lower Critical Solution Temperature of Linear and Crosslinked Poly(N-ethylacrylamide) in Aqueous Media. *Macromolecular Chemistry and Physics* **2003**, *204* (16), 1956-1965.
  44. Baltes, T.; Garret-Flaudy, F.; Freitag, R., Investigation of the LCST of polyacrylamides as a function of molecular parameters and the solvent composition. *Journal of Polymer Science Part A: Polymer Chemistry* **1999**, *37* (15), 2977-2989.
  45. Tong, Z.; Zeng, F.; Zheng, X.; Sato, T., Inverse Molecular Weight Dependence of Cloud Points for Aqueous Poly(N-isopropylacrylamide) Solutions. *Macromolecules* **1999**, *32* (13), 4488-4490.
  46. Zheng, X.; Tong, Z.; Xie, X.; Zeng, F., Phase Separation in Poly(N-isopropyl acrylamide)/Water Solutions I. Cloud Point Curves and Microgelation. *Polymer Journal* **1998**, *30* (4), 284-288.
  47. Ru, G.; Feng, J., Effects of end groups on phase transition and segmental mobility of poly(N-isopropylacrylamide) chains in D<sub>2</sub>O. *Journal of Polymer Science Part B: Polymer Physics* **2011**, *49* (10), 749-755.
  48. Fujishige, S.; Kubota, K.; Ando, I., Phase transition of aqueous solutions of poly(N-isopropylacrylamide) and poly(N-isopropylmethacrylamide). *The Journal of Physical Chemistry* **1989**, *93* (8), 3311-3313.
  49. Huber, S.; Hutter, N.; Jordan, R., Effect of end group polarity upon the lower critical solution temperature of poly(2-isopropyl-2-oxazoline). *Colloid and Polymer Science* **2008**, *286* (14), 1653-1661.
  50. Chung, J. E.; Yokoyama, M.; Aoyagi, T.; Sakurai, Y.; Okano, T., Effect of molecular architecture of hydrophobically modified poly(N-isopropylacrylamide) on the formation of thermoresponsive core-shell micellar drug carriers. *Journal of Controlled Release* **1998**, *53* (1), 119-130.

51. Xia, Y.; Burke, N. A. D.; Stöver, H. D. H., End Group Effect on the Thermal Response of Narrow-Disperse Poly(N-isopropylacrylamide) Prepared by Atom Transfer Radical Polymerization. *Macromolecules* **2006**, *39* (6), 2275-2283.
52. Chung, J. E.; Yokoyama, M.; Suzuki, K.; Aoyagi, T.; Sakurai, Y.; Okano, T., Reversibly thermo-responsive alkyl-terminated poly(N-isopropylacrylamide) core-shell micellar structures. *Colloids and Surfaces B: Biointerfaces* **1997**, *9* (1), 37-48.
53. Ohnsorg, M. L.; Ting, J. M.; Jones, S. D.; Jung, S.; Bates, F. S.; Reineke, T. M., Tuning PNIPAm self-assembly and thermoresponse: roles of hydrophobic end-groups and hydrophilic comonomer. *Polymer Chemistry* **2019**, *10* (25), 3469-3479.
54. Okada, Y.; Tanaka, F.; Kujawa, P.; Winnik, F. M., Unified model of association-induced lower critical solution temperature phase separation and its application to solutions of telechelic poly(ethylene oxide) and of telechelic poly(N-isopropylacrylamide) in water. *The Journal of Chemical Physics* **2006**, *125* (24), 244902.
55. Bebis, K.; Jones, M. W.; Haddleton, D. M.; Gibson, M. I., Thermoresponsive behaviour of poly[oligo(ethyleneglycol methacrylate)]s and their protein conjugates: importance of concentration and solvent system. *Polymer Chemistry* **2011**, *2* (4), 975-982.
56. Hoogenboom, R.; Popescu, D.; Steinhauer, W.; Keul, H.; Möller, M., Nitroxide-Mediated Copolymerization of 2-Hydroxyethyl Acrylate and 2-Hydroxypropyl Acrylate: Copolymerization Kinetics and Thermoresponsive Properties. *Macromolecular Rapid Communications* **2009**, *30* (23), 2042-2048.
57. Hua, F.; Jiang, X.; Li, D.; Zhao, B., Well-defined thermosensitive, water-soluble polyacrylates and polystyrenics with short pendant oligo(ethylene glycol) groups synthesized by nitroxide-mediated radical polymerization. *Journal of Polymer Science Part A: Polymer Chemistry* **2006**, *44* (8), 2454-2467.
58. Eggenhuisen, T. M.; Becer, C. R.; Fijten, M. W. M.; Eckardt, R.; Hoogenboom, R.; Schubert, U. S., Libraries of Statistical Hydroxypropyl Acrylate Containing Copolymers with LCST Properties Prepared by NMP. *Macromolecules* **2008**, *41* (14), 5132-5140.
59. Park, J.-S.; Akiyama, Y.; Winnik, F. M.; Kataoka, K., Versatile Synthesis of End-Functionalized Thermosensitive Poly(2-isopropyl-2-oxazolines). *Macromolecules* **2004**, *37* (18), 6786-6792.
60. Freitag, R.; Garret-Flaudy, F., Salt Effects on the Thermoprecipitation of Poly-(N-isopropylacrylamide) Oligomers from Aqueous Solution. *Langmuir* **2002**, *18* (9), 3434-3440.
61. Mori, T.; Hamada, M.; Kobayashi, T.; Okamura, H.; Minagawa, K.; Masuda, S.; Tanaka, M., Effect of alkyl substituents structures and added ions on the phase transition of polymers and gels prepared from methyl 2-alkylamidoacrylates. *Journal of Polymer Science Part A: Polymer Chemistry* **2005**, *43* (20), 4942-4952.
62. Okamura, H.; Mori, T.; Minagawa, K.; Masuda, S.; Tanaka, M., A novel thermosensitive polymer, poly(methyl 2-propionamidoacrylate), with geminal substituents. *Polymer* **2002**, *43* (13), 3825-3828.
63. Kunz, W., Specific ion effects in colloidal and biological systems. *Current Opinion in Colloid & Interface Science* **2010**, *15* (1), 34-39.
64. Hamley, I. W., The Amyloid Beta Peptide: A Chemist's Perspective. Role in Alzheimer's and Fibrillization. *Chem. Rev.* **2012**, *112* (10), 5147-5192.
65. Hamley, I. W., Peptide Fibrillization. *Angew. Chem. Int. Ed.* **2007**, *46* (43), 8128-8147.
66. Gopalswamy, M.; Kumar, A.; Adler, J.; Baumann, M.; Henze, M.; Kumar, S. T.; Fändrich, M.; Scheidt, H. A.; Huster, D.; Balbach, J., Structural characterization of amyloid fibrils from the human parathyroid hormone. *Biochim. Biophys. Acta* **2015**, *1854* (4), 249-257.

67. Fowler, D. M.; Koulov, A. V.; Alory-Jost, C.; Marks, M. S.; Balch, W. E.; Kelly, J. W., Functional amyloid formation within mammalian tissue. *PLoS Biol.* **2006**, *4* (1), e6-e6.
68. Barnhart, M. M.; Chapman, M. R., Curli biogenesis and function. *Annu. Rev. Microbiol.* **2006**, *60*, 131-147.
69. Iconomidou, V. A.; Vriend, G.; Hamodrakas, S. J., Amyloids protect the silkworm oocyte and embryo. *FEBS Lett.* **2000**, *479* (3), 141-145.
70. Maddelein, M.-L.; Dos Reis, S.; Duvezin-Caubet, S.; Coulary-Salin, B.; Saupe, S. J., Amyloid aggregates of the HET-s prion protein are infectious. *Proc. Natl. Acad. Sci. U.S.A.* **2002**, *99* (11), 7402-7407.
71. Rambaran, R. N.; Serpell, L. C., Amyloid fibrils: Abnormal protein assembly. *Prion* **2008**, *2* (3), 112-117.
72. Verma, M.; Vats, A.; Taneja, V., Toxic species in amyloid disorders: Oligomers or mature fibrils. *Annals of Indian Academy of Neurology* **2015**, *18* (2), 138-145.
73. Sweeney, P.; Park, H.; Baumann, M.; Dunlop, J.; Frydman, J.; Kopito, R.; McCampbell, A.; Leblanc, G.; Venkateswaran, A.; Nurmi, A.; Hodgson, R., Protein misfolding in neurodegenerative diseases: implications and strategies. *Translational neurodegeneration* **2017**, *6*, 6-6.
74. Tan, S.; Wong, E., Chapter Fifteen - Kinetics of Protein Aggregates Disposal by Aggrephagy. In *Methods in Enzymology*, Galluzzi, L.; Bravo-San Pedro, J. M.; Kroemer, G., Eds. Academic Press: 2017; Vol. 588, pp 245-281.
75. Sakai, K.; Piao, Y.-S.; Kikugawa, K.; Ohara, S.; Hasegawa, M.; Takano, H.; Fukase, M.; Nishizawa, M.; Kakita, A.; Takahashi, H., Corticobasal degeneration with focal, massive tau accumulation in the subcortical white matter astrocytes. *Acta Neuropathol* **2006**, *112* (3), 341-348.
76. Jellinger, K. A., Multiple System Atrophy: An Oligodendroglioneuronal Synucleinopathy1. *Journal of Alzheimer's disease : JAD* **2018**, *62* (3), 1141-1179.
77. Martinez-Naharro, A.; Hawkins, P. N.; Fontana, M., Cardiac amyloidosis. *Clinical medicine (London, England)* **2018**, *18* (Suppl 2), s30-s35.
78. Lakshminarayanan, R.; Chaurasia, S. S.; Murugan, E.; Venkatraman, A.; Chai, S.-M.; Vithana, E. N.; Beuerman, R. W.; Mehta, J. S., Biochemical Properties and Aggregation Propensity of Transforming Growth Factor-Induced Protein (TGFBIp) and the Amyloid Forming Mutants. *The Ocular Surface* **2015**, *13* (1), 9-25.
79. Adamcik, J.; Mezzenga, R., Proteins Fibrils from a Polymer Physics Perspective. *Macromolecules* **2012**, *45* (3), 1137-1150.
80. Arosio, P.; Knowles, T. P. J.; Linse, S., On the lag phase in amyloid fibril formation. *Phys. Chem. Chem. Phys.* **2015**, *17* (12), 7606-7618.
81. Cohen, S. I. A.; Linse, S.; Luheshi, L. M.; Hellstrand, E.; White, D. A.; Rajah, L.; Otzen, D. E.; Vendruscolo, M.; Dobson, C. M.; Knowles, T. P. J., Proliferation of amyloid- $\beta$ 42 aggregates occurs through a secondary nucleation mechanism. *Proc. Natl. Acad. Sci.* **2013**, *110* (24), 9758-9763.
82. Meisl, G.; Yang, X.; Hellstrand, E.; Frohm, B.; Kirkegaard, J. B.; Cohen, S. I. A.; Dobson, C. M.; Linse, S.; Knowles, T. P. J., Differences in nucleation behavior underlie the contrasting aggregation kinetics of the A $\beta$ 40 and A $\beta$ 42 peptides. *Proc. Natl. Acad. Sci. U.S.A.* **2014**, *111* (26), 9384-9389.
83. Cohen, S. I. A.; Cukalevski, R.; Michaels, T. C. T.; Šarić, A.; Törnquist, M.; Vendruscolo, M.; Dobson, C. M.; Buell, A. K.; Knowles, T. P. J.; Linse, S., Distinct thermodynamic signatures of oligomer generation in the aggregation of the amyloid- $\beta$  peptide. *Nature chemistry* **2018**, *10* (5), 523-531.
84. Linse, S., Mechanism of amyloid protein aggregation and the role of inhibitors. *Pure and Applied Chemistry* **2019**, *9* (2), 211-229.

85. Abelein, A.; Jarvet, J.; Barth, A.; Gräslund, A.; Danielsson, J., Ionic Strength Modulation of the Free Energy Landscape of A $\beta$ 40 Peptide Fibril Formation. *Journal of the American Chemical Society* **2016**, *138* (21), 6893-6902.
86. Zhang, H.; Zheng, X.; Kwok, R. T. K.; Wang, J.; Leung, N. L. C.; Shi, L.; Sun, J. Z.; Tang, Z.; Lam, J. W. Y.; Qin, A.; Tang, B. Z., In situ monitoring of molecular aggregation using circular dichroism. *Nature Communications* **2018**, *9* (1), 4961.
87. Korn, A.; McLennan, S.; Adler, J.; Krueger, M.; Surendran, D.; Maiti, S.; Huster, D., Amyloid  $\beta$  (1–40) Toxicity Depends on the Molecular Contact between Phenylalanine 19 and Leucine 34. *ACS Chem. Neurosci.* **2017**.
88. Taraban, M. B.; Truong, H. C.; Feng, Y.; Jouravleva, E. V.; Anisimov, M. A.; Yu, Y. B., Water Proton NMR for In Situ Detection of Insulin Aggregates. *Journal of Pharmaceutical Sciences* **2015**, *104* (12), 4132-4141.
89. Seshadri, S.; Khurana, R.; Fink, A. L., Fourier transform infrared spectroscopy in analysis of protein deposits. In *Methods in Enzymology*, Academic Press: 1999; Vol. 309, pp 559-576.
90. Giehm, L.; Svergun, D. I.; Otzen, D. E.; Vestergaard, B., Low-resolution structure of a vesicle disrupting  $\alpha$ -synuclein oligomer that accumulates during fibrillation. *Proceedings of the National Academy of Sciences* **2011**, *108* (8), 3246-3251.
91. Carrotta, R.; Manno, M.; Bulone, D.; Martorana, V.; Biagio, P. L. S., Protofibril Formation of Amyloid  $\beta$ -Protein at Low pH via a Non-cooperative Elongation Mechanism. *Journal of Biological Chemistry* **2005**, *280* (34), 30001-30008.
92. Bolisetty, S.; Adamcik, J.; Mezzenga, R., Snapshots of fibrillation and aggregation kinetics in multistranded amyloid  $\beta$ -lactoglobulin fibrils. *Soft Matter* **2011**, *7* (2), 493-499.
93. Greenfield, N. J., Using circular dichroism spectra to estimate protein secondary structure. *Nat. Protoc.* **2006**, *1* (6), 2876-2890.
94. Shire, S. J., 2 - Analytical tools used in the formulation and assessment of stability of monoclonal antibodies (mAbs). In *Monoclonal Antibodies*, Shire, S. J., Ed. Woodhead Publishing: 2015; pp 17-44.
95. K. Debnath; Shekhar, S.; Kumar, V.; Jana, N. R., Efficient Inhibition of Protein Aggregation, Disintegration of Aggregates, and Lowering of Cytotoxicity by Green Tea Polyphenol-Based Self-Assembled Polymer Nanoparticles. *ACS Appl. Mater. Interfaces* **2016**, *8* (31), 20309-20318.
96. Ladiwala, A. R. A.; Lin, J. C.; Bale, S. S.; Marcelino-Cruz, A. M.; Bhattacharya, M.; Dordick, J. S.; Tessier, P. M., Resveratrol Selectively Remodels Soluble Oligomers and Fibrils of Amyloid A $\beta$  into Off-pathway Conformers. *J. Biol. Chem.* **2010**, *285* (31), 24228-24237.
97. Liu, H.; Xie, B.; Dong, X.; Zhang, L.; Wang, Y.; Liu, F.; Sun, Y., Negatively charged hydrophobic nanoparticles inhibit amyloid  $\beta$ -protein fibrillation: The presence of an optimal charge density. *React. Funct. Polym.* **2016**, *103*, 108-116.
98. Gladytz, A.; Wagner, M.; Häupl, T.; Elsner, C.; Abel, B., Structure-Making Effects of Metal Nanoparticles in Amyloid Peptide Fibrillation. *Part. Part. Syst. Char.* **2015**, *32* (5), 573-582.
99. Hellstrand, E.; Sparr, E.; Linse, S., Retardation of A $\beta$  Fibril Formation by Phospholipid Vesicles Depends on Membrane Phase Behavior. *Biophys. J.* **2010**, *98* (10), 2206-2214.
100. Aisenbrey, C.; Borowik, T.; Byström, R.; Bokvist, M.; Lindström, F.; Misiak, H.; Sani, M.-A.; Gröbner, G., How is protein aggregation in amyloidogenic diseases modulated by biological membranes? *Eur. Biophys. J.* **2008**, *37* (3), 247-255.
101. Heegaard, P. M. H.; Boas, U.; Otzen, D. E., Dendrimer Effects on Peptide and Protein Fibrillation. *Macromol. Biosci.* **2007**, *7* (8), 1047-1059.

102. Klajnert, B.; Cortijo-Arellano, M.; Cladera, J.; Bryszewska, M., Influence of dendrimer's structure on its activity against amyloid fibril formation. *Biochem. Biophys. Res. Commun.* **2006**, *345* (1), 21-28.
103. Castelletto, V.; Newby, G. E.; Hermida Merino, D.; Hamley, I. W.; Liu, D.; Noirez, L., Self-assembly of an amyloid peptide fragment-PEG conjugate: lyotropic phase formation and influence of PEG crystallization. *Polym. Chem.* **2010**, *1* (4), 453-459.
104. Dehn, S.; Castelletto, V.; Hamley, I. W.; Perrier, S., Altering Peptide Fibrillization by Polymer Conjugation. *Biomacromolecules* **2012**, *13* (9), 2739-2747.
105. Lin, J.-M.; Lin, T.-L.; Jeng, U. S.; Huang, Z.-H.; Huang, Y.-S., Aggregation structure of Alzheimer amyloid-[small beta](1-40) peptide with sodium dodecyl sulfate as revealed by small-angle X-ray and neutron scattering. *Soft Matter* **2009**, *5* (20), 3913-3919.
106. Abelein, A.; Kaspersen, J. D.; Nielsen, S. B.; Jensen, G. V.; Christiansen, G.; Pedersen, J. S.; Danielsson, J.; Otzen, D. E.; Gräslund, A., Formation of Dynamic Soluble Surfactant-induced Amyloid  $\beta$  Peptide Aggregation Intermediates. *J. Biol. Chem.* **2013**, *288* (32), 23518-23528.
107. Cohen, S. I. A.; Arosio, P.; Presto, J.; Kurudenkandy, F. R.; Biverstål, H.; Dolfe, L.; Dunning, C.; Yang, X.; Frohm, B.; Vendruscolo, M.; Johansson, J.; Dobson, C. M.; Fisahn, A.; Knowles, T. P. J.; Linse, S., A molecular chaperone breaks the catalytic cycle that generates toxic A $\beta$  oligomers. *Nat. Struct. Mol. Biol.* **2015**, *22*, 207.
108. Willander, H.; Presto, J.; Askarieh, G.; Biverstål, H.; Frohm, B.; Knight, S. D.; Johansson, J.; Linse, S., BRICHOS Domains Efficiently Delay Fibrillation of Amyloid  $\beta$ -Peptide. *J. Biol. Chem.* **2012**, *287* (37), 31608-31617.
109. Stanyon, H. F.; Viles, J. H., Human Serum Albumin Can Regulate Amyloid- $\beta$  Peptide Fiber Growth in the Brain Interstitium: Implications for Alzheimer disease. *J. Biol. Chem.* **2012**, *287* (33), 28163-28168.
110. Takahashi, T.; Mihara, H., Peptide and Protein Mimetics Inhibiting Amyloid  $\beta$ -Peptide Aggregation. *Acc. Chem. Res.* **2008**, *41* (10), 1309-1318.
111. Serpell, L. C., Alzheimer's amyloid fibrils: structure and assembly. *Biochim. Biophys. Acta - Mol. Basis. Dis.* **2000**, *1502* (1), 16-30.
112. Enache, T. A.; Chiorcea-Paquim, A.-M.; Oliveira-Brett, A. M., Amyloid- $\beta$  peptides time-dependent structural modifications: AFM and voltammetric characterization. *Analytica Chimica Acta* **2016**, *926*, 36-47.
113. Oliver, D. M. A.; Reddy, P. H., Small molecules as therapeutic drugs for Alzheimer's disease. *Molecular and Cellular Neuroscience* **2019**, *96*, 47-62.
114. Casey, D. A.; Antimisiaris, D.; O'Brien, J., Drugs for Alzheimer's disease: are they effective? *P & T: a peer-reviewed journal for formulary management* **2010**, *35* (4), 208-211.
115. Fu, Z.; Aucoin, D.; Ahmed, M.; Ziliox, M.; Van Nostrand, W. E.; Smith, S. O., Capping of A $\beta$ 42 Oligomers by Small Molecule Inhibitors. *Biochemistry* **2014**, *53* (50), 7893-7903.
116. Ge, J.-F.; Qiao, J.-P.; Qi, C.-C.; Wang, C.-W.; Zhou, J.-N., The binding of resveratrol to monomer and fibril amyloid beta. *Neurochemistry International* **2012**, *61* (7), 1192-1201.
117. Ehrnhoefer, D. E.; Bieschke, J.; Boeddrich, A.; Herbst, M.; Masino, L.; Lurz, R.; Engemann, S.; Pastore, A.; Wanker, E. E., EGCG redirects amyloidogenic polypeptides into unstructured, off-pathway oligomers. *Nat. Struct. Mol. Biol.* **2008**, *15*, 558.
118. Bieschke, J.; Russ, J.; Friedrich, R. P.; Ehrnhoefer, D. E.; Wobst, H.; Neugebauer, K.; Wanker, E. E., EGCG remodels mature  $\alpha$ -synuclein and amyloid- $\beta$  fibrils and reduces cellular toxicity. *Proceedings of the National Academy of Sciences* **2010**, *107* (17), 7710-7715.
119. Andrich, K.; Bieschke, J., The Effect of (-)-Epigallo-catechin-(3)-gallate on Amyloidogenic Proteins Suggests a Common Mechanism. In *Natural Compounds as*

- .....
- Therapeutic Agents for Amyloidogenic Diseases*, Vassallo, N., Ed. Springer International Publishing: Cham, 2015; pp 139-161.
120. Palhano, F. L.; Lee, J.; Grimster, N. P.; Kelly, J. W., Toward the Molecular Mechanism(s) by Which EGCG Treatment Remodels Mature Amyloid Fibrils. *J. Am. Chem. Soc.* **2013**, *135* (20), 7503-7510.
121. Porat, Y.; Abramowitz, A.; Gazit, E., Inhibition of Amyloid Fibril Formation by Polyphenols: Structural Similarity and Aromatic Interactions as a Common Inhibition Mechanism. *Chemical Biology & Drug Design* **2006**, *67* (1), 27-37.
122. Gervais, F.; Paquette, J.; Morissette, C.; Krzywkowski, P.; Yu, M.; Azzi, M.; Lacombe, D.; Kong, X.; Aman, A.; Laurin, J.; Szarek, W. A.; Tremblay, P., Targeting soluble A $\beta$  peptide with Tramiprosate for the treatment of brain amyloidosis. *Neurobiology of Aging* **2007**, *28* (4), 537-547.
123. Kocis, P.; Tolar, M.; Yu, J.; Sinko, W.; Ray, S.; Blennow, K.; Fillit, H.; Hey, J. A., Elucidating the A $\beta$ 42 Anti-Aggregation Mechanism of Action of Tramiprosate in Alzheimer's Disease: Integrating Molecular Analytical Methods, Pharmacokinetic and Clinical Data. *CNS Drugs* **2017**, *31* (6), 495-509.
124. Ono, K.; Hirohata, M.; Yamada, M.,  $\alpha$ -Lipoic acid exhibits anti-amyloidogenicity for  $\beta$ -amyloid fibrils in vitro. *Biochemical and Biophysical Research Communications* **2006**, *341* (4), 1046-1052.
125. Felice, F. G. D.; Houzel, J.-C.; Garcia-Abreu, J.; Paulo Roberto F. Louzada, J.; Afonso, R. C.; Meirelles, M. N. L.; Lent, R.; Neto, V. M.; Ferreira, S. T., Inhibition of Alzheimer's disease  $\beta$ -amyloid aggregation, neurotoxicity, and in vivo deposition by nitrophenols: implications for Alzheimer's therapy. *The FASEB Journal* **2001**, *15* (7), 1297-1299.
126. Ono, K.; Hasegawa, K.; Naiki, H.; Yamada, M., Anti-Parkinsonian agents have anti-amyloidogenic activity for Alzheimer's  $\beta$ -amyloid fibrils in vitro. *Neurochemistry International* **2006**, *48* (4), 275-285.
127. Ono, K.; Hirohata, M.; Yamada, M., Ferulic acid destabilizes preformed  $\beta$ -amyloid fibrils in vitro. *Biochemical and Biophysical Research Communications* **2005**, *336* (2), 444-449.
128. Ono, K.; Yoshiike, Y.; Takashima, A.; Hasegawa, K.; Naiki, H.; Yamada, M., Vitamin A exhibits potent anti-amyloidogenic and fibril-destabilizing effects in vitro. *Experimental Neurology* **2004**, *189* (2), 380-392.
129. Sinha, S.; Lopes, D. H. J.; Du, Z.; Pang, E. S.; Shanmugam, A.; Lomakin, A.; Talbiersky, P.; Tennstaedt, A.; McDaniel, K.; Bakshi, R.; Kuo, P.-Y.; Ehrmann, M.; Benedek, G. B.; Loo, J. A.; Klärner, F.-G.; Schrader, T.; Wang, C.; Bitan, G., Lysine-Specific Molecular Tweezers Are Broad-Spectrum Inhibitors of Assembly and Toxicity of Amyloid Proteins. *Journal of the American Chemical Society* **2011**, *133* (42), 16958-16969.
130. Koziara, J. M.; Lockman, P. R.; Allen, D. D.; Mumper, R. J., In Situ Blood-Brain Barrier Transport of Nanoparticles. *Pharmaceutical Research* **2003**, *20* (11), 1772-1778.
131. Cabaleiro-Lago, C.; Quinlan-Pluck, F.; Lynch, I.; Dawson, K. A.; Linse, S., Dual Effect of Amino Modified Polystyrene Nanoparticles on Amyloid  $\beta$  Protein Fibrillation. *ACS Chem. Neurosci.* **2010**, *1* (4), 279-287.
132. Yoo, S. I.; Yang, M.; Brender, J. R.; Subramanian, V.; Sun, K.; Joo, N. E.; Jeong, S.-H.; Ramamoorthy, A.; Kotov, N. A., Inhibition of Amyloid Peptide Fibrillation by Inorganic Nanoparticles: Functional Similarities with Proteins. *Angew. Chem. Int. Ed.* **2011**, *50* (22), 5110-5115.
133. Skaat, H.; Chen, R.; Grinberg, I.; Margel, S., Engineered Polymer Nanoparticles Containing Hydrophobic Dipeptide for Inhibition of Amyloid- $\beta$  Fibrillation. *Biomacromolecules* **2012**, *13* (9), 2662-2670.

134. Saraiva, A. M.; Cardoso, I.; Pereira, M. C.; Coelho, M. A. N.; Saraiva, M. J.; Möhwald, H.; Brezesinski, G., Controlling Amyloid- $\beta$  Peptide(1–42) Oligomerization and Toxicity by Fluorinated Nanoparticles. *ChemBioChem* **2010**, *11* (13), 1905-1913.
135. Rocha, S.; Thünemann, A. F.; Pereira, M. d. C.; Coelho, M.; Möhwald, H.; Brezesinski, G., Influence of fluorinated and hydrogenated nanoparticles on the structure and fibrillogenesis of amyloid beta-peptide. *Biophysical Chemistry* **2008**, *137* (1), 35-42.
136. Liao, Y.-H.; Chang, Y.-J.; Yoshiike, Y.; Chang, Y.-C.; Chen, Y.-R., Negatively Charged Gold Nanoparticles Inhibit Alzheimer's Amyloid- $\beta$  Fibrillization, Induce Fibril Dissociation, and Mitigate Neurotoxicity. *Small* **2012**, *8* (23), 3631-3639.
137. Moore, K. A.; Pate, K. M.; Soto-Ortega, D. D.; Lohse, S.; van der Munnik, N.; Lim, M.; Jackson, K. S.; Lyles, V. D.; Jones, L.; Glassgow, N.; Napumecho, V. M.; Mobley, S.; Uline, M. J.; Mahtab, R.; Murphy, C. J.; Moss, M. A., Influence of gold nanoparticle surface chemistry and diameter upon Alzheimer's disease amyloid- $\beta$  protein aggregation. *Journal of Biological Engineering* **2017**, *11* (1), 5.
138. Palmal, S.; Maity, A. R.; Singh, B. K.; Basu, S.; Jana, N. R.; Jana, N. R., Inhibition of Amyloid Fibril Growth and Dissolution of Amyloid Fibrils by Curcumin–Gold Nanoparticles. *Chemistry – A European Journal* **2014**, *20* (20), 6184-6191.
139. Gao, G.; Zhang, M.; Gong, D.; Chen, R.; Hu, X.; Sun, T., The size-effect of gold nanoparticles and nanoclusters in the inhibition of amyloid- $\beta$  fibrillation. *Nanoscale* **2017**, *9* (12), 4107-4113.
140. Palmal, S.; Jana, N. R.; Jana, N. R., Inhibition of Amyloid Fibril Growth by Nanoparticle Coated with Histidine-Based Polymer. *J. Phys. Chem. C* **2014**, *118* (37), 21630-21638.
141. Mudshinge, S. R.; Deore, A. B.; Patil, S.; Bhalgat, C. M., Nanoparticles: Emerging carriers for drug delivery. *Saudi Pharmaceutical Journal* **2011**, *19* (3), 129-141.
142. Milojevic, J.; Raditsis, A.; Melacini, G., Human serum albumin inhibits Abeta fibrillization through a "monomer-competitor" mechanism. *Biophysical journal* **2009**, *97* (9), 2585-2594.
143. Milojevic, J.; Esposito, V.; Das, R.; Melacini, G., Understanding the Molecular Basis for the Inhibition of the Alzheimer's A $\beta$ -Peptide Oligomerization by Human Serum Albumin Using Saturation Transfer Difference and Off-Resonance Relaxation NMR Spectroscopy. *Journal of the American Chemical Society* **2007**, *129* (14), 4282-4290.
144. Reyes Barcelo, A. A.; Gonzalez-Velasquez, F. J.; Moss, M. A., Soluble aggregates of the amyloid- $\beta$  peptide are trapped by serum albumin to enhance amyloid- $\beta$  activation of endothelial cells. *Journal of Biological Engineering* **2009**, *3* (1), 5.
145. Kuo, Y.-M.; Kokjohn, T. A.; Kalback, W.; Luehrs, D.; Galasko, D. R.; Chevallier, N.; Koo, E. H.; Emmerling, M. R.; Roher, A. E., Amyloid- $\beta$  Peptides Interact with Plasma Proteins and Erythrocytes: Implications for Their Quantitation in Plasma. *Biochemical and Biophysical Research Communications* **2000**, *268* (3), 750-756.
146. Różga, M.; Kłoniecki, M.; Jabłowska, A.; Dadlez, M.; Bal, W., The binding constant for amyloid A $\beta$ 40 peptide interaction with human serum albumin. *Biochemical and Biophysical Research Communications* **2007**, *364* (3), 714-718.
147. Bohrmann, B.; Tjernberg, L.; Kuner, P.; Poli, S.; Levet-Trafit, B.; Näslund, J.; Richards, G.; Huber, W.; Döbeli, H.; Nordstedt, C., Endogenous Proteins Controlling Amyloid  $\beta$ -Peptide Polymerization: POSSIBLE IMPLICATIONS FOR  $\beta$ -AMYLOID FORMATION IN THE CENTRAL NERVOUS SYSTEM AND IN PERIPHERAL TISSUES. *Journal of Biological Chemistry* **1999**, *274* (23), 15990-15995.
148. Evans, K. C.; Berger, E. P.; Cho, C. G.; Weisgraber, K. H.; Lansbury, P. T., Apolipoprotein E is a kinetic but not a thermodynamic inhibitor of amyloid formation:

- .....
- implications for the pathogenesis and treatment of Alzheimer disease. *Proceedings of the National Academy of Sciences* **1995**, 92 (3), 763-767.
149. Villmow, M.; Baumann, M.; Malesevic, M.; Sachs, R.; Hause, G.; Fändrich, M.; Balbach, J.; Schiene-Fischer, C., Inhibition of A $\beta$ (1–40) fibril formation by cyclophilins. *Biochem. J.* **2016**, 473 (10), 1355-1368.
150. Smith, T. J.; Stains, C. I.; Meyer, S. C.; Ghosh, I., Inhibition of  $\beta$ -Amyloid Fibrillization by Directed Evolution of a  $\beta$ -Sheet Presenting Miniature Protein. *Journal of the American Chemical Society* **2006**, 128 (45), 14456-14457.
151. Chalifour, R. J.; McLaughlin, R. W.; Lavoie, L.; Morissette, C.; Tremblay, N.; Boulé, M.; Sarazin, P.; Stéa, D.; Lacombe, D.; Tremblay, P.; Gervais, F., Stereoselective Interactions of Peptide Inhibitors with the  $\beta$ -Amyloid Peptide. *Journal of Biological Chemistry* **2003**, 278 (37), 34874-34881.
152. Lu, J.; Cao, Q.; Wang, C.; Zheng, J.; Luo, F.; Xie, J.; Li, Y.; Ma, X.; He, L.; Eisenberg, D.; Nowick, J.; Jiang, L.; Li, D., Structure-Based Peptide Inhibitor Design of Amyloid- $\beta$  Aggregation. *Frontiers in Molecular Neuroscience* **2019**, 12 (54).
153. Qiuming, W.; Xiang, Y.; Lingyan, L.; Jie, Z., Inhibition of Amyloid- $\beta$  Aggregation in Alzheimer's Disease. *Current Pharmaceutical Design* **2014**, 20 (8), 1223-1243.
154. Austen, B. M.; Paleologou, K. E.; Ali, S. A. E.; Qureshi, M. M.; Allsop, D.; El-Agnaf, O. M. A., Designing Peptide Inhibitors for Oligomerization and Toxicity of Alzheimer's  $\beta$ -Amyloid Peptide. *Biochemistry* **2008**, 47 (7), 1984-1992.
155. Tjernberg, L. O.; Lilliehöök, C.; Callaway, D. J. E.; Näslund, J.; Hahne, S.; Thyberg, J.; Terenius, L.; Nordstedt, C., Controlling Amyloid  $\beta$ -Peptide Fibril Formation with Protease-stable Ligands. *Journal of Biological Chemistry* **1997**, 272 (19), 12601-12605.
156. Tjernberg, L. O.; Näslund, J.; Lindqvist, F.; Johansson, J.; Karlström, A. R.; Thyberg, J.; Terenius, L.; Nordstedt, C., Arrest of  $\beta$ -Amyloid Fibril Formation by a Pentapeptide Ligand. *Journal of Biological Chemistry* **1996**, 271 (15), 8545-8548.
157. Goyal, D.; Shuaib, S.; Mann, S.; Goyal, B., Rationally Designed Peptides and Peptidomimetics as Inhibitors of Amyloid- $\beta$  (A $\beta$ ) Aggregation: Potential Therapeutics of Alzheimer's Disease. *ACS Combinatorial Science* **2017**, 19 (2), 55-80.
158. Yamin, G.; Ruchala, P.; Teplow, D. B., A Peptide Hairpin Inhibitor of Amyloid  $\beta$ -Protein Oligomerization and Fibrillogenesis. *Biochemistry* **2009**, 48 (48), 11329-11331.
159. Fradinger, E. A.; Monien, B. H.; Urbanc, B.; Lomakin, A.; Tan, M.; Li, H.; Spring, S. M.; Condrón, M. M.; Cruz, L.; Xie, C.-W.; Benedek, G. B.; Bitan, G., C-terminal peptides coassemble into A $\beta$ 42 oligomers and protect neurons against A $\beta$ 42-induced neurotoxicity. *Proceedings of the National Academy of Sciences* **2008**, 105 (37), 14175-14180.
160. Hetényi, C.; Szabó, Z.; Klement, É.; Datki, Z.; Körtvélyesi, T.; Zarándi, M.; Penke, B., Pentapeptide Amides Interfere with the Aggregation of  $\beta$ -Amyloid Peptide of Alzheimer's Disease. *Biochemical and Biophysical Research Communications* **2002**, 292 (4), 931-936.
161. Blanchard, B. J.; Konopka, G.; Russell, M.; Ingram, V. M., Mechanism and prevention of neurotoxicity caused by  $\beta$ -amyloid peptides: relation to Alzheimer's disease. *Brain Research* **1997**, 776 (1), 40-50.
162. Kawashima, H.; Sohma, Y.; Nakanishi, T.; Kitamura, H.; Mukai, H.; Yamashita, M.; Akaji, K.; Kiso, Y., A new class of aggregation inhibitor of amyloid- $\beta$  peptide based on an O-acetyl isopeptide. *Bioorganic & Medicinal Chemistry* **2013**, 21 (21), 6323-6327.
163. Flashner, E.; Raviv, U.; Friedler, A., The effect of tachykinin neuropeptides on amyloid  $\beta$  aggregation. *Biochemical and Biophysical Research Communications* **2011**, 407 (1), 13-17.
164. Aloisi, A.; Barca, A.; Romano, A.; Guerrieri, S.; Storelli, C.; Rinaldi, R.; Verri, T., Anti-Aggregating Effect of the Naturally Occurring Dipeptide Carnosine on A $\beta$ 1-42 Fibril Formation. *PLOS ONE* **2013**, 8 (7), e68159.

165. Richman, M.; Wilk, S.; Chemerovski, M.; Wärmländer, S. K. T. S.; Wahlström, A.; Gräslund, A.; Rahimpour, S., In Vitro and Mechanistic Studies of an Antiamyloidogenic Self-Assembled Cyclic d,l- $\alpha$ -Peptide Architecture. *Journal of the American Chemical Society* **2013**, *135* (9), 3474-3484.
166. Rajasekhar, K.; Suresh, S. N.; Manjithaya, R.; Govindaraju, T., Rationally Designed Peptidomimetic Modulators of A $\beta$  Toxicity in Alzheimer's Disease. *Scientific Reports* **2015**, *5* (1), 8139.
167. Devanathan, S.; Salamon, Z.; Lindblom, G.; Gröbner, G.; Tollin, G., Effects of sphingomyelin, cholesterol and zinc ions on the binding, insertion and aggregation of the amyloid A $\beta$ 1–40 peptide in solid-supported lipid bilayers. *The FEBS Journal* **2006**, *273* (7), 1389-1402.
168. Matsuzaki, K., Physicochemical interactions of amyloid  $\beta$ -peptide with lipid bilayers. *Biochimica et Biophysica Acta (BBA) - Biomembranes* **2007**, *1768* (8), 1935-1942.
169. Ji, S.-R.; Wu, Y.; Sui, S.-f., Cholesterol Is an Important Factor Affecting the Membrane Insertion of  $\beta$ -Amyloid Peptide (A $\beta$ 1–40), Which May Potentially Inhibit the Fibril Formation. *Journal of Biological Chemistry* **2002**, *277* (8), 6273-6279.
170. Gellermann, G. P.; Appel, T. R.; Tannert, A.; Radestock, A.; Hortschansky, P.; Schroeckh, V.; Leisner, C.; Lütkepohl, T.; Shtrasburg, S.; Röcken, C.; Pras, M.; Linke, R. P.; Diekmann, S.; Fändrich, M., Raft lipids as common components of human extracellular amyloid fibrils. *Proceedings of the National Academy of Sciences of the United States of America* **2005**, *102* (18), 6297-6302.
171. Murphy, R. M., Kinetics of amyloid formation and membrane interaction with amyloidogenic proteins. *Biochimica et Biophysica Acta (BBA) - Biomembranes* **2007**, *1768* (8), 1923-1934.
172. Lindberg, D. J.; Wesén, E.; Björkeröth, J.; Rocha, S.; Esbjörner, E. K., Lipid membranes catalyse the fibril formation of the amyloid- $\beta$  (1–42) peptide through lipid-fibril interactions that reinforce secondary pathways. *Biochimica et Biophysica Acta (BBA) - Biomembranes* **2017**, *1859* (10), 1921-1929.
173. Adler, J.; Scheidt, H. A.; Lemmnitzer, K.; Krueger, M.; Huster, D., N-terminal lipid conjugation of amyloid [small beta](1-40) leads to the formation of highly ordered N-terminally extended fibrils. *Phys. Chem. Chem. Phys.* **2017**, *19* (3), 1839-1846.
174. Dahse, K.; Garvey, M.; Kovermann, M.; Vogel, A.; Balbach, J.; Fändrich, M.; Fahr, A., DHPC Strongly Affects the Structure and Oligomerization Propensity of Alzheimer's A $\beta$ (1–40) Peptide. *J. Mol. Biol.* **2010**, *403* (4), 643-659.
175. Chang, C.-C.; Edwald, E.; Veatch, S.; Steel, D. G.; Gafni, A., Interactions of amyloid- $\beta$  peptides on lipid bilayer studied by single molecule imaging and tracking. *Biochimica et Biophysica Acta (BBA) - Biomembranes* **2018**, *1860* (9), 1616-1624.
176. Shao, H.; Jao, S.-c.; Ma, K.; Zagorski, M. G., Solution structures of micelle-bound amyloid  $\beta$ -(1-40) and  $\beta$ -(1-42) peptides of Alzheimer's disease. Edited by P. E. Wright. *J. Mol. Biol.* **1999**, *285* (2), 755-773.
177. Österlund, N.; Kulkarni, Y. S.; Misiaszek, A. D.; Wallin, C.; Krüger, D. M.; Liao, Q.; Mashayekhy Rad, F.; Jarvet, J.; Strodel, B.; Wärmländer, S. K. T. S.; Ilag, L. L.; Kamerlin, S. C. L.; Gräslund, A., Amyloid- $\beta$  Peptide Interactions with Amphiphilic Surfactants: Electrostatic and Hydrophobic Effects. *ACS Chemical Neuroscience* **2018**, *9* (7), 1680-1692.
178. Maity, S.; Pramanik, A.; Lyubchenko, Y. L., Probing Intermolecular Interactions within the Amyloid  $\beta$  Trimer Using a Tethered Polymer Nanoarray. *Bioconjugate chemistry* **2018**, *29* (8), 2755-2762.
179. Assarsson, A.; Linse, S.; Cabaleiro-Lago, C., Effects of Polyamino Acids and Polyelectrolytes on Amyloid  $\beta$  Fibril Formation. *Langmuir* **2014**, *30* (29), 8812-8818.

- .....
180. Rocha, S.; Cardoso, I.; Börner, H.; Pereira, M. C.; Saraiva, M. J.; Coelho, M., Design and biological activity of  $\beta$ -sheet breaker peptide conjugates. *Biochem. Biophys. Res. Commun.* **2009**, *380* (2), 397-401.
181. Sun, H.; Liu, J.; Li, S.; Zhou, L.; Wang, J.; Liu, L.; Lv, F.; Gu, Q.; Hu, B.; Ma, Y.; Wang, S., Reactive Amphiphilic Conjugated Polymers for Inhibiting Amyloid  $\beta$  Assembly. *Angew. Chem. Int. Ed.* **2019**, *58* (18), 5988-5993.
182. Sahoo, B. R.; Genjo, T.; Nakayama, T. W.; Stoddard, A. K.; Ando, T.; Yasuhara, K.; Fierke, C. A.; Ramamoorthy, A., A cationic polymethacrylate-copolymer acts as an agonist for  $\beta$ -amyloid and an antagonist for amylin fibrillation. *Chemical Science* **2019**, *10* (14), 3976-3986.
183. Chowdhury, S. R.; Agarwal, M.; Meher, N.; Muthuraj, B.; Iyer, P. K., Modulation of Amyloid Aggregates into Nontoxic Coaggregates by Hydroxyquinoline Appended Polyfluorene. *ACS Appl. Mater. Interfaces* **2016**, *8* (21), 13309-13319.
184. Song, Y.; Cheng, P.-N.; Zhu, L.; Moore, E. G.; Moore, J. S., Multivalent Macromolecules Redirect Nucleation-Dependent Fibrillar Assembly into Discrete Nanostructures. *J. Am. Chem. Soc.* **2014**, *136* (14), 5233-5236.
185. Marx, U. C.; Adermann, K.; Bayer, P.; Forssmann, W.-G.; Rösch, P., Solution Structures of Human Parathyroid Hormone Fragments hPTH(1-34) and hPTH(1-39) and Bovine Parathyroid Hormone Fragment bPTH(1-37). *Biochem. Biophys. Res. Commun.* **2000**, *267* (1), 213-220.
186. Ehrnhoefer, D. E.; Bieschke, J.; Boeddrich, A.; Herbst, M.; Masino, L.; Lurz, R.; Engemann, S.; Pastore, A.; Wanker, E. E., EGCG redirects amyloidogenic polypeptides into unstructured, off-pathway oligomers. *Nature Structural & Molecular Biology* **2008**, *15* (6), 558-566.
187. Guo, J.; Khatri, A.; Maeda, A.; Potts, J. T.; Jüppner, H.; Gardella, T. J., Prolonged Pharmacokinetic and Pharmacodynamic Actions of a Pegylated Parathyroid Hormone (1-34) Peptide Fragment. *J. Bone Miner. Res.* **2017**, *32* (1), 86-98.
188. Evgrafova, Z.; Rothmund, S.; Voigt, B.; Hause, G.; Balbach, J.; Binder, W. H., Synthesis and Aggregation of Polymer-Amyloid  $\beta$  Conjugates. *Macromolecular Rapid Communications* **2019**, *0* (0), 1900378.

## VI. Appendix

### Appendix A – *Polymers* 2016, 8 (5)

#### *Amyloid Beta Aggregation in the Presence of Temperature-Sensitive Polymers*

#### Characterization of poly(methoxydi(ethylene glycol)acrylate)

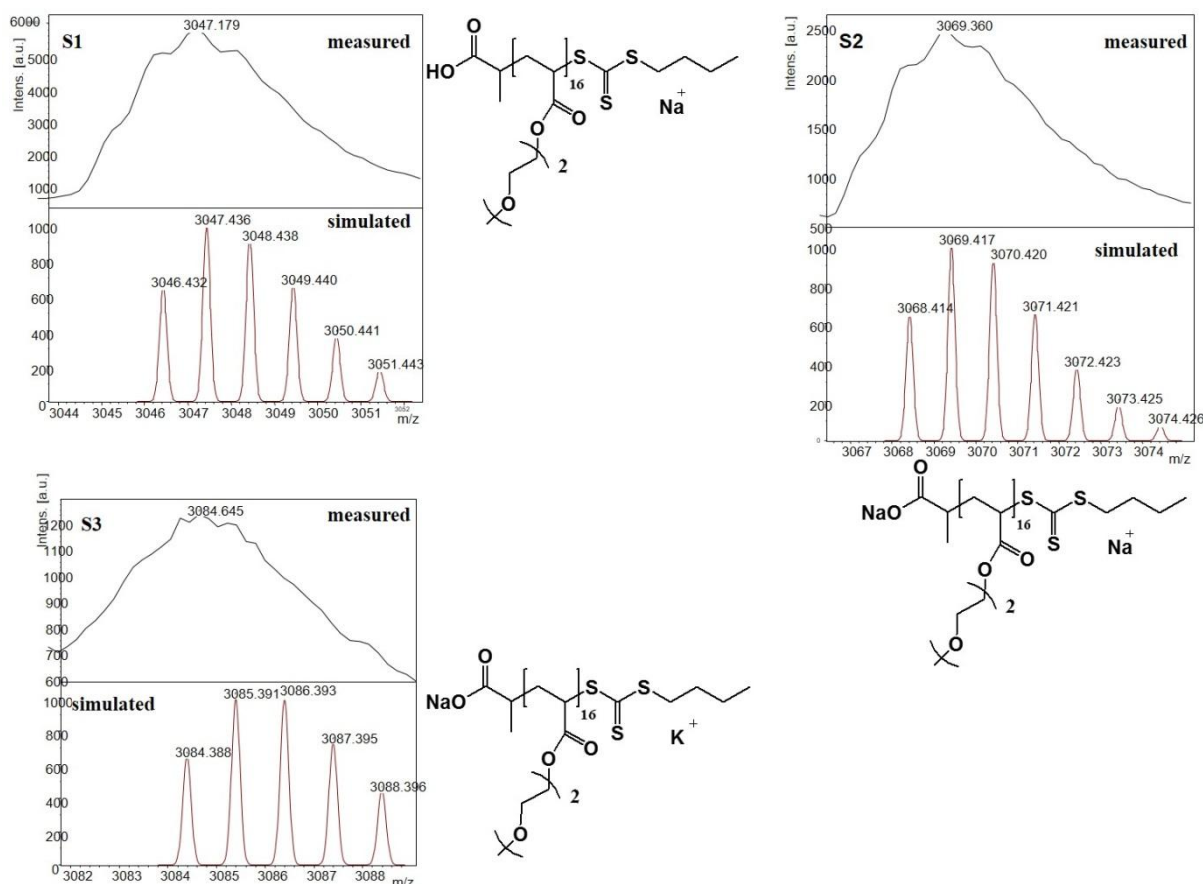


**Figure S1.** MALDI-TOF spectrum of poly(methoxydi(ethylene glycol)acrylate) (**3a**).

The structure of the obtained poly(methoxydiethylene glycol)acrylate (**3a**) and the presence of the both end-groups were also verified by <sup>1</sup>H-NMR spectroscopy (Figure S2). Thus, an end-group methine proton (a) is visible as a multiplet from 4.85 to 4.82 ppm. The methylene protons (e) of the repeating unit appeared as a broad singlet at 4.19 ppm, while methylene protons (f) + (g) and (h) are present as a multiplet from 3.67 to 3.62 ppm and a multiplet at 3.53 ppm respectively. Three methyl protons of the repeating unit (i) were found as a wide singlet at 3.36 ppm. The broad signal at 2.34 ppm can be ascribed to the methine proton (d) and a number of signals from 1.92 to 1.41 ppm are including protons (c), (k) and (l). The presence of both end-groups is verified by the appearance of the protons (b) at 1.15 ppm and (m) at 0.93 ppm. The molecular weight ( $M_n$ ) of the obtained polymer was assessed as 3600 g/mol using integration values under signal (d) and a molecular weight of the repeating unit equal to 174 g/mol.

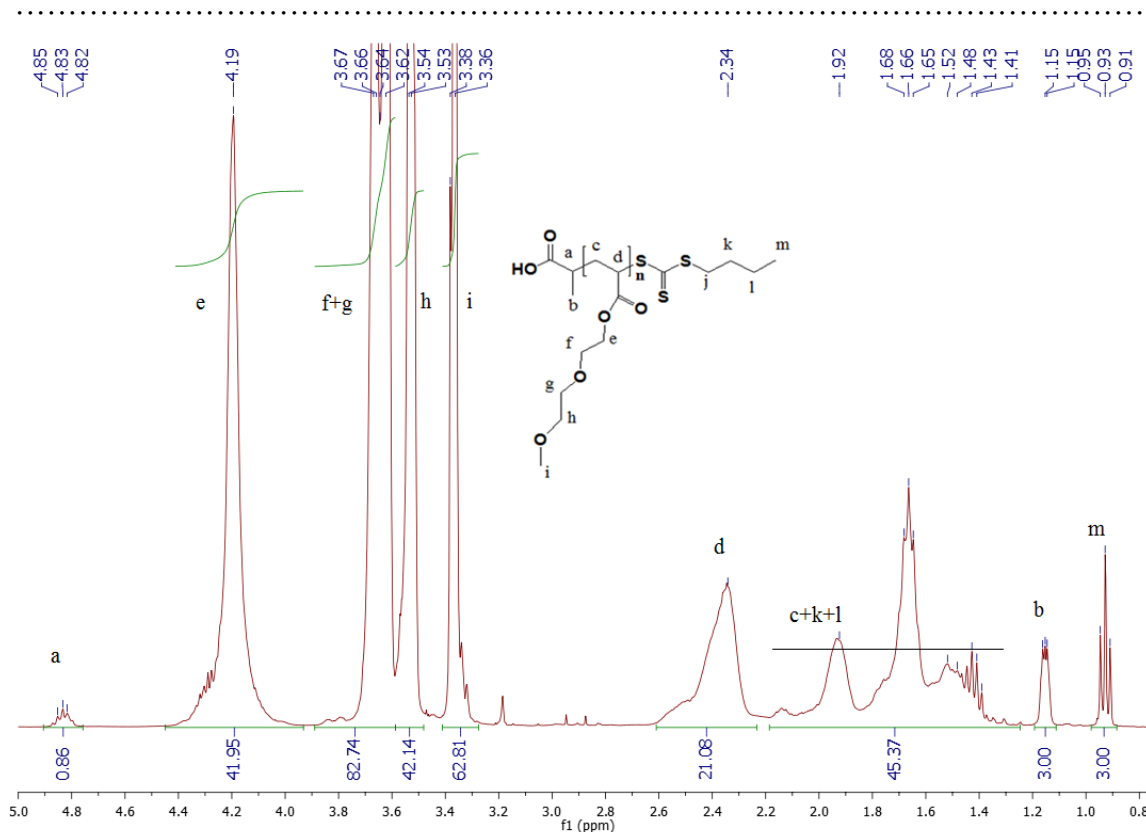


**Figure S2.**  $^1\text{H}$ -NMR-spectrum of poly(methoxydi(ethylene glycol)acrylate) (**3a**).

### Oxazoline syntheses

The procedure for the syntheses of the 2-oxazoline monomers, starting from ethanolamine and the corresponding nitrile, was adopted from Witte and Seeliger.[1]

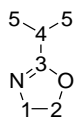
#### Synthesis of 2-isopropyl-2-oxazoline

To zinc acetate dihydrate (2.2 g, 10 mmol) the isobutyronitrile was added (18.0 mL, 200.0 mmol). Subsequently the mixture was heated to 130 °C and the ethanolamine (14.5 mmol, 240.0 mmol) was added dropwise to avoid an excessive formation of ammonia. After refluxing for 24 hours the orange solution was distilled under reduced pressure (60 °C, 40 mbar) to yield the pure, colorless product.

Characterization:

Properties: Colourless, characteristic smelling liquid, boiling point: 41 °C (50 mbar)

Yield: 13.3 mL, 111 mmol (56 %)



$^1\text{H}$ -NMR (400 MHz,  $\text{CDCl}_3$ , 27 °C):  $\delta$  (ppm) = 4.03 (t, 2H,  $H_2$ ,  $^3J_{\text{H,H}} = 9.5$  Hz), 3.62 (t, 2H,  $H_1$ ,  $^3J_{\text{H,H}} = 9.5$  Hz), 2.43 – 2.31 (m, 1H,  $H_4$ ), 1.01 (d, 6H,  $H_5$ ,  $^3J_{\text{H,H}} = 7.0$  Hz).

$^{13}\text{C}$ -NMR (100 MHz,  $\text{CDCl}_3$ , 27 °C):  $\delta$  (ppm) = 172.5 ( $C_3$ ), 67.1 ( $C_2$ ), 54.1 ( $C_1$ ), 27.9 ( $C_4$ ), 19.5 ( $C_5$ ).

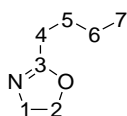
### Synthesis of 2-*n*-butyl-oxazoline

A mixture of zinc acetate dihydrate (1.9 g, 8.6 mmol) and valeronitrile (18.0 mL, 173.0 mmol) was heated to 130 °C. Ethanolamine (11.0 mL, 181.0 mmol) was added dropwise to avoid an excessive formation of ammonia. Consecutively the mixture was refluxed for 24 hours before it was distilled (85 °C, 19 mbar) to obtain the pure, colorless product.

Characterization:

Properties: Colourless, characterisitic smelling liquid, boiling point: 55 °C (15 mbar)

Yield: 9.6 g, 75 mmol (44 %)



$^1\text{H-NMR}$  (400 MHz,  $\text{CDCl}_3$ , 27 °C):  $\delta$  (ppm) = 4.14 (t, 2H,  $H_2$ ,  $^3J_{\text{H,H}} = 9.4$  Hz), 3.75 (t, 2H,  $H_1$ ,  $^3J_{\text{H,H}} = 9.4$  Hz), 2.23 – 2.18 (m, 2H,  $H_4$ ), 1.59 – 1.51 (m, 2H,  $H_5$ ), 1.36 – 1.26 (m, 2H,  $H_6$ ), 0.86 (t, 3H,  $H_7$ ,  $^3J_{\text{H,H}} = 7.4$  Hz).

$^{13}\text{C-NMR}$  (100 MHz,  $\text{CDCl}_3$ , 27 °C):  $\delta$  (ppm) = 168.5 ( $C_3$ ), 67.0 ( $C_3$ ), 54.3 ( $C_1$ ), 28.0 ( $C_4$ ), 27.6 ( $C_5$ ), 22.2, ( $C_6$ ), 13.7 ( $C_7$ ).

### Synthesis of poly(2-isopropyl-2-oxazoline)

The polymerization of the oxazolines were done according to Winnik *et al.*[2], but were carried out with an increased temperature (80 °C) due to lower reaction times.

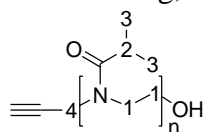
#### Initiation with propargyl tosylate

In the glove box 2-isopropyl-2-oxazoline (2.00 g, 2.10 mL, 17.63 mmol), dry ACN (8.81 mL) and propargyl tosylate were added to a Schlenk tube, which was sealed with a rubber septum afterwards. The mixture was stirred at room temperature for one hour and consecutively for 48 hours at 80 °C until gas chromatography (GC) showed complete conversion. The living chain ends were quenched by addition of water (74.75  $\mu\text{L}$ , 74.75 mL, 4.15 mmol) and further stirring for 24 hours at 60 °C. After evaporation of the solvent the residue was dissolved in DCM (5.0 mL) and was extracted with water (5 x 30.0 mL). The combined aqueous phases were back extracted using DCM (10 x 30.0 mL). Subsequently the organic phases were combined and dried over sodium sulfate. After filtration most of the solvent was removed using a rotary evaporator. The remaining viscous solution was precipitated three times in a cold mixture of diethyl ether / *n*-hexane to obtain the pure polymer. To increase the yield the solvent was centrifuged after every precipitation.

Characterization:

Properties: yellowish-orange solid

Yield: 1.65 g, 1.03 mmol (82 %)



$^1\text{H-NMR}$  (400 MHz,  $\text{CDCl}_3$ , 27 °C):  $\delta$  (ppm) = 4.09 (s, 2H,  $H_4$ ), 3.76 – 3.26 (m,  $\text{CH}_2$  of the repetitive unit), 3.01 – 2.55 (m,  $\text{CH}$  of the repetitive unit), 1.09 (s,  $\text{CH}_3$  of the repetitive unit).

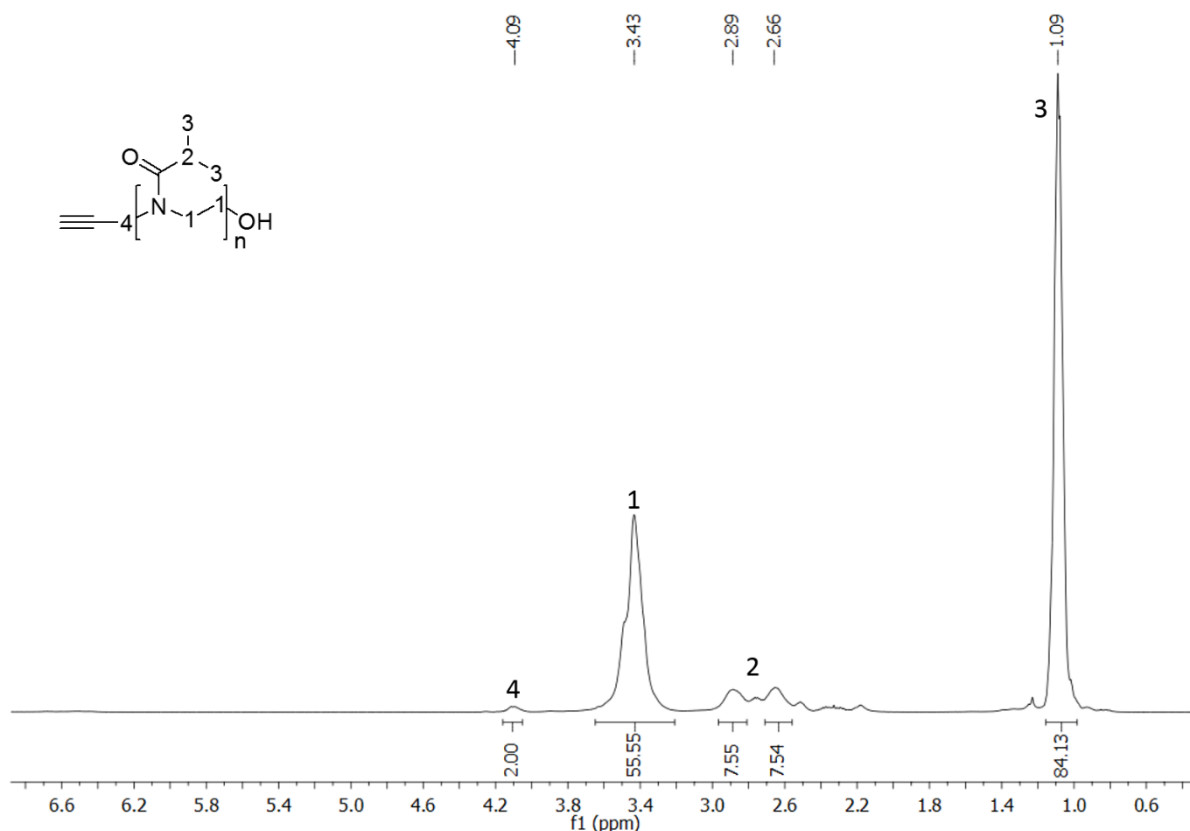


**Figure S3.** Exemplary  $^1\text{H-NMR}$ -spectrum from a poly(2-isopropyl-2-oxazoline) homopolymer that was initiated with propargyl tosylate.

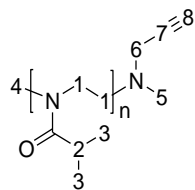
### Initiation with methyl triflate

The polymerization was carried out as described for the polymerization with propargyl tosylate. 2-Isopropyl-2-oxazoline (0.48 g, 0.50 mL, 4.20 mmol), ACN (1.88 mL) and methyl triflate (0.45 M in ACN, 0.21 mL) were mixed in a Schlenk tube and stirred at room temperature for one hour. Subsequently the mixture was stirred for 48 hours at 80 °C. The quench was done by adding *N*-methylpropargylamine (16.88  $\mu\text{L}$ , 13.82 mg, 0.20 mmol) and stirring for 36 hours at 42 °C. Work-up was done as described for the polymerization with propargyl tosylate as initiator.

Characterization:

Properties: slightly brownish solid

Yield: 268.0 mg, 51.5  $\mu\text{mol}$  (56 %)



$^1\text{H-NMR}$  (400 MHz,  $\text{CDCl}_3$ , 27 °C):  $\delta$  (ppm) = 4.09 (s, 2H,  $H_6$ ), 3.70 – 3.30 (m,  $\text{CH}_2$  of the repetitive unit), 3.05 (s, 3H,  $H_4$ ), 3.00 – 2.50 (m,  $\text{CH}$  of the repetitive unit), 1.09 (s,  $\text{CH}_3$  of the repetitive unit).

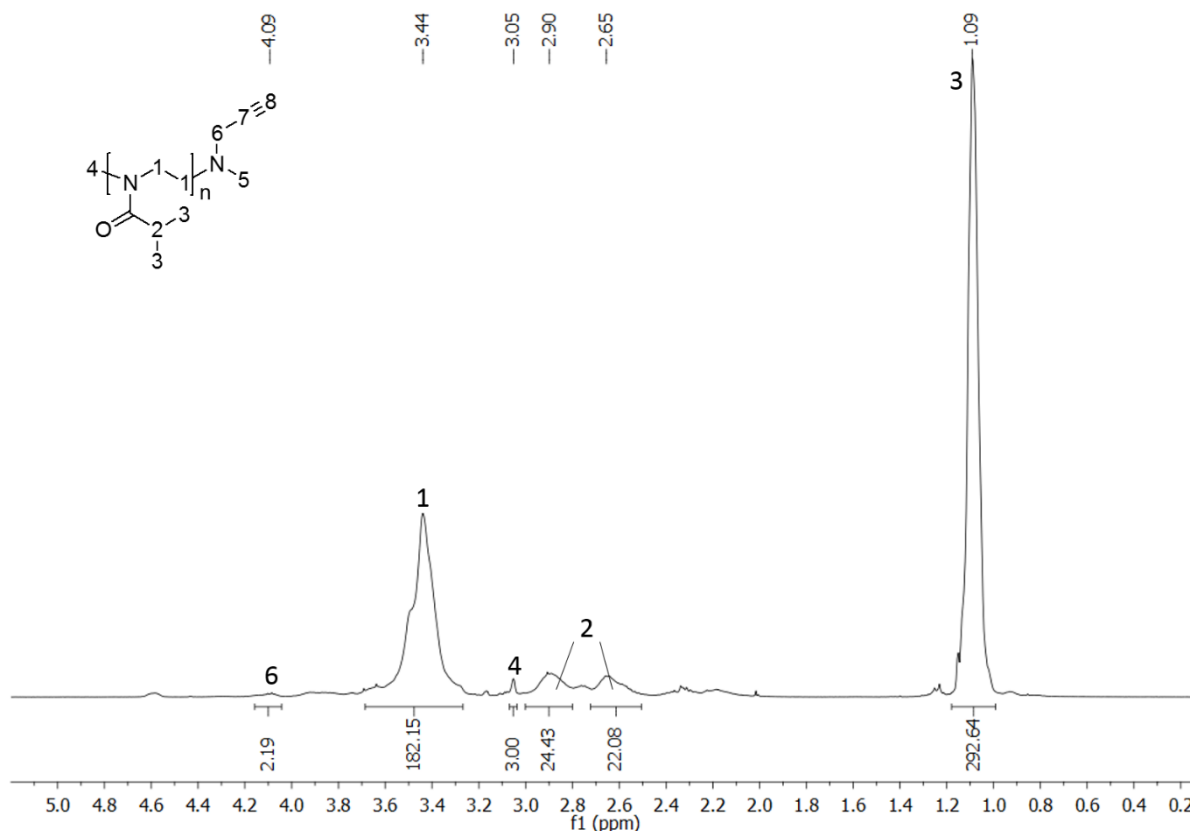


**Figure S4.** Exemplary  $^1\text{H}$ -NMR-spectrum from a poly(2-isopropyl-2-oxazoline) homopolymer that was initiated with methyl triflate.

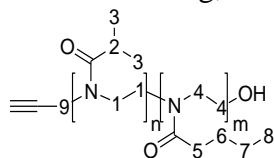
### Synthesis of poly(2-isopropyl-2-oxazoline-*grad*-2-*n*-butyl-2-oxazoline) copolymer [3]

The procedure was done as described for the homopolymerization of 2-isopropyl-oxazoline. A mixture of 2-isopropyl-2-oxazoline (0.54 mL, 0.51 g, 4.50 mmol), 2-*n*-butyl-oxazoline (63.60 mg, 0.50 mmol), propargyl tosylate (50.86  $\mu\text{L}$ , 61.80 mg, 0.29 mmol) and ACN (2.50 mL) was stirred for one hour at room temperature in a Schlenk tube. After stirring for 48 hours at 80  $^\circ\text{C}$  the reaction was quenched by the addition of water (20.90  $\mu\text{L}$ , 20.90 mg, 1.16 mmol). The reaction was stirred for further 24 hours at 60  $^\circ\text{C}$ . The work-up was done as described for the poly(2-isopropyl-2-oxazoline).

Characterization:

Properties: colorless, slightly yellowish solid

Yield: 527.0 mg, 0.31 mmol (92 %)



$^1\text{H}$ -NMR (400 MHz,  $\text{CDCl}_3$ , 27  $^\circ\text{C}$ ):  $\delta$  (ppm) = 4.03 (s, 2H,  $H_9$ ), 3.50 – 3.25 (m,  $\text{CH}_2$  of the repetitive unit,  $H_1 + H_4$ ), 2.90 – 2.50 (m,  $\text{CH}$  of the repetitive unit), 2.32 – 2.15 (m,  $\text{CH}_2$  of the repetitive unit,  $H_5$ ), 1.50 (s,  $\text{CH}_2$  of the repetitive unit,  $H_6$ ), 1.25 (s,  $\text{CH}_2$  of the repetitive unit,  $H_7$ ), 1.02 (s,  $\text{CH}_3$  of the repetitive unit,  $H_3$ ), 0.82 (s,  $\text{CH}_3$  of the repetitive unit,  $H_8$ ).

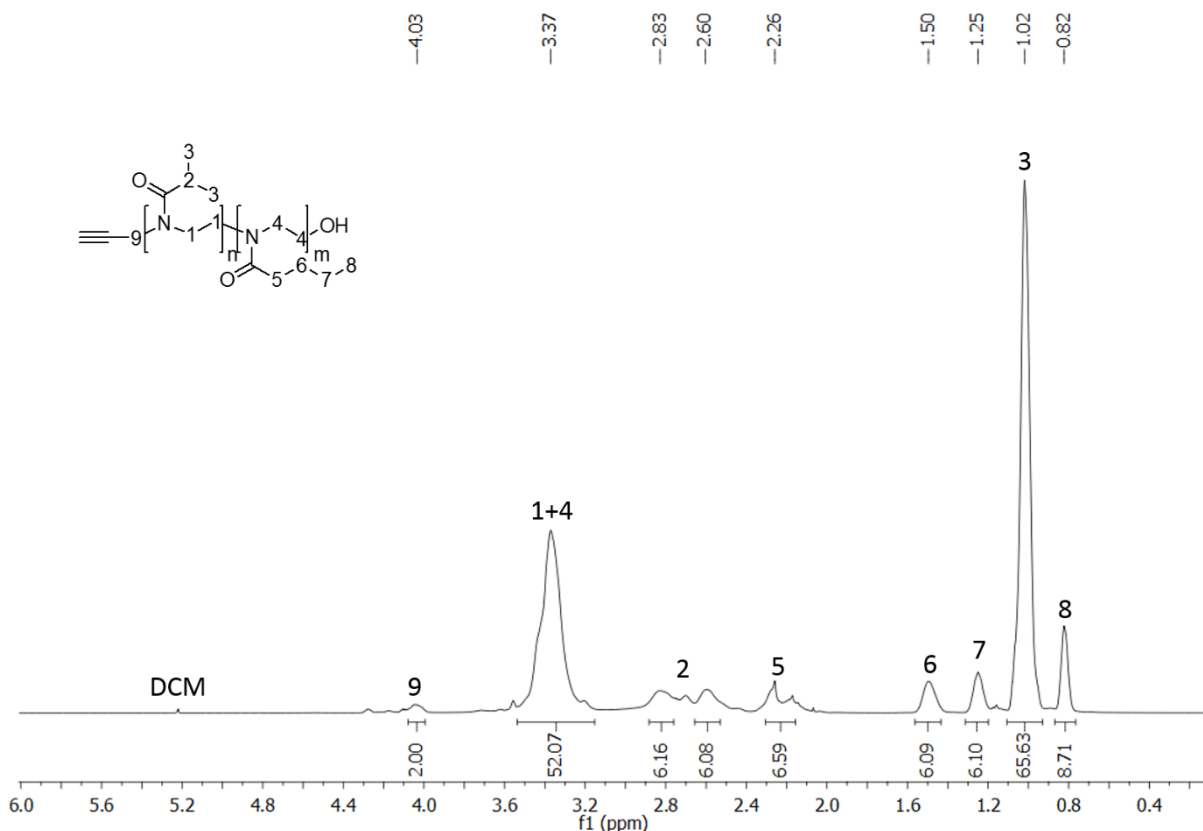


**Figure S5.** Exemplary  $^1\text{H-NMR}$ -spectrum from poly(2-isopropyl-2-oxazoline-grad-2-n-butyl-2-oxazoline) copolymer that was initiated with propargyl tosylate.

**Table S1.** Obtained molecular weights, PDIs and compositions for the synthesized copolymers **9**. Polymerizations were carried out in ACN ( $c = 2 \text{ mol/L}$ ) at  $80^\circ\text{C}$  with propargyl tosylate as initiator and water as quencher.

Entry	$n_{\text{th.}}^1$ (4)	$n_{\text{th.}}^1$ (5)	$M_{\text{theo.}}$ (g/mol)	$M_{\text{NMR}}^2$ (g/mol)	$M_{\text{GPC}}^3$ (g/mol)	PDI	$n_{\text{NMR}}^1$ (4)	$n_{\text{NMR}}^1$ (5)	Polymer
<b>9a</b>	0.90	0.10	2,000	1,700	3,600	1.3	0.79	0.21	P( $n\text{BuOx}_3i\text{PrOx}_{11}$ )
<b>9b</b>	0.75	0.25	2,040	1,600	3,600	1.3	0.80	0.20	P( $n\text{BuOx}_{2.6}i\text{PrOx}_{10.4}$ )
<b>9c</b>	0.65	0.35	2,060	1,700	4,200	1.4	0.61	0.39	P( $n\text{BuOx}_{5.5}i\text{POx}_{8.5}$ )

<sup>1</sup> fraction of monomer for the copolymer, <sup>2</sup> the  $^1\text{H-NMR}$  signal from the methylene group next to the alkyne group at  $\delta = 4.05 \text{ ppm}$  was used as reference, <sup>3</sup> measured in DMF with polystyrene ( $M_{\text{P}} = 1,000 - 115,000 \text{ g/mol}$ ) as standard.

### LCST measurements for the poly(2-isopropyl-2-oxazoline) homopolymer (**7**)

**Table S2.** Concentration dependency of the LCST for the PiPrOx **7** (3,100 g/mol) in water as 1 wt% solutions.

	0.25 wt%	0.50 wt%	0.75 wt%	1.00 wt%	1.25 wt%	1.50 wt%
$T_{\text{CP}} (^\circ\text{C})$	48.2	45.4	44.0	43.4	42.3	41.3

.....

### LCST measurements for the poly(2-isopropyl-2-oxazoline-grad-2-*n*-butyl-2-oxazoline) copolymers

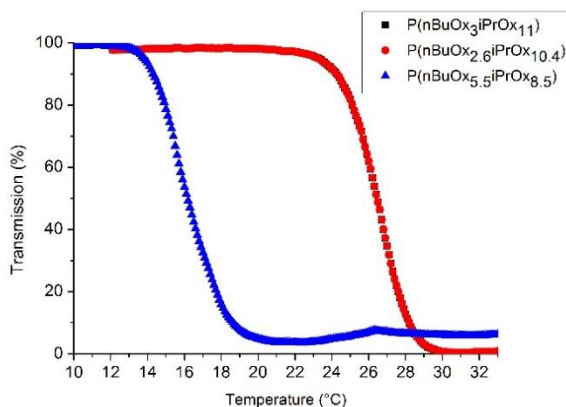


**Figure S6.** Measured curves for the copolymers **9a**, **9b**, and **9c** in sodium borate buffer (50 mmol, pH = 9.0) as 0.25 wt% solution. The presence of the hydrophobic nBuOx moieties significantly decreases the LCST. Because of the similar composition of the polymers **6a** (squares) and **6b** (circles) the curves overlap each other.

### LCST measurements for the poly(methoxydiethylene glycol)acrylates

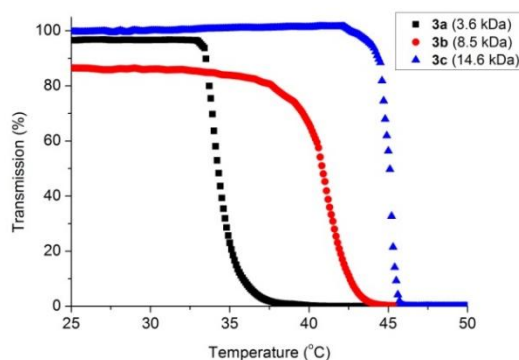


**Figure S7.** Dependency of the LCST from the molecular weight for 1 wt%-solutions of poly(methoxydi(ethylene glycol)acrylates) in H<sub>2</sub>O. With an increasing molecular weight the LCST is increasing.

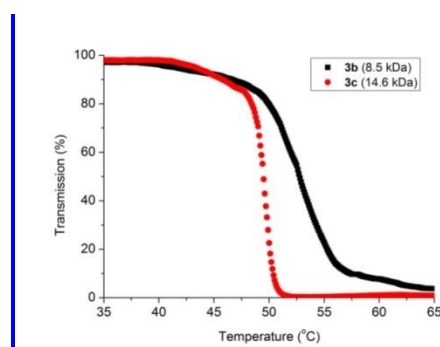
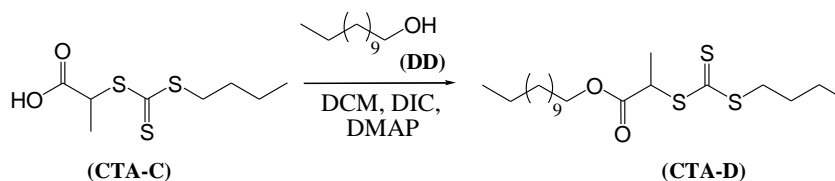


**Figure S8.** Influence of sodium phosphate (25 mmol/L, pH = 9.2, contained 150 mmol NaCl) on the LCST of poly(methoxy(diethylene glycol)acrylates) **3b** and **3c** ( $c = 230 \mu\text{mol/L}$ ). The presence of the salt increases the LCST of the polymer whereas this affect is much more pronounced for lower molecular weights.

- 
1. Witte, H. and W. Seeliger, *Cyclische Imidsäureester aus Nitrilen und Aminoalkoholen*. Justus Liebigs Annalen der Chemie, 1974. **1974**(6): p. 996-1009.
  2. Park, J.-S., et al., *Versatile Synthesis of End-Functionalized Thermosensitive Poly(2-isopropyl-2-oxazolines)*. Macromolecules, 2004. **37**(18): p. 6786-6792.
  3. Huber, S. and R. Jordan, *Modulation of the lower critical solution temperature of 2-Alkyl-2-oxazoline copolymers*. Colloid and Polymer Science, 2008. **286**(4): p. 395-402.

.....  
**Appendix B** – *Physical Chemistry Chemical Physics* **2019**, *21* (37), 20999-21006  
*Modulation of amyloid  $\beta$  peptide aggregation by hydrophilic polymers*

### Synthesis of *S*-Butyl-*S*-dodecyltrithiocarbonate (CTA-D)



**Scheme S1** Synthetic pathway for preparation of *S*-Butyl-*S*-dodecyltrithiocarbonate (CTA-D)

The synthesis of *S*-Butyl-*S*-dodecyltrithiocarbonate (CTA-D) was performed similarly to the procedure described in literature (Scheme S1)<sup>1</sup>. 2-[[*(*Butylsulfanyl)carbonothioyl]sulfanyl]propanoic acid (CTA-C)<sup>2</sup> (462.3 mg; 1.94 mmol), dodecanol (DD) (479.1  $\mu$ L; 2.13 mmol) and 12 ml of dry and degassed DCM were added into a dry oxygen-free double-neck reaction flask equipped with a magnetic stirrer, a rubber septum and a gas tap. 4-(Dimethylamino)-pyridin (DMAP) (23.7 mg; 0.194 mmol) was added and the mixture was cooled to 0 °C by means of the ice-bath. Then, *N,N'*-diisopropylcarbodiimide (DIC) (330.4  $\mu$ L; 2.13 mmol) solution in DCM (4 ml) was added dropwise while stirring. The reaction was hold at 0 °C for the next 2h and subsequently at room temperature overnight. Afterwards, all insoluble residues were filtered off and the crude product (CTA-D) was concentrated by rotary evaporation. Purification via column chromatography using chlorophorm was applied, obtaining a brownish product ( $R_f=0.86$ ). The product (CTA-D) was dried in a high vacuum and analyzed by <sup>1</sup>H-NMR spectroscopy.

Yield: 83.7 %

Characterization data: **CTA-D**: <sup>1</sup>H-NMR (400 MHz, CDCl<sub>3</sub>):  $\delta$  = ppm 4.80 (q, 1H<sub>n</sub>, -CHCH<sub>3</sub>), 4.11 (m, 2H<sub>l</sub>, -CH<sub>2</sub>CH<sub>2</sub>O), 3.35 (t, 2H<sub>o</sub>, -SCH<sub>2</sub>CH<sub>2</sub>), 1.68 (m, 4H<sub>c,p</sub>, -CH<sub>2</sub>CH<sub>2</sub>CH<sub>3</sub>), 1.58 (d, 3H<sub>m</sub>, -CHCH<sub>3</sub>), 1.42 (dt, 2H<sub>q</sub>, -CH<sub>2</sub>CH<sub>3</sub>), 1.26 (m, 16H<sub>d-k</sub>, -CH<sub>2</sub>CH<sub>2</sub>CH<sub>2</sub>), 0.93 (t, 3H<sub>r</sub>, -CH<sub>2</sub>CH<sub>3</sub>), 0.87 (t, 3H<sub>a</sub>, -(CH<sub>2</sub>)<sub>11</sub>CH<sub>3</sub>)

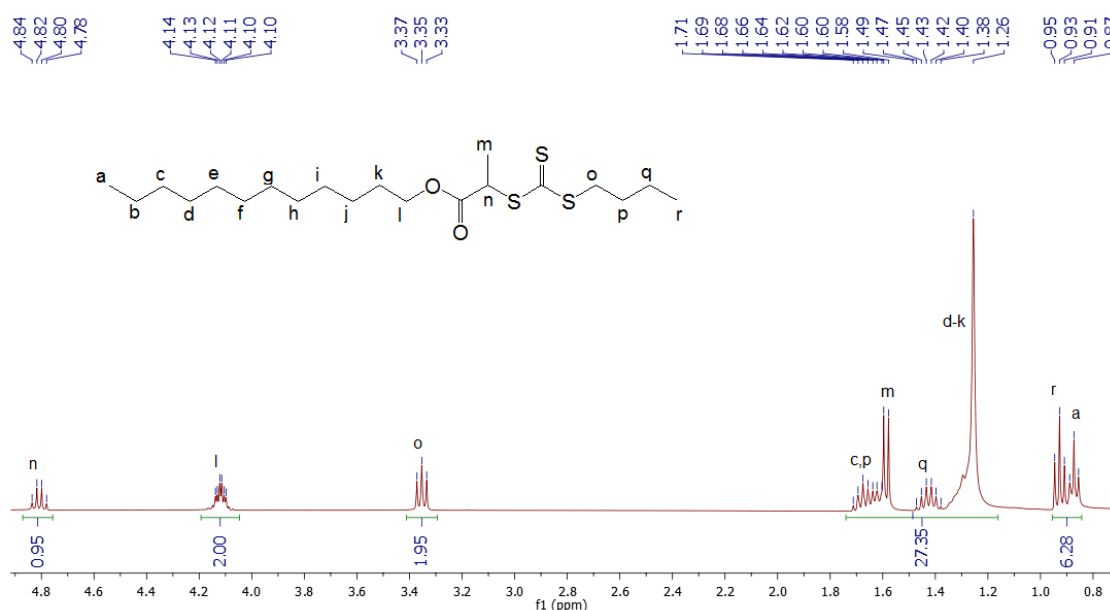


**Figure S1.** <sup>1</sup>H-NMR spectrum of *S*-Butyl-*S*-dodecyltrithiocarbonate (CTA-D).

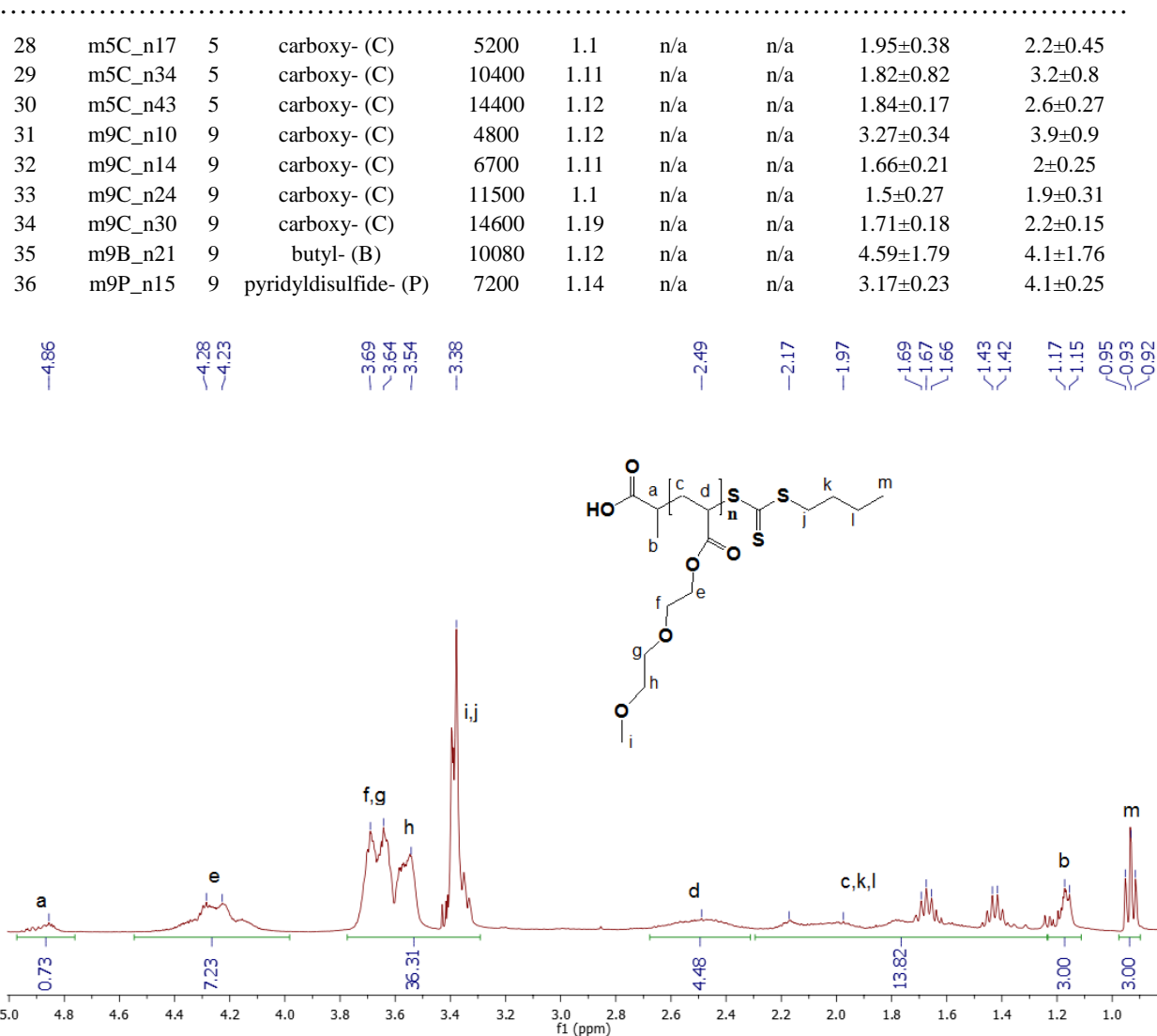
.....

**General procedure for the syntheses of the poly(methoxydi(ethylene glycol)acrylates) on example of m2C\_n16:**

RAFT polymerization of **m2C\_n16** was carried out using a standard Schlenk technique. The 2-[[[(Butylsulfanyl)carbonothioyl]sulfanyl] propanoic acid **CTA-C**<sup>2</sup> (40.1 mg, 0.168 mmol), methoxydi(ethylene glycol)acrylate (**Mon-2**) (425  $\mu$ L, 2.52 mmol) and 2,2'-Azobis(2-methylpropionitrile) AIBN (2.76 mg, 0.0168 mmol) in a molar ratio of (**Mon-2**):(**CTA-C**):AIBN 15:1:0.1 were dissolved in 0.85 mL of DMF. The mixture of (**Mon-2**), (**CTA-C**), AIBN and DMF were bubbled with argon for 30 minutes prior to the reaction and placed into a preheated oil bath at 70 °C. The reaction was stirred for six hours before it was cooled by means of a methanol/liquid nitrogen bath to -80 °C. The resulting yellow polymer was precipitated three times into a high excess of *n*-hexane and dried in high vacuum for three days. The polymeric product **m2C\_n16** was characterized via <sup>1</sup>H-NMR (Figure S3), matrix-assisted laser desorption/ionization mass spectrometry (MALDI-TOF MS) (Figure S12), size exclusion chromatography (SEC), and turbidimetry proving its chemical structure including the end-groups.

**Table S2** Summary of the synthesized polymers (Scheme 2). Molecular mass  $M_n$  of the polymers obtained via <sup>1</sup>H-NMR spectroscopy and PDI values obtained from RI signals of GPC in THF. The name of every sample comprises: m(1-9) - the number of ethylene glycol units in the side chain of the polymer; (C), (D), (B), (P) - the end group of the polymer; (n) followed by a number – the degree of polymerization. n/a:  $T_{cp}$  above 90 °C or no sufficient solubility at RT. As reference,  $A\beta_{1-40}$  in the absence of polymer showed values of  $t_{lag} = 3.25 \pm 0.12$  h and  $t_{char} = 3.83 \pm 0.1$  h. Mean values and corresponding standard deviations ( $\pm$ ) for  $t_{lag}$  and  $t_{char}$  obtained from three independent measurements using piecewise linear fits are given.

Entry	Name	m	End group	$M_n^{NMR}$ , g/mol	PDI	$T_{cp}$ , °C fib.buf	$T_{cp}$ , °C water	$t_{lag}$ , h	$t_{char}$ , h
1	m1C_n12	1	carboxy- (C)	1560	1.19	n/a	n/a	3.88±0.75	4.3±0.75
2	m1C_n32	1	carboxy- (C)	4200	1.16	42.4	<5	22.43±1.9	24.5±1.4
3	m1C_n53	1	carboxy- (C)	9200	1.12	n/a	n/a	-	-
4	m1D_n17	1	dodecyl- (D)	1900	1.1	n/a	n/a	-	-
5	m2C_n4	2	carboxy- (C)	700	1.25	n/a	n/a	3.48±0.49	4.6±0.5
6	m2C_n8	2	carboxy- (C)	1400	1.2	n/a	n/a	3.44±0.2	4±0.13
7	m2C_n16	2	carboxy- (C)	2800	1.15	n/a	n/a	2.78±0.06	3.6±0.1
8	m2C_n21	2	carboxy- (C)	3600	1.17	n/a	n/a	2.34±0.13	3.2±0.2
9	m2C_n32	2	carboxy- (C)	5600	1.14	80.4	75	1.6±0.19	2.5±0.1
10	m2C_n49	2	carboxy- (C)	8500	1.14	78	74.7	1.23±0.05	2.3±0.1
11	m2B_n19	2	butyl- (B)	3300	1.16	60.5	68.4	2.95±0.1	4.7±0.7
12	m2B_n27	2	butyl- (B)	4700	1.12	55.2	64.9	7.5±0.11	11±0.45
13	m2B_n36	2	butyl- (B)	6300	1.12	54.1	63.8	4.72±0.89	6.6±0.9
14	m2D_n16	2	dodecyl- (D)	2800	1.1	n/a	n/a	9.18±0.73	16±1.75
15	m2D_n23	2	dodecyl- (D)	4000	1.12	43.2	51.2	20.89±0.47	29.5±0.9
16	m2D_n56	2	dodecyl- (D)	9800	1.11	45	51.9	10.53±0.45	16.9±0.9
17	m2P_n18	2	pyridyldisulfide- (P)	3200	1.16	n/a	n/a	2.0±0.17	3.8±0.63
18	m2P_n38	2	pyridyldisulfide- (P)	6600	1.19	65.2	65.6	1.51±0.12	2.1±0.11
19	m2P_n50	2	pyridyldisulfide- (P)	8700	1.15	55.8	64.1	8.52±0.33	12.3±0.46
20	m3C_n10	3	carboxy- (C)	2180	1.18	n/a	n/a	3.59±0.52	4.1±0.7
21	m3C_n18	3	carboxy- (C)	3900	1.15	n/a	n/a	2.63±0.44	3.3±0.57
22	m3C_n35	3	carboxy- (C)	7600	1.21	n/a	n/a	3.09±0.26	3.6±0.1
23	m3C_n38	3	carboxy- (C)	8300	1.17	n/a	n/a	1.64±0.12	2.4±0.1
24	m3C_n47	3	carboxy- (C)	10250	1.17	n/a	n/a	3.38±0.38	4.2±0.39
25	m3P_n16	3	pyridyldisulfide- (P)	3500	1.14	n/a	n/a	3.48±0.24	4.3±0.36
26	m3B_n20	3	butyl- (B)	4360	1.11	n/a	n/a	2.08±0.28	2.8±0.2
27	m5C_n13	5	carboxy- (C)	4000	1.12	n/a	n/a	3.15±0.82	3.2±0.9



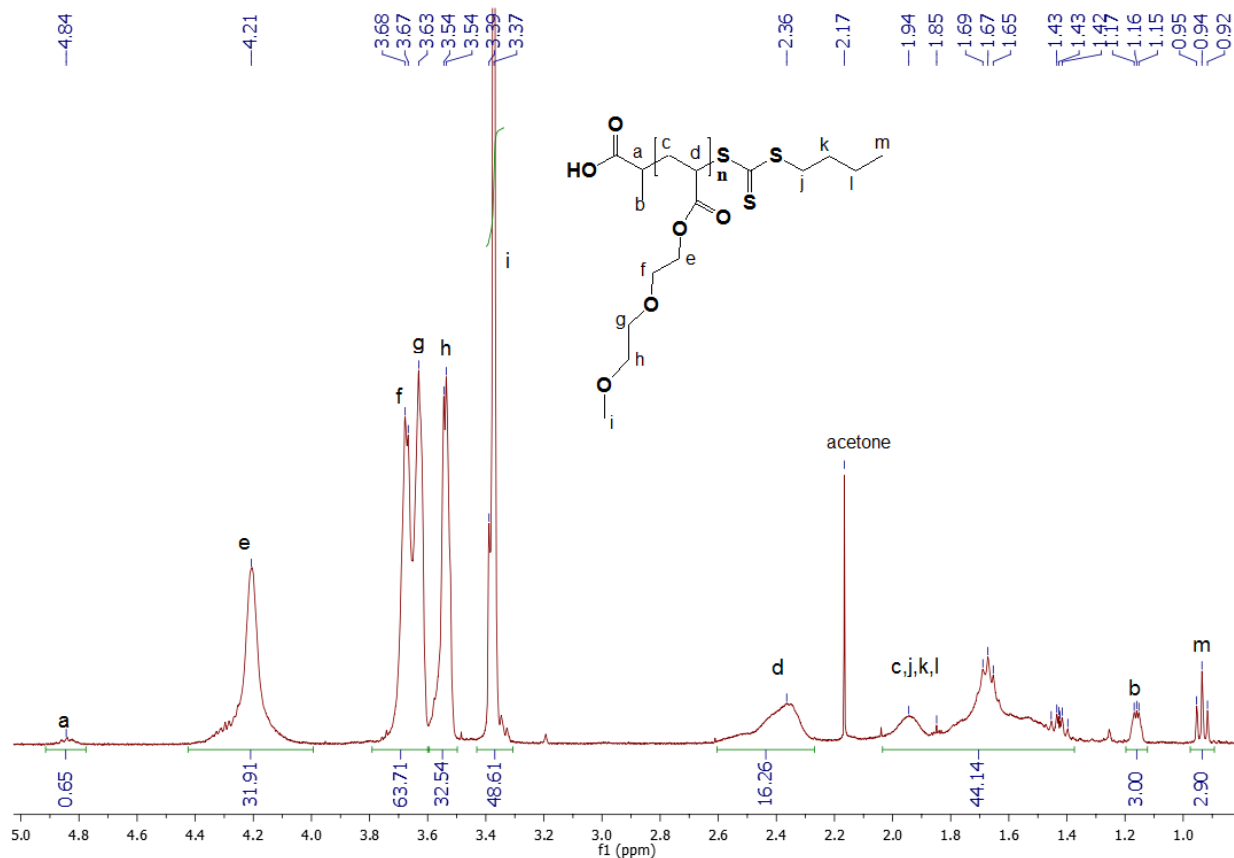


Figure S3.  $^1\text{H-NMR}$  spectrum of poly(methoxy di(ethylene glycol)acrylate) (m2C\_n16).

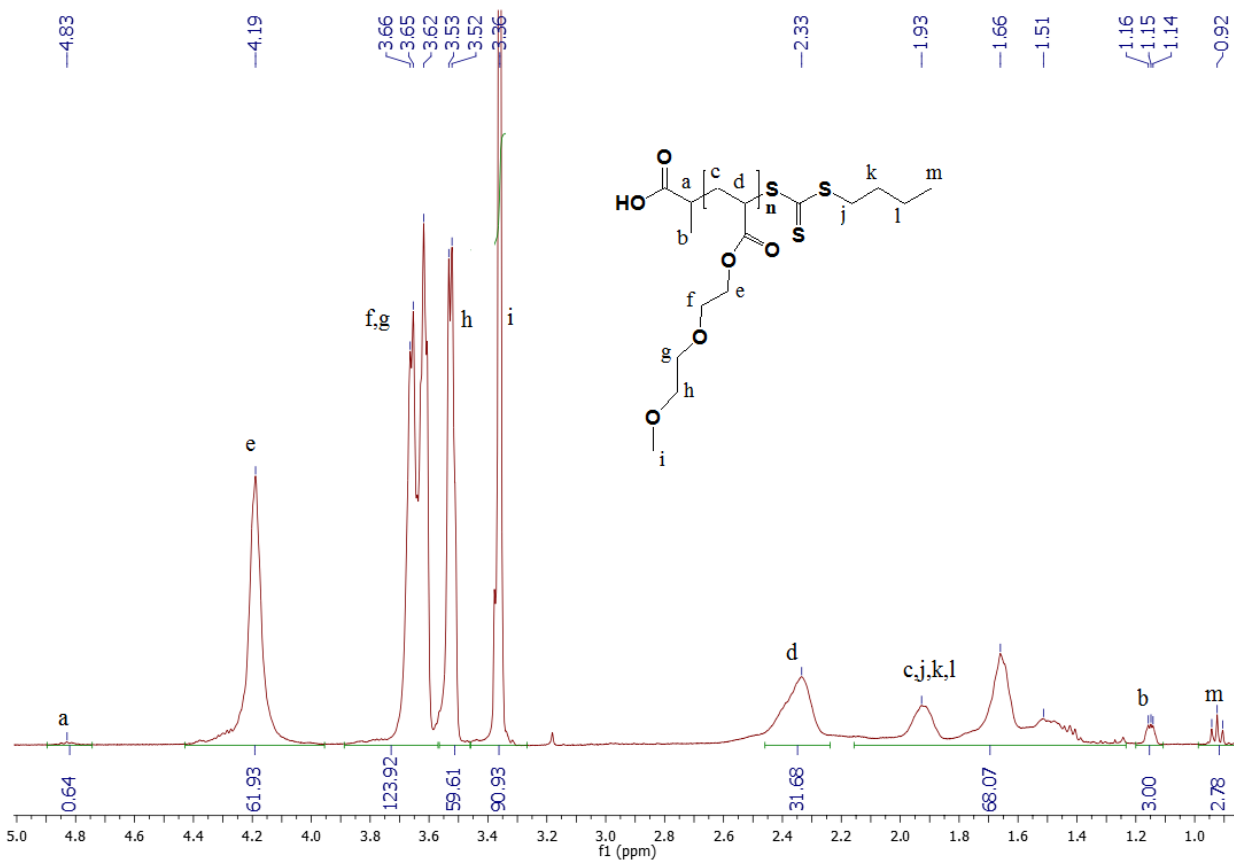


Figure S4.  $^1\text{H-NMR}$  spectrum of poly(methoxy di(ethylene glycol)acrylate) (m2C\_n32).

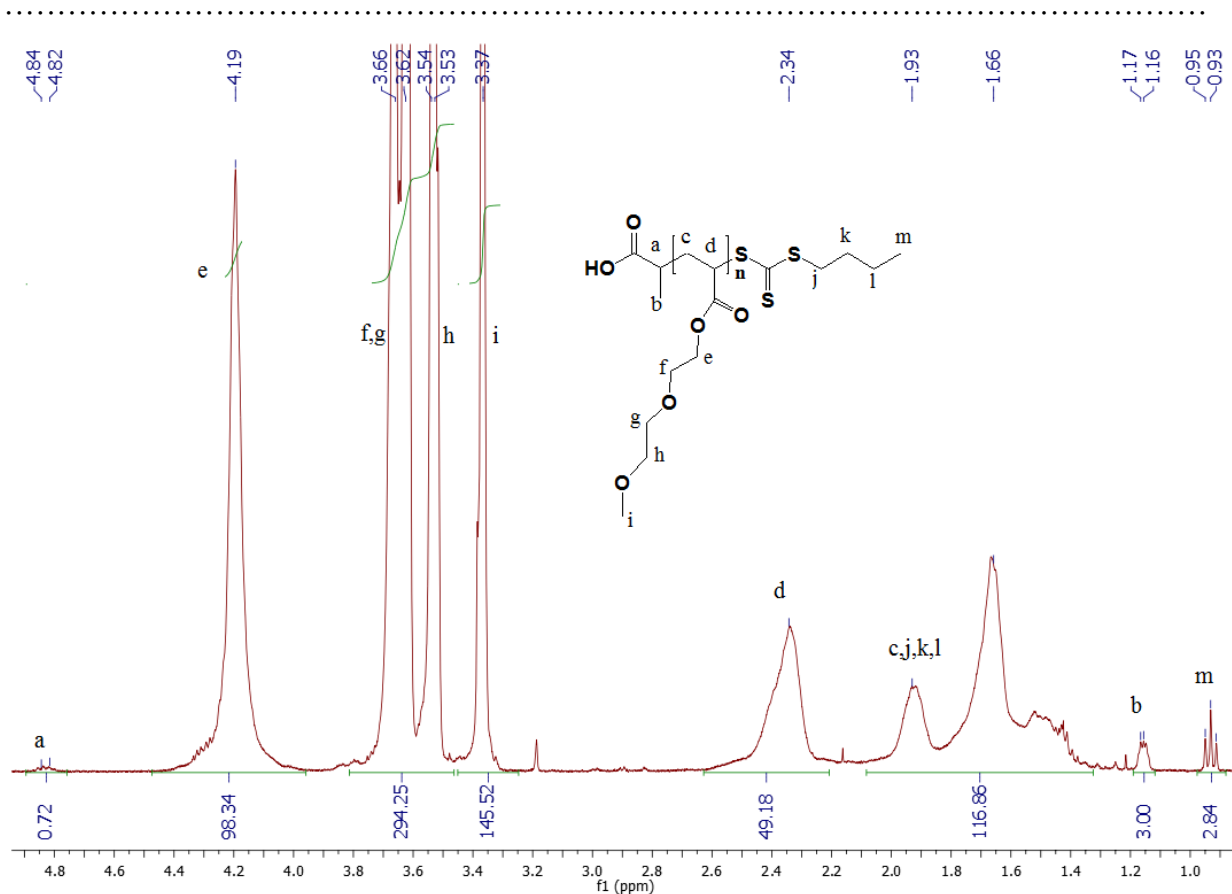


Figure S5.  $^1\text{H-NMR}$  spectrum of poly(methoxy di(ethylene glycol)acrylate) (**m2C<sub>n</sub>49**).

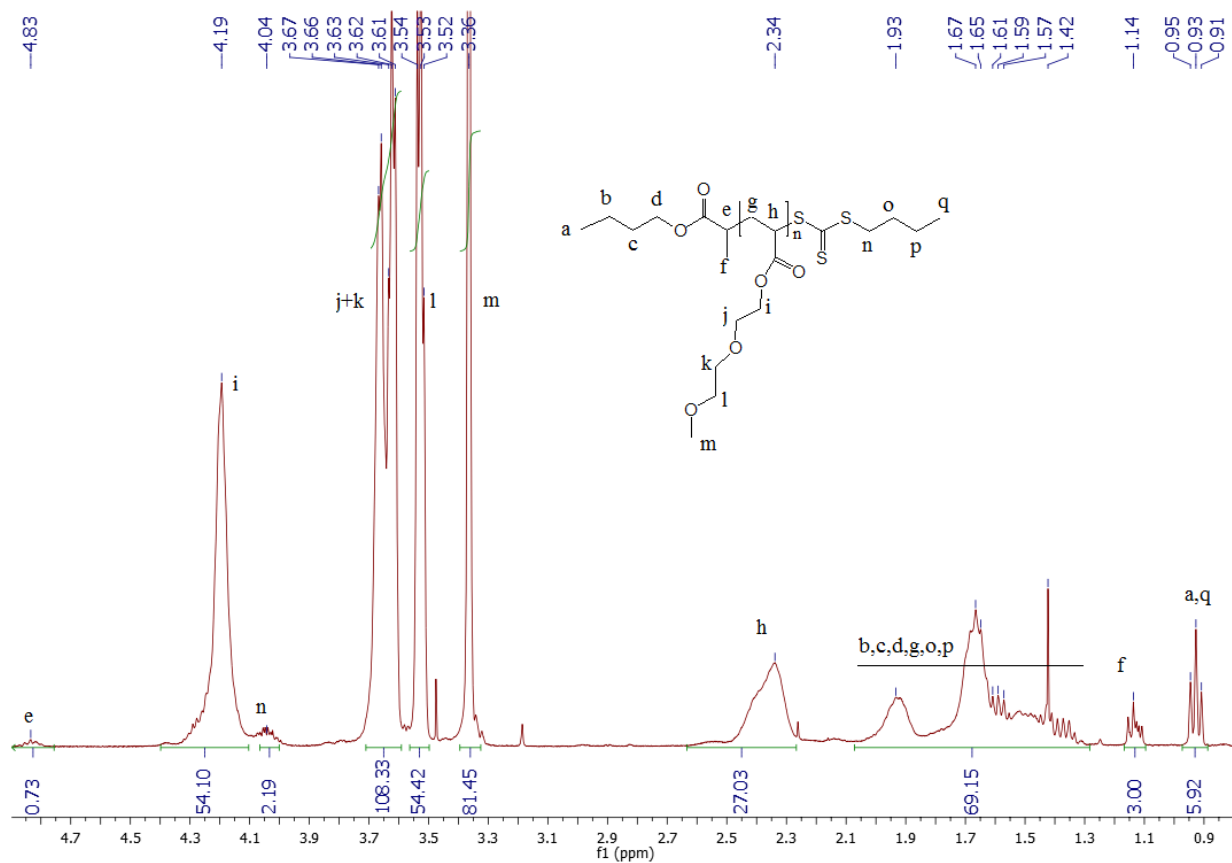


Figure S6.  $^1\text{H-NMR}$  spectrum of poly(methoxy di(ethylene glycol)acrylate) (**m2B<sub>n</sub>27**).

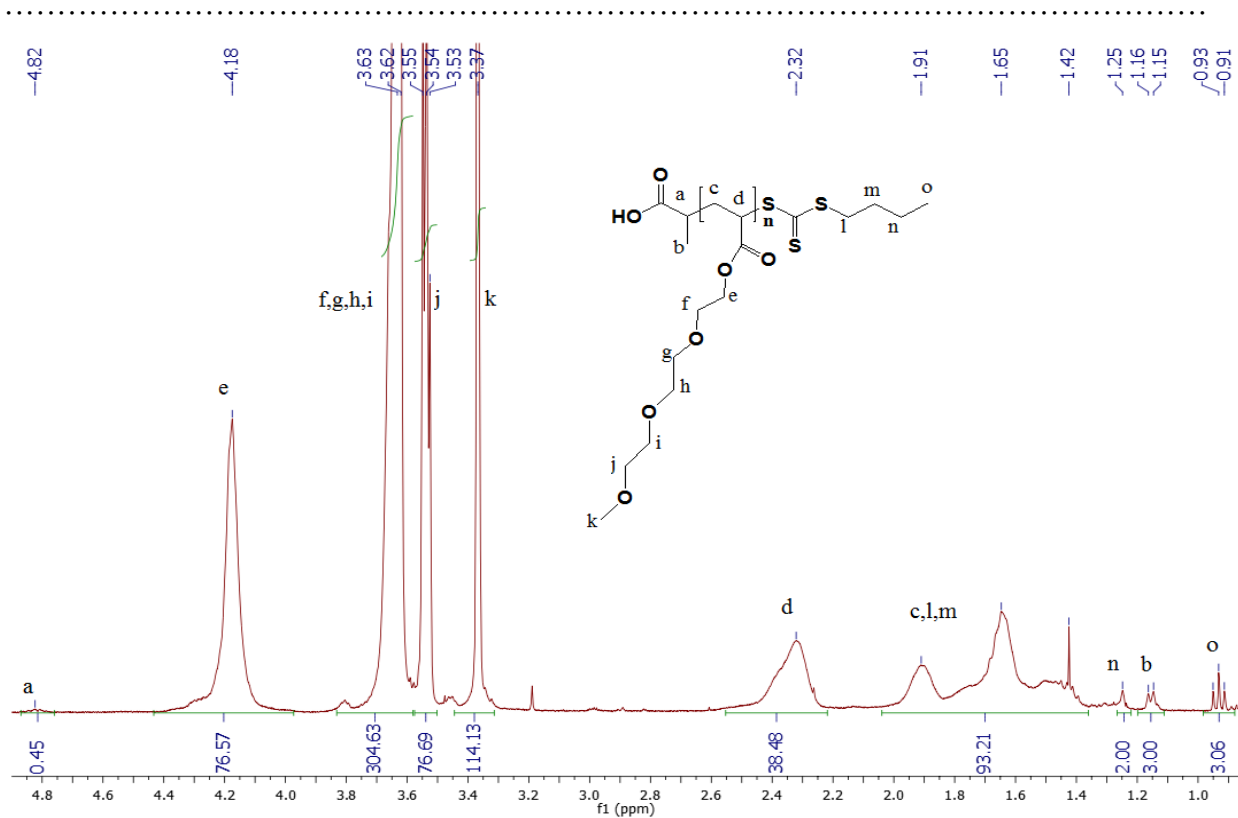


Figure S7.  $^1\text{H-NMR}$  spectrum of poly(methoxy tri(ethylene glycol)acrylate) (**m3C\_n38**).

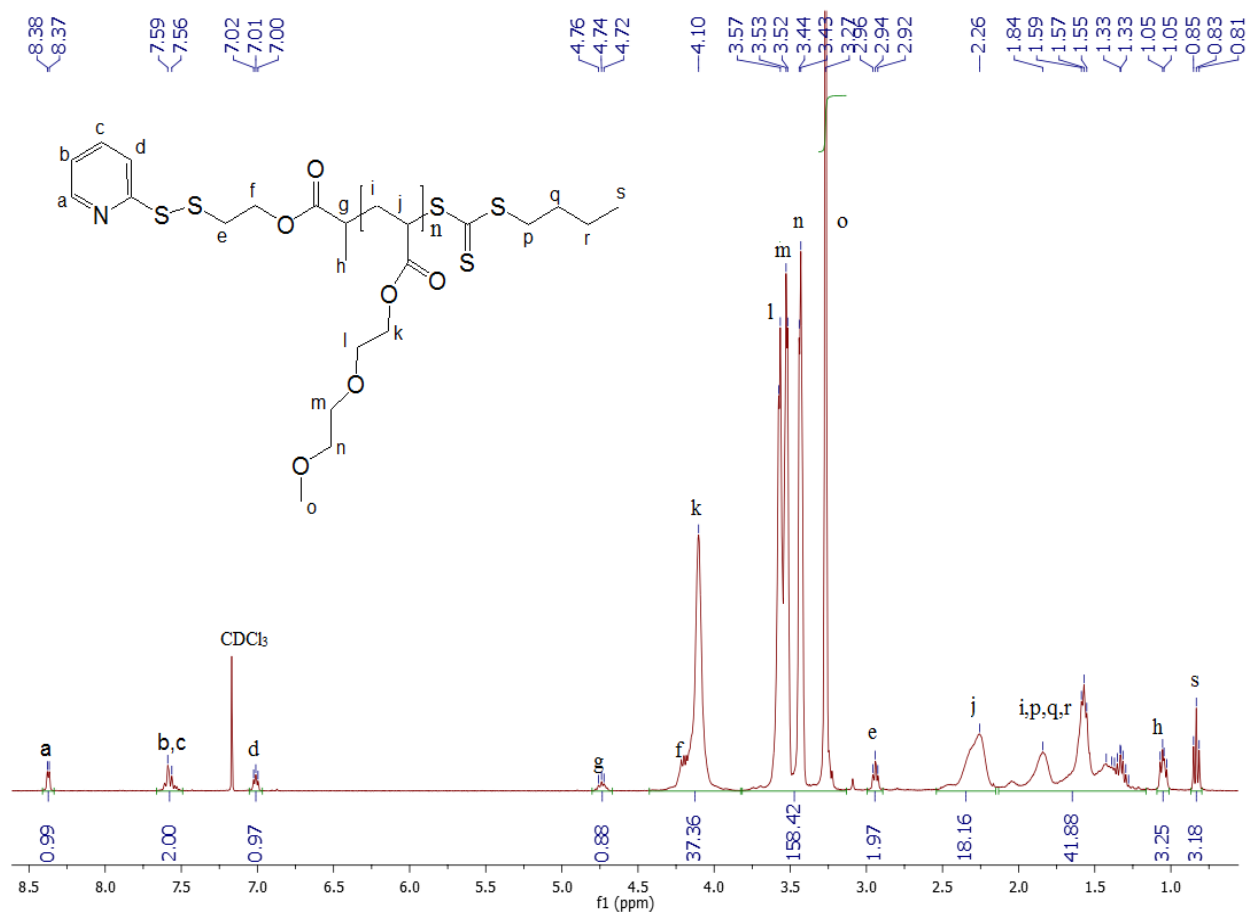


Figure S8.  $^1\text{H-NMR}$  spectrum of poly(methoxy di(ethylene glycol)acrylate) (**m2P\_n18**).

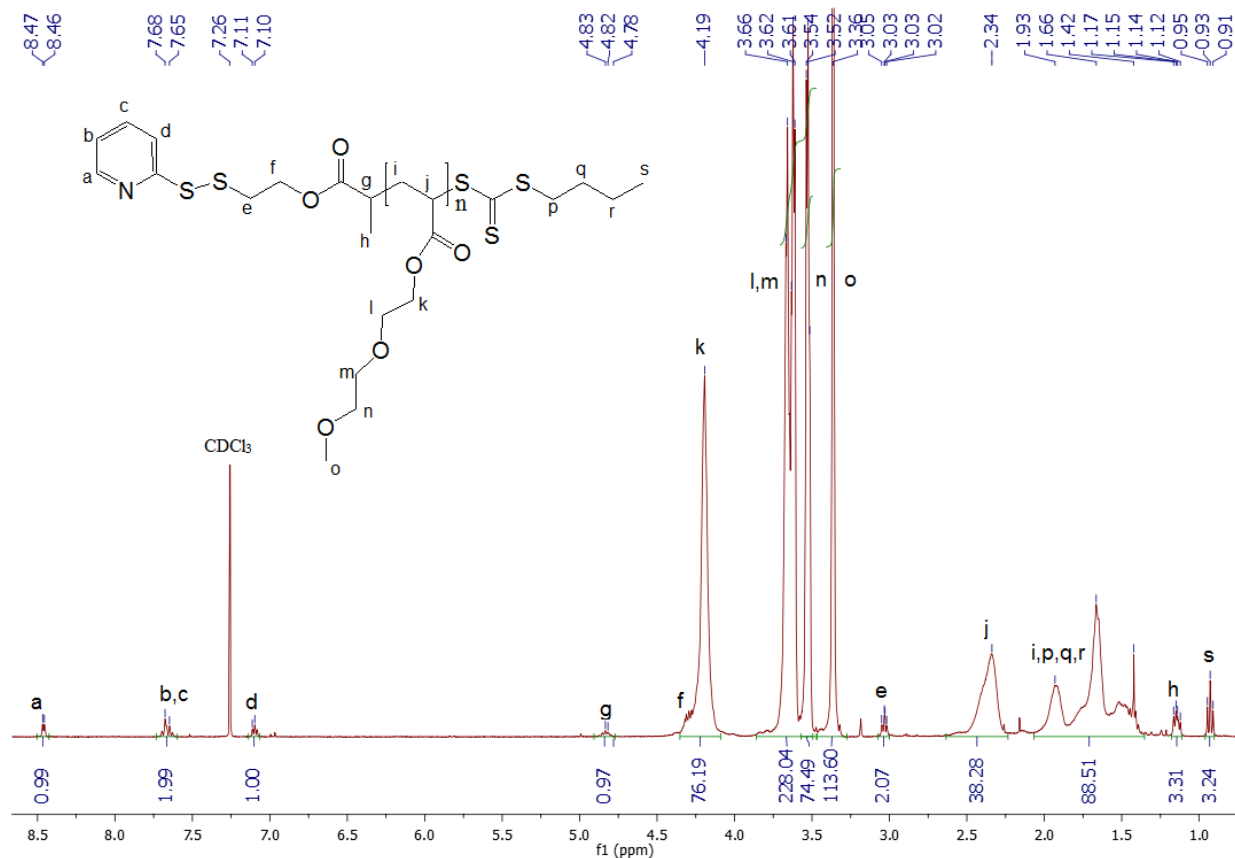


Figure S9. <sup>1</sup>H-NMR spectrum of poly(methoxy di(ethylene glycol)acrylate) (m2P\_n38).

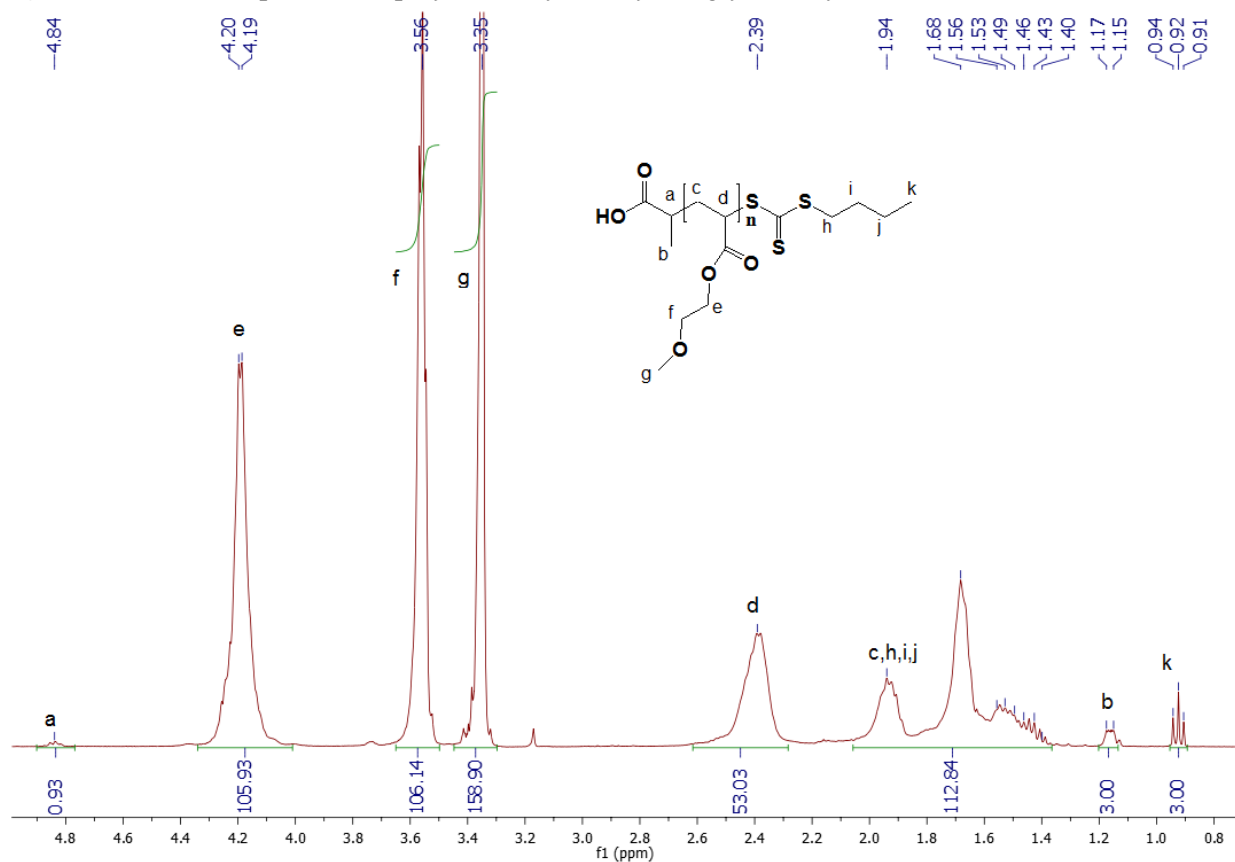
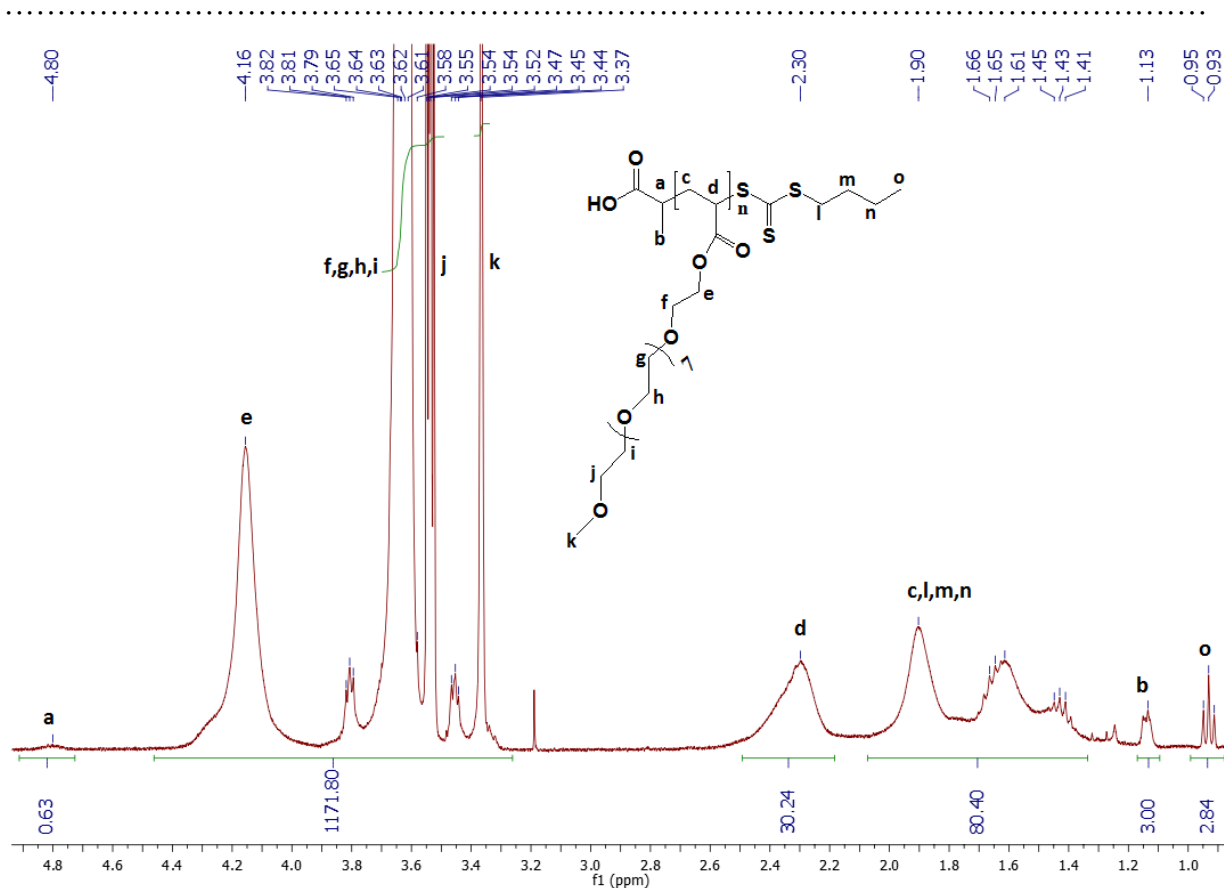


Figure S10. <sup>1</sup>H-NMR spectrum of poly(methoxy (ethylene glycol)acrylate) (m1C\_n53).



**Figure S11.**  $^1\text{H-NMR}$  spectrum of poly(methoxy nona(ethylene glycol)acrylate) (**m9C\_n30**).

**m2C\_n4:**  $^1\text{H-NMR}$  (400 MHz,  $\text{CDCl}_3$ ):  $\delta =$  ppm 4.86 (m,  $1\text{H}_a$ ,  $-\text{CHCH}_3$ ), 4.21 (bm,  $8\text{H}_e$ ,  $-\text{OCH}_2\text{CH}_2$ ), 3.64 (bm,  $16\text{H}_{f,g}$ ,  $-\text{OCH}_2\text{CH}_2\text{OCH}_2$ ), 3.54 (m,  $8\text{H}_h$ ,  $-\text{CH}_2\text{OCH}_3$ ), 3.38 (m,  $13\text{H}_{i,j}$ ,  $-\text{CH}_2\text{OCH}_3$ ;  $-\text{SCH}_2$ ), 2.49 (bs,  $4\text{H}_d$ ,  $-\text{CHCH}_2$ ), 1.67 (m,  $12\text{H}_{c,k,l}$ ,  $-\text{CHCH}_2$ ;  $-\text{SCH}_2\text{CH}_2\text{CH}_2$ ;  $\text{H}_2\text{O}$  from  $\text{CDCl}_3$ ), 1.17 (m,  $3\text{H}_b$ ,  $-\text{CHCH}_3$ ), 0.93 (t,  $3\text{H}_m$ ,  $-\text{CH}_2\text{CH}_3$ )

**m2C\_n8:**  $^1\text{H-NMR}$  (400 MHz,  $\text{CDCl}_3$ ):  $\delta =$  ppm 4.84 (m,  $1\text{H}_a$ ,  $-\text{CHCH}_3$ ), 4.21 (bm,  $16\text{H}_e$ ,  $-\text{OCH}_2\text{CH}_2$ ), 3.63 (bm,  $32\text{H}_{f,g}$ ,  $-\text{OCH}_2\text{CH}_2\text{OCH}_2$ ), 3.53 (m,  $16\text{H}_h$ ,  $-\text{CH}_2\text{OCH}_3$ ), 3.37 (m,  $26\text{H}_{i,j}$ ,  $-\text{CH}_2\text{OCH}_3$ ;  $-\text{SCH}_2$ ), 2.43 (bs,  $8\text{H}_d$ ,  $-\text{CHCH}_2$ ), 1.67 (m,  $20\text{H}_{c,k,l}$ ,  $-\text{CHCH}_2$ ;  $-\text{SCH}_2\text{CH}_2\text{CH}_2$ ), 1.16 (m,  $3\text{H}_b$ ,  $-\text{CHCH}_3$ ), 0.93 (t,  $3\text{H}_m$ ,  $-\text{CH}_2\text{CH}_3$ )

**m2C\_n16:**  $^1\text{H-NMR}$  (400 MHz,  $\text{CDCl}_3$ ):  $\delta =$  ppm 4.84 (m,  $1\text{H}_a$ ,  $-\text{CHCH}_3$ ), 4.21 (bm,  $32\text{H}_e$ ,  $-\text{OCH}_2\text{CH}_2$ ), 3.63 (bm,  $64\text{H}_{f,g}$ ,  $-\text{OCH}_2\text{CH}_2\text{OCH}_2$ ), 3.54 (m,  $32\text{H}_h$ ,  $-\text{CH}_2\text{OCH}_3$ ), 3.37 (m,  $48\text{H}_i$ ,  $-\text{CH}_2\text{OCH}_3$ ), 2.36 (bs,  $16\text{H}_d$ ,  $-\text{CHCH}_2$ ), 1.67 (m,  $38\text{H}_{c,j,k,l}$ ,  $-\text{CHCH}_2$ ;  $-\text{SCH}_2\text{CH}_2\text{CH}_2$ ;  $\text{H}_2\text{O}$  from  $\text{CDCl}_3$ ), 1.16 (m,  $3\text{H}_b$ ,  $-\text{CHCH}_3$ ), 0.94 (t,  $3\text{H}_m$ ,  $-\text{CH}_2\text{CH}_3$ )

**m2C\_n32:**  $^1\text{H-NMR}$  (400 MHz,  $\text{CDCl}_3$ ):  $\delta =$  ppm 4.83 (m,  $1\text{H}_a$ ,  $-\text{CHCH}_3$ ), 4.19 (bm,  $62\text{H}_e$ ,  $-\text{OCH}_2\text{CH}_2$ ), 3.62 (bm,  $124\text{H}_{f,g}$ ,  $-\text{OCH}_2\text{CH}_2\text{OCH}_2$ ), 3.52 (m,  $62\text{H}_h$ ,  $-\text{CH}_2\text{OCH}_3$ ), 3.36 (m,  $93\text{H}_i$ ,  $-\text{CH}_2\text{OCH}_3$ ), 2.33 (bs,  $31\text{H}_d$ ,  $-\text{CHCH}_2$ ), 1.66 (m,  $68\text{H}_{c,j,k,l}$ ,  $-\text{CHCH}_2$ ;  $-\text{SCH}_2\text{CH}_2\text{CH}_2$ ), 1.15 (m,  $3\text{H}_b$ ,  $-\text{CHCH}_3$ ), 0.92 (t,  $3\text{H}_m$ ,  $-\text{CH}_2\text{CH}_3$ )

**m2C\_n49:**  $^1\text{H-NMR}$  (400 MHz,  $\text{CDCl}_3$ ):  $\delta =$  ppm 4.84 (m,  $1\text{H}_a$ ,  $-\text{CHCH}_3$ ), 4.19 (bm,  $98\text{H}_e$ ,  $-\text{OCH}_2\text{CH}_2$ ), 3.62 (bm,  $196\text{H}_{f,g}$ ,  $-\text{OCH}_2\text{CH}_2\text{OCH}_2$ ), 3.53 (m,  $98\text{H}_h$ ,  $-\text{CH}_2\text{OCH}_3$ ), 3.37 (m,  $147\text{H}_i$ ,  $-\text{CH}_2\text{OCH}_3$ ), 2.34 (bs,  $49\text{H}_d$ ,  $-\text{CHCH}_2$ ), 1.66 (m,  $38\text{H}_{c,j,k,l}$ ,  $-\text{CHCH}_2$ ;  $-\text{SCH}_2\text{CH}_2\text{CH}_2$ ;  $\text{H}_2\text{O}$  from  $\text{CDCl}_3$ ), 1.16 (m,  $3\text{H}_b$ ,  $-\text{CHCH}_3$ ), 0.93 (t,  $3\text{H}_m$ ,  $-\text{CH}_2\text{CH}_3$ )

.....  
**m2B\_n27:**  $^1\text{H-NMR}$  (400 MHz,  $\text{CDCl}_3$ ):  $\delta =$  ppm 4.83 (m,  $1\text{H}_e$ ,  $-\text{CHCH}_3$ ), 4.19 (bs,  $54\text{H}_i$ ,  $-\text{OCH}_2\text{CH}_2$ ), 4.19 (m,  $2\text{H}_n$ ,  $-\text{SCH}_2$ ), 3.62 (bm,  $108\text{H}_{j,k}$ ,  $-\text{OCH}_2\text{CH}_2\text{OCH}_2$ ), 3.53 (m,  $54\text{H}_l$ ,  $-\text{CH}_2\text{OCH}_3$ ), 3.36 (s,  $81\text{H}_m$ ,  $-\text{CH}_2\text{OCH}_3$ ), 2.34 (bs,  $27\text{H}_h$ ,  $-\text{CH}_2\text{CH}$ ), 1.67 (m,  $64\text{H}_{b,c,d,g,o,p}$ ,  $-\text{OCH}_2\text{CH}_2\text{CH}_2\text{CH}_3$ ;  $-\text{CH}_2\text{CH}$ ;  $-\text{SCH}_2\text{CH}_2\text{CH}_2$ ;  $-\text{CH}_2\text{CH}_3$ ;  $\text{H}_2\text{O}$  from  $\text{CDCl}_3$ ), 1.14 (m,  $3\text{H}_f$ ,  $-\text{CHCH}_3$ ), 0.93 (t,  $6\text{H}_{a,q}$ ,  $-\text{CH}_2\text{CH}_3$ )

**m3C\_n38:**  $^1\text{H-NMR}$  (400 MHz,  $\text{CDCl}_3$ ):  $\delta =$  ppm 4.82 (m,  $1\text{H}_a$ ,  $-\text{CHCH}_3$ ), 4.18 (bm,  $76\text{H}_e$ ,  $-\text{OCH}_2\text{CH}_2$ ), 3.63 (bm,  $304\text{H}_{f,g,h,i}$ ,  $-\text{CH}_2\text{OCH}_2\text{CH}_2\text{OCH}_2$ ), 3.54 (m,  $76\text{H}_j$ ,  $-\text{CH}_2\text{OCH}_3$ ), 3.37 (m,  $114\text{H}_k$ ,  $-\text{CH}_2\text{OCH}_3$ ), 2.32 (bs,  $38\text{H}_d$ ,  $-\text{CHCH}_2$ ), 1.65 (m,  $80\text{H}_{c,l,m}$ ,  $-\text{CHCH}_2$ ;  $-\text{SCH}_2\text{CH}_2$ ;  $\text{H}_2\text{O}$  from  $\text{CDCl}_3$ ), 1.25 (m,  $2\text{H}_j$ ,  $-\text{CH}_2\text{CH}_3$ ); 1.15 (m,  $3\text{H}_b$ ,  $-\text{CHCH}_3$ ), 0.93 (t,  $3\text{H}_m$ ,  $-\text{CH}_2\text{CH}_3$ )

**m2P\_n18:**  $^1\text{H-NMR}$  (400 MHz,  $\text{CDCl}_3$ ):  $\delta =$  ppm 8.38 (d,  $1\text{H}_a$ ,  $-\text{NCH}$ ), 7.59 (m,  $2\text{H}_{b,c}$ ,  $-\text{NCHCHCH}$ ), 7.01 (m,  $1\text{H}_d$ ,  $-\text{NCCH}$ ), 4.74 (m,  $1\text{H}_g$ ,  $-\text{CHCH}_3$ ), 4.10 (bm,  $38\text{H}_{f,k}$ ,  $-\text{CH}_2\text{OCO}$ ;  $-\text{OCH}_2\text{CH}_2$ ), 3.53 (bm,  $72\text{H}_{l,m}$ ,  $-\text{OCH}_2\text{CH}_2\text{OCH}_2$ ), 3.43 (bm,  $36\text{H}_n$ ,  $-\text{CH}_2\text{OCH}_3$ ), 3.27 (bs,  $54\text{H}_o$ ,  $-\text{CH}_2\text{OCH}_3$ ), 2.94 (t,  $2\text{H}_e$ ,  $-\text{SSCH}_2$ ), 2.26 (bs,  $18\text{H}_j$ ,  $-\text{CHCH}_2$ ), 1.57 (m,  $42\text{H}_{i,p,q,r}$ ,  $-\text{CHCH}_2$ ;  $-\text{SCSCH}_2\text{CH}_2\text{CH}_2\text{CH}_3$ ), 1.05 (m,  $3\text{H}_h$ ,  $-\text{CHCH}_3$ ), 0.83 (t,  $3\text{H}_s$ ,  $-\text{CH}_2\text{CH}_3$ )

**m2P\_n38:**  $^1\text{H-NMR}$  (400 MHz,  $\text{CDCl}_3$ ):  $\delta =$  ppm 8.47 (d,  $1\text{H}_a$ ,  $-\text{NCH}$ ), 7.68 (m,  $2\text{H}_{b,c}$ ,  $-\text{NCHCHCH}$ ), 7.10 (m,  $1\text{H}_d$ ,  $-\text{NCCH}$ ), 4.82 (m,  $1\text{H}_g$ ,  $-\text{CHCH}_3$ ), 4.19 (bm,  $76\text{H}_k$ ,  $-\text{CHCH}_3$ ), 3.62 (m,  $152\text{H}_{l,m}$ ,  $-\text{OCH}_2\text{CH}_2\text{OCH}_2$ ), 3.52 (m,  $76\text{H}_n$ ,  $-\text{CH}_2\text{OCH}_3$ ), 3.36 (bs,  $114\text{H}_o$ ,  $-\text{CH}_2\text{OCH}_3$ ), 3.03 (m,  $2\text{H}_e$ ,  $-\text{SSCH}_2$ ), 2.34 (bs,  $38\text{H}_j$ ,  $-\text{CHCH}_2$ ), 1.66 (m,  $82\text{H}_{i,p,q,r}$ ,  $-\text{CHCH}_2$ ;  $-\text{SCSCH}_2\text{CH}_2\text{CH}_2$ ;  $\text{H}_2\text{O}$  from  $\text{CDCl}_3$ ), 1.15 (m,  $3\text{H}_h$ ,  $-\text{CHCH}_3$ ), 0.93 (t,  $3\text{H}_s$ ,  $-\text{CH}_2\text{CH}_3$ )

**m2P\_n50:**  $^1\text{H-NMR}$  (400 MHz,  $\text{CDCl}_3$ ):  $\delta =$  ppm 8.60 (d,  $1\text{H}_a$ ,  $-\text{NCH}$ ), 7.93 (m,  $2\text{H}_{b,c}$ ,  $-\text{NCHCHCH}$ ), 7.35 (m,  $1\text{H}_d$ ,  $-\text{NCCH}$ ), 4.83 (m,  $1\text{H}_g$ ,  $-\text{CHCH}_3$ ), 4.19 (bs,  $102\text{H}_{f,k}$ ,  $-\text{CH}_2\text{OCO}$ ;  $-\text{OCH}_2\text{CH}_2$ ), 3.65 (m,  $202\text{H}_{l,m,p}$ ,  $-\text{OCH}_2\text{CH}_2\text{OCH}_2$ ;  $-\text{SCH}_2$ ), 3.52 (m,  $100\text{H}_n$ ,  $-\text{CH}_2\text{OCH}_3$ ), 3.36 (s,  $150\text{H}_o$ ,  $-\text{CH}_2\text{OCH}_3$ ), 3.12 (m,  $2\text{H}_e$ ,  $-\text{SSCH}_2$ ), 2.33 (bs,  $50\text{H}_j$ ,  $-\text{CHCH}_2$ ), 1.65 (m,  $104\text{H}_{i,q,r}$ ,  $-\text{CHCH}_2$ ;  $-\text{SCSCH}_2\text{CH}_2$ ;  $-\text{CH}_2\text{CH}_3$ ;  $\text{H}_2\text{O}$  from  $\text{CDCl}_3$ ), 1.15 (m,  $3\text{H}_h$ ,  $-\text{CHCH}_3$ ), 0.93 (t,  $3\text{H}_s$ ,  $-\text{CH}_2\text{CH}_3$ )

**m1C\_n53:**  $^1\text{H-NMR}$  (400 MHz,  $\text{CDCl}_3$ ):  $\delta =$  ppm 4.84 (m,  $1\text{H}_a$ ,  $-\text{CHCH}_3$ ), 4.19 (bm,  $106\text{H}_e$ ,  $-\text{OCH}_2\text{CH}_2$ ), 3.56 (m,  $106\text{H}_f$ ,  $-\text{CH}_2\text{OCH}_3$ ), 3.35 (bs,  $159\text{H}_g$ ,  $-\text{CH}_2\text{OCH}_3$ ), 2.39 (bs,  $53\text{H}_d$ ,  $-\text{CHCH}_2$ ), 1.68 (m,  $112\text{H}_{c,h,i,j}$ ,  $-\text{CHCH}_2$ ;  $-\text{SCH}_2\text{CH}_2\text{CH}_2$ ), 1.17 (m,  $3\text{H}_b$ ,  $-\text{CHCH}_3$ ), 0.92 (t,  $3\text{H}_k$ ,  $-\text{CH}_2\text{CH}_3$ )

**m9C\_n14:**  $^1\text{H-NMR}$  (400 MHz,  $\text{CDCl}_3$ ):  $\delta =$  ppm 4.82 (m,  $1\text{H}_a$ ,  $-\text{CHCH}_3$ ), 4.17 (bs,  $28\text{H}_e$ ,  $-\text{OCH}_2\text{CH}_2$ ), 3.63 (bm,  $476\text{H}_{f,g,h,i}$ ,  $-\text{CH}_2\text{OCH}_2\text{CH}_2\text{OCH}_2$ ), 3.55 (m,  $28\text{H}_j$ ,  $-\text{CH}_2\text{OCH}_3$ ), 3.36 (m,  $42\text{H}_k$ ,  $-\text{CH}_2\text{OCH}_3$ ), 2.32 (bs,  $14\text{H}_d$ ,  $-\text{CHCH}_2$ ), 1.66 (m,  $64\text{H}_{c,l,m,n}$ ,  $-\text{CHCH}_2$ ;  $-\text{SCH}_2\text{CH}_2\text{CH}_2$ ;  $\text{H}_2\text{O}$  from  $\text{CDCl}_3$ ), 1.13 (m,  $3\text{H}_b$ ,  $-\text{CHCH}_3$ ), 0.93 (t,  $3\text{H}_o$ ,  $-\text{CH}_2\text{CH}_3$ )

**m9C\_n30:**  $^1\text{H-NMR}$  (400 MHz,  $\text{CDCl}_3$ ):  $\delta =$  ppm 4.80 (m,  $1\text{H}_a$ ,  $-\text{CHCH}_3$ ), 4.16 (bs,  $62\text{H}_{e,l}$ ,  $-\text{OCH}_2\text{CH}_2$ ;  $-\text{SCSCH}_2$ ), 3.63 (bm,  $960\text{H}_{f,g,h,i}$ ,  $-\text{CH}_2\text{OCH}_2\text{CH}_2\text{OCH}_2$ ), 3.54 (m,  $60\text{H}_j$ ,  $-\text{CH}_2\text{OCH}_3$ ), 3.37 (m,  $90\text{H}_k$ ,  $-\text{CH}_2\text{OCH}_3$ ), 2.30 (bs,  $30\text{H}_d$ ,  $-\text{CHCH}_2$ ), 1.67 (m,  $64\text{H}_{c,m,n}$ ,  $-\text{CHCH}_2$ ;  $-\text{SCH}_2\text{CH}_2$ ;  $\text{H}_2\text{O}$  from  $\text{CDCl}_3$ ), 1.13 (m,  $3\text{H}_b$ ,  $-\text{CHCH}_3$ ), 0.93 (t,  $3\text{H}_o$ ,  $-\text{CH}_2\text{CH}_3$ )

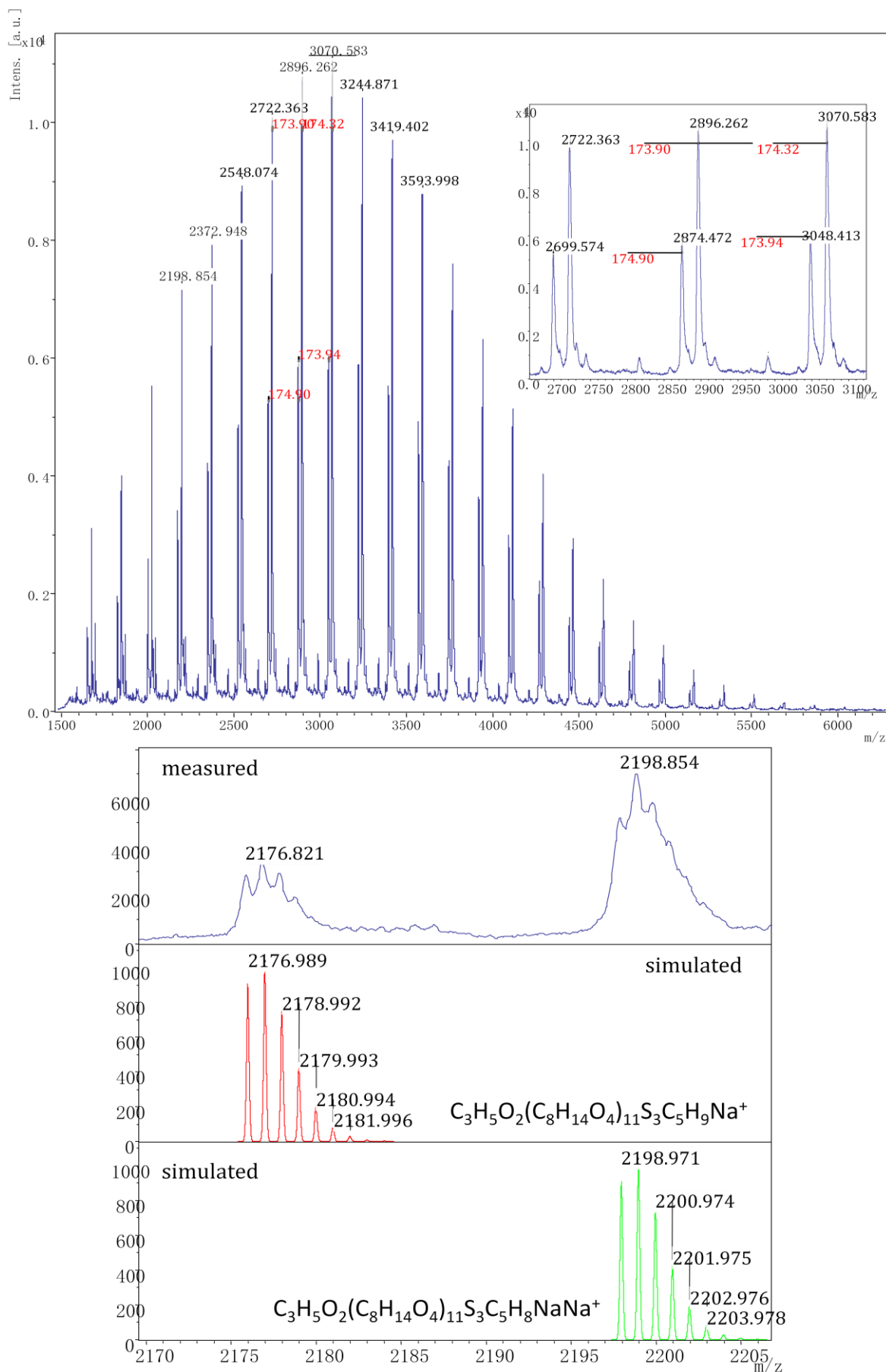


**Figure S12.** MALDI-TOF spectrum of poly(methoxy di(ethylene glycol)acrylate) (m2C\_n16).

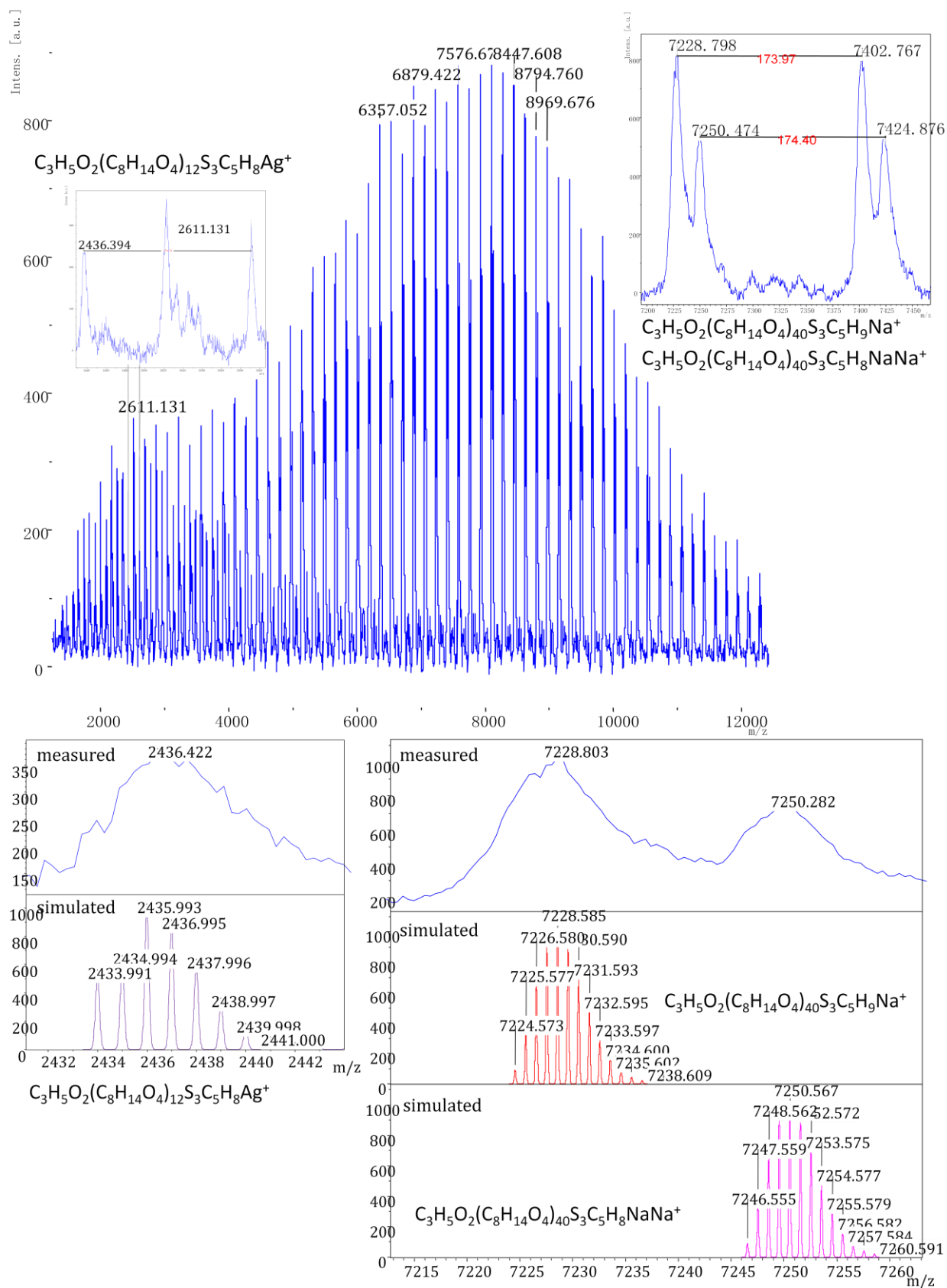
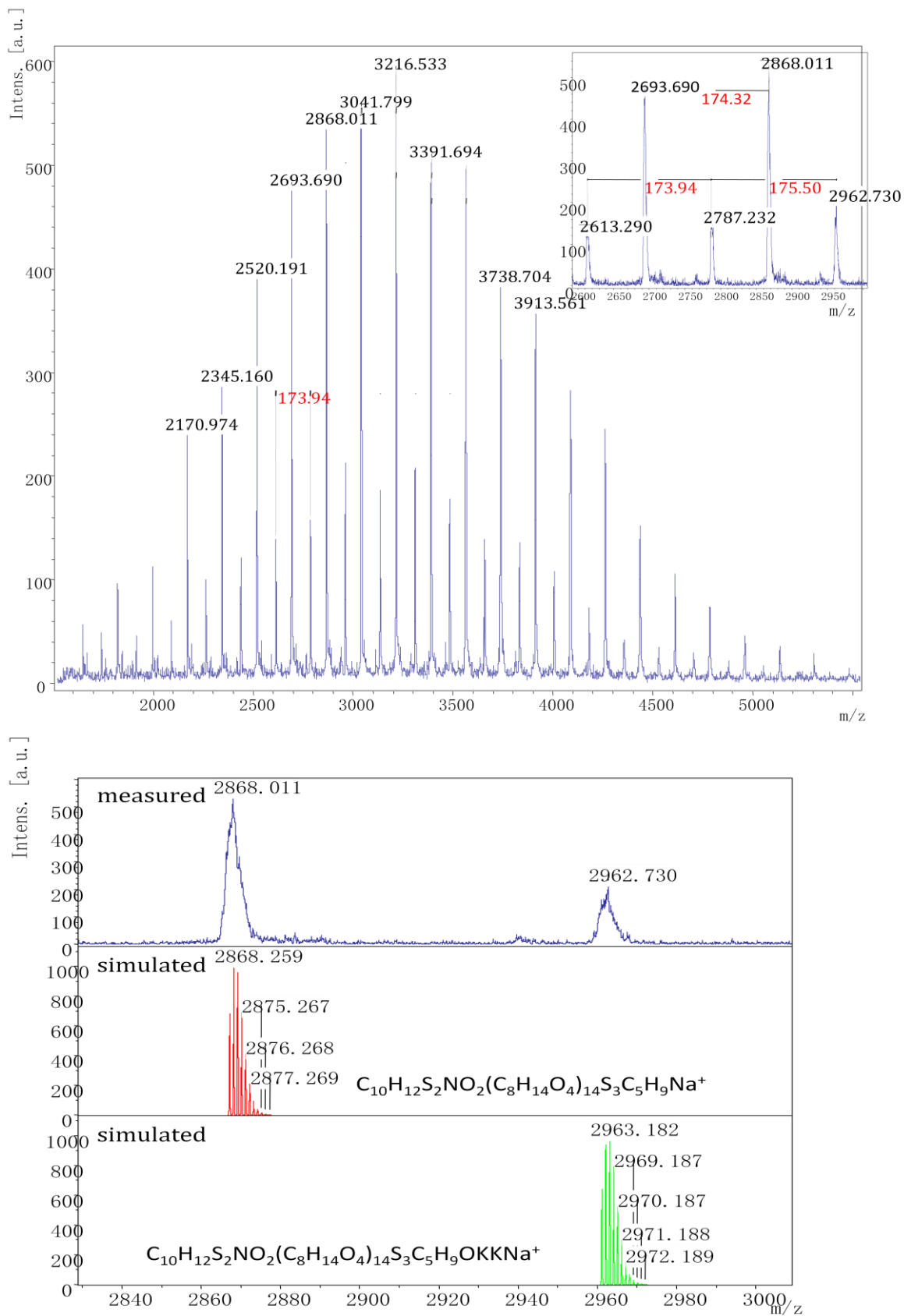
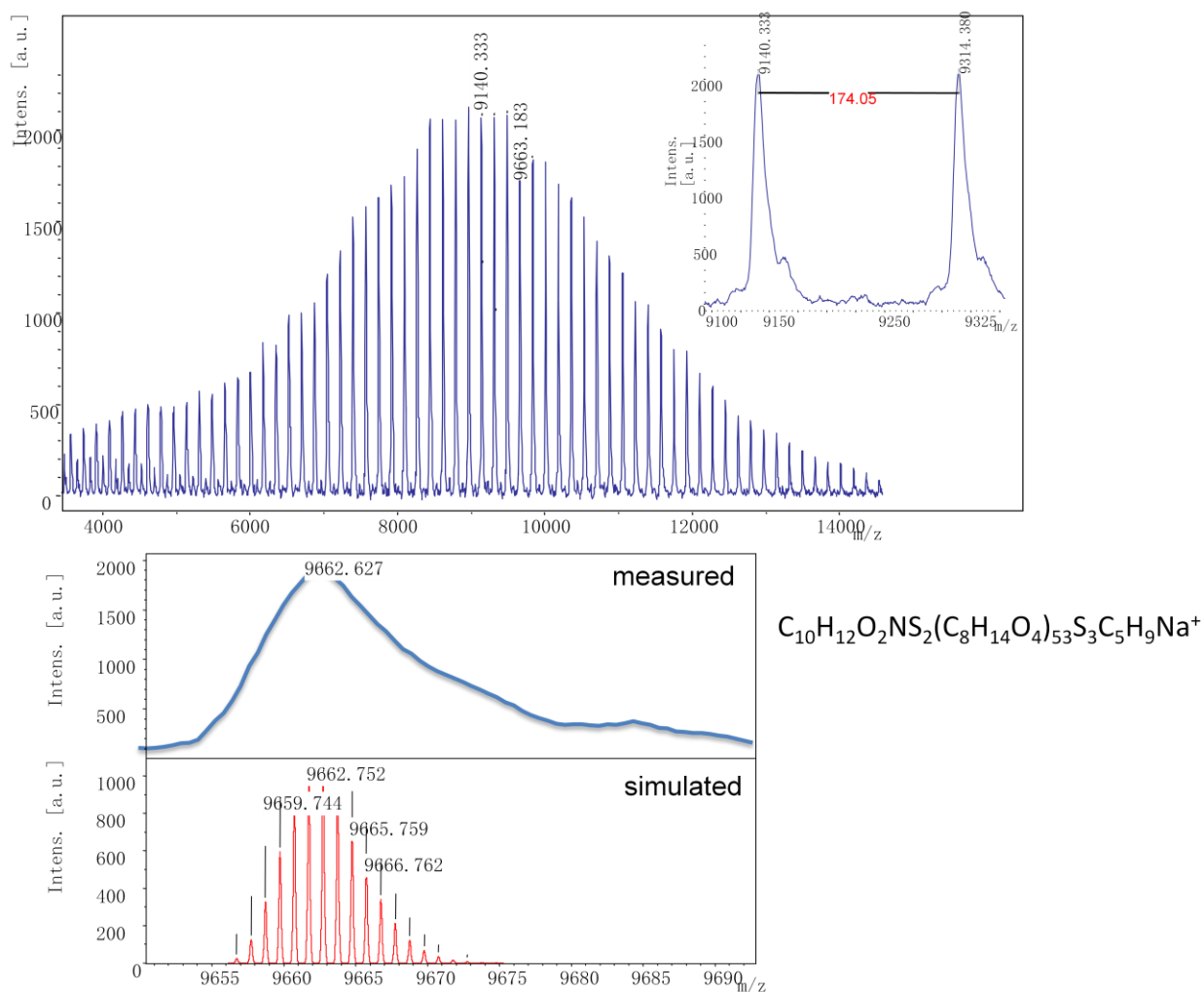


Figure S13. MALDI-TOF spectrum of poly(methoxy di(ethylene glycol)acrylate) (**m2C<sub>n</sub>49**).



**Figure S14.** MALDI-TOF spectrum of poly(methoxy di(ethylene glycol)acrylate) (m2P\_n18).



**Figure S15.** MALDI-TOF spectrum of poly(methoxy di(ethylene glycol)acrylate) (**m2P\_n50**).

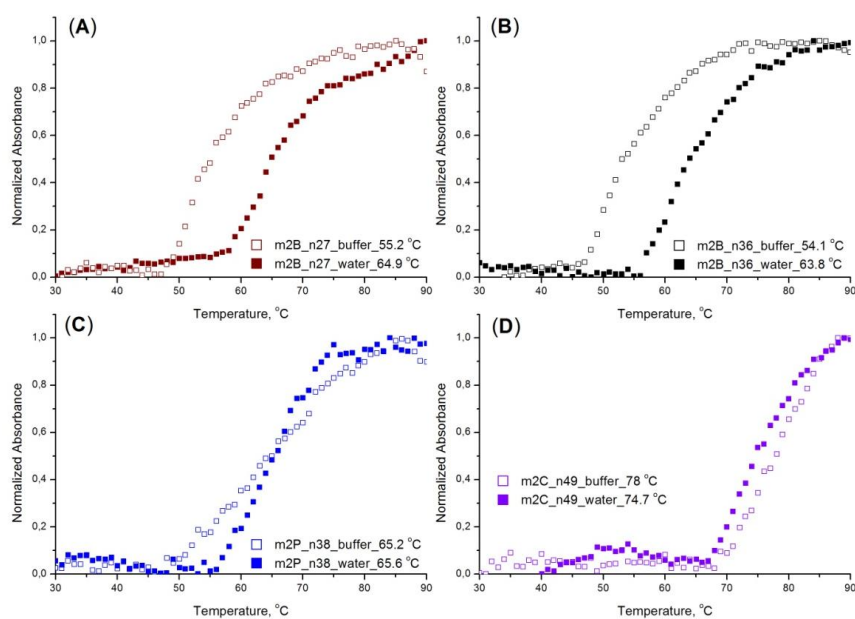


**Figure S16.** LCST ( $T_{cp}$ ) measurements for the polymers (A) **m2B\_n27**, (B) **m2B\_n36**, (C) **m2P\_n38**, (D) **m2C\_n49** either as 10  $\mu$ M solution in a 50 mM  $Na_2HPO_4$  buffer (pH 7.4) supplemented with 150 mM NaCl or as 10  $\mu$ M solution in water.

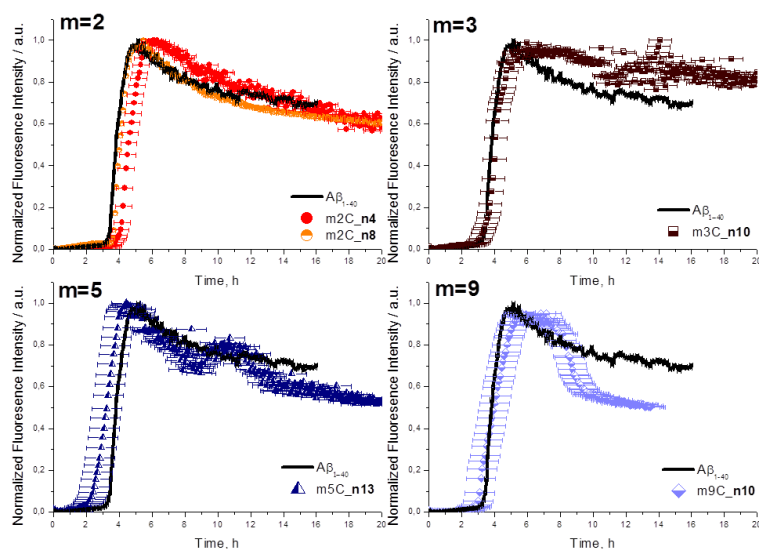


**Figure S17.** Time evolution of the ThT fluorescence intensity of the poly(oligo(ethylene glycol)<sub>m</sub> acrylates) /  $A\beta_{1-40}$  mixtures at  $\lambda = 480$  nm. Black solid line corresponds to  $A\beta_{1-40}$  wild type. The hydrophilicity is varied by the number of ethylene glycol units (m). Degree of polymerization (n) is indicated for every sample and highlighted in bold. Error bars based on three independent measurements are shown.

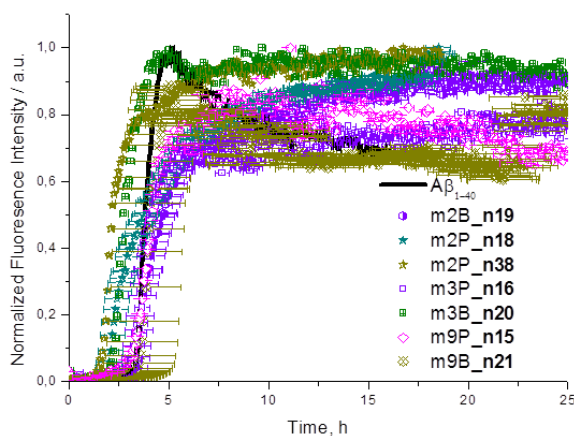


**Figure S18.** Effect of the polymer's end-group on the  $t_{lag}$  and  $t_{char}$  of the  $A\beta_{1-40}$  fibrillation demonstrated as a time evolution of the ThT fluorescence intensity at  $\lambda = 480$  nm. Error bars based on three independent measurements are shown.

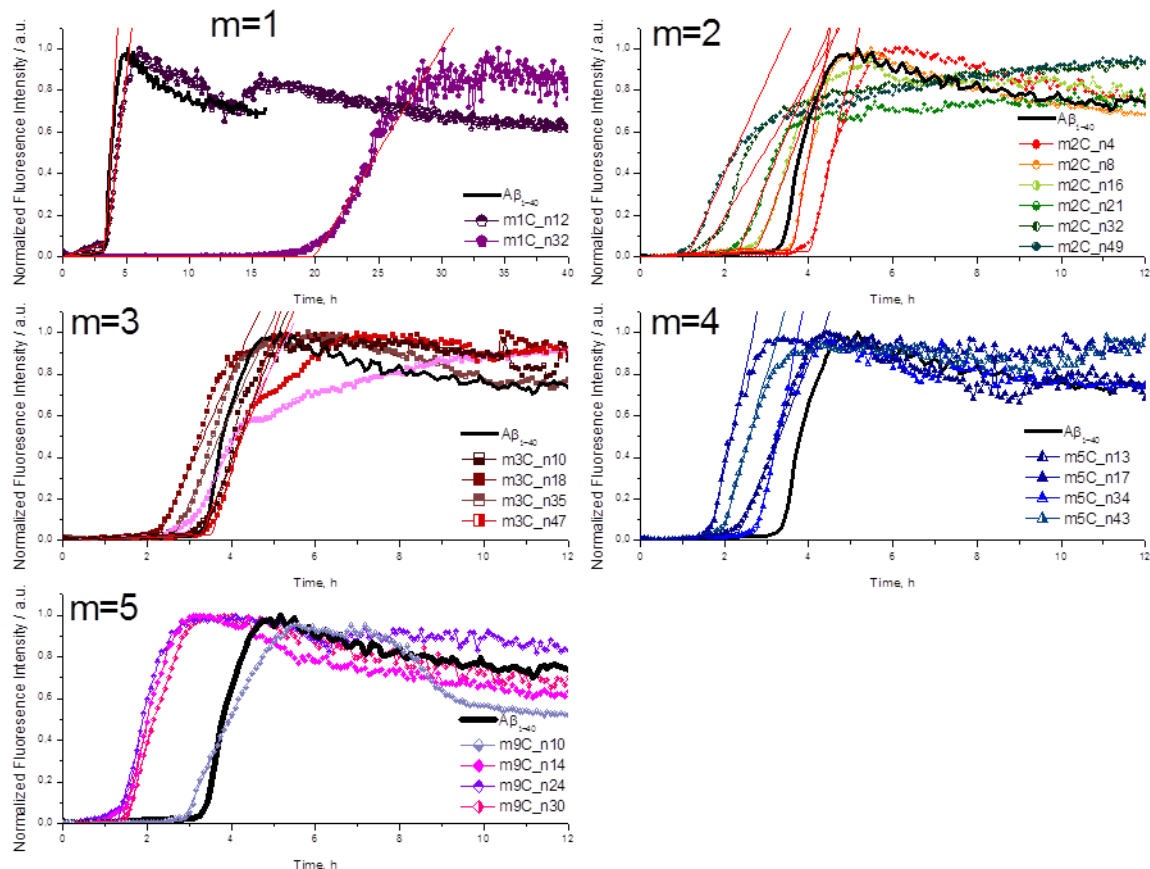


**Figure S19.** Time evolution of the ThT fluorescence intensity of the poly(oligo(ethylene glycol) $_m$  acrylates) /  $A\beta_{1-40}$  mixtures at  $\lambda = 480$  nm. Black solid line corresponds to  $A\beta_{1-40}$  wild type. The hydrophilicity is varied by the number of ethylene glycol units ( $m$ ). Degree of polymerization ( $n$ ) is indicated for every sample and highlighted in bold. Piecewise linear fits are demonstrated respectively.

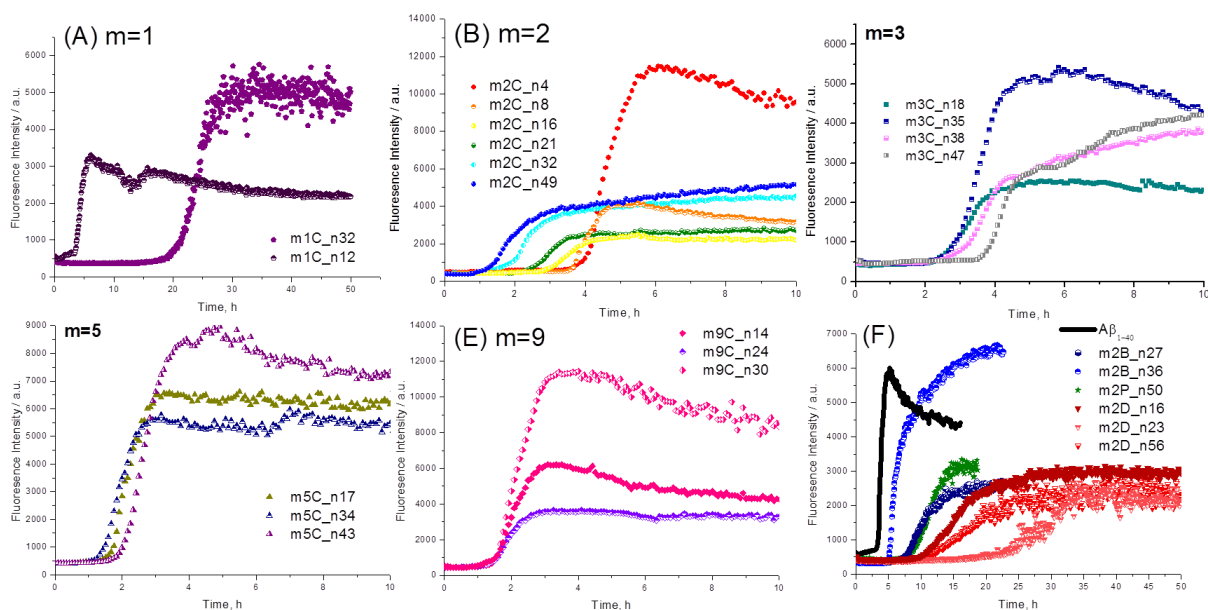


**Figure S20.** Time evolution of the ThT fluorescence intensity of the poly(oligo(ethylene glycol) $_m$  acrylates) /  $A\beta_{1-40}$  mixtures at  $\lambda = 480$  nm. Black solid line corresponds to  $A\beta_{1-40}$  wild type. The raw

.....  
 data are presented. The hydrophilicity is varied by the number of ethylene glycol units ( $m=1-9$ ) ((A)-(E)) and by choice of the end groups (F).

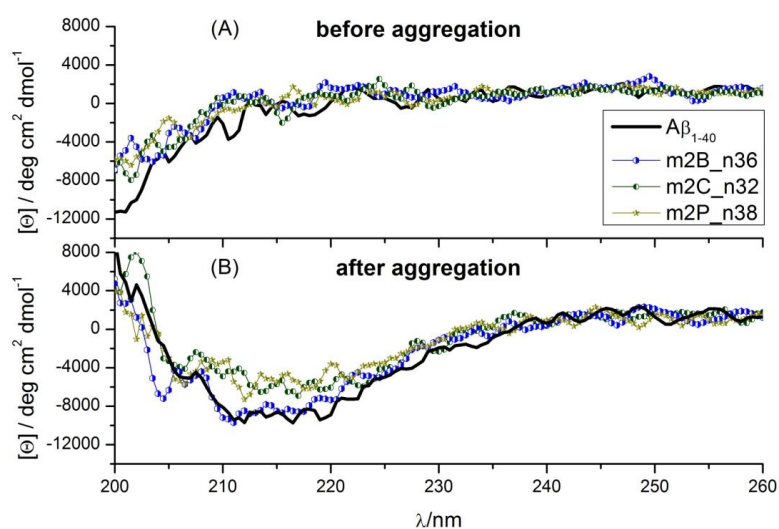


**Figure S21.** UV-CD spectra of the  $A\beta_{1-40}$  / poly(oligo(ethylene glycol) $_m$  acrylates) **m2B\_n36**, **m2C\_n32**, **m2P\_n38** 10  $\mu$ M/10  $\mu$ M mixtures as solution in a 50 mM  $Na_2HPO_4$  buffer (pH 7.4) supplemented with 150 mM NaCl, measured (A) just before ThT kinetic measurements and (B) just after ThT kinetic measurements. The resulting CD spectra display a transition from the non-aggregated freshly prepared native peptides (A) to the  $\beta$ -sheet rich fibrils (B).

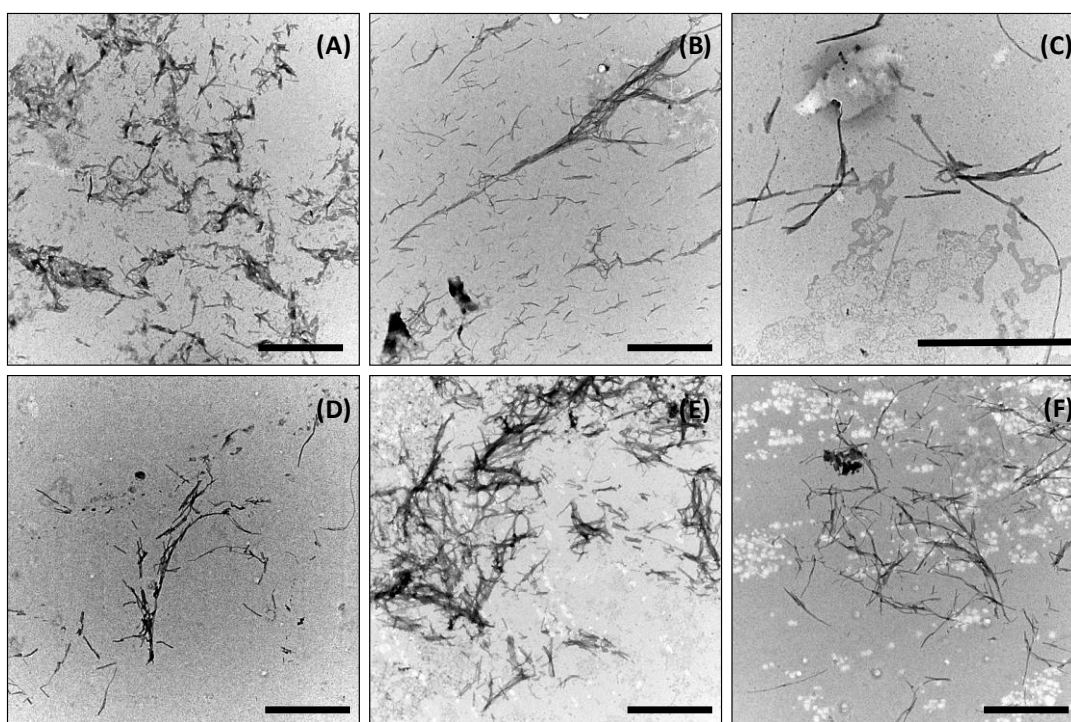


**Figure S22.** TEM images of the fibrils obtained after ThT kinetic measurements (A)  $A\beta_{1-40}$  / m2P\_n38 ; (B)  $A\beta_{1-40}$  / m1C\_n32; (C)  $A\beta_{1-40}$  / m2D\_n16; (D)  $A\beta_{1-40}$  / m3C\_n10; (E)  $A\beta_{1-40}$  / m5C\_n13; (F)  $A\beta_{1-40}$  / m9C\_n10. The scale bar corresponds to 1000 nm.

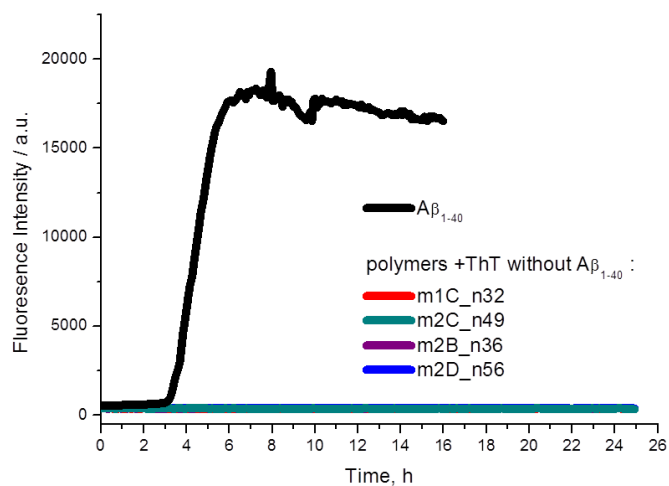


**Figure S23.** Time evolution of the ThT fluorescence intensity of the poly(oligo(ethylene glycol)<sub>m</sub> acrylates) m1C\_n32, m2C\_n49, m2B\_n36 and m2D\_n56 at  $\lambda = 480$  nm. Black solid line corresponds to A $\beta_{1-40}$  wild type.

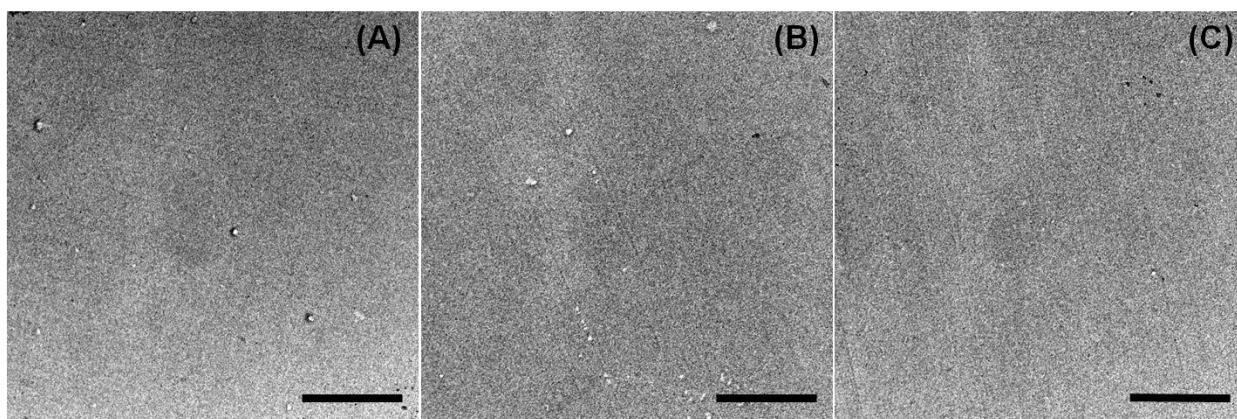


**Figure S24.** TEM images of the polymers (A) m1C\_n32, (B) m2D\_n56 and (C) m2C\_n49 obtained after ThT kinetics studies.

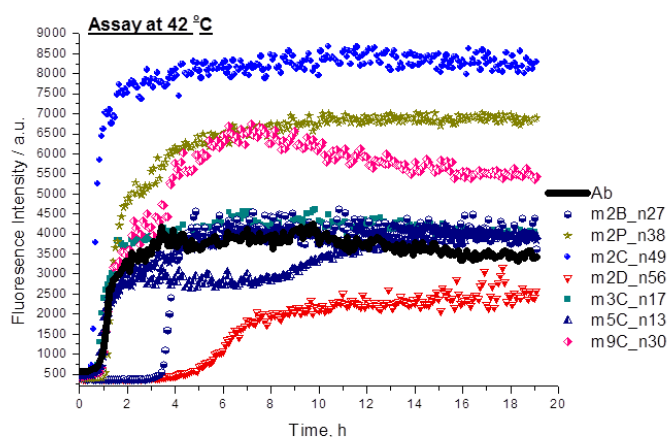


**Figure S25** Time evolution of the ThT fluorescence intensity of the poly(oligo(ethylene glycol)<sub>m</sub> acrylates) / A $\beta_{1-40}$  mixtures at  $\lambda = 480$  nm and 42 °C. Black solid line corresponds to A $\beta_{1-40}$  wild type. The raw data are presented.

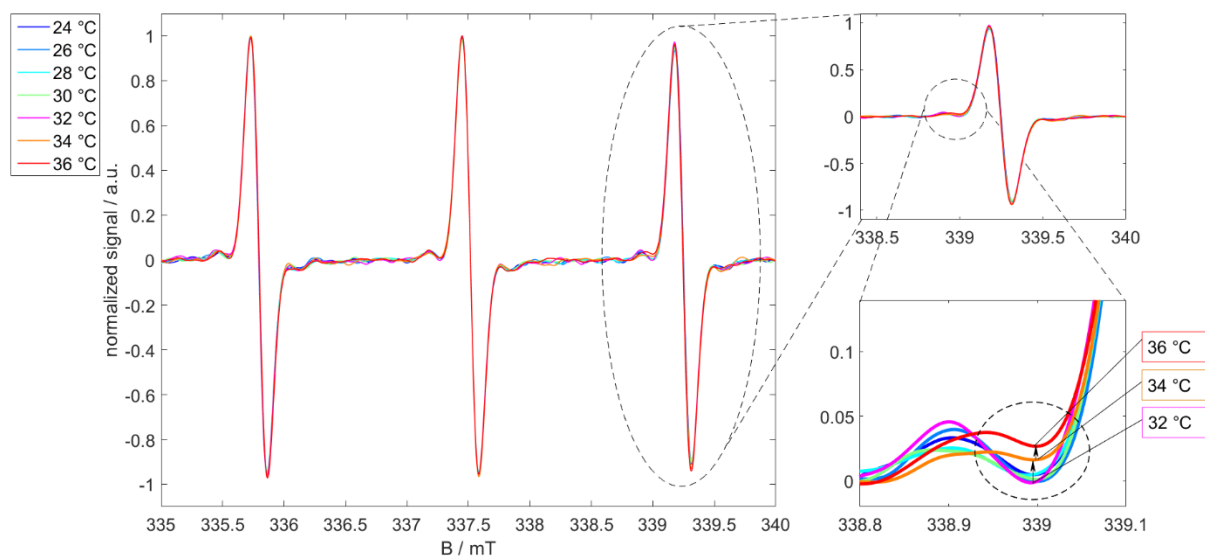
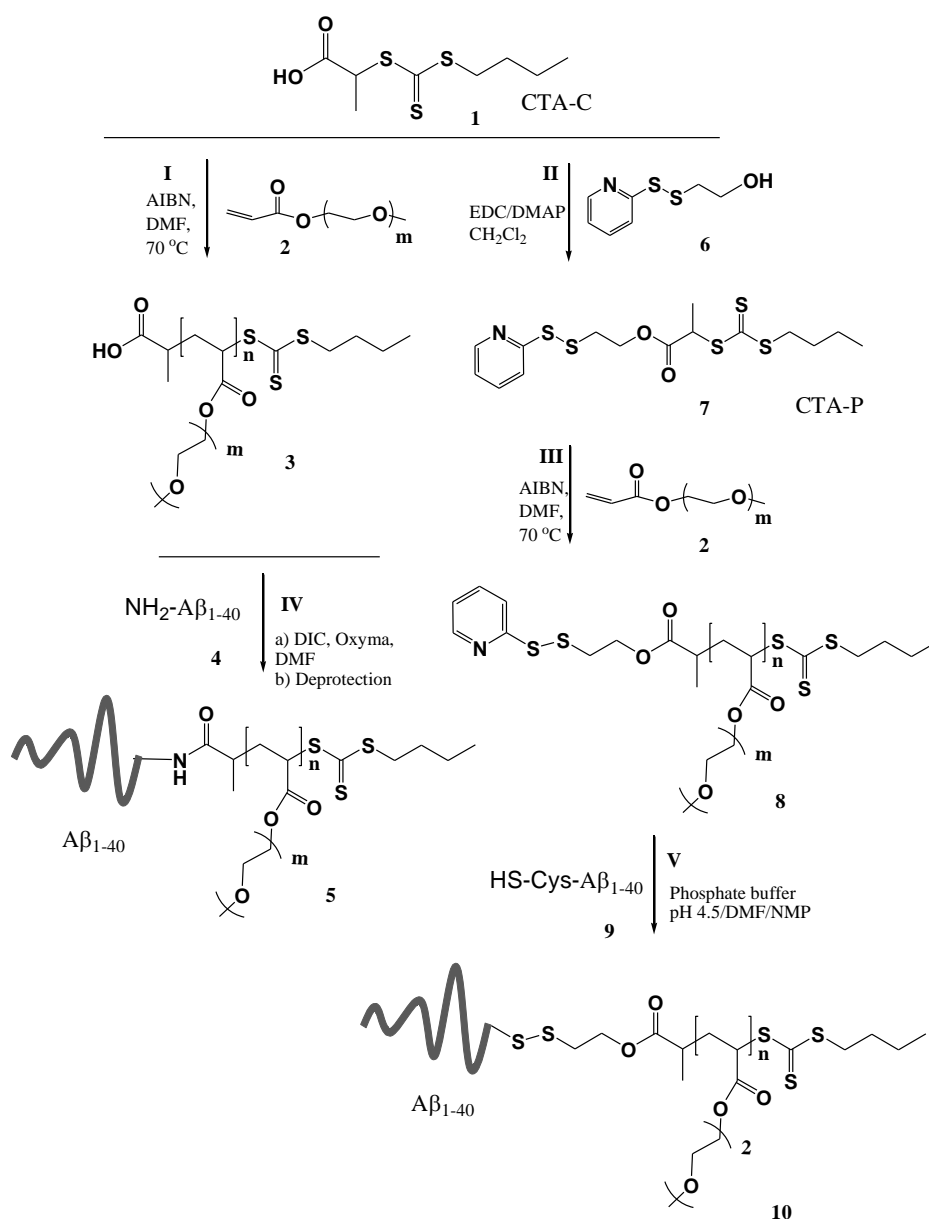


**Figure S26** CW EPR spectra of the physical mixture of polymer (15) m2D\_n23 and A $\beta_{1-40}$  at different temperatures. Starting at temperatures of 34 °C, a second type of spectral component becomes visible in particular at the high-field EPR line (see inset and zoom), which clearly stems from TEMPO probe molecules that on the timescale of our EPR experiment (nanoseconds) reside in water-depleted, polymer-enriched "hydrophobic" nano-inhomogeneities.

**Appendix C – Macromolecular Rapid Communications 2019, 0 (0), 1900378**  
**Synthesis and Aggregation of Polymer-Amyloid  $\beta$  Conjugates**



**Scheme S1.** Synthesis of polymer- $A\beta_{1-40}$  conjugates described in details in this study. **I, III** - RAFT polymerization; **II** - synthesis of the pyridyldisulfide functional CTA via esterification reaction; **IV** - a) polymer conjugation to N-terminal amino group of the  $A\beta_{1-40}$  performed over night in DMF, followed by b) deprotection in TFA, TIPS,  $H_2O$  and phenol for 4 h at RT; **V** -  $A\beta_{1-40}$ -polymer conjugation through thiol-disulfide exchange for 2 h at RT. For details see general procedure described below. All synthesized products are labeled with the respective number (**1-10**). Namely, two functional CTAs (**1, 7**) were synthesized and used in RAFT polymerization of oligo(ethylene glycol)<sub>m</sub> acrylates ( $m=1-3,9$ ). Obtained polymers (**3, 8**) were coupled with peptides giving the respective products (**5, 10**).

**Table S1.** Overview of the synthesized polymers including experimental data.

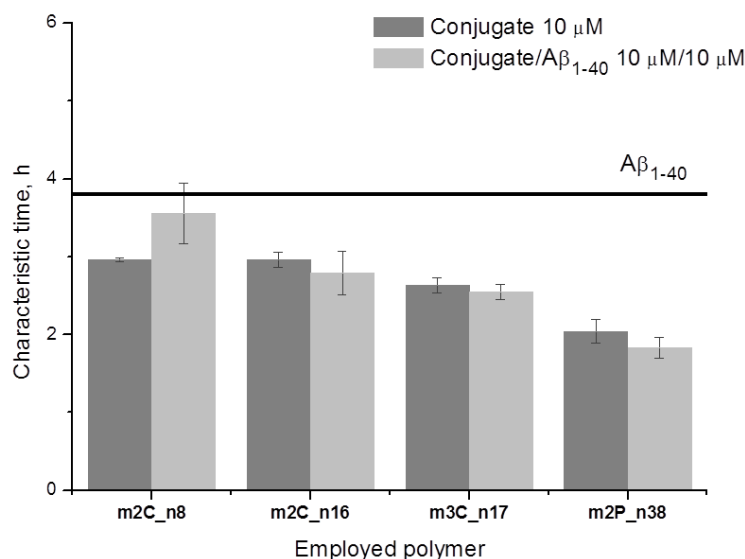
Polymer	CTA -R	Mon -m	[Mon]: [CTA]: [Initiator]	DP (NMR)	Amount CTA, mmol	Amount monomer, mmol	Amount Initiator, mmol	Amount CTA, mg	Amount monomer, $\mu\text{L}$	Amount Initiator, mg	Amount solvent, $\mu\text{L}$
m1C_n90	C	1	100:1:0.1	90	0.037	3.7	0.0037	8.84	476	0.6	950
m2P_n18	P	2	15:1:0.1	18	0.15	2.25	0.015	60.9	380	2.5	570
m2P_n38	P	2	35:1:0.1	38	0.087	3.05	0.0087	35.3	514	1.4	770
m2P_n44	P	2	50:1:0.1	44	0.012	0.6	0.0012	4.7	96.8	0.2	200
m2C_n8	C	2	14:1:0.1	8	0.165	2.31	0.0165	39.4	390	2.7	600
m2C_n16	C	2	15:1:0.1	16	0.168	2.52	0.0168	40.1	425	2.8	850
m2C_n21	C	2	18:1:0.1	21	0.063	1.14	0.0063	15.1	198.6	1.1	340
m2C_n49	C	2	50:1:0.1	49	0.064	3.2	0.064	15.1	536	1	800
m3C_n17	C	3	15:1:0.1	17	0.161	2.42	0.0161	38.3	513	2.6	650
m3C_n38	C	3	50:1:0.1	38	0.054	2.7	0.0054	13	574	0.9	860
m9C_n14	C	9	20:1:0.1	14	0.07	1.4	0.007	16.7	616.5	1.2	950
m9P_n15	P	9	15:1:0.1	14	0.06	0.9	0.006	24.5	398	1	600

**Table S2.** Overview of the synthesized polymers including  $^1\text{H}$  NMR and GPC data. Deviations between  $M_n$  obtained from  $^1\text{H}$  NMR and GPC analyses arise since a polystyrene standard was used for external calibration of GPC.

Entry	Name	m	End group	NMR, $M_n$ g/mol	GPC, $M_n$ g/mol	GPC PDI
1	m1C_n90	1	carboxy- (C)	11700	9100	1.13
2	m2P_n18	2	pyridyldisulfide- (P)	3200	2500	1.16
3	m2P_n38	2	pyridyldisulfide- (P)	6600	3400	1.19
4	m2P_n44	2	pyridyldisulfide- (P)	7800	4100	1.19
5	m2C_n8	2	carboxy- (C)	1400	1250	1.2
6	m2C_n16	2	carboxy- (C)	2800	1200	1.15
7	m2C_n21	2	carboxy- (C)	3600	2700	1.16
8	m2C_n49	2	carboxy- (C)	8500	5600	1.14
9	m3C_n17	3	carboxy- (C)	3700	3900	1.2
10	m3C_n38	3	carboxy- (C)	8300	6200	1.17
11	m9C_n14	9	carboxy- (C)	6700	3400	1.11
12	m9P_n15	9	pyridyldisulfide- (P)	7200	5700	1.14

**Table S3.** Overview of the synthesized polymer-A $\beta_{1-40}$  conjugates including experimental data.

Entry	Conjugate	Amount polymer, mmol	Amount polymer, mg	Amount A $\beta_{1-40}$ , mmol	Amount A $\beta_{1-40}$ , mg	Amount conjugate, mg	Yields, %
1	m2C_n8_A $\beta_{1-40}$	0.053	74	0.011	50	17	26.5
2	m2C_n16_A $\beta_{1-40}$	0.043	120	0.011	50	9.4	11.8
3	m2C_n21_A $\beta_{1-40}$	0.022	79	0.011	50	7.3	8.4
4	m2C_n32_A $\beta_{1-40}$	0.024	135	0.011	50	9	8.1
5	m2C_n49_A $\beta_{1-40}$	0.010	84.5	0.011	50	<1	<1
6	m2P_n18_A $\beta_{1-40}$	0.032	101	0.0045	20	7.4	21.7
7	m2P_n38_A $\beta_{1-40}$	0.018	122	0.0045	20	16.7	33.6
8	m3C_n17_A $\beta_{1-40}$	0.025	98	0.011	50	21.4	23.2

**Scheme S2.** Summary of polymer-A $\beta_{1-40}$  conjugates, regarding to their characteristic times of aggregate formation. The data are obtained from the ThT detected fibrillation kinetics of native A $\beta_{1-40}$  (showed as a black bold line), polymer-A $\beta_{1-40}$  conjugates (gray) or physical mixture of the conjugates with the native A $\beta_{1-40}$  peptide (light gray). Error bars based on averaged three independent measurements are also shown.

## Materials

Deuterated chloroform (CDCl<sub>3</sub>) was purchased from Chemotrade. The following solvents were purchased in technical grade and distilled at least once prior use: dichloromethane (DCM) was predried over calcium chloride (CaCl<sub>2</sub>) and then refluxed over calcium hydride (CaH<sub>2</sub>) for several hours, methanol and dimethylformamide (DMF) were refluxed over calcium hydride (CaH<sub>2</sub>) for several hours and distilled under an inert atmosphere. For synthesis of chain transfer agents (CTAs): acryloyl chloride was purchased from abcr GmbH & Co, 2,2'-dipyridyl disulfide was obtained from TCI, N-(3-dimethylaminopropyl)-N'-ethylcarbodiimide (EDC) was bought by Alfa Aesar. For synthesis of polymers: all CTAs and methoxyoligo(ethylene glycol) acrylates were synthesized in our lab, 2-methoxyethyl acrylate was obtained from TCI. A $\beta_{40}$  peptide (DAEFRHDSGY EVHHQKLVFF AEDVGSNKGKGA

.....  
 IIGLMVGGVV) was synthesized using standard Fmoc solid phase synthesis (Peptide Core Unit, Leipzig University, Germany) on a preloaded resin (PHB-TentaGel R resin, Rapp Polymere GmbH, Germany). 1,8-Diazabicyclo[5.4.0]undec-7-ene (DBU) was purchased from Fluka. All other chemicals were received from Sigma Aldrich and used without further purification unless otherwise stated.

## Methods

$^1\text{H}$ - and  $^{13}\text{C}$ -NMR spectra of polymers were recorded on a Varian Gemini 2000 (400 MHz) or on a Varian Unity Inova 500 (500 MHz) using MestReNova software (version 6.0.2-5475) for the evaluation of the results. NMR spectra were measured at 27 °C using  $\text{CDCl}_3$ . All chemical shifts ( $\delta$ ) were given in parts per million (ppm) relative to trimethylsilane (TMS) and referred to the solvent signal ( $\text{CDCl}_3$ : 7.26 ppm ( $^1\text{H}$ ), 77.0 ppm ( $^{13}\text{C}$ )).

ESI-TOF-MS analyses were measured using *Focus microTOF* by *Bruker Daltonics*. 1-2 mg of the sample was dissolved in HPLC grade solvents (THF/Methanol 100:1 [v/v]). All spectra were obtained by means of direct injection with the rate 180  $\mu\text{L}/\text{h}$  using the positive mode.

MALDI-TOF MS analysis of all polymers was carried out using a *Bruker Autoflex III Smartbeam* equipped with a nitrogen laser (337 nm) working in linear and reflection modes. The obtained data were evaluated using flexAnalysis software (version 3.0.). The matrix solution was prepared by dissolving 1,8,9-anthracenetriol (Dithranol) or trans-2-[3-(4-tert-Butylphenyl)-2-methyl-2-propenylidene]malononitrile (DCTB) in THF at a concentration of 20 mg/mL. All polymers were dissolved in THF (20 mg/mL, purchased from Sigma Aldrich in HPLC grade) and mixed with sodium trifluoroacetate (20 mg/mL in THF). The ratio between the matrix, the analyte, and the salt was 100:10:1 [v/v].

MALDI-TOF MS analysis of conjugates was carried out using a *Bruker Microflex LT* equipped with a nitrogen laser at 337 nm working in linear mode. The obtained data were evaluated using flexAnalysis software (version 3.4). The matrix solution was prepared by dissolving trans-3,5-dimethoxy-4-hydroxycinnamic acid (sinapinic acid) in solvent (50:50 [v/v] acetonitrile/0.1% TFA in water) at a concentration of 20 mg/mL. The conjugate was dissolved in acetonitrile/water (50:50) 0.1% TFA and mixed with the matrix at the ratio 1:2.

Preparative RP-HPLC (Gilson, Limburg, Germany) was implemented to purify the crude peptides to >95% purity. For both analytical and preparative use, the mobile phases were water (A) and acetonitrile (B), respectively, each containing 0.1 % trifluoroacetic acid, with detection at 220 nm. Samples were eluted with a linear gradient from 5 % B to 90 % B in 15 min for analytical runs and in 90 min for preparative runs. Finally, all peptides were characterized by analytical HPLC Dionex Ultimate 3000 (Thermo Scientific, Germany) using a PLRP-S column (Agilent Technologies, 150x3mm, 3 $\mu\text{m}$ ).

Gel permeation chromatography (GPC) measurements of polymers were done using Viscotek GPCmax VE 2002 using a  $\text{H}_{\text{HR}}\text{-H}$  Guard-17360 precolumn and a  $\text{GMH}_{\text{HR}}\text{-N-18055}$  column with THF as solvent and VE 3580 IR detector for refractive index determination. A polystyrene standard ( $M_{\text{p}} = 1,000 - 115,000$  g/mol) was used for external calibration. Column and detector temperatures were held at 22 °C and 35 °C respectively and the flow rate was set to 1 mL/min. The concentration of all samples was 5 mg/mL.

ThT dependent fibrillation kinetics of  $\text{A}\beta_{1-40}$  and the conjugates were recorded on a BMG Labtech FLUOStar Omega platereader using a 96-well plate (150  $\mu\text{L}$  each)<sup>[1-2]</sup>. In order to completely dissolve  $\text{A}\beta_{1-40}$  and the conjugates, an ultrasound treatment for 2 min was applied<sup>[3]</sup>. A consequent centrifugation at 4 °C and 10000 rpm for 2 hours prior to every measurement was carried out, according to previously reported protocols.<sup>[3-5]</sup> Subsequently, the concentration of the samples was determined using a Jasco J-650 UV-VIS spectrometer

.....

and set to 10  $\mu\text{M}$ . The shaking protocol comprised of 300 s long cycles including 240 s double-orbital shaking at 300 rpm before the measurement, using an excitation wavelength of 450 nm and an emission wavelength of 480 nm. All experiments were performed independently three times at 37  $^{\circ}\text{C}$ . Fluorescence intensities were normalized to the range from 0 to 1. The lag times ( $t_{\text{lag}}$ ) were determined as intercepts of piecewise linear fits performed from the zero-intensity up to the inflexion points of the ThT fluorescence intensity curves

$$\begin{cases} at, & t < t_{\text{lag}} \\ at_{\text{lag}} + b(t - t_{\text{lag}}), & t \geq t_{\text{lag}} \end{cases},$$

where  $a, b$  are the slopes of the linear fits before and after the lag time  $t_{\text{lag}}$ , respectively, and  $t$  is the experimental time. The characteristic times ( $t_{\text{char}}$ ) were determined as times at which the fluorescence intensity reaches a half of its maximum.

Transmission Electron Microscopy (TEM) was employed to explore the morphology of aggregated samples. 5  $\mu\text{l}$  samples, taken from the well plates after ThT dependent kinetic measurements, were applied on carbon film coated copper grids and incubated for three minutes. The grids were further washed three times (20 seconds each time) in double distilled water and incubated for 60 seconds in 1% (w/v) uranyl acetate solution. The grids were dried for 24 h on filter paper. TEM analysis was done with a Zeiss EM 900 transmission electron microscope (acceleration voltage 80 kV). Images were taken by a Variospeed SSCCD camera (SM-1k-120, TRS, Moorenweis) operating with ImageSP Viewer software.

Turbidimetry measurements were carried out using an UV-VIS spectrometer JASCO Corp., J-815 using a 0.1 cm diameter quartz cuvette. By coupling with a peltier element PTC-423L from Jasco a controlled heating rate of 1 K/min could be utilized. The observed wavelength was  $\lambda = 500$  nm. For measurements in buffer 10  $\mu\text{M}$  solutions of poly(oligo(ethylene glycol)<sub>m</sub> acrylates) or 10  $\mu\text{M}$  solutions of conjugates in 50 mM  $\text{Na}_2\text{HPO}_4$  buffer (pH 7.4), supplemented with 150 mM NaCl were used. Cloud point temperatures ( $T_{\text{cp}}$ ) were detected at 50% of maximum absorbance.

#### **General procedure for the syntheses of the poly(methoxydi(ethylene glycol)acrylates) on example of m2P\_n44:**

RAFT polymerization of **m2P\_n44** was performed using a standard Schlenk technique. The pyridyl disulfide functionalized **CTA-P** (4.7 mg, 0.012 mmol), methoxydi(ethylene glycol)acrylate (**Mon-2**) (96.8  $\mu\text{L}$ , 0.6 mmol) and AIBN (0.2 mg, 0.0012 mmol) in a molar ratio of (**Mon-2**):(**CTA-P**):AIBN 50:1:0.1 were dissolved in 0.2 mL of DMF. The mixture of (**Mon-2**), (**CTA-P**), AIBN and DMF was bubbled with argon for 30 minutes prior to the reaction and placed into a preheated oil bath at 70  $^{\circ}\text{C}$ . The reaction was stirred for six hours before it was cooled by means of a methanol/liquid nitrogen bath to -80  $^{\circ}\text{C}$ . The resulting yellow polymer was precipitated three times into high excess of *n*-hexane and dried in high vacuum within three days. The polymeric product **m2P\_n44** was characterized via  $^1\text{H-NMR}$  (Figure S15), matrix-assisted laser desorption/ionization mass spectrometry (MALDI-TOF MS) (Figure S16) and size exclusion chromatography (SEC). Therefore the synthesis of the polymer was truly proven via these experimental methods.

#### **General procedure for the syntheses of A $\beta$ <sub>1-40</sub>-polymer conjugates:**

Solid-phase peptide synthesis of the A $\beta$ <sub>1-40</sub> variants (**Scheme 1A**) was utilized on an automated microwave peptide synthesizer Liberty Blue, (CEM GmbH, Germany) using

.....

standard Fmoc-chemistry and preloaded resin. The polymers with the carboxy- end group (m2C\_n8-m9C\_n14) were coupled to the N-terminal amino group in excess of 2-5 equiv. in DMF over night using DIC (2-5 equiv.), and HOBT (1-hydroxybenzotriazole, 2-5 equiv.) at room temperature. The final side chain deprotection and cleavage from the resin was conducted by adding a mixture of trifluoroacetic acid, triisopropylsilane, water and phenol (92.5:2.5:2.5:2.5 [v/v]) with gentle agitation for 4 h at room temperature. The crude conjugates were filtrated and then precipitated in cold ether (10ml x 3) and consequently dried. The coupling of pyridyldisulfide-functionalized polymers (m2P\_n18-m2P\_n44) was utilized with N-terminally cysteine-containing A $\beta$ <sub>1-40</sub> (SH-Cys-A $\beta$ <sub>1-40</sub>). The polymers were dissolved in 1 ml 0.5 M phosphate buffer pH 4.5, while 20 mg of the peptide was dissolved in 1 ml DMF/NMP 50:50 [v/v]. The peptide solution was subsequently added to the polymer solutions. After 10 min 1 ml buffer (pH 4.5) was added, followed by 1.5 ml buffer in 20 min and then 4 ml in 30 min. The reaction was held for 1 h at room temperature, while shaking. Finally, the polymer-peptide conjugates were separated by centrifugation (13000 rpm) for 20 min. The precipitates were then dissolved in 2 ml DMSO. The crude conjugates were purified to >95% purity using preparative RP-HPLC. The purified conjugates were obtained in yields of 8.1-33.6 %.

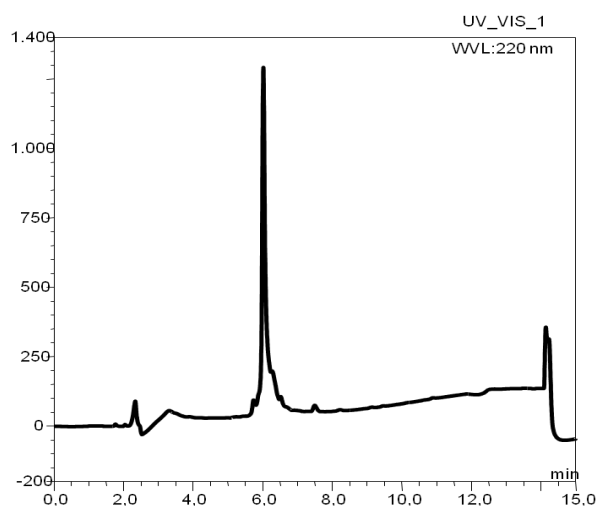


**Figure S1.** HPLC traces of HS-Cys-A $\beta$ <sub>1-40</sub> at 6 min.

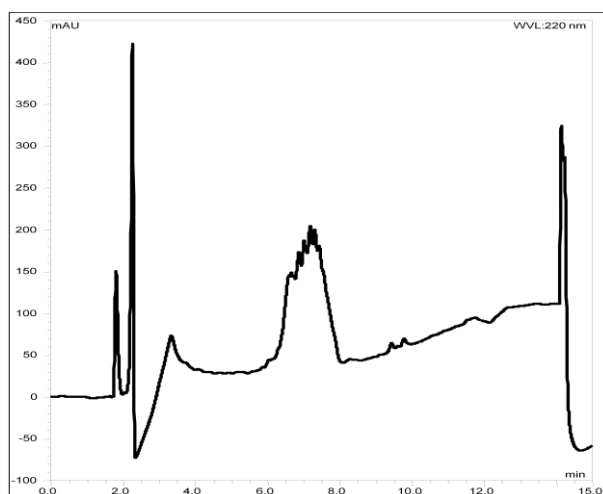


**Figure S2.** HPLC chromatogram of the m2C\_n8\_A $\beta$ <sub>1-40</sub> conjugate. The peak at 7.1 min represents the purified product.

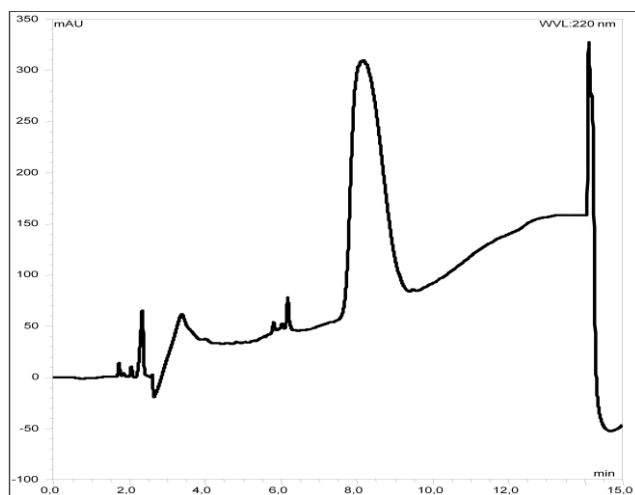


**Figure S3.** HPLC chromatogram of the m2C\_n16\_A $\beta$ <sub>1-40</sub> conjugate. The peak at 8.2 min represents the purified product.

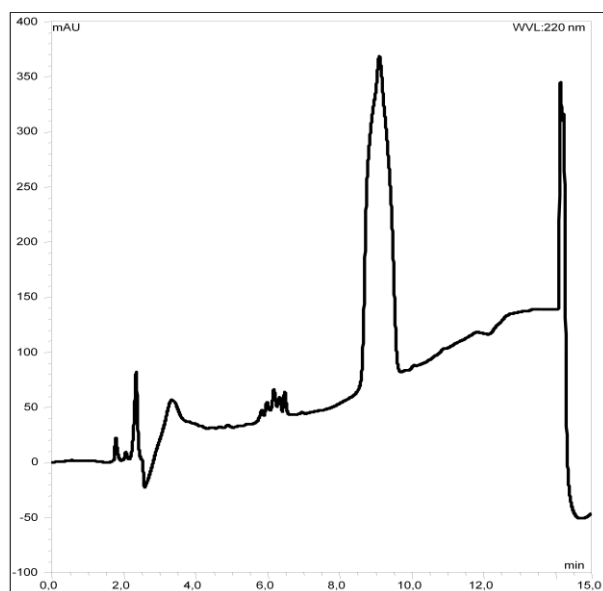


**Figure S4.** HPLC chromatogram of the m2P\_n38\_A $\beta$ <sub>1-40</sub> conjugate. The peak at 9 min represents the purified product.

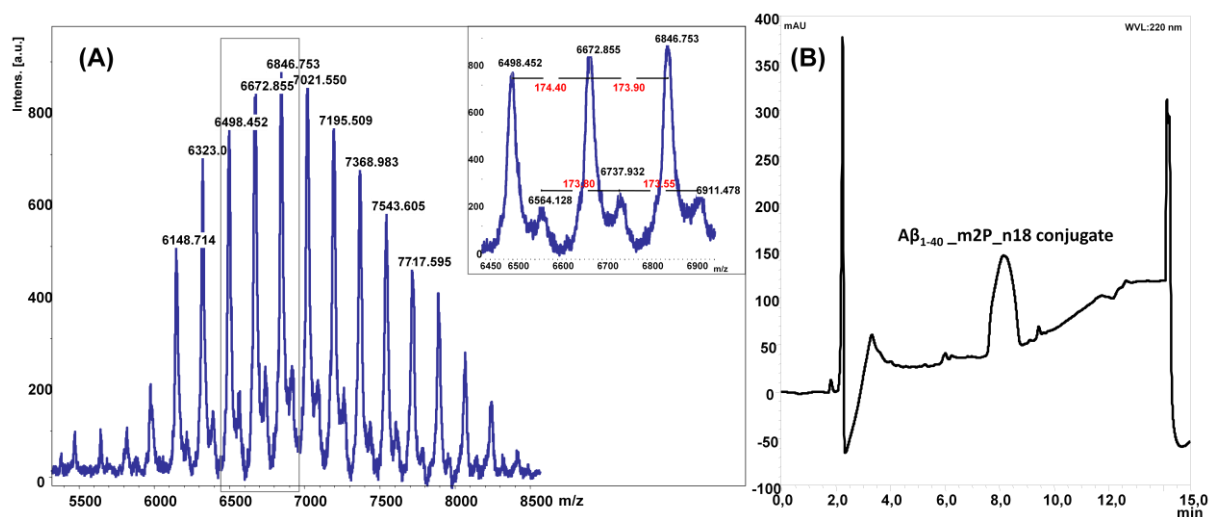


**Figure S5.** (A) MALDI-TOF MS spectrum of poly(methoxy di(ethylene glycol)acrylate)-A $\beta_{1-40}$  conjugate m2P\_n18\_A $\beta_{1-40}$ . (B) HPLC chromatogram of m2P\_n18\_A $\beta_{1-40}$  conjugate. The peak at 8.2 min represents the purified product.

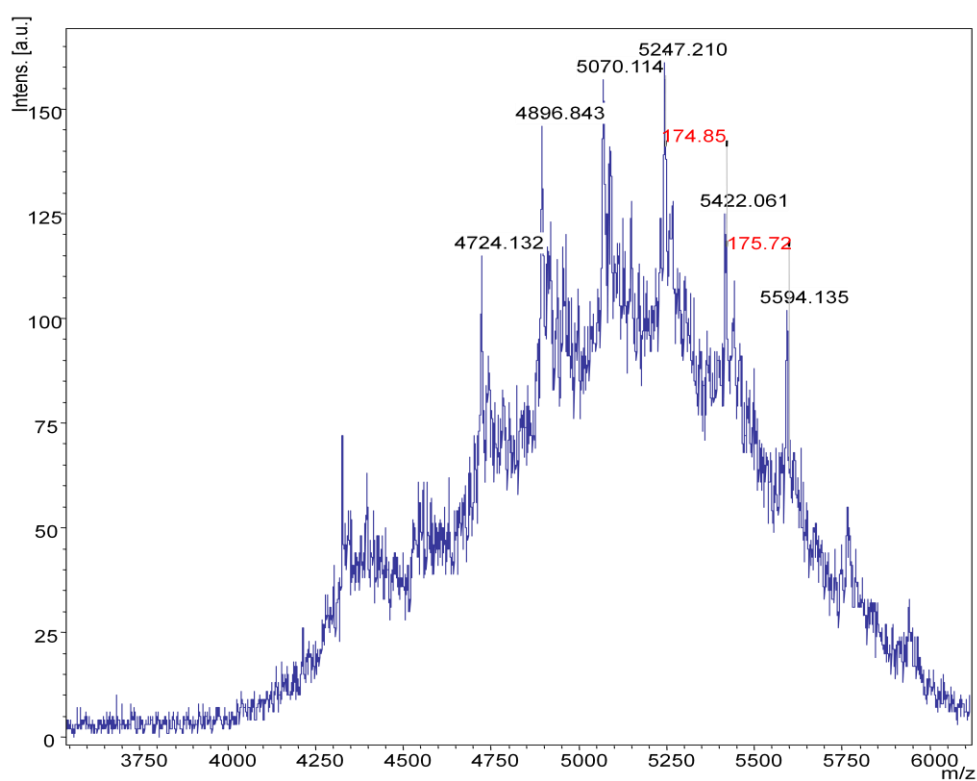


**Figure S6.** MALDI-TOF MS spectrum of poly(methoxy di(ethylene glycol)acrylate)-A $\beta_{1-40}$  conjugate m2C\_n8\_A $\beta_{1-40}$ .

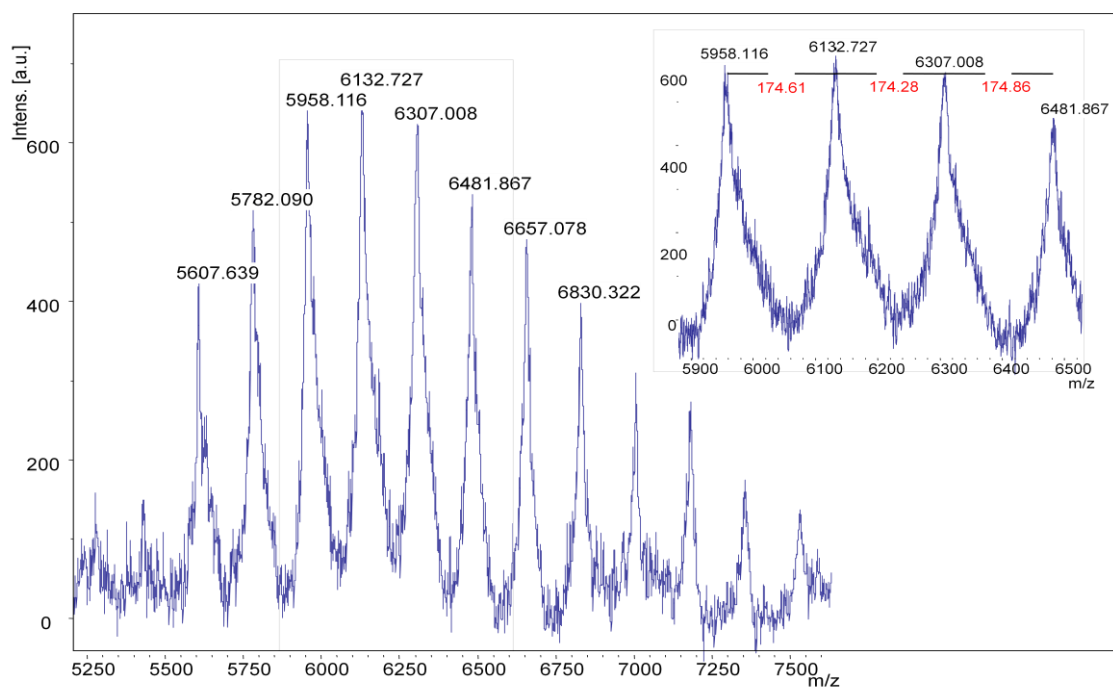


**Figure S7.** MALDI-TOF MS spectrum of poly(methoxy di(ethylene glycol)acrylate)-A $\beta$ <sub>1-40</sub> conjugate m2C\_n16\_A $\beta$ <sub>1-40</sub>.

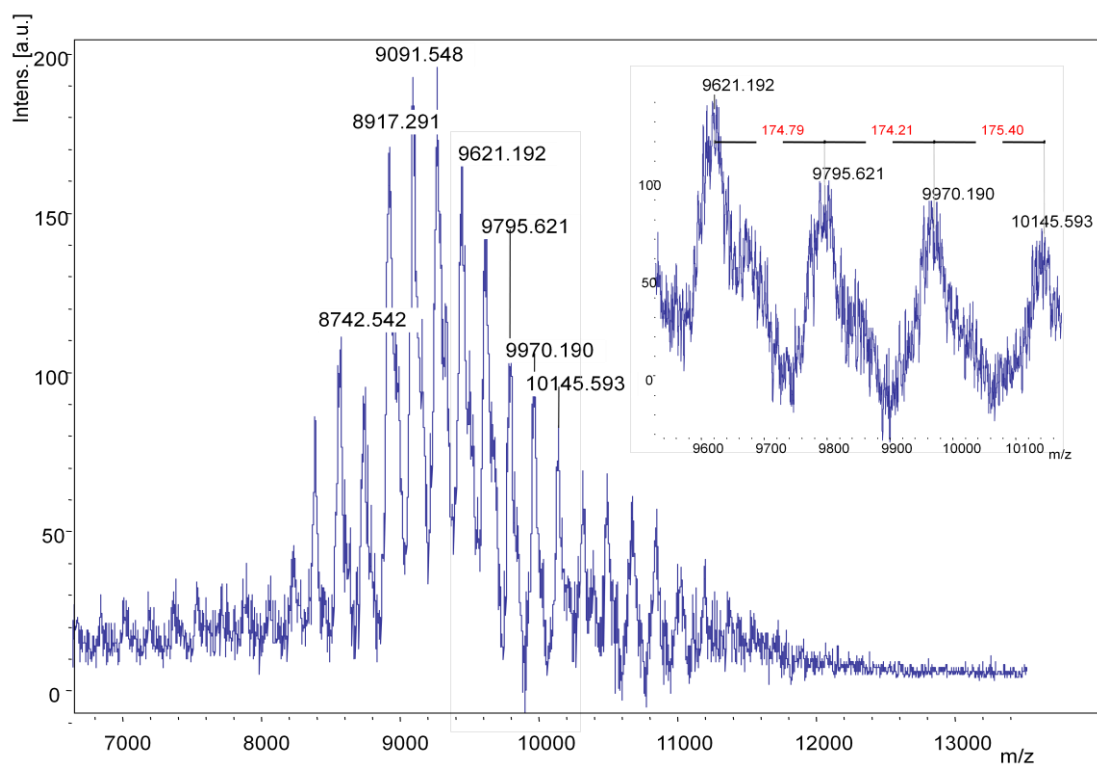


**Figure S8.** MALDI-TOF MS spectrum of poly(methoxy di(ethylene glycol)acrylate)-A $\beta$ <sub>1-40</sub> conjugate m2P\_n38\_A $\beta$ <sub>1-40</sub>.

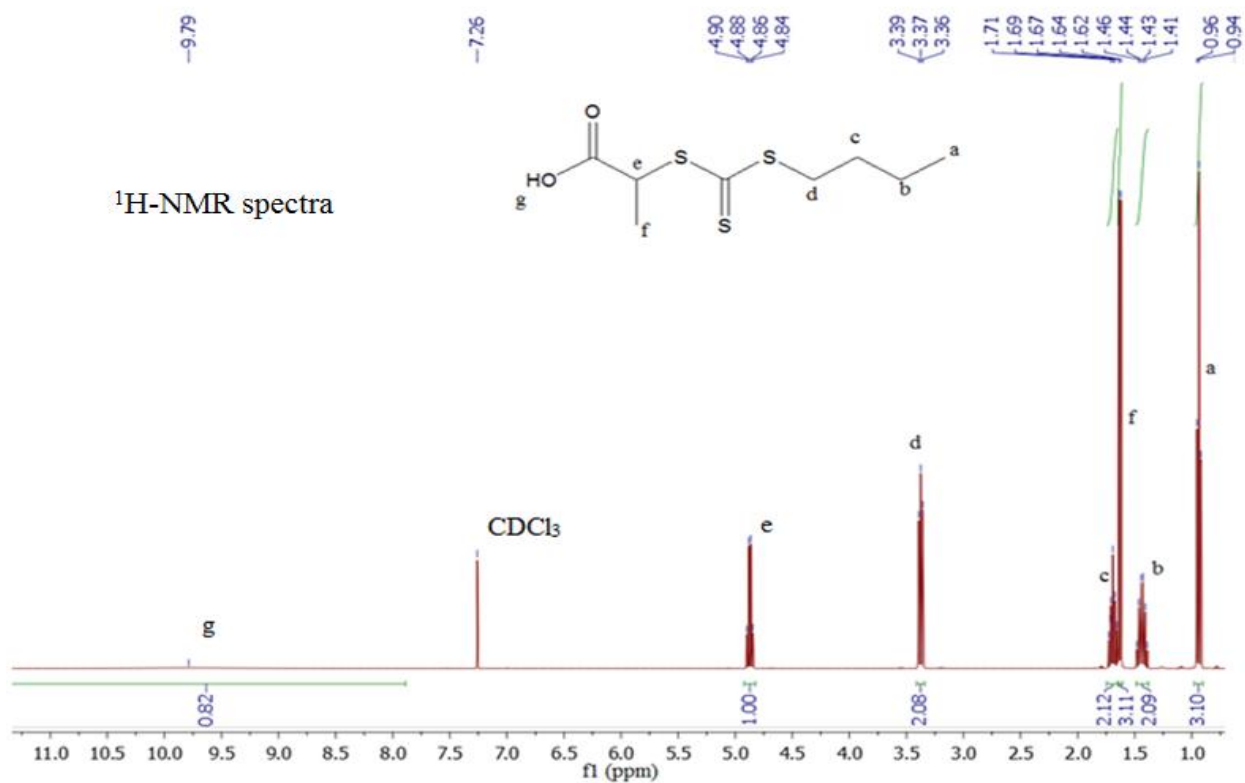


**Figure S9.** <sup>1</sup>H-NMR spectrum of 2-(n-butyltrithiocarbonylthio) propionic acid (1).

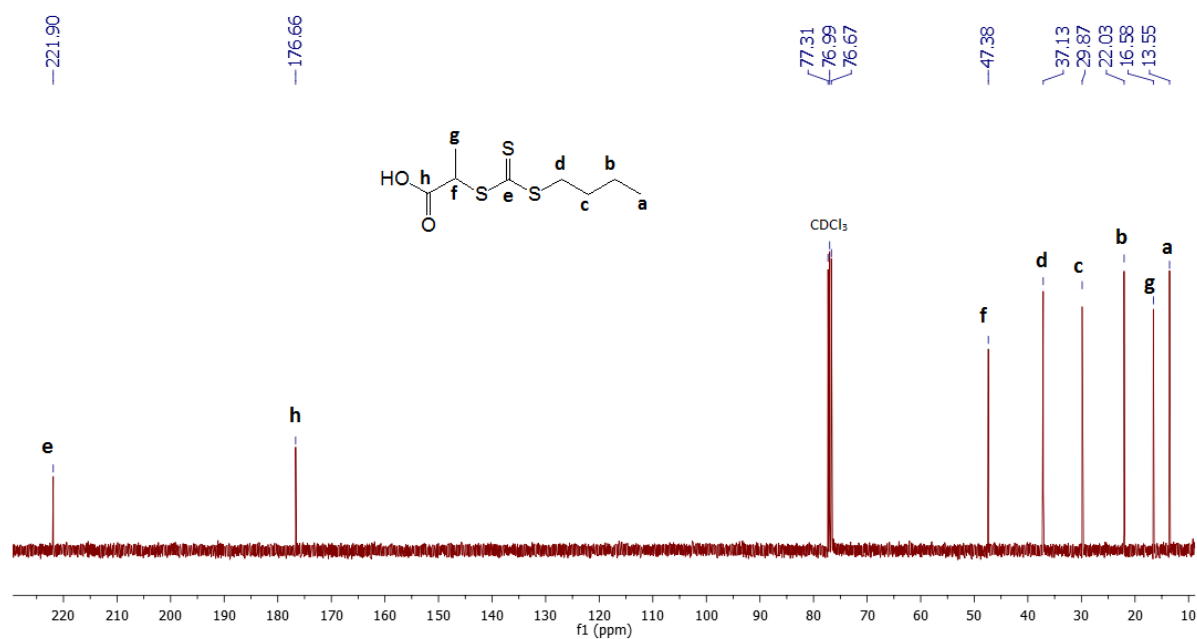


**Figure S10.** <sup>13</sup>C-NMR spectrum of 2-(n-butyltrithiocarbonylthio) propionic acid (1).

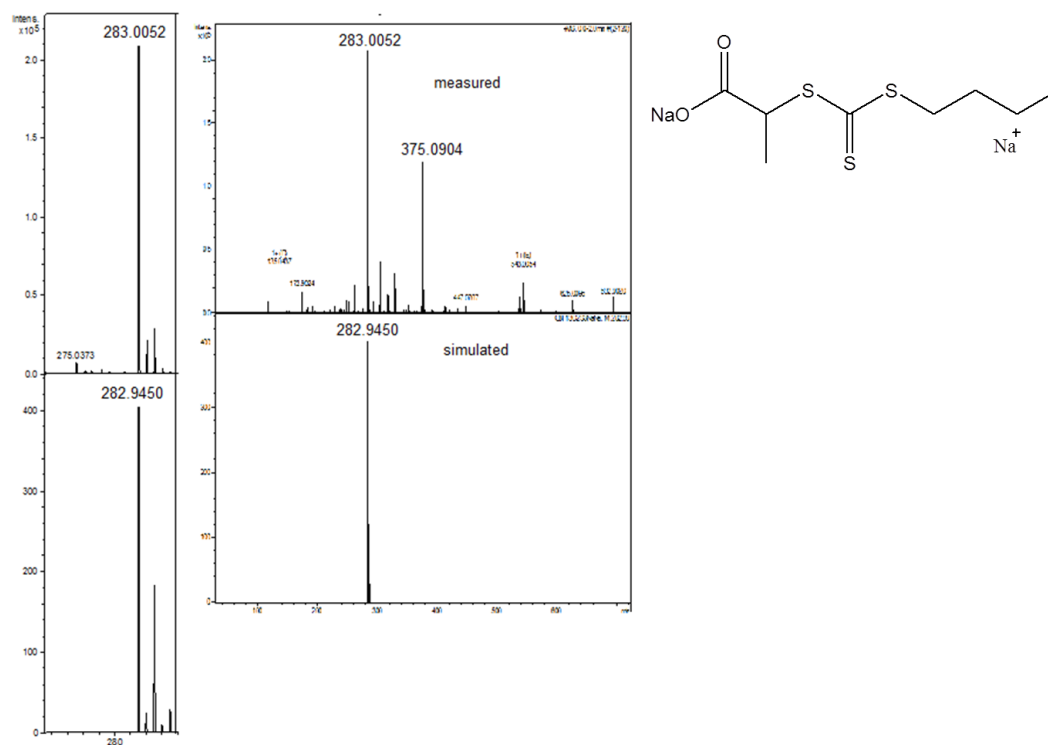


**Figure S11.** ESI-TOF MS spectrum of 2-(n-butyltrithiocarbonylthio) propionic acid (1).

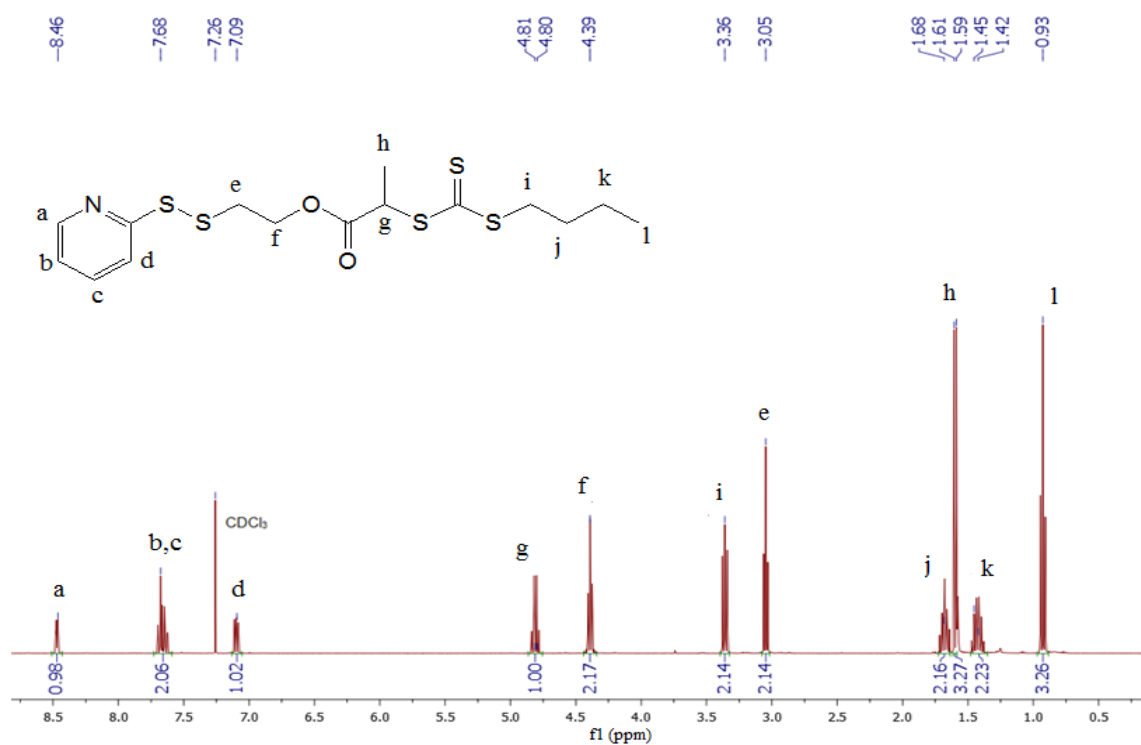


**Figure S12.**  $^1\text{H-NMR}$  spectrum of pyridyl disulfide containing CTA (7).

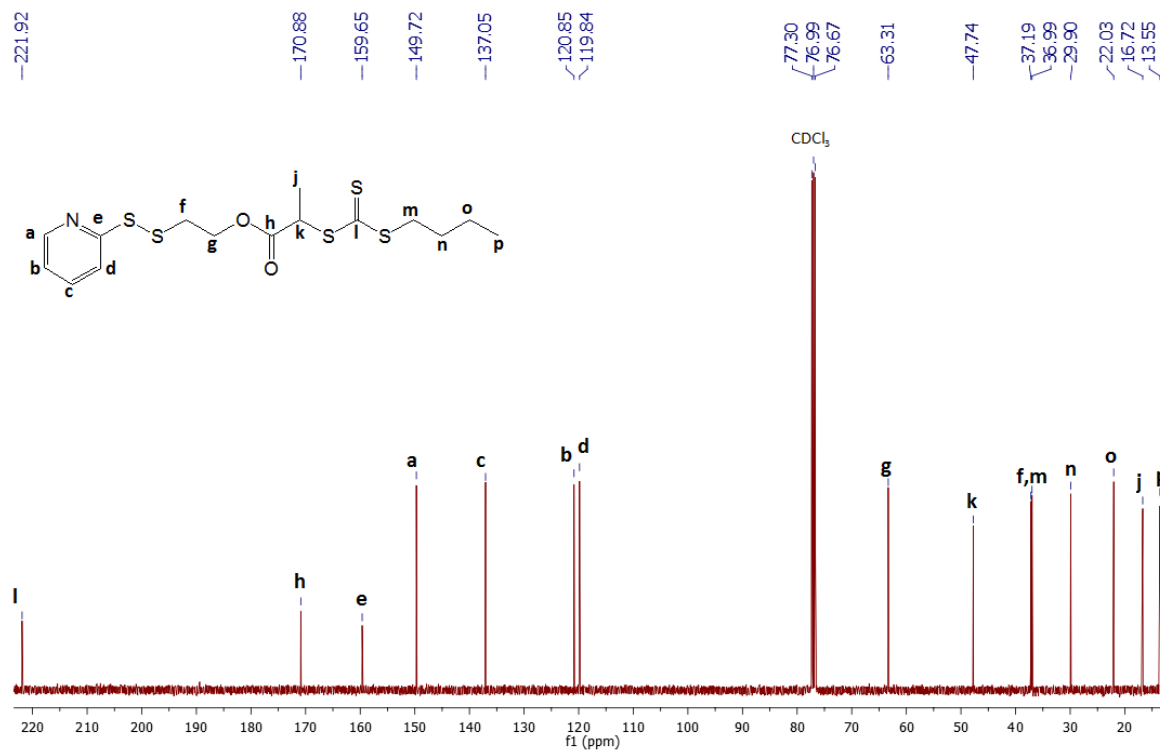


**Figure S13.**  $^{13}\text{C}$ -NMR spectrum of pyridyl disulfide containing CTA (7).

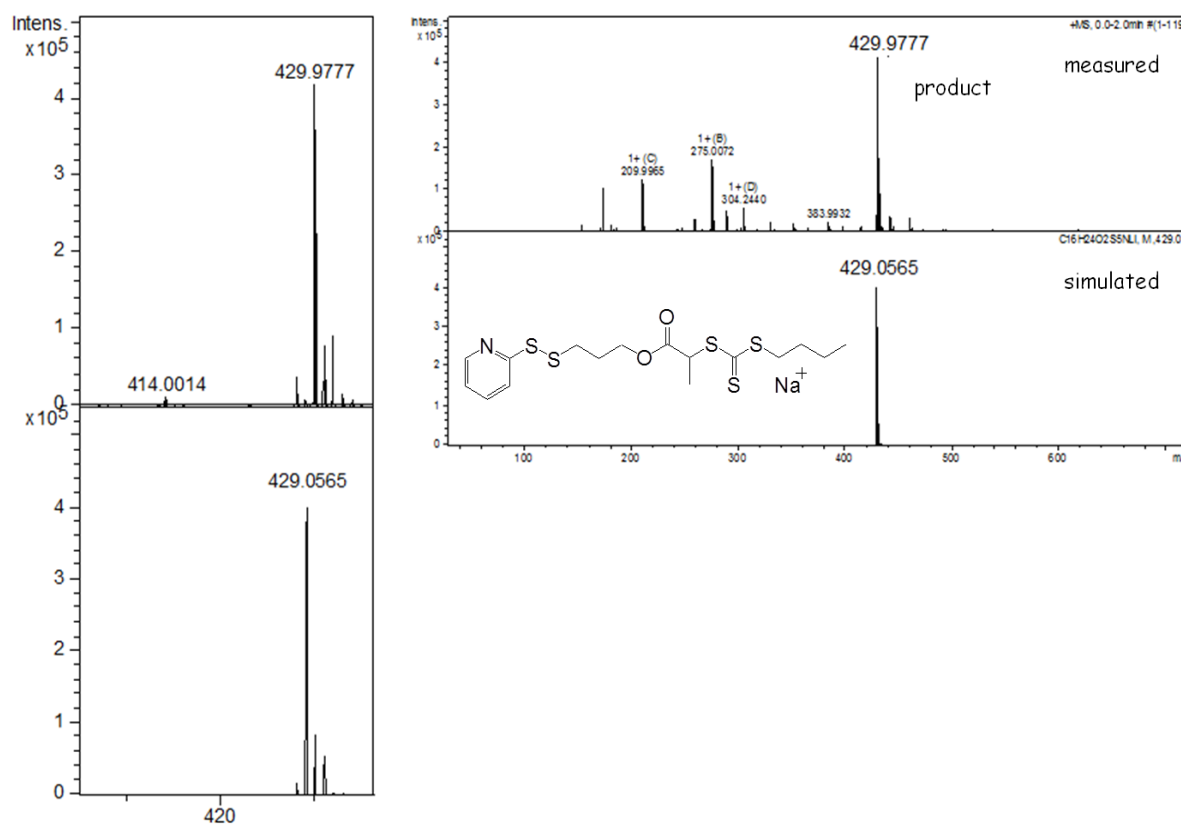


**Figure S14.** ESI-TOF MS spectrum of pyridyl disulfide containing CTA (7).

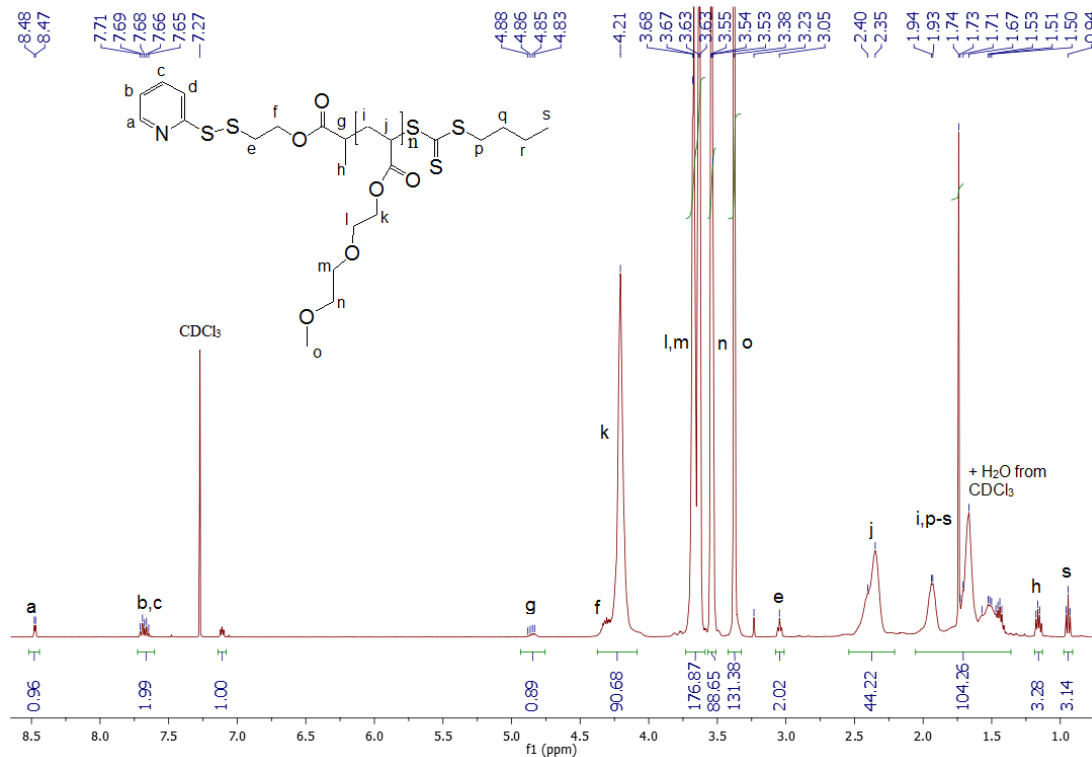
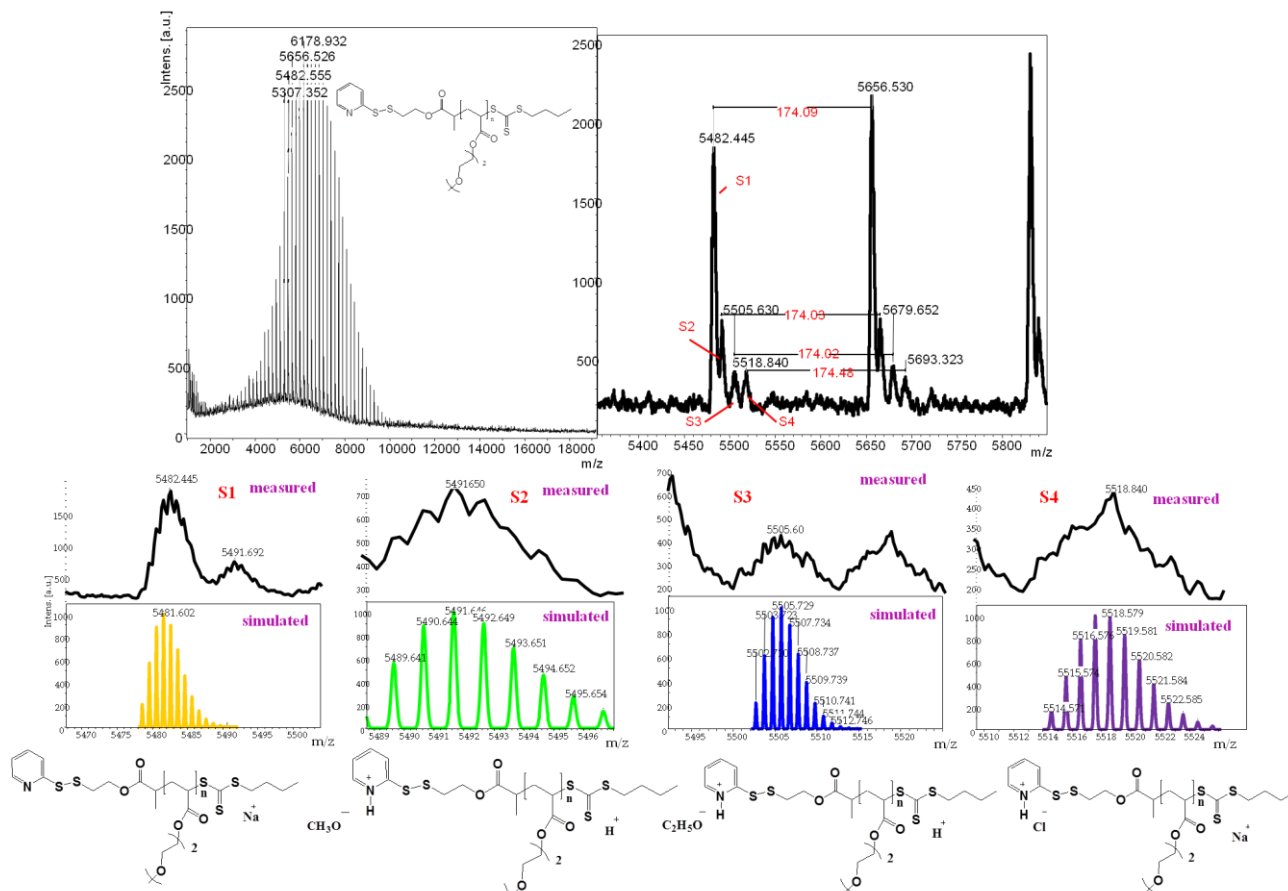
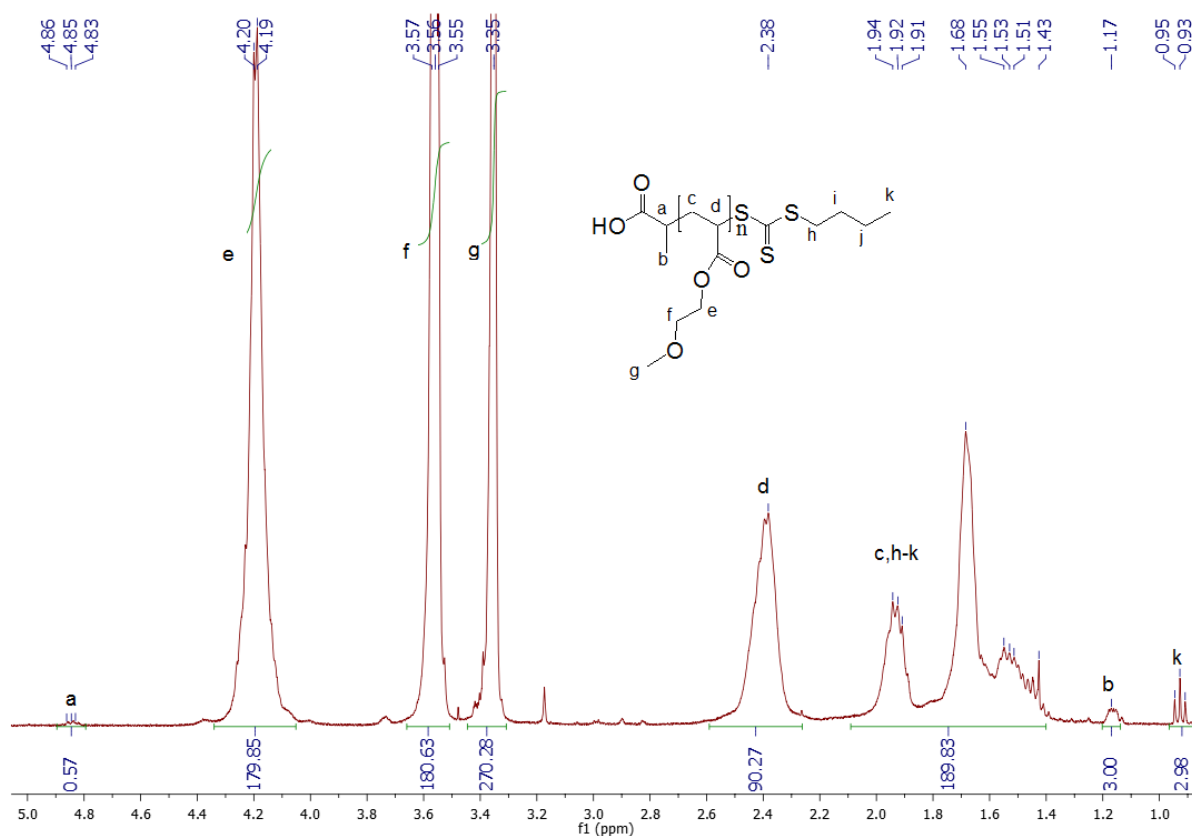
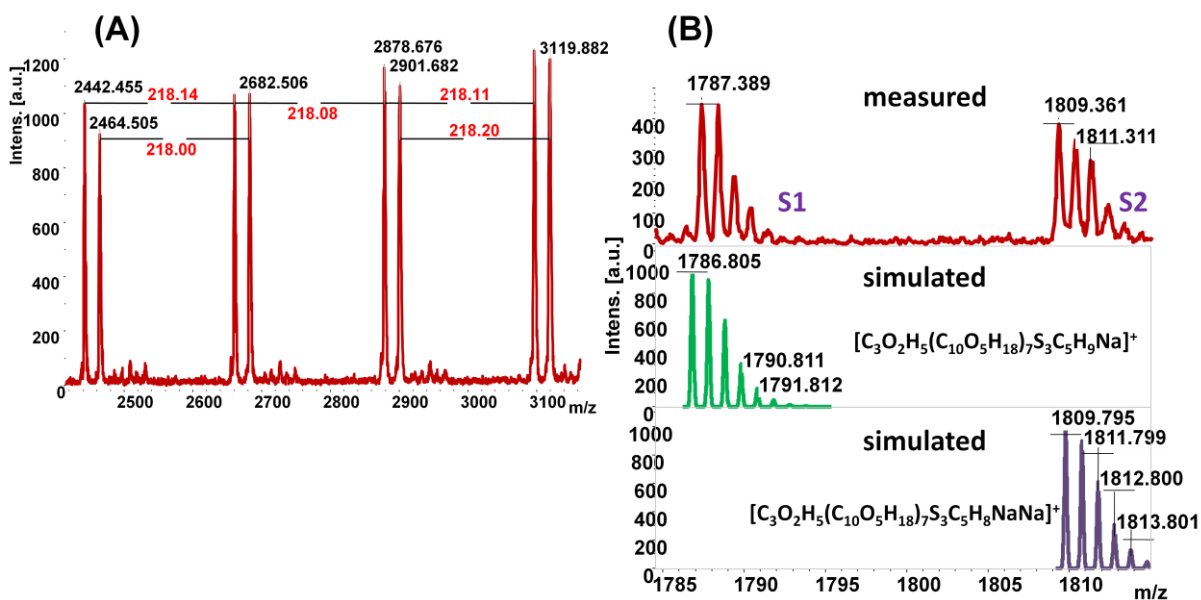
Figure S15.  $^1\text{H-NMR}$  spectrum of the polymer m2P\_n44.

Figure S16. MALDI-TOF MS spectrum of the polymer m2P\_n44.



**Figure S17.**  $^1\text{H-NMR}$  spectrum of the polymer m1C\_n90.



**Figure S18.** (A) MALDI-TOF MS spectrum of the polymer m3C\_n17 (see also Figure 1). (A) Differences between maximums correspond to repeating unit of the polymer ( $\sim 218$  g/mol). (B) Measured and simulated isotopic patterns of the chosen series are shown.

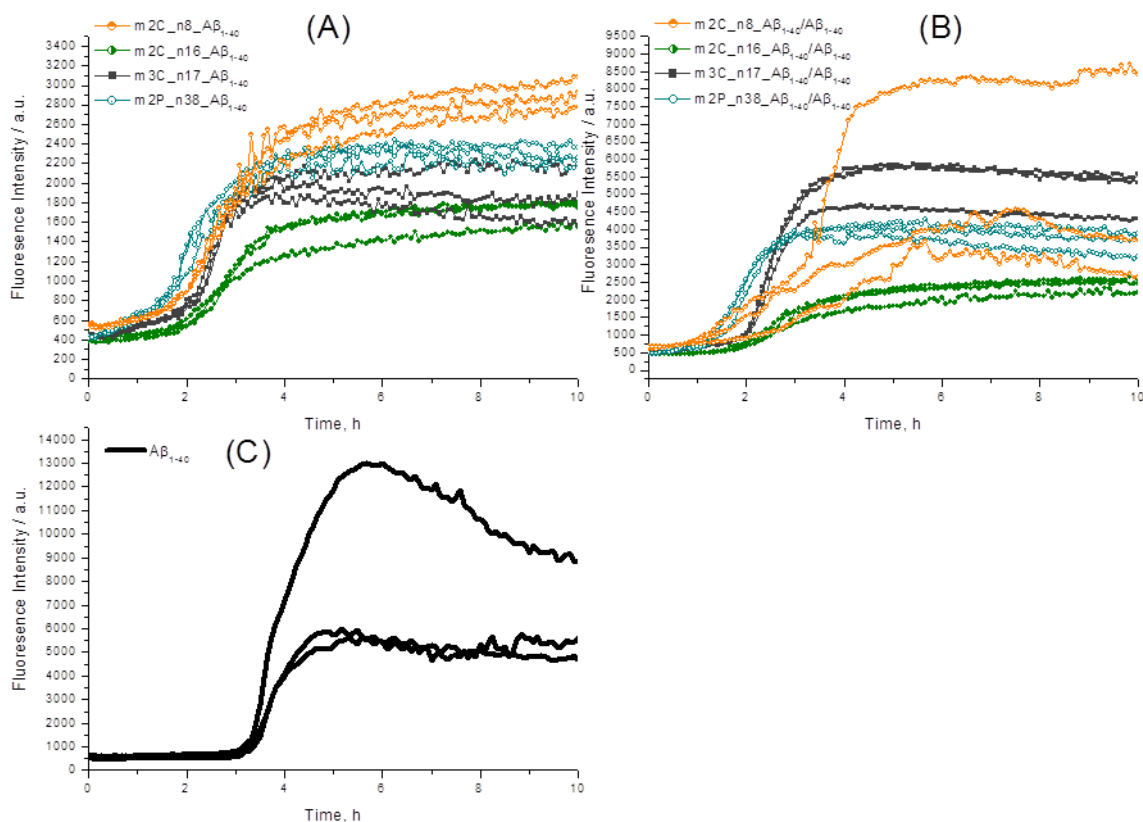


**Figure S19.** Time evolution of the ThT fluorescence intensity of the 10 μM solutions of poly(oligo(ethylene glycol)<sub>m</sub> acrylates)-Aβ<sub>1-40</sub> conjugates, (B) 10 μM/10 μM solutions of poly(oligo(ethylene glycol)<sub>m</sub> acrylates)-Aβ<sub>1-40</sub> conjugates / Aβ<sub>1-40</sub> and (C) Aβ<sub>1-40</sub> wild type. The raw data are presented.

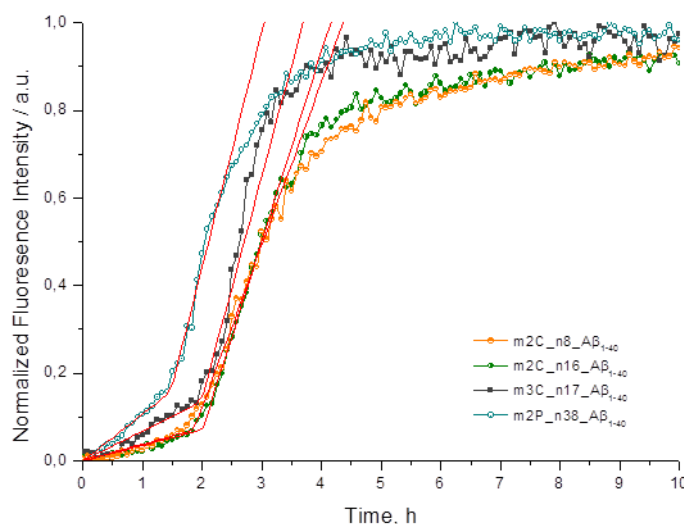


**Figure S20.** Time evolution of the ThT fluorescence intensity of the 10 μM solutions of poly(oligo(ethylene glycol)<sub>m</sub> acrylates)-Aβ<sub>1-40</sub> conjugates. Piecewise linear fits are demonstrated respectively.

[1] J. Wägele, S. De Sio, B. Voigt, J. Balbach, M. Ott, *Biophys. J.* **2019**, *116*, 227.

- .....
- [2] Z. Evgrafova, B. Voigt, M. Baumann, M. Stephani, W. H. Binder, J. Balbach, *ChemPhysChem* **2019**, *20*, 236.
- [3] D. Jiang, I. Rauda, S. Han, S. Chen, F. Zhou, *Langmuir* **2012**, *28*, 12711.
- [4] T. J. Esparza, N. C. Wildburger, H. Jiang, M. Gangolli, N. J. Cairns, R. J. Bateman, D. L. Brody, *Scientific Reports* **2016**, *6*, 38187.
- 20
- [5] P. Arosio, T. Cedervall, T. P. J. Knowles, S. Linse, *Analytical Biochemistry* **2016**, *504*, 7.

.....  
**Appendix D – ChemPhysChem 2019, 20 (2), 236-240**

*Probing Polymer Chain Conformation and Fibril Formation of Peptide Conjugates*

**Experimental Section**

**Materials.** Deuterated chloroform was purchased from Chemotrade, DMF, DMF (HPLC grade) and THF (HPLC grade) were purchased from Grüssing and VWR – Prolabo respectively. Hexane was bought from Overlack. All other chemicals were received from Sigma Aldrich or Carl Roth GmbH and used without further purification unless otherwise stated.

**Analytical methods for the poly(methoxydi(ethylene glycol)acrylates).**  $^1\text{H-NMR}$  spectra of RP-22 (Figure S8) and RP-23 (Figure S9) were recorded on a Varian Gemini 2000 (400 MHz) or on a Varian Unity Inova 500 (500 MHz) using MestReNova software (version 6.0.2-5475) for the evaluation of the results. NMR spectra were measured at 27 °C using deuterated chloroform ( $\text{CDCl}_3$ ). All chemical shifts ( $\delta$ ) were given in parts per million (ppm) relative to trimethylsilane (TMS) and referred to the solvent signal ( $\text{CDCl}_3$ : 7.26 ppm ( $^1\text{H}$ ), 77.0 ppm ( $^{13}\text{C}$ )).

**RP-22:**  $^1\text{H-NMR}$  (400 MHz,  $\text{CDCl}_3$ ):  $\delta =$  ppm 8.60 (d,  $1\text{H}_a$ , -NCH), 7.93 (m,  $2\text{H}_{b,c}$ , -NCHCHCH), 7.35 (m,  $1\text{H}_d$ , -NCCH), 4.83 (m,  $1\text{H}_g$ , -CHCH $_3$ ), 4.19 (bs,  $102\text{H}_{f,k}$ , -CHCH $_3$ ), 3.65 (m,  $202\text{H}_{l,m,p}$  -OCH $_2$ CH $_2$ OCH $_2$ ; -SCH $_2$ ), 3.52 (m,  $100\text{H}_n$ , -CH $_2$ OCH $_3$ ), 3.36 (s,  $150\text{H}_o$ , -CH $_2$ OCH $_3$ ), 3.12 (m,  $2\text{H}_e$ , -SSCH $_2$ ), 2.33 (bs,  $50\text{H}_j$ , -CH $_2$ CH), 1.65 (m,  $104\text{H}_{i,q,r}$ , -CH $_2$ CH; -CSSCH $_2$ CH $_2$ ; -CH $_2$ CH $_3$ ; H $_2$ O from  $\text{CDCl}_3$ ), 1.15 (m,  $3\text{H}_h$ , -CHCH $_3$ ), 0.93 (t,  $3\text{H}_s$ , -CH $_2$ CH $_3$ )

**RP-23:**  $^1\text{H-NMR}$  (400 MHz,  $\text{CDCl}_3$ ):  $\delta =$  ppm 8.52 (d,  $1\text{H}_a$ , -NCH), 7.78 (m,  $2\text{H}_{b,c}$ , -NCHCHCH), 7.20 (m,  $1\text{H}_d$ , -NCCH), 4.84 (m,  $1\text{H}_g$ , -CHCH $_3$ ), 4.19 (bs,  $44\text{H}_{f,k}$ , -CHCH $_3$ ), 3.67 (m,  $84\text{H}_{l,m,p}$  -OCH $_2$ CH $_2$ OCH $_2$ ; -SCH $_2$ ), 3.52 (m,  $42\text{H}_n$ , -CH $_2$ OCH $_3$ ), 3.36 (s,  $63\text{H}_o$ , -CH $_2$ OCH $_3$ ), 3.07 (m,  $2\text{H}_e$ , -SSCH $_2$ ), 2.34 (bs,  $21\text{H}_j$ , -CH $_2$ CH), 1.66 (m,  $48\text{H}_{i,q,r}$ , -CH $_2$ CH; -CSSCH $_2$ CH $_2$ ; -CH $_2$ CH $_3$ ; H $_2$ O from  $\text{CDCl}_3$ ), 1.15 (m,  $3\text{H}_h$ , -CHCH $_3$ ), 0.93 (t,  $3\text{H}_s$ , -CH $_2$ CH $_3$ )

MALDI-TOF-MS analysis was carried out using a *Bruker Autoflex III Smartbeam* equipped with a nitrogen laser (337 nm) working in linear and reflection modes. The obtained data were evaluated using flexAnalysis software (version 3.0). In case of polymer the matrix solution was prepared by dissolving trans-2-[3-(4-tert-Butylphenyl)-2-methyl-2-propenylidene]malononitrile (DCTB) in THF at a concentration of 20 mg·mL $^{-1}$ . The polymer was dissolved in THF (20 mg·mL $^{-1}$ ) and mixed with sodium trifluoroacetate (20 mg·mL $^{-1}$  in THF). The ratio between the matrix, the analyte and the salt was 100:10:1. In case of polymer-peptide conjugates the matrix solution was prepared by dissolving (trans-3,5-dimethoxy-4-hydroxycinnamic acid (sinapinic acid) in TA50 solvent (50:50 [v/v] acetonitrile : 0.1% TFA in water) at a concentration of 20 mg·mL $^{-1}$ . The conjugate was dissolved in TA50 (100 pmol· $\mu\text{l}^{-1}$ ) and mixed with the matrix. The ratio between the matrix and the analyte was 100:10.

Gel permeation chromatography (GPC) measurements were performed on a Viscotek GPCmax VE 2002 using a H $_{\text{HR}}$ -H Guard-17360 precolumn and a GMH $_{\text{HR}}$ -N-18055 column with THF as solvent and VE 3580 IR detector for refractive index determination. A polystyrene standard ( $M_{\text{P}} = 1,000 - 115,000 \text{ g}\cdot\text{mol}^{-1}$ ) was used for external calibration. Column and detector temperatures were held at 22 °C and 35 °C respectively and the flow rate was set to 1 mL·min $^{-1}$ . The concentration of all samples was 3 mg·mL $^{-1}$ .

Turbidimetry measurements were performed using an UV-VIS spectrometer HP 8543 from Agilent. By coupling with a peltier element HP 89090A from Agilent controlled heating with

.....  
 a heating rate of  $0.5\text{ }^{\circ}\text{C}\cdot\text{min}^{-1}$  was possible. The observed wavelength was  $\lambda = 500\text{ nm}$ . For all measurements in water a 1 wt% solution of the polymer was used. The measurements in buffers were done as follows: for the poly(methoxydi(ethylene glycol)acrylates) 700  $\mu\text{M}$  solutions in sodium borate buffer (50mM  $\text{H}_3\text{BO}_3/\text{NaOH}$ , pH 9,0) was used.  $T_{\text{CP}}$  was detected at 50% of transmission.

Thin-layer chromatography (TLC) was performed using ``Merck silica gel 60`` plates. Spots on TLC plate were visualized using oxidizing agent ``blue`` stain or UV light (254 or 366 nm). ``Blue`` stain was prepared as follows:  $(\text{NH}_4)_6\text{Mo}_7\text{O}_{24}\cdot 4\text{H}_2\text{O}$  (1 g) and  $\text{Ce}(\text{SO}_4)_2\cdot 4\text{H}_2\text{O}$  (1 g) were dissolved in a mixture of distilled water (90 mL) and concentrated sulphuric acid (6 mL).

Column chromatography was carried out using high purity grade Merck 60 (230 – 400 mesh particle size) silica gel.

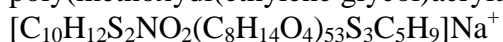
**General procedure for the syntheses of the poly(methoxydi(ethylene glycol)acrylates):**

RAFT polymerization of RP-23 was performed using a standard Schlenk technique. The pyridyl disulfide functionalized CTA (**1**)<sup>[23]</sup> (30.5 mg, 0.128 mmol), methoxydi(ethylene glycol)acrylate (**2**)<sup>[24]</sup> (431,5  $\mu\text{L}$ , 2.56 mmol) and AIBN (2.1 mg, 0.0128 mmol) in a molar ratio of (**2**):(**1**):AIBN 20:1:0.1 were dissolved in 1.2 mL of DMF. The mixture of (**2**), (**1**), AIBN and DMF was bubbled with argon for 30 minutes prior to the reaction and placed into a preheated oil bath at  $70\text{ }^{\circ}\text{C}$ . The reaction was stirred for six hours before it was cooled by means of a methanol/liquid nitrogen bath to  $-80\text{ }^{\circ}\text{C}$ . The resulting yellow polymer was precipitated three times into high excess of *n*-hexane and dried in high vacuum within three days. The polymeric product RP-23 was characterized via  $^1\text{H-NMR}$  (Figure S9), matrix-assisted laser desorption/ionization mass spectrometry (MALDI-TOF MS) (Figure S3), size exclusion chromatography (SEC) (Figure S10), and turbidimetry (Figure S1). Therefore the obtained polymer was truly proven via these experimental methods.

As an example the MALDI-TOF of the polymer RP-23 is shown in Figure S3, displaying one main series, corresponding to the repeating unit (difference  $\sim 174\text{ Da}$ ). The first series at 4087.510 Da can be assigned to poly(methoxydi(ethylene glycol)acrylate) with a formula of  $[\text{C}_{10}\text{H}_{12}\text{S}_2\text{NO}_2(\text{C}_8\text{H}_{14}\text{O}_4)_{21}\text{S}_3\text{C}_5\text{H}_9]\text{Na}^+$ . The main signal of the multiplet chosen for Series S2, which appears at 2541.684 Da and can be assigned to



For RP-22 the difference between multiplets ( $\sim 174\text{ Da}$ ) coincides with the repeating unit of the polymer. The signal appearing at 9662.627 Da (Figure S2) can be assigned to poly(methoxydi(ethylene glycol)acrylate) with a formula of



**Recombinant expression of PTH.** Human PTH(1-84) was purified with minor modifications according to a reported protocol.<sup>[25]</sup> The pET SUMOadapt vector transformed into *E. coli* BL21 (DE3) CodonPlus RIL was used as the expression system. The *N* and *C* terminal cysteine variants PTH(1-84) V2C and PTH(1-84) Q84C, respectively, have been obtained by site-directed mutagenesis. Isotope labelling for NMR studies has been achieved by supplementation of the MSM CHP2 expression medium with  $^{15}\text{NH}_4\text{Cl}$ .

The peptide was purified by Ni-NTA affinity chromatography followed by cleavage of the SUMO fusion tag with SUMO protease ( $50\text{-}150\text{ }\mu\text{g}\cdot\text{ml}^{-1}$ ). The solution was further purified by hydrophobic interaction chromatography (HIC) using a butyl sepharose 4 fast flow medium. In a final step the solution was applied to a S75 size exclusion chromatography column. The purified PTH(1-84) was lyophilized and then stored at  $-20\text{ }^{\circ}\text{C}$ .

.....  
**Conjugation reaction and product purification.** For the synthesis of the peptide-polymer conjugates a strategy based on thiol disulfide exchange was used. The respective PTH(1-84) variant was solubilised in reduction buffer (50 mM Na<sub>2</sub>HPO<sub>4</sub>, pH8.0) and mixed with dithiothreitol (DTT) in a molar ratio of 1:200 in a 1,5 ml glass tube. Previously formed PTH homodimers have been reduced for two hours at room temperature. DTT separation and buffer exchange to conjugation buffer (50 mM Na<sub>2</sub>HPO<sub>4</sub>, 100 mM NaCl, 1 mM EDTA, pH6.8) were performed using a PD MiniTrap G25 column. For the final reaction mixture, the peptide concentration was adjusted to 250 μM. The reaction was started by adding the polymer RP-22 or RP-23 in a 1:10 molar ratio, allowing the conjugation over 3 hours at 23 °C or 15 °C, respectively.

After the reaction the temperature was adjusted to a value above the transition point of the respective free polymer (37 °C or 25 °C). The sample was centrifuged (16200 g, 30 min) to separate the aggregated non-conjugated polymer. The supernatant was applied to a sulphopropyl fast flow 1 ml cation exchange chromatography medium equilibrated with 20 mM Na<sub>2</sub>HPO<sub>4</sub> (pH 6.8). For the elution the same buffer complemented with 1 M NaCl was used. Size exclusion chromatography (50 mM Na<sub>2</sub>HPO<sub>4</sub>, pH7.4) was used as the final purification step.

**Protein NMR spectroscopy.** For structural analyses two dimensional <sup>1</sup>H-<sup>15</sup>N-heteronuclear single quantum coherence spectra (<sup>1</sup>H-<sup>15</sup>N-HSQC) have been obtained on a Bruker Avance III 800 MHz NMR spectrometer in the liquid state. The experiments were carried out at 25 °C (RP-22 and RP-23) and at 15 °C (RP-23). As a reference <sup>15</sup>N labelled PTH(1-84) was used at the respective temperatures. For the analysis of interactions in physical mixtures <sup>1</sup>H-<sup>15</sup>N-HSQC spectra of PTH (c = 500 μM) were acquired in the presence of 0 μM or 250 μM polymer. The NMR experiments for the conjugates were carried out at concentrations of 20-50 μM.

The apparent hydrodynamic radii were calculated from diffusion coefficients determined by pulsed field gradient (PFG) stimulated spin echos.<sup>[26]</sup> The gradient strength was varied from 0.0175 T·m<sup>-1</sup> to 0.3325 T·m<sup>-1</sup>. The duration of the gradient was adjusted to 3 ms and diffusion of the molecules was allowed for 100 ms. For the analysis the spectra were integrated from 1.71 ppm to 2.10 ppm and from 3.56 ppm to 3.83 ppm. Dioxane was used as an external reference due to its known hydrodynamic radius of  $r_H = 0,212$  nm.

**ThT dependent kinetic assay.** ThT detected fibrillation kinetics of PTH and PTH conjugates were recorded according to earlier reports<sup>[16]</sup> on a BMG Labtech FLUOStar Omega plater reader using a 96-well plate. 600 μM PTH and equimolar polymer concentrations were incubated in 50 mM Na<sub>2</sub>HPO<sub>4</sub>, pH 7.4, supplemented with 150 mM or 300 mM NaCl and 50 μM ThT at 37 °C. The shaking protocol consisted of 30 s double-orbital shaking at 100 rpm prior to the measurement followed by 270 s incubation at 0 rpm. After excitation at 450 nm emission was monitored at 480 nm. The very reproducible assay was recorded three times at 300 mM NaCl for PTH and in its physical mixtures with RP-23 and RP-22. The corresponding kinetics at 150mM NaCl were recorded as duplicates

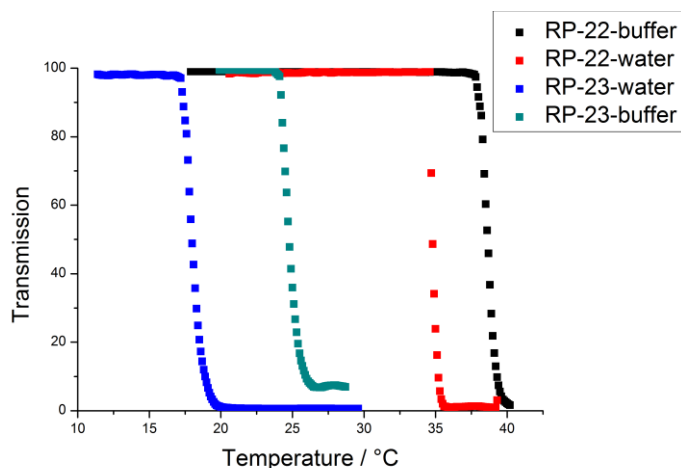


**Figure S1.** LCST measurements of the poly(methoxydi(ethylene glycol)acrylates) as 1 wt% water solutions or in sodium borate buffer (50mM  $\text{H}_3\text{BO}_3/\text{NaOH}$ , pH 9,0; 700 mM (ca. 0.26 wt% for RP-23 and ca. 0.61 wt% for RP-22)). The blue and red curves refer to the measurement in water of RP-23 (3,700 g/mol) and RP-22 (8,700 g/mol), where dark green and black curves refer to measurements of the RP-22 and RP-23 in buffer respectively. LCST under measured conditions can be detected at 50% of transmission and is determined as: RP-22 (1wt% water) 34.8 °C; RP-22 (buffer) 38.6 °C; RP-23 (1wt% water) 18.01 °C; RP-23 (buffer) 24.7 °C. With an increasing molecular weight the LCST is also increasing.

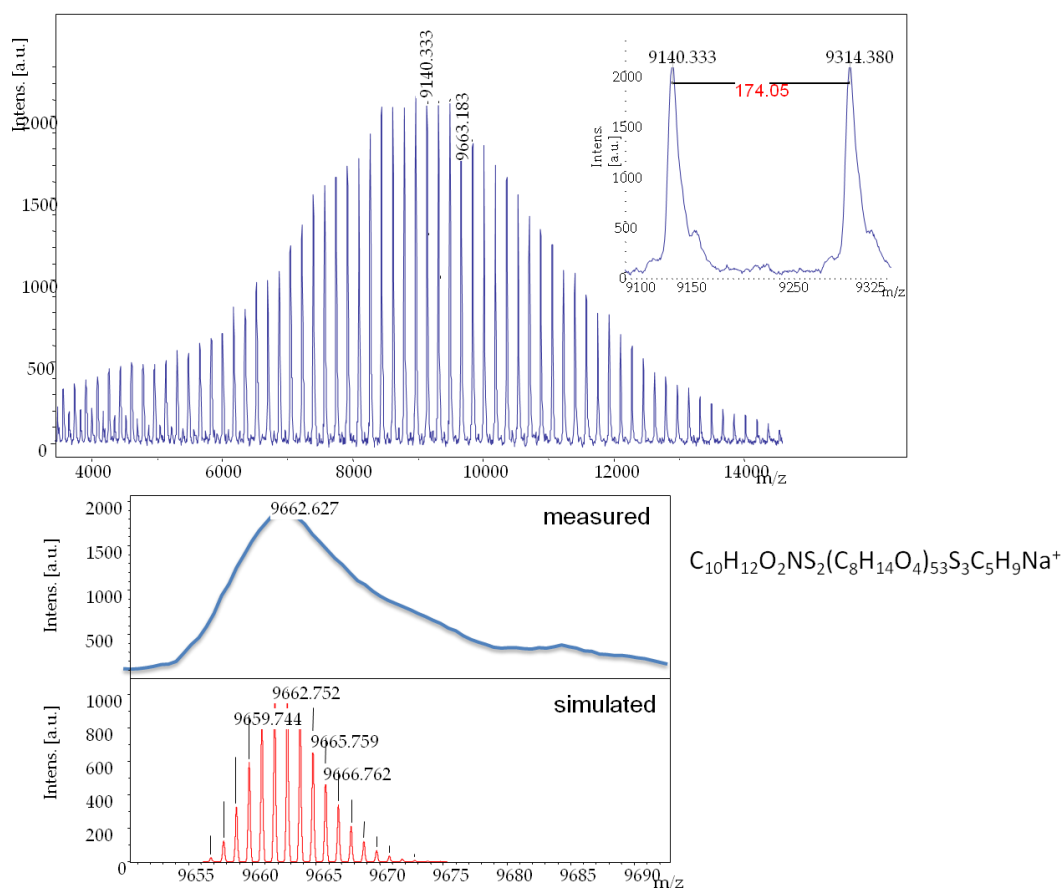


**Figure S2.** MALDI-TOF spectrum of poly(methoxydi(ethylene glycol)acrylate) RP-22

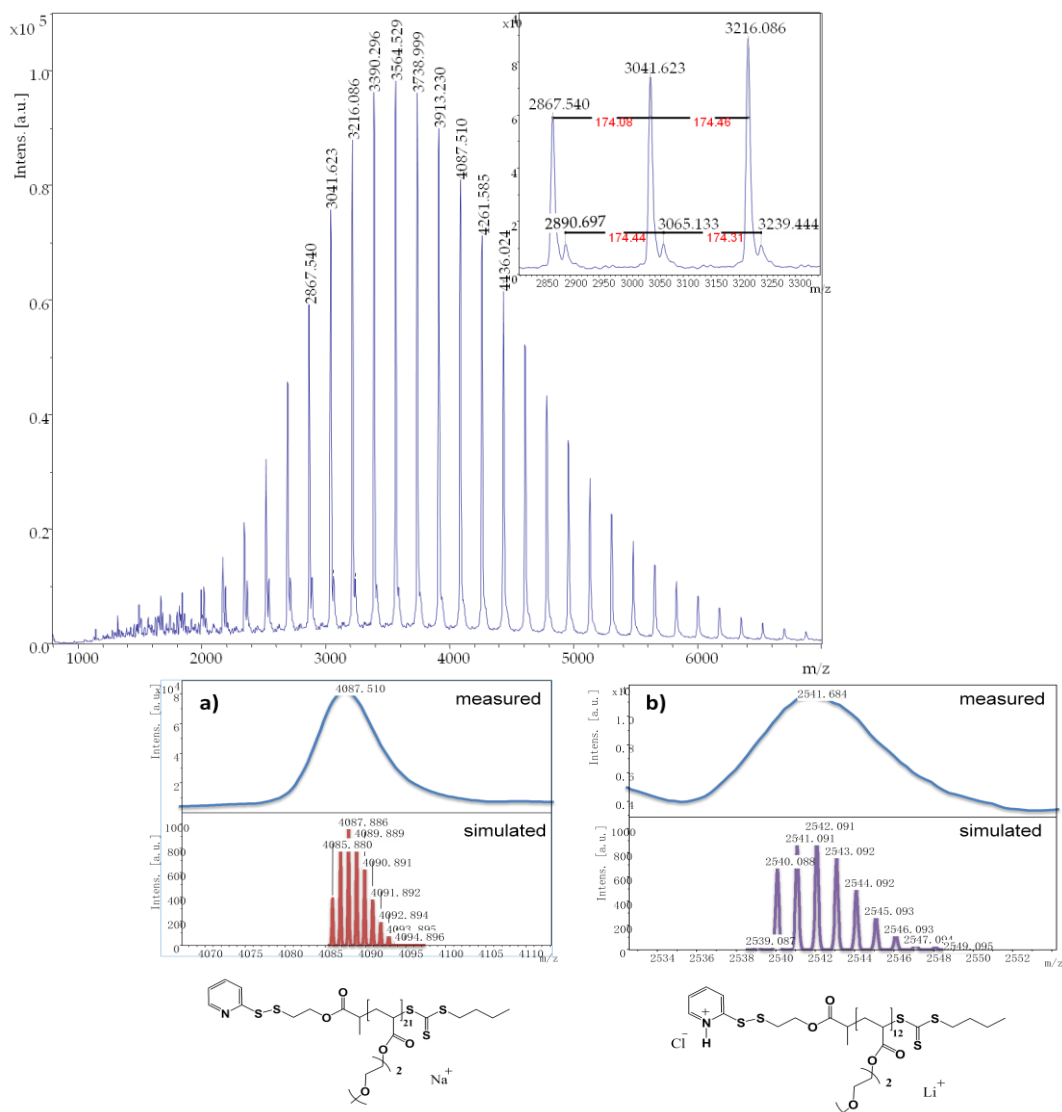


**Figure S3.** MALDI-TOF spectrum of poly(methoxydi(ethylene glycol)acrylate) RP-23 a) measured and simulated isotopic patterns of series 1 with the structure  $[C_{10}H_{12}S_2NO_2(C_8H_{14}O_4)_{21}S_3C_5H_9]Na^+$  and b) measured and simulated isotopic patterns of series 2 with the structure  $[C_{10}H_{13}S_2NO_2Cl(C_8H_{14}O_4)_{12}S_3C_5H_9]Li^+$ .

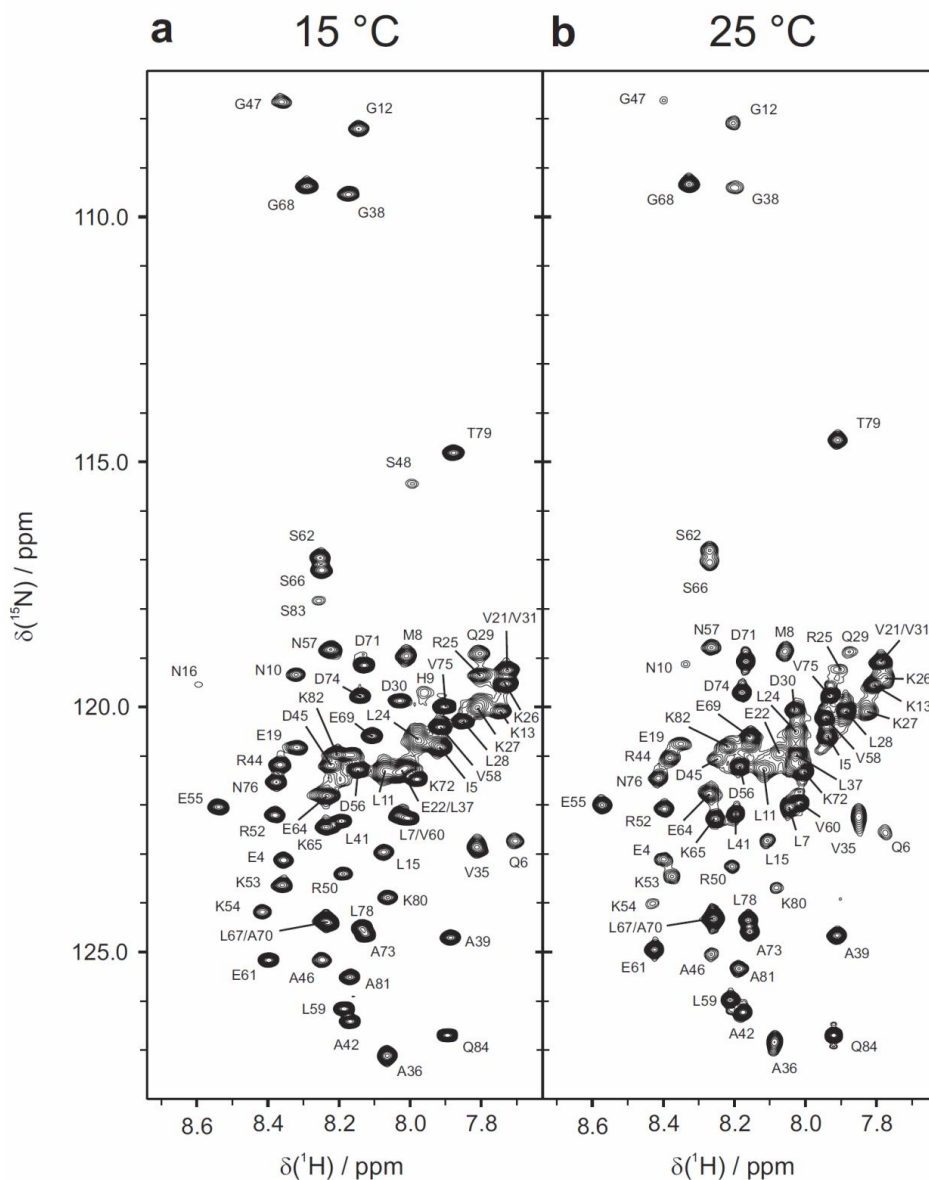


**Figure S4.** 2D  $^1\text{H}$ - $^{15}\text{N}$  HSQC spectra of  $^{15}\text{N}$  PTH at 15 °C (a) and 25 °C (b) in 50 mM sodium phosphate, pH 7.4, including backbone assignments of the NMR cross peaks (one letter abbreviations for the amino acids and primary sequence number). 80% of the published assignments<sup>[16,27]</sup> could be transferred to the here used buffer conditions.

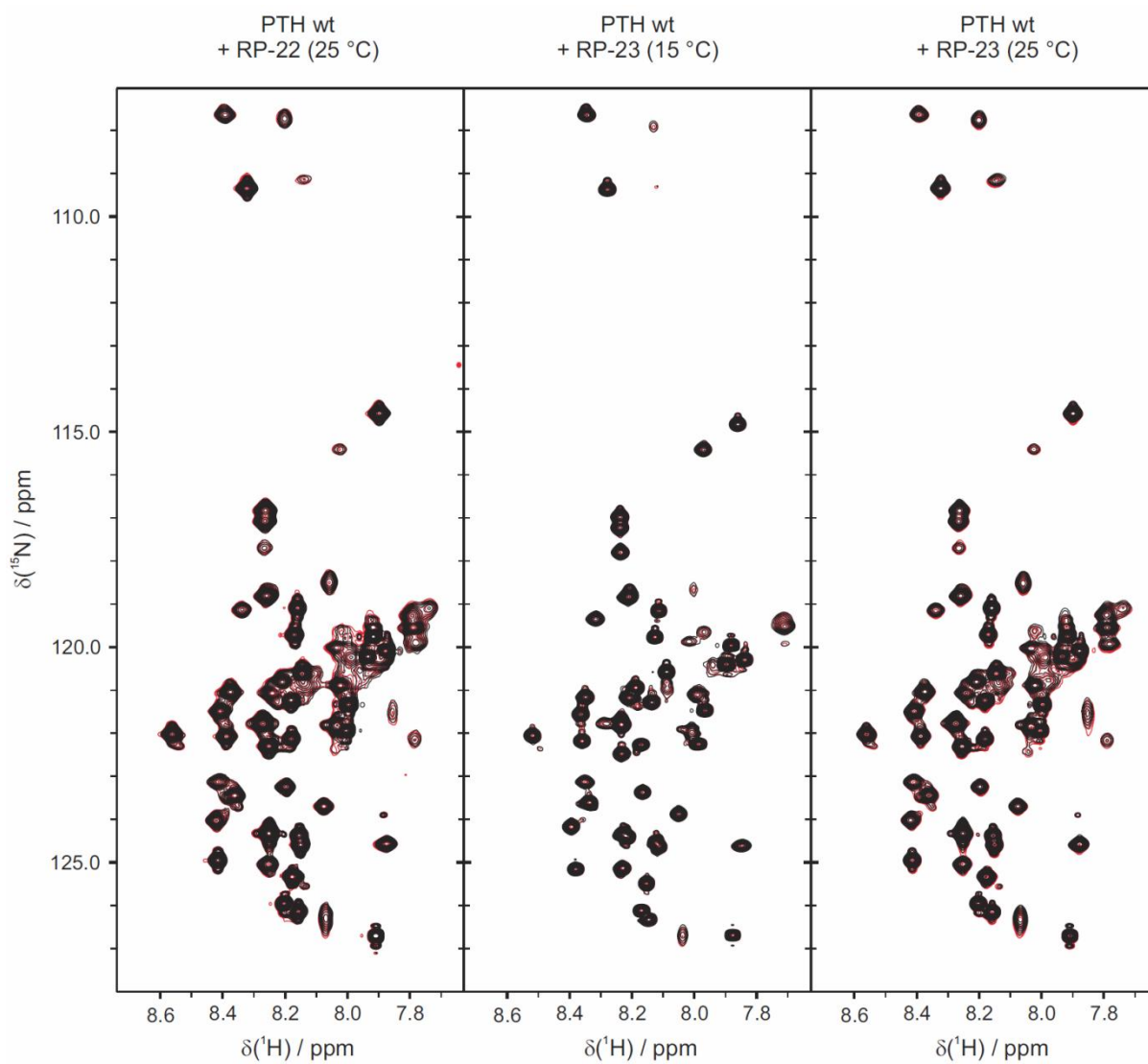


**Figure S5.** 2D  $^1\text{H}$ - $^{15}\text{N}$  HSQC spectra of 500  $\mu\text{M}$   $^{15}\text{N}$  PTH wt in the absence (red) and in the presence (black) of 250  $\mu\text{M}$  non-conjugated RP-22 at 25  $^\circ\text{C}$  (left) and RP-23 at 15  $^\circ\text{C}$  (middle) or 25  $^\circ\text{C}$  (right).

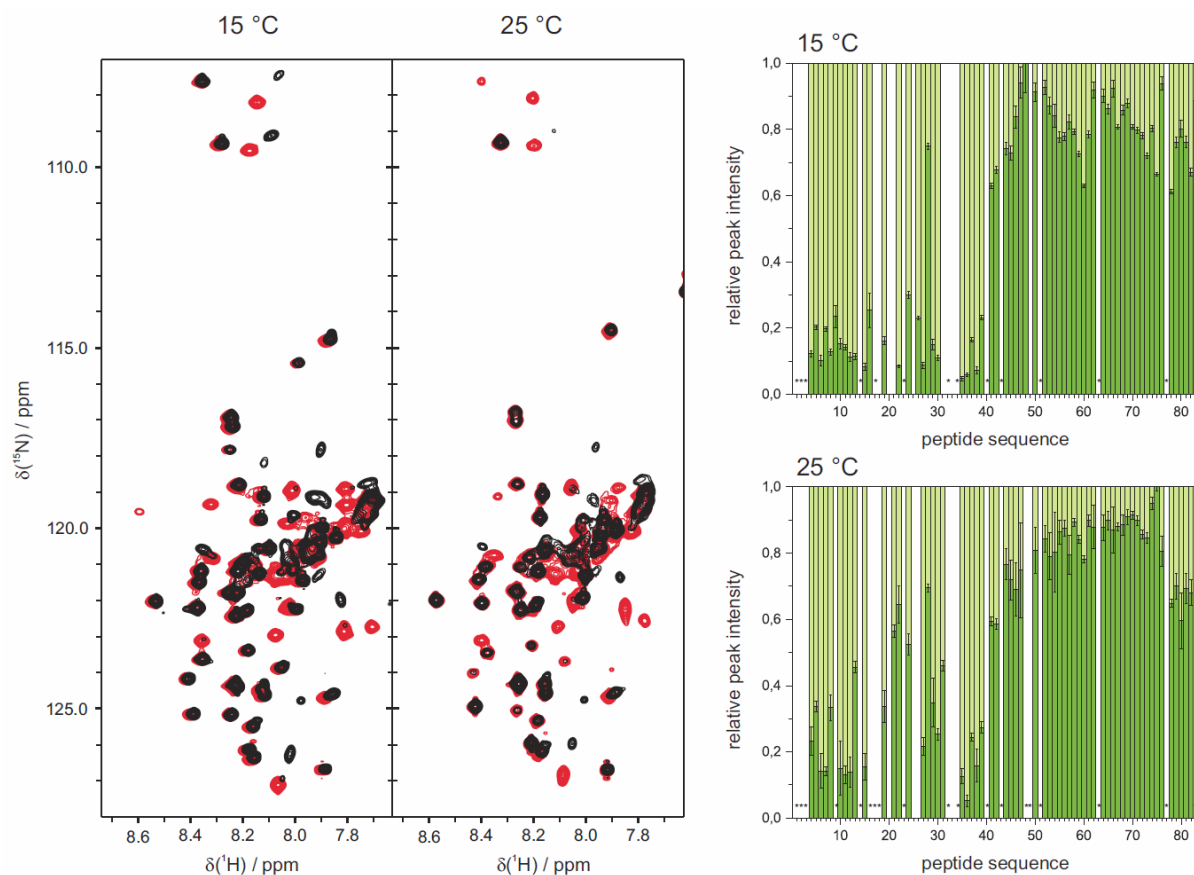


**Figure S6.** 2D  $^1\text{H}$ - $^{15}\text{N}$  HSQC NMR spectra of  $^{15}\text{N}$  PTH V2C-RP-23 (black) at 15 °C and 25 °C compared to the spectra of the non-conjugated  $^{15}\text{N}$  PTH variants (red). The diagrams illustrate the relative intensity changes at the respective cross peak positions in the  $^{15}\text{N}$  PTH spectrum along the peptide sequence. Prolines and residues with non-detectable cross peaks are indicated by an asterisk.

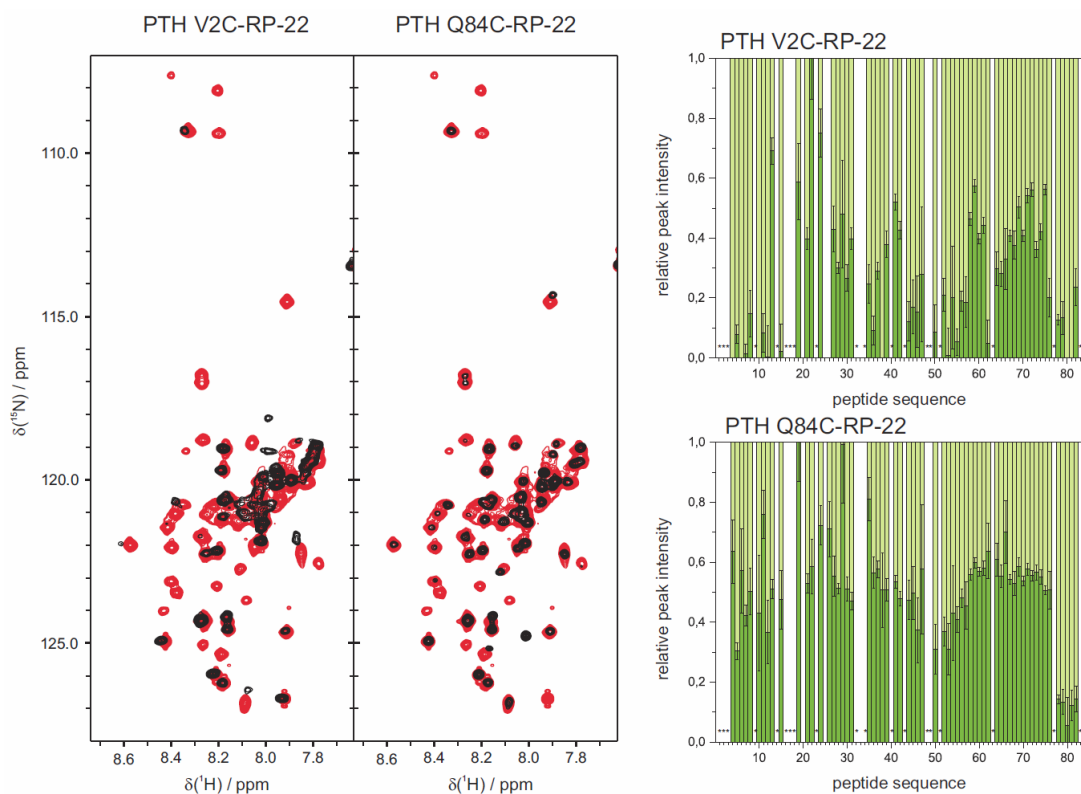


**Figure S7.** 2D  $^1\text{H}$ - $^{15}\text{N}$  HSQC spectra of  $^{15}\text{N}$  PTH V2C-RP-22 (left, black) and  $^{15}\text{N}$  PTH Q84C-RP-22 (right, black) at 25 °C compared to the non-conjugated  $^{15}\text{N}$  PTH variants (red). The diagrams illustrate the relative intensity changes at the respective cross peak positions in the  $^{15}\text{N}$  PTH spectrum along the peptide sequence. Prolines and residues with non-detectable cross peaks are indicated by an asterisk.

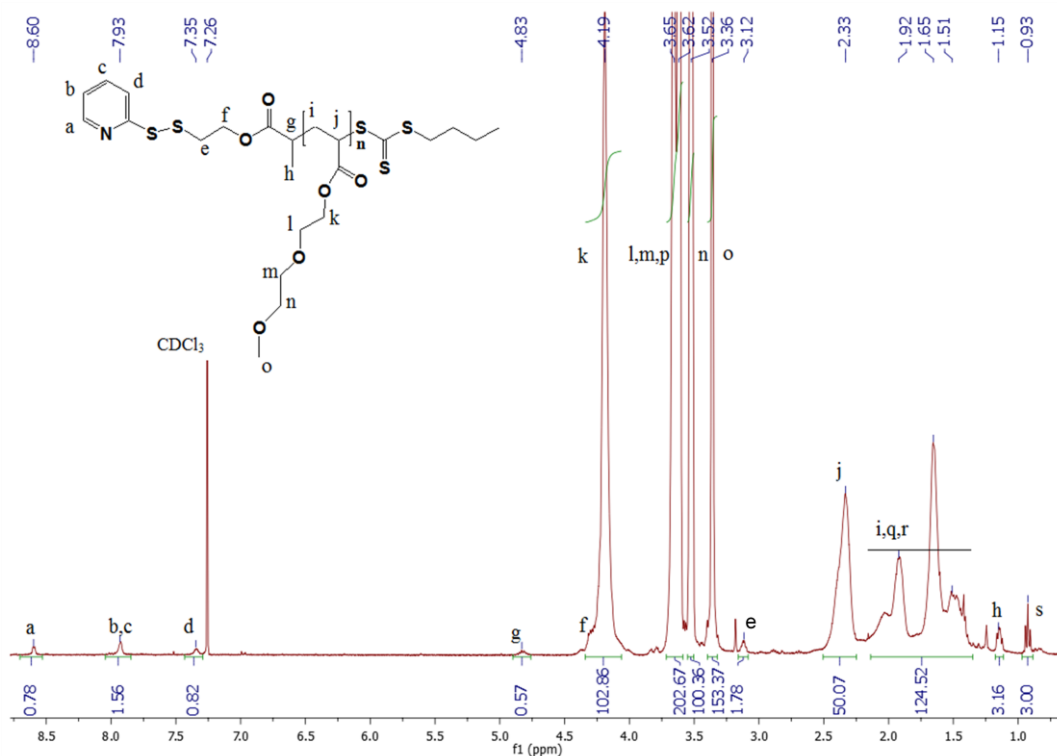


**Figure S8.**  $^1\text{H}$ -NMR spectrum of poly(methoxydi(ethylene glycol)acrylate RP-22.

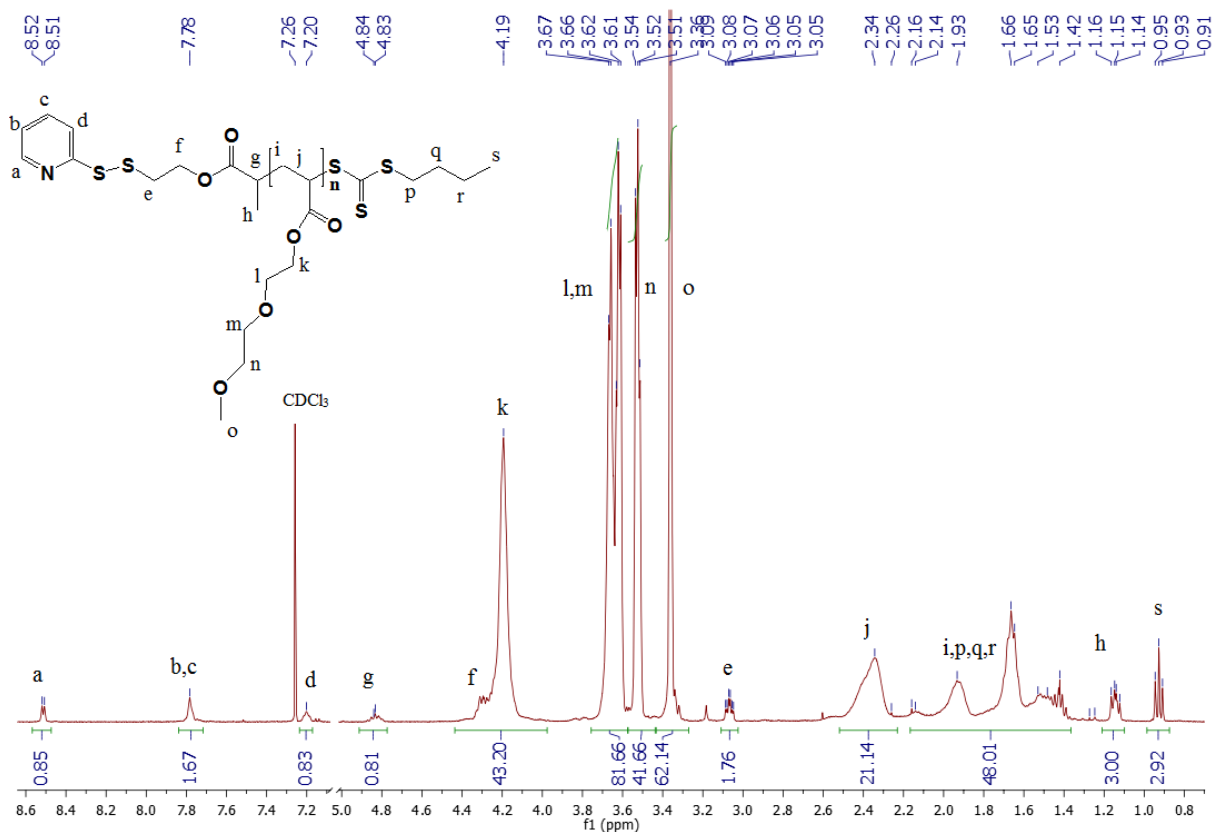


**Figure S9.**  $^1\text{H-NMR}$  spectrum of poly(methoxydi(ethylene glycol)acrylate RP-23.

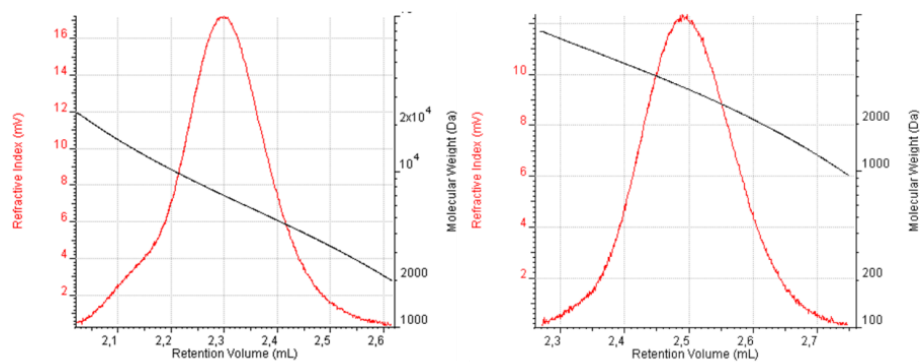


**Figure S10.** SEC traces of poly(methoxydi(ethylene glycol)acrylates) RP-22 (PDI=1.15) and RP-23 (PDI=1.11).

## BILDUNG

---

- Februar 2015 – Dezember 2019 - Martin-Luther-Universität Halle-Wittenberg, Institut für Makromolekulare Chemie, Doktorandin
  - Thema der Doktorarbeit: “Modulation der Amyloidpeptidaggregation durch hydrophile Polymere”
- Oktober 2012 – Januar 2015 - Martin-Luther-Universität Halle-Wittenberg, Polymer Materials Science Masterprogram
  - Thema der Masterarbeit: “Mikrophasenetrennte polymer-ionische Flüssigkeiten”
- September, 2006 – Juni, 2011 - Chemisch-Technische Dmitri-Mendelejew-Universität von Russland, Institut für Makromolekulare Chemie, Diplom Chemieingenieur
  - Thema der Diplomarbeit: “Synthese und Eigenschaften von Polyarylenetherketonen, erhalten durch Reaktion der nukleophilen Substitution”
- September, 1996 – Juni, 2006 – Städtische Allgemeine Bildungseinrichtung Stadtgymnasium von Dimitrovgrad

## BERUFSERFAHRUNG

---

- Februar 2015 – Dezember 2019 - Martin-Luther-Universität Halle-Wittenberg, Institut für Makromolekulare Chemie, Wissenschaftliche Mitarbeiterin
- August 2011 – September 2012 – Spezialist in der Abteilung für Forschung und Entwicklung von Verpackungsmaterialien bei Danone Company
- September 2010 – Juli 2011 – Wissenschaftliche Hilfskraft in Nesmeyanov-Institut für Elementorganische Verbindungen der Russischen Akademie der Wissenschaften in Moskau

## AUSZEICHUNGEN

---

30.04.2013 – Halle Young Polymer Scientist Scholarship

### SPRACHEN

---

Russisch ●●●●●●  
Deutsch ●●●●○  
Englisch ●●●●○

### SCHLÜSSELFERTIGKEITEN

---

- Projektmanagement
- Polymer- und Proteincharakterisierungstechniken (NMR, EPR, GPC, MALDI-TOF, ESI-TOF, DLS, Turbidimetrie, HPLC, CD, IR, Fluoreszenzspektroskopie, TEM)
- Methoden des Verpackungslabor (Zugfestigkeitsprüfung, Schrumpftest)
- Datenverarbeitungssoftware (Origin, SAP, MS Office)

Geburtsdatum 29/09/1989

Verheiratet

### Liste der Publikationen:

1. Synthesis and aggregation of polymer-amyloid  $\beta$  conjugates. Zhanna Evgrafova, Sven Rothmund, Bruno Voigt, Gerd Hause, Jochen Balbach, Wolfgang H. Binder\*, *Macromol. Rapid Commun.* 2019, *Macromolecular Rapid Communications* 2019, 0, 1900378,
2. Modulation of Amyloid beta-Peptide Aggregation by Hydrophilic Polymers. Zhanna Evgrafova, Bruno Voigt, Andreas H. Roos, Gerd Hause, Dariush Hinderberger, Jochen Balbach and Wolfgang H. Binder\*, *Physical Chemistry Chemical Physics*, 2019, 20999 - 21006,
3. Probing polymer chain conformation and fibril formation of peptide conjugates. Zhanna Evgrafova, Bruno Voigt, Monika Baumann, Madlen Stephani, Wolfgang H. Binder\* and Jochen Balbach\*, *ChemPhysChem*, 2019, 236-240,
4. Amyloid beta aggregation in the presence of temperature-sensitive polymers. Sebastian Funtan, Zhanna Evgrafova, Juliane Adler, Daniel Huster and Wolfgang H. Binder\*, *Polymers MDPI*, 2016, 8, 178.

### Präsentation auf Konferenzen:

1. Z. Evgrafova, S. Deike, A. Paschold, B. Voigt, J. Balbach, W. H. Binder; "Assembly of peptide/polymer hybrid molecules", 7th SFB-TRR 102 (Polymers under multiple constraints) Miniworkshop, 08. November 2019, Leipzig, Deutschland, Poster
2. Z. Evgrafova, B. Voigt, J. Balbach, W. H. Binder; "Assembly of peptide/polymer hybrid molecules", Review of the proposal of continuation of the SFB TRR 102 (Polymers under multiple constraints), 12.–13. März 2019, Halle (Saale), Deutschland, Poster
3. Z. Evgrafova, J. Adler, B. Voigt, J. Balbach, D. Huster, W. H. Binder; "Changes in amyloid-aggregation by (non)-covalently polymers: influence of hydrophilicity on aggregation of amyloid-A-beta (40) and PTH (1-84)", 6th SFB-TRR 102 (Polymers under multiple constraints) Miniworkshop, 09. Juli 2018, Halle (Saale), Deutschland, Poster
4. Z. Evgrafova, S. Kumar, B. Voigt, J. Adler, D. Huster, J. Balbach, W. H. Binder; "Amyloid beta aggregation in the presence of temperature-sensitive polymers", International Discussion Meeting on Polymer Crystallization, 17.–20. September 2017, Wittenberg, Deutschland, Poster
5. Z. Evgrafova, J. Adler, D. Huster, W. H. Binder; "Amyloid beta aggregation in the presence of temperature-sensitive polymers", APME (Advanced Polymer via Macromolecular Engineering), 21.–25. Mai 2017, Ghent, Belgien, Poster
6. Z. Evgrafova, J. Adler, D. Huster, W. H. Binder; "Amyloid beta aggregation in the presence of temperature-sensitive polymers", Biennial Meeting of the GDCh-Division Macromolecular Chemistry, 11.–13. September 2016, Halle (Saale), Deutschland, Poster
7. Z. Evgrafova, A. Stojanovic, P. Michael, W. H. Binder; "Microphase separated polymeric ionic liquids", European Polymer Federation Congress (EPF), 22.–26. Juni 2015, Dresden, Deutschland, Poster

---

Zhanna Evgrafova

## **Eigenständigkeitserklärung**

Hiermit erkläre ich an Eides statt, dass ich die vorliegende Dissertation selbstständig und ohne fremde Hilfe verfasst und keine anderen, als die von mir angegebenen Quellen und Hilfsmittel verwendet habe.

Außerdem erkläre ich, dass die vorliegende Dissertation an keiner anderen wissenschaftlichen Einrichtung zur Erlangung eines akademischen Grades eingereicht wurde.

Halle (Saale), 24.03.2020

---

Zhanna Evgrafova